THE UNIVERSITY OF
ARIZONA
TUCSON ARIZONA

FINAL REPORT

for

NASA Research Grant NAG-1-1041

Development of Deterministic Transport Methods for Low Energy Neutrons for Shielding in Space

Submitted to

The National Aeronautics and Space Administration
Langley Research Center
Hampton Virginia

by

Dr. Barry Ganapol

of the

Department of Nuclear and Energy Engineering
The University of Arizona

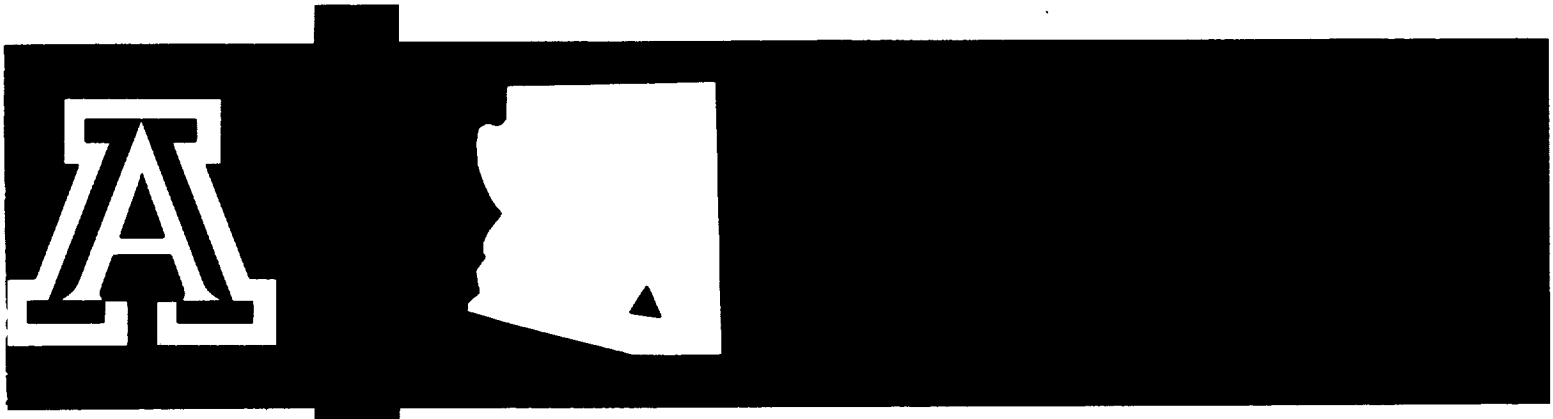

ENGINEERING EXPERIMENT STATION
COLLEGE OF ENGINEERING AND MINES
THE UNIVERSITY OF ARIZONA
TUCSON, ARIZONA 85721

THE UNIVERSITY OF ARIZONA
GRADUATE COLLEGE

As members of the Final Examination Committee, we certify that we have read the dissertation prepared by Robert Clay Singleterry, Jr.

entitled Neutron Transport Associated with the Galactic Cosmic Ray Cascade

and recommend that it be accepted as fulfilling the dissertation requirement for the Degree of Doctor of Philosophy - Engineering

Barry Ganapol	Barry Ganapol	8/2/93 Date
William Filippone	William Filippone	8/3/93 Date
David Hetrick	David L Hetrick	8/2/93 Date
Morris Farr	Morris Farr	8/23/93 Date
		Date

Final approval and acceptance of this dissertation is contingent upon the candidate's submission of the final copy of the dissertation to the Graduate College.

I hereby certify that I have read this dissertation prepared under my direction and recommend that it be accepted as fulfilling the dissertation requirement.

Barry Ganapol Barry Ganapol 8/2/93
Dissertation Director Date

Statement By Author

This dissertation has been submitted in partial fulfillment of requirements for an advanced degree at the University of Arizona and is deposited in the University Library to be made available to borrowers under rules of the Library.

Brief quotations from this dissertation are allowable without special permission, provided that accurate acknowledgment of source is made. Requests for permission for extended quotation from or reproduction of this manuscript in whole or in part may be granted by the head of the major department or the Dean of the Graduate College when in his or her judgment the proposed use of the material is in the interests of scholarship. In all other instances, however, permission must be obtained from the author.

Signed: 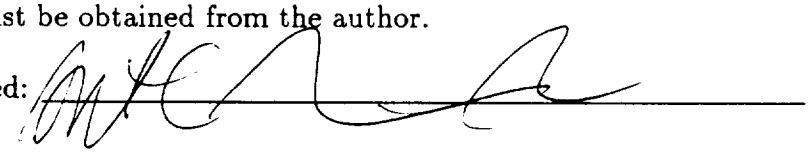

Acknowledgment

I would like to thank John Wilson and Larry Townsend at NASA Langley for supporting and Dr. Barry Ganapol for directing this work. Dr. Ganapol also provided extensive comments while I planned and wrote the manuscript. I would also like to thank Maria Groshner and Grant Schmieder for time spent editing the final draft of the manuscript. For granting me a doctoral degree based on this manuscript, I would like to thank my committee members: Dr. William Dallas, Dr. William Filippone, Dr. David Hetrick, Dr. Morris Farr, and my dissertation director Dr. Barry Ganapol. Without these people, this research and manuscript would not exist.

Dedication

This dissertation and my entire scholastic career is dedicated to Maria Groshner, my partner in life. She put up with living apart for four and a half years while I attended graduate school. I can never show her how much that means to me.

Table of Contents

List of Illustrations

LIST OF TABLES

ABSTRACT

Transport of low energy neutrons associated with the galactic cosmic ray cascade is analyzed in this dissertation. A benchmark quality analytical algorithm is demonstrated for use with BRYNTRN, a computer program written by the High Energy Physics Division of NASA Langley Research Center, which is used to design and analyze shielding against the radiation created by the cascade. BRYNTRN uses numerical methods to solve the integral transport equations for baryons with the straight-ahead approximation, and numerical and empirical methods to generate the interaction probabilities. The straight-ahead approximation is adequate for charged particles, but not for neutrons. As NASA Langley improves BRYNTRN to include low energy neutrons, a benchmark quality solution is needed for comparison. The neutron transport algorithm demonstrated in this dissertation uses the closed-form Green's function solution to the galactic cosmic ray cascade transport equations to generate a source of neutrons. A basis function expansion for finite heterogeneous and semi-infinite homogeneous slabs with multiple energy groups and isotropic scattering is used to generate neutron fluxes resulting from the cascade. This method, called the F_N method, is used to solve the neutral particle linear Boltzmann transport equation. As a demonstration of the algorithm coded in the programs MGSLAB and MGSEMI, neutron and ion fluxes are shown for a beam of fluorine ions at 1000 MeV per nucleon incident on semi-infinite and

finite aluminum slabs. Also, to demonstrate that the shielding effectiveness against the radiation from the galactic cosmic ray cascade is not directly proportional to shield thickness, a graph of transmitted total neutron scalar flux versus slab thickness is shown. A simple model based on the nuclear liquid drop assumption is used to generate cross sections for the galactic cosmic ray cascade. The ENDF/B V database is used to generate the total and scattering cross sections for neutrons in aluminum. As an external verification, the results from MGSLAB and MGSEMI were compared to ANISN/PC, a routinely used neutron transport code, showing excellent agreement. In an application to an aluminum shield, the F_N method seems to generate reasonable results.

CHAPTER 1

INTRODUCTION

The advance of man and machines into space presents concerns about damage caused by radiation. This damage can disrupt electronic and biological systems to the point of failure. To protect against radiation damage, three mechanisms are available: distance, time, and shielding. Providing distance between the radiation source and the systems in a space environment is expensive because of size and weight limitations. Time considerations are not applicable because the spacecraft is exposed continuously to radiation sources. Therefore shielding must be used as the primary protection mechanism.

The radiation of concern in the space environment is highly energetic (billions of electron volts per nucleon) heavy ions and their secondary radiation. The primary ions originate from deep space sources or from our sun and are called galactic cosmic rays. The secondary radiations are fragments resulting from collisions of galactic cosmic rays with the material used to shield the systems in question. As these fragments collide with shield material, smaller fragments are created. Eventually, the fragments generated are neutrons and protons. The resultant radiation shower created by this phenomenon is called the galactic cosmic ray cascade. The prediction of the radiation dose resulting from this source

is very important for the proper design of shields for occupants and electronic components.

The nuclear power industry uses mass to shield systems. This mass attenuates particles by multiple scattering collisions or by absorption. The particles being shielded usually do not fragment and create a secondary radiation shower. Using current nuclear power industry shield designs, large quantities of mass would be placed into orbit which is expensive and time consuming. To reduce mass in a spacecraft, the shielding used for galactic cosmic rays must perform other tasks, such as being part of a pressure vessel, a micro-meteor shield, or a structural component. A spacecraft's less massive shielding must not only shield the internal systems from galactic cosmic rays, it must perform its other design tasks without creating a secondary radiation field that is worse than the original radiation field it was meant to shield.

Through various efforts, personnel at the High Energy Physics division of the NASA Langley Research Center have developed a computational algorithm which employs numerical methods and various empirical and analytical nuclear physics computations to predict the radiation dose from the galactic cosmic ray cascade. The transport model used in this algorithm, while being realistic for charged particles, is not realistic for low energy neutrons. The work presented in this dissertation addresses the neutron problem by coupling an analytical solution to the galactic cosmic ray cascade with an algorithm that treats low energy

neutrons realistically.

1.1 Motivation

Various solution methodologies are available to predict the radiation dose from the galactic cosmic ray cascade. The computer program that NASA has created is called BRYNTRN (Reference [1]). It is a compromise between computational accuracy and ease of use in design tasks. The use of the Monte Carlo method or perturbation theory to design shielding can be highly accurate at the expense of long turn-around times and extensive computational resources. An S_N based deterministic method utilizing SMART scattering (References [2] and [3]) could be used to solve the problem in one, two, or three dimensions. While being faster than the Monte Carlo method and almost as accurate, it still consumes large amounts of computer resources. Resource usage could be reduced by limiting the number of particles treated and the number of dimensions. Of course, a reduction in utility and accuracy is also incurred. The numerical solution method employed by BRYNTRN using the integral transport equation requires a small fraction of the computational resources needed by Monte Carlo and is comparable to the S_N method. Unfortunately, the physics approximations for neutrons reduce the applicability of the results in comparison to the other methods. In addition, verification of the BRYNTRN program, using a quality benchmark, is required to determine the accuracy of the dose calculation.

The BRYNTRN program numerically solves a set of coupled integral

transport equations for the initial ion distribution and each subsequent fragment distribution created (including protons and neutrons) in energy and space to determine dose rates. The interaction and particle generation probabilities are determined from analytical and empirical nuclear physics calculations. The results for relatively low energy (100 to 400 MeV) neutrons and protons on tissue agrees well with various studies using three dimensional Monte Carlo codes (References [4] and [5]), but with more efficient use of computer resources.

To verify the numerical solution technique used in BRYNTRN, a closed-form analytical solution to the galactic cosmic ray cascade equations was developed in Reference [6] and used as a benchmark. The two methods generated virtually identical results over a wide range of input parameters. This verified the solution technique, but not the physics models on which they were based. To continue the development process, the models used in BRYNTRN must be expanded to encompass more realistic physics. To verify these new models, new benchmarks must be developed which is one purpose of the effort.

The current BRYNTRN model treats neutrons as monoenergetic and monodirectional; therefore, they are not included in the overall dose calculation. In this dissertation, the closed-form analytical solution to the galactic cosmic ray cascade is coupled to an analytical neutral particle transport solver to generate a benchmark quality analytical solution to the cascade that includes a multiple energy group (multigroup) and angular dependent neutron description. With this

new algorithm as a benchmark, a better neutron model can be introduced into BRYNTRN, tested, and verified. This will allow neutrons to more easily be included in the overall dose calculation.

1.2 Background

Radiation is very damaging to the systems of a spacecraft. Radiation damage is the destruction of the structure of system components by energetic particles. An extensive effort has been expended in formulating techniques to predict the damage caused by radiation, called dose, in various situations encountered in space. These dose predictions allow the design and building of shields to protect systems that are sensitive to radiation.

Analysis techniques for solving shielding problems are widespread in the nuclear industry; however, only neutrons of no more than 20 MeV, alpha particles, protons, beta particles, and gamma rays have been studied in great detail. Fission fragments in nuclear reactors, which are heavier and more energetic than the above particles, are assumed to be confined to the nuclear fuel under normal operating scenarios. Fission fragment behavior is closer to the situation addressed in this dissertation than the other particles mentioned above, but the analysis techniques are almost entirely empirical. The main issue regarding fission fragment behavior centers on how long a fuel pellet can be exposed in a reactor before damage is extensive enough to warrant concern. The industry estimates the problem of fission fragment damage to the fuel pellet by using the integrated exposure, or

burnup, of the fuel pellet as a basis to measure other performance parameters. This large body of knowledge is of little use in generating a benchmark quality solution that contains the necessary detail for the galactic cosmic ray cascade.

Since prior knowledge about charged particle interaction with matter cannot be used and built upon, a first principles approach is required to construct models that can be used to generate the necessary shield design. Experience has shown that the linear Boltzmann particle transport equation (hereafter, referred to as the Boltzmann equation) can be used as an approximate mathematical model for most problems concerning particle interactions. The full Boltzmann equation is difficult, if not impossible, to solve analytically. To create a tractable mathematical problem, various physical approximations and restrictions are required to simplify the full Boltzmann formulation. Previous work on the galactic cosmic ray cascade has shown that the Boltzmann equation without angular deflection is appropriate for high energy, heavy ion and subsequent proton fluxes (References [7], [8], and [9]).

1.3 Specific Objectives

As indicated above, the current models used in BRYNTRN should be expanded to include energy and angular dependent neutron distributions because the straight-ahead approximation, no angular deflection, does not accurately describe neutron motion in general. This is accomplished by coupling an existing analytical solution to the galactic cosmic ray cascade to an analytical neutral

particle transport solution. Two geometries are utilized in the neutral particle transport method: homogeneous semi-infinite and heterogeneous finite slabs. Both geometries are used to solve the galactic cosmic ray cascade problem. Homogeneous finite slabs can be used because the straight-ahead approximation does not allow the back-propagation of information about a boundary. The particles incident on a slab travel straight into the slab, but are not allowed to scatter, so they never travel back towards the slab boundary where they entered. Therefore, the particles never detect a boundary until they cross it, then they never re-cross that boundary.

The closed-form analytical solution to the galactic cosmic ray cascade is determined by applying the Laplace transform to the appropriate Boltzmann equations. A set of ordinary, first order differential equations is generated and solved. Using a partial fraction expansion for the resultant solution, the inverse Laplace transform can be performed analytically. This determines the number, position, and energy of all the ions in transport media. To determine the number, position, and energy of the neutrons created, the Boltzmann equation is solved for neutrons without considering their motion in space and energy. The result is used in the source for the neutral particle algorithm.

The neutral particle Boltzmann transport equation for one-dimensional heterogeneous finite and homogeneous semi-infinite media with multiple energy groups and isotropic down scatter is used as the model for the neutrons resulting

from the galactic cosmic ray cascade. This formulation contains an isotropic distributed neutral particle source. Since the neutron source described above is monodirectional, the collision operator from the Boltzmann equation is applied to the monodirectional source to create an isotropic source. The Boltzmann equation is transformed into two singular integral equations obtained by essentially taking the Laplace transform with respect to both the positive and negative directions and restricting the complex transform variable to be on the cut along the real axis. From the definition of a principle value of a Cauchy type integral, a set of Fredholm integral equations and constraints follow. These equations are solved using the standard method of expanding the solution in basis functions (Reference [10]) originally developed by C. E. Siewert in References [11] through [14]. To produce an answer relatively free from truncation error, a post processor based on integral transport theory provides the ultimate angular fluxes.

The neutral particle transport algorithm can be decoupled from the galactic cosmic ray cascade source to provide a general benchmark quality neutral particle solution algorithm. A beam or isotropic source incident on the left face of the slab or a distributed source is available for heterogeneous finite or homogeneous semi-infinite slabs.

The results generated by the neutral particle transport programs are angular and scalar fluxes. When the programs are in the galactic cosmic ray cascade source mode, ion fluxes and neutron source values are generated. This

information is presented in printable data files and data files that can be used to generate two-dimensional and three-dimensional plots.

In Chapter 2, the physical theory and the associated mathematical models are described. Once the mathematical models have been developed, the numerical methods used to solve the model equations are described in Chapter 3. Since the neutral particle transport program has been created for this dissertation, it is verified as described in Chapter 4. Once the program is verified, it is applied to the galactic cosmic ray cascade, and the results are discussed in Chapter 5. Concluding remarks and observations are contained in Chapter 6. Details of the derivation for the analytical neutron transport model can be found in Appendix A. A user's manual for the programs is found in Appendix B.

CHAPTER 2

THEORY

The galactic cosmic ray cascade is a complicated particle interaction that can be treated using classical physics. This chapter outlines physical and mathematical arguments required to simplify the problem so it can be solved using analytical techniques. To perform this task, a physical model is described. This physical model is then transformed into a mathematical model.

The physical model details the interactions between the incident ion and the target material. Because of its speed, the ion is treated as a randomly configured mass of neutrons and protons traveling in a straight line. From the ion point of view, the target material is an evenly distributed proton and electron mass with distinct interaction centers. The evenly distributed mass acts continuously to slow the ion down though electrostatic interactions. Eventually, the ion slows and stops or encounters an interaction center and fragments creating smaller ions. The fragmenting continues until protons and neutrons are created. The protons act like the ions and eventually slow down and stop. The neutrons interact with the target material through scattering and absorption.

The mathematical model used to represent the physical model is based on classical statistical mechanics through the linear Boltzmann particle transport

equation. This imposes physical and mathematical requirements on the solution; however, the assumptions required to use this equation generally exclude quantum mechanical and single particle effects through using a statistically large number of classical point particles. These assumptions do not effect the physical model enough to warrant concern.

This chapter details the physical and mathematical models plus solution methods for the mathematical model equations. Once a solution method exists, numerical techniques can be used to generate numerical values which must then be verified.

2.1 Physical Models

The physical models required to describe this problem in a detailed manner do not represent the physics of the entire problem, but describe the physics sufficiently well to generate useful results. Definitions of various entities are needed to establish a basis for building a physical model. There are standard assumptions associated with the statistical, non-relativistic Boltzmann equation solutions which are described in detail and justified in Reference [15], Section 1.4. The first assumption is that all particles are treated as point particles; that is, a particle is completely described by its position and momentum. Spatial and temporal scales of the particles are sufficiently large to exclude quantum mechanical effects. Large numbers of each particle are present so deviations from the expectation value of the number densities can be ignored. The transport medium (target) does not

change on time scales of importance to particle transport. The density of particles relative to the density of the medium is small so that particle-particle interactions can be neglected.

2.1.1 Galactic Cosmic Ray Interaction

This model represents the interaction of heavy, high energy ions (galactic cosmic rays) with a shield or target material. The two modes of interaction considered are ions having coulombic collisions with target nuclei and slowing down, and ions colliding by direct impact with target nuclei creating nuclear fragments. Other modes of interaction exist and are occurring in galactic cosmic ray interactions with nuclei, but these are less significant and ignored in this treatment to reduce the complexity of the mathematical model. Detailed definitions of these two interactions are needed prior to generating mathematical models.

As a heavy fast ion travels through matter, it loses energy by interacting with the matter through electronic excitation. This excitation is caused by the protons of the ion interacting with the protons and electrons of the target nuclei. In this process, energy and momentum are transferred to the nuclei from the ion by the electrostatic forces between the ion and the nuclei. This results in the ion slowing down and losing energy with each interaction. For this model, the gain in energy by the target nuclei is ignored. Since the target nuclei surround the ion, the media is considered continuous, so the slowing down process is considered

continuous. The ion is traveling at great speeds, so its direction is not changed substantially by the small pushes and pulls of the surrounding target nuclei. Therefore, the ion path is assumed to be a straight line.

If the ion trajectory intersects a target nucleus, then a direct impact collision occurs called an abrasive collision. The result of an abrasive collision is fragmentation of the ion into other nuclear particles in a statistically random manner while conserving charge, energy, and momentum. To reduce the complexity of the model, the fragmentation of the target nuclei is ignored.

These definitions can be restated by adding physical assumptions to the original assumptions required for the Boltzmann equation. Because the target material protons do not change the direction of the ions and fragments, the straight-ahead approximation is used to model the particle motion. Energy is lost by the ions in a continuous manner so the continuous slowing down approximation is used. All interactions are statistically random while conserving charge, energy, and momentum. Fragmentation and energy gain of the target nucleus is neglected. From these assumptions and approximations, an appropriate mathematical interaction model can be formed.

2.1.2 Neutral Particle Transport

This model represents the interactions of neutrons with the target material. Since there is no coulombic charge associated with the neutron, only direct interactions are modeled. These interactions are either scattering collisions or

absorptions. The probability of each depends on the target material and the energy of the neutron. The F_N method, a robust mathematical and computational solution technique, is chosen to solve the neutron-Boltzmann transport equation for one-dimensional heterogeneous finite and homogeneous semi-infinite media with multiple energy groups and isotropic down scatter. An isotropic source is used to couple this model to the galactic cosmic ray cascade model.

2.2 Mathematical Formulation

The previous section described the physical models that require translation into a mathematical formulation. From the physical assumptions outlined, a statistical mechanics approach is taken. Therefore, a particular form of the Boltzmann equation is used for each model. This equation was originally used to describe the behavior of dilute gases; however, with appropriate modifications, it can be used to describe the behavior of dilute charged and neutral particles interacting with an appropriate medium. Appendix A describes the derivation of the Boltzmann equation for the F_N method.

2.2.1 Boltzmann Equation

There are various ways to derive the Boltzmann equation. The most fundamental is a physically based heuristic method (References [16] and [15]). This involves describing the various physical interactions and movements of particles in an infinitesimal phase volume. The Boltzmann equation can also be derived

directly from the statistical mechanical Liouville Equation (Reference [17]). The result of these derivations including only scattering and absorption interactions is

$$\left[\frac{1}{v}\frac{\partial}{\partial t} + \mathbf{\Omega}\cdot\nabla_{\mathbf{r}} + \mathbf{a}\cdot\nabla_{\mathbf{v}} + \sigma(\mathbf{r},\mathrm{E})\right]\Phi(\mathbf{r},\mathbf{\Omega},\mathrm{E},t) =$$
$$= \int_0^\infty \mathrm{dE}' \int_{4\pi} \mathrm{d}\mathbf{\Omega}'\,\sigma(\mathbf{r},\mathrm{E}')\,\mathrm{f}(\mathbf{r};\mathbf{\Omega}',\mathrm{E}'\rightarrow\mathbf{\Omega},\mathrm{E})\,\Phi(\mathbf{r},\mathbf{\Omega}',\mathrm{E}',t) + \qquad (2.1)$$
$$+ \mathrm{Q}(\mathbf{r},\mathbf{\Omega},\mathrm{E},t),$$

where,

$\mathbf{v}$ - Particle velocity,

v - Particle speed = $|\mathbf{v}|$,

$\mathbf{a}$ - *External force* term acting on the particle = $\frac{\mathbf{F}_{ext}}{mv}$, where, m is the particle mass,

$\mathbf{r}$ - Position vector (three components),

$\mathbf{\Omega}$ - Direction unit vector (two components) from the particle momentum $= \frac{\mathbf{p}}{mv}$, where, $\mathbf{p}$ is the particle momentum,

E - Particle kinetic energy = $\frac{1}{2}mv^2$,

t - Time,

$\sigma(\mathbf{r},\mathrm{E})$ - Total interaction probability at position $\mathbf{r}$ and energy E per particle length of travel,

$\Phi(\mathbf{r},\mathbf{\Omega},\mathrm{E},t)$ - Particle angular flux $[vN(\mathbf{r},\mathbf{\Omega},\mathrm{E},t)]$ which is the speed times the particle density in particles per phase volume,

$f(\mathbf{r}; \Omega', E' \rightarrow \Omega, E)d\Omega dE$ - Probability density for particle transfer from Ω' and E' to Ω and E in $d\Omega$ and dE,

$Q(\mathbf{r}, \Omega, E, t)$ - External particle sources.

To determine a unique solution to this equation, initial and boundary conditions are required. The existence and uniqueness of a solution to the Boltzmann equation are not discussed here, but Reference [18] gives various proofs for the existence and uniqueness of a solution. A general, analytical solution to equation (2.1) at this point is impossible to obtain; however, the physical model is restrictive in various respects to allow simplifications to be made to the Boltzmann equation allowing a solution. A balance is struck between the physical restrictions and the mathematical simplifications in order to maintain a worthwhile problem relating to spacecraft shielding.

2.2.2 Galactic Cosmic Rays

As already indicated, the Boltzmann equation will be adapted to describe the galactic ray cascade by applying assumptions and approximations to reduce its complexity. If steady state conditions, straight-ahead motion, continuous slowing down, and multiple species considerations are assumed, then equation (2.1) reduces to the following set of equations for each ion species of charge number j

$$\left[\frac{\partial}{\partial \tau} - \frac{\partial}{\partial E} S_j(E) + \sigma_j\right] \psi_j(\tau, E) = \sum_{k=j+1}^{J} M_{j,k}\, \sigma_k\, \psi_k(\tau, E), \qquad (2.2a)$$

with boundary conditions of

$$\psi_j(0, \mathrm{E}) = f_j(\mathrm{E}), \tag{2.2b}$$

where,

τ - Optical path length in grams per square centimeter,

j - Charge number, $0, \ldots, J$, where J is the charge number of the largest ion,

$\mathrm{S}_j(\mathrm{E})$ - Stopping power associated with ion j,

σ_j - Total interaction cross section for ion j,

$\psi_j(\tau, \mathrm{E})$ - Particle flux for ion j,

$\mathrm{M}_{j,k}$ - Multiplicity, or the probability of creating fragments of ion j from an abrasive collision of ion k,

$f_j(\mathrm{E})$ - A known flux at the slab boundary as a function energy for ion j.

The second term in the transport operator, $\frac{\partial}{\partial \mathrm{E}}\mathrm{S}_j(\mathrm{E})$, is from the continuous slowing down approximation with the external force term in the original transport equation, equation (2.1). The external force being the electrostatic force between the target material's protons and electrons and the ion's protons. The stopping power of ion j is inside the differential, so a functional form of this term must be

found to continue the derivation. It can be related through a scaling constant to the stopping power of the proton, a well studied quantity,

$$S_j(E) = \overline{\nu}_j S_P(E), \tag{2.3}$$

where, $\overline{\nu}_j$ is the scaling constant $\frac{Z_j^2}{A_j}$ (Reference [19]), and $S_P(E)$ is the stopping power of a proton as a function of energy. This approximation treats the incoming ion and target material as a sea of protons interacting separately instead of as discrete bundled atoms. The ion energies are large enough so that this approximation is valid.

2.2.2.1 Transformation from Energy to Path Length. When equation (2.3) is introduced into equation (2.2a), the stopping power of the proton is still inside the partial derivative term. This is transformed by scaling the energy variable in terms of the stopping power of the proton. The resultant variable transformation is from the energy of the particle to the energy integrated path length of the particle in the medium. The path length is defined as the penetration distance of a proton of initial energy E_0 as it slows down to energy E

$$s \equiv s(E, E_0) = \int_E^{E_0} dE' \frac{1}{S_P(E')}. \tag{2.4}$$

After changing the variable from energy to path length, the resultant set of equations is

$$\left[\frac{\partial}{\partial \tau} - \overline{\nu}_j \frac{\partial}{\partial s} + \sigma_j\right] \psi_j(\tau, s) = \sum_{k=j+1}^{J} M_{j,k}\, \sigma_k\, \psi_k(\tau, s), \tag{2.5a}$$

with boundary conditions of

$$\psi_j(0,s) \;=\; f_j(s). \tag{2.5b}$$

The original energy dependent fluxes are obtained as follows

$$\psi_j(\tau,s) \;=\; \mathrm{S}_P(\mathrm{E})\;\psi_j(\tau,\mathrm{E}), \tag{2.5c}$$

and

$$f_j(s) \;=\; \mathrm{S}_P(\mathrm{E})\;f_j(\mathrm{E}). \tag{2.5d}$$

2.2.2.2 Green's Function Solution to the Galactic Cosmic Ray Cascade Equations. General solutions to this set of equations for various boundary conditions can be found in Reference [6]; however, for clarity, a short synopsis of the Green's function solution is given here. To generate an impulse forcing function, the boundary conditions are set to $f_j(s) = \delta(s)\delta_{jJ}$. The Laplace transform of equations (2.5) is taken with respect to s and the resultant set of ordinary differential equations is solved analytically. The coefficients in the solution are dependent on the complex variable used in the transform. A recursion relation exists that can determine these coefficients (Reference [20]). Using a partial fraction expansion, the inverse Laplace transform can be determined analytically. In order to simplify the equation notation, all partial fraction coefficients are included even though some of the coefficients are identical or zero. Using an analytical mathematical argument, these coefficients can be identified.

The resultant equations determine the flux of any ion at any position and path length

$$\psi_{J-l}(\tau,s) = \sum_{r=1}^{N_l} e^{-\frac{a_r}{b_r}s-(\sigma_{J-i_1}-\frac{a_r}{b_r}\overline{\nu}_{J-i_1})\tau}\times \\ \times\ \tilde{\mathrm{Y}}_{i_1,r}^{J-l}\left[\theta(s-\overline{\nu}_{J-i_1}\tau)-\theta(s-\overline{\nu}_{J-i_2}\tau)\right], \tag{2.6}$$

where,

N_l - The number of partial fraction terms for the $J-l$ equation is $l(l+1)/2$,

a_r - $\sigma_{m(r)}-\sigma_{n(r)}$,

b_r - $\overline{\nu}_{m(r)}-\overline{\nu}_{n(r)}$,

$m(r)$ - Index: $J-l$,

$n(r)$ - Index: $J-k$ where $k=0,\ldots,l-1$,

i_1 - Index: k where $k=0,\ldots,l-1$,

i_2 - Index: l,

$\tilde{\mathrm{Y}}_{i_1,r}^{J-l}$ - Modified partial fraction coefficients.

For $1\le r\le N_{l-1}$, the recursion relation for the modified partial fraction coefficients are

$$\tilde{\mathrm{Y}}_{i_1,r}^{J-l} = \hat{X}_{1,i_1,r}^{J-l}\sum_{k=J-l+1}^{J-i_1}\mathrm{M}_{J-l,k}\sigma_k\tilde{Y}_{i_1,r}^{k}\theta\left(N_{J-k}-r\right), \tag{2.7a}$$

where,

$$\hat{X}_{1,i_1,r}^{J-l} \equiv -\left(\frac{b_{J-l,J-i_1}}{a_{J-l,J-i_1}b_r-a_rb_{J-l,J-i_1}}\right). \tag{2.7b}$$

For $N_{l-1}+1 \leq r \leq N_l$, the recursion relation is

$$\tilde{Y}^{J-l}_{i_1,r} = \sum_{r'=1}^{N_{l-1}} \left(\frac{b_{J-l,J-i}}{b_{r'}} \right) P_{r'} \tilde{Y}^{J-l}_{i_1,r'} + \mathrm{M}_{J-l,J} \sigma_J \delta_{i,0}, \tag{2.8}$$

where, $P_{r'}$ selects only the non-zero values of $\tilde{Y}^{J-l}_{i_1,r'}$. With this Green's function solution, all other distribution functions for $f_j(s)$ can be obtained with the appropriate integration over the Green's function.

2.2.3 Neutral Particle Transport

The Boltzmann equation is simplified mathematically in Appendix Section A.1 to describe the physical model for neutral particle transport. Steady state conditions, planer geometry, and isotropic scattering media are assumed. The source is an isotropically distributed source, and the particles cannot gain energy from scattering. The Boltzmann equation is then reduced to the heterogeneous slab, multigroup, neutral particle transport equation for group g, where $g = 1, 2, \ldots, G$

$$\left[\mu \frac{\partial}{\partial x} + \sigma^{\mathrm{i}}_g \right] \phi_g(x,\mu) = \frac{1}{2} \sum_{g'=1}^{g} \sigma^{\mathrm{i}}_{g' \to g} \int_{-1}^{+1} \mathrm{d}\mu' \, \phi_{g'}(x,\mu') + \frac{1}{2} \mathrm{S}^{\mathrm{i}}_g(x), \tag{2.9a}$$

with a set of boundary conditions for each slab

$$\phi_g(x_{i-1},\mu) = \mathrm{F}^{g,\mathrm{i}}_{\mathrm{L}}(\mu), \quad \text{and} \quad \phi_g(x_i,-\mu) = \mathrm{F}^{g,\mathrm{i}}_{\mathrm{R}}(\mu), \quad \text{for } \mu > 0, \tag{2.9b}$$

where,

i - Slab number, $1, 2, \ldots,$ NS, where NS is the total number of slabs,

μ - Angular direction $= \Omega \cdot \hat{x}$,

$\phi_g(x,\mu)$ - Steady state group flux in one dimension $= \int_{E_g}^{E_{g-1}} dE\ \Phi(\mathbf{r},\Omega,E,t)$,

σ_g^i - Steady state group constant in one dimension $= \frac{\int_{E_g}^{E_{g-1}} dE\ \sigma(\mathbf{r},E)\Phi(\mathbf{r},\Omega,E,t)}{\int_{E_g}^{E_{g-1}} dE\ \Phi(\mathbf{r},\Omega,E,t)}$,

$\sigma_{g'\to g}^i$ - Steady state group transfer cross section in one dimension,

$S_g^i(x)$ - Steady state distributed group source in one dimension,

x_{i-1} - Position of left boundary for slab i,

x_i - Position of right boundary for slab i,

$F_L^{g,i}(\mu)$ - Known general function of μ in positive half range $(0 \le \mu < 1)$,

$F_R^{g,i}(\mu)$ - Known general function of μ in negative half range $(-1 \le \mu < 0)$.

2.2.3.1 Singular Integral Equation Formulation. Equation (2.9a) can be solved in many different ways. The angular and spatial variables can be discretized and a finite difference formulation substituted for the derivative terms to create the S_N method. The angular dependance in the flux and source functions can be expanded in spherical harmonics to create the P_N method. Analytical methods can be used to solve for the flux. If the medium is infinite in extent in all dimensions, then a Fourier transform can be used to solve for the flux. If two semi-infinite mediums meet at the boundary, then a Laplace transform can be used to solve for the flux. The method of choice for this application is based on an integral form of equation (2.9a). To create a set of integral equations, equations (2.9) are

analytically continued into the complex plane. Through the Plemelj relations, the integrals are then evaluated on the real axis. This is accomplished as shown below with details shown in Appendix Section A.2

Using equation (2.9a) μ is replaced with $-\mu$ and then multiplied by $e^{-\frac{\sigma_g^i x}{s}}$. The result is integrated over x on $[z_1, z_2]$ to obtain

$$\frac{s\mu}{\mu - s} B_g(\mu, s) \; - \; \sigma_g^i \int_{z_1}^{z_2} \mathrm{d}x \, e^{-\frac{\sigma_g^i x}{s}} \phi_g(x, -\mu) \; = \\ = \; \sum_{g'=1}^{g} \frac{\sigma_{g'}^i}{2} \; \frac{s}{\mu - s} \; \rho_{gg'}^*(s) \; + \; \frac{1}{2} \frac{s}{\mu - s} \; \mathrm{S}_g^*(s, z_1, z_2), \tag{2.10a}$$

with,

$$B_g(\mu, s) \; = \; e^{-\frac{\sigma_g^i z_1}{s}} \phi_g(z_1, -\mu) - e^{-\frac{\sigma_g^i z_2}{s}} \phi_g(z_2, -\mu), \tag{2.10b}$$

$$\rho_{gg'}^*(s) \; = \; \int_{z_1}^{z_2} \mathrm{d}x \, e^{-\frac{\sigma_g^i x}{s}} \int_{-1}^{+1} \mathrm{d}\mu' \, \phi_{g'}(x, -\mu'), \tag{2.10c}$$

$$\mathrm{S}_g^*(s, z_1, z_2) \; = \; \int_{z_1}^{z_2} \mathrm{d}x \, e^{-\frac{\sigma_g^i x}{s}} \mathrm{S}_g^i(x). \tag{2.10d}$$

Next, μ is integrated on $[-1, +1]$ to obtain

$$\int_{-1}^{+1} \mathrm{d}\mu \, \frac{\mu}{\mu - s} B_g(\mu, s) \; = \; \sigma_g^i \sum_{g'=1}^{g} \frac{\rho_{gg'}^*(s)}{s} \Lambda_{g'g}(s) + \\ + \; \mathrm{L}(s) \mathrm{S}_g^*(s, z_1, z_2), \tag{2.11a}$$

where,

$$\Lambda_{g'g}(s) \; = \; \delta_{g'g} \; + \; \frac{s\sigma_{g' \to g}^i}{\sigma_g^i} \mathrm{L}(s), \tag{2.11b}$$

$$\mathrm{L}(s) \; = \; \frac{1}{2} \int_{-1}^{+1} \mathrm{d}\mu \, \frac{1}{\mu - s} \; = \; \frac{1}{2} \ln \left(\frac{s+1}{s-1} \right), \tag{2.11c}$$

$$\delta_{g'g} \; = \; \begin{cases} 1 & g' = g \\ 0 & g' \neq g \end{cases}. \tag{2.11d}$$

Equation (2.11a) is multiplied by $e^{\frac{\sigma_g^i x_1}{s}}$ to obtain

$$\int_{-1}^{+1} d\mu \, \frac{\mu}{\mu - s} C_g(\mu, s) = \sigma_g^i \sum_{g'=1}^{g} I_{gg'}^{*i}(s, z_1, z_2) \Lambda_{g'g}(s) + \\ + L(s) S_g^*(s, z_1, z_2) e^{\frac{\sigma_g^i x_1}{s}}, \tag{2.12a}$$

where,

$$C_g(\mu, s) = e^{\frac{\sigma_g^i x_1}{s}} B_g(\mu, s) \\ = \phi_g(z_1, -\mu) - e^{-\frac{\sigma_g^i (x_2 - x_1)}{s}} \phi_g(z_2, -\mu), \tag{2.12b}$$

$$I_{gg'}^{*i}(s, z_1, z_2) = \frac{e^{\frac{\sigma_g^i x_1}{s}}}{s} \rho_{gg'}^*(s) \\ = \frac{1}{s} \int_{z_1}^{z_2} dx \, e^{-\frac{\sigma_g^i (x - z_1)}{s}} \int_{-1}^{+1} d\mu \, \phi_{g'}(x, -\mu). \tag{2.12c}$$

To form a second equation, the signs of s and μ in equation (2.10a) are changed and the equation is multiplied by $e^{-\frac{\sigma_g^i z_2}{s}}$ to obtain

$$\int_{-1}^{+1} d\mu \, \frac{\mu}{\mu - s} D_g(\mu, s) = \sigma_g^i \sum_{g'=1}^{g} J_{gg'}^{*i}(s, z_1, z_2) \Lambda_{g'g}(s) + \\ + L(s) S_g^*(-s, z_1, z_2) e^{-\frac{\sigma_g^i z_2}{s}}, \tag{2.13a}$$

where,

$$D_g(\mu, s) = -e^{-\frac{\sigma_g^i z_2}{s}} B_g(-\mu, -s) \\ = \phi_g(z_2, \mu) - e^{-\frac{\sigma_g^i (z_2 - z_1)}{s}} \phi_g(z_1, \mu), \tag{2.13b}$$

$$J_{gg'}^{*i}(s, z_1, z_2) = \frac{e^{-\frac{\sigma_g^i z_2}{s}}}{s} \rho_{gg'}^*(s) \\ = \frac{1}{s} \int_{z_1}^{z_2} dx \, e^{-\frac{\sigma_g^i (z_2 - x)}{s}} \int_{-1}^{+1} d\mu \, \phi_{g'}(x, -\mu). \tag{2.13c}$$

By defining ν_0^g to be the positive root of the infinite medium dispersion relation, $\Lambda_{gg}(s)$, the integral equations, when evaluated at ν_0^g, become a set of

constraints

$$\int_{-1}^{+1} \mathrm{d}\mu \, \frac{\mu}{\mu - \nu_0^g} C_g(\mu, \nu_0^g) \;=\; -\frac{\sigma_g^i}{\nu_0^g \sigma_{g\to g}^i} \mathrm{S}_g^*(\nu_0^g, z_1, z_2) e^{\frac{\sigma_g^i z_1}{\nu_0^g}}, \tag{2.14a}$$

$$\int_{-1}^{+1} \mathrm{d}\mu \, \frac{\mu}{\mu - \nu_0^g} D_g(\mu, \nu_0^g) \;=\; -\frac{\sigma_g^i}{\nu_0^g \sigma_{g\to g}^i} \mathrm{S}_g^*(-\nu_0^g, z_1, z_2) e^{-\frac{\sigma_g^i z_2}{\nu_0^g}}. \tag{2.14b}$$

The above integrals are not singular because if $\frac{\sigma_{g\to g}^i}{\sigma_g^i} < 1$ then $|\nu_0^g| > 1$ and real (Reference [21]).

The integral terms in equations (2.12a) and (2.13a) are restricted to the real axis by use of the Plemelj relations (Reference [22])

$$\lim_{\epsilon \to 0} \frac{1}{\eta - (\nu \pm i\epsilon)} \;=\; \wp \left[\frac{1}{\eta - \nu} \right] \pm i\pi\delta(\eta - \nu). \tag{2.15a}$$

If the Plemelj relations are applied to this Cauchy type integral

$$\chi(s) = \int_{-1}^{+1} \mathrm{d}\eta \, \frac{f(\eta)}{\eta - s}, \tag{2.15b}$$

then, the result is

$$\lim_{\epsilon \to 0} \chi(\nu \pm i\epsilon) = \chi^{\pm}(\nu) = \fint_{-1}^{+1} \mathrm{d}\eta \, \frac{f(\eta)}{\eta - \nu} \pm i\pi f(\nu). \tag{2.15c}$$

All integration variables have been changed to η and $\nu \in [0, 1] \cup \nu_0^g$.

These rules are applied to the integral equations (2.12a) and (2.13a) to obtain

$$\begin{aligned} &\fint_{-1}^{+1} \mathrm{d}\eta \, \frac{\eta}{\eta - \nu} C_g(\eta, \nu) \;\pm\; i\pi\nu C_g(\nu, \nu) \;= \\ &\quad = \sigma_g^i \sum_{g'=1}^{g} \Lambda_{g'g}^{\pm}(\nu) \; \mathrm{I}_{gg'}^{*i}(\nu, z_1, z_2) \;+\; e^{\frac{\sigma_g^i z_1}{\nu}} \mathrm{S}_g^*(\nu, z_1, z_2) \mathrm{L}^{\pm}(\nu), \end{aligned} \tag{2.16a}$$

$$\begin{aligned} &\fint_{-1}^{+1} d\eta \, \frac{\eta}{\eta - \nu} D_g(\eta, \nu) \pm i\pi\nu D_g(\nu, \nu) = \\ &\quad = \sigma_g^i \sum_{g'=1}^{g} \Lambda_{g'g}^{\pm}(\nu) \, J_{gg'}^{*i}(\nu, z_1, z_2) + e^{-\frac{\sigma_g^i z_2}{\nu}} S_g^*(-\nu, z_1, z_2) L^{\pm}(\nu), \end{aligned} \tag{2.16b}$$

where,

$$L^{\pm}(\nu) = \frac{1}{2} \fint_{-1}^{+1} d\eta \, \frac{1}{\eta - \nu} \pm \frac{i\pi}{2} = \frac{1}{2} \ln \left| \frac{1 - \nu}{1 + \nu} \right| \pm \frac{i\pi}{2}, \tag{2.16c}$$

$$\Lambda_{g'g}^{\pm}(\nu) = \lambda_{g'g}(\nu) \pm \frac{i\pi\nu\sigma_{g' \to g}^i}{2\sigma_g^i}, \tag{2.16d}$$

$$\lambda_{g'g}(\nu) = \delta_{g'g} + \frac{\nu\sigma_{g' \to g}^i}{2\sigma_g^i} \fint_{-1}^{+1} d\eta \, \frac{1}{\eta - \nu} = \delta_{g'g} + \frac{\nu\sigma_{g' \to g}^i}{2\sigma_g^i} \ln \left| \frac{1 - \nu}{1 + \nu} \right|. \tag{2.16e}$$

Eliminating $I_{gg}^{*i}(\nu, z_1, z_2)$ and $J_{gg}^{*i}(\nu, z_1, z_2)$ by adding and subtracting the positive and negative branches of equations (2.16) to obtain

$$\begin{aligned} &\fint_{-1}^{+1} d\eta \, \frac{\eta}{\eta - \nu} C_g(\eta, \nu) - \frac{2\sigma_g^i}{\sigma_{g \to g}^i} \lambda_{gg}(\nu) C_g(\nu, \nu) = \\ &\quad = -\frac{\sigma_g^i e^{\frac{\sigma_g^i z_1}{\nu}}}{\nu\sigma_{g \to g}^i} S_g^*(\nu, z_1, z_2) + \frac{\sigma_{g \to g}^i}{\sigma_g^i} \sum_{g'=1}^{g-1} \sigma_{g' \to g}^i \, I_{gg'}^{*i}(\nu, z_1, z_2), \end{aligned} \tag{2.17a}$$

$$\begin{aligned} &\fint_{-1}^{+1} d\eta \, \frac{\eta}{\eta - \nu} D_g(\eta, \nu) - \frac{2\sigma_g^i}{\sigma_{g \to g}^i} \lambda_{gg}(\nu) D_g(\nu, \nu) = \\ &\quad = -\frac{\sigma_g^i e^{-\frac{\sigma_g^i z_2}{\nu}}}{\nu\sigma_{g \to g}^i} S_g^*(-\nu, z_1, z_2) + \frac{\sigma_{g \to g}^i}{\sigma_g^i} \sum_{g'=1}^{g-1} \sigma_{g' \to g}^i \, J_{gg'}^{*i}(\nu, z_1, z_2). \end{aligned} \tag{2.17b}$$

Rewriting the integral equations in terms of the fluxes and changing the

integration variables so that they are evaluated on the interval $[0,1]$ gives

$$\begin{aligned}
&\fint_0^1 d\eta\, \frac{\eta}{\eta-\nu}\phi_g(x_{i-1},-\eta) \;+\; \int_0^1 d\eta\, \frac{\eta}{\eta+\nu}\phi_g(x_{i-1},\eta) \;- \\
&\quad -e^{-\frac{\Delta_g^i}{\nu}}\left[\fint_0^1 d\eta\, \frac{\eta}{\eta-\nu}\phi_g(x_i,-\eta) + \int_0^1 d\eta\, \frac{\eta}{\eta+\nu}\phi_g(x_i,\eta)\right] - \\
&\quad -\frac{2\sigma_g^i}{\sigma_{g\to g}^i}\lambda_{gg}(\nu)\left[\phi_g(x_{i-1},-\nu) \;-\; \phi_g(x_i,-\nu)e^{-\frac{\Delta_g^i}{\nu}}\right] \;= \\
&= \;-\frac{\sigma_g^i}{\sigma_{g\to g}^i}\sum_{g'=1}^{g-1}\sigma_{g'\to g}^i \mathrm{I}_{gg'}^{*i}(\nu,x_{i-1},x_i) \;- \\
&\quad -\frac{\sigma_g^i e^{\frac{\sigma_g^i x_{i-1}}{\nu}}}{\nu\sigma_{g\to g}^i}\mathrm{S}_g^*(\nu,x_{i-1},x_i),
\end{aligned} \tag{2.18a}$$

$$\begin{aligned}
&\fint_0^1 d\eta\, \frac{\eta}{\eta-\nu}\phi_g(x_i,\eta) \;+\; \int_0^1 d\eta\, \frac{\eta}{\eta+\nu}\phi_g(x_i,-\eta) \;- \\
&\quad -e^{-\frac{\Delta_g^i}{\nu}}\left[\fint_0^1 d\eta\, \frac{\eta}{\eta-\nu}\phi_g(x_{i-1},\eta) + \int_0^1 d\eta\, \frac{\eta}{\eta+\nu}\phi_g(x_{i-1},-\eta)\right] - \\
&\quad -\frac{2\sigma_g^i}{\sigma_{g\to g}^i}\lambda_{gg}(\nu)\left[\phi_g(x_i,\nu) \;-\; \phi_g(x_{i-1},\nu)e^{-\frac{\Delta_g^i}{\nu}}\right] \;= \\
&= \;-\frac{\sigma_g^i}{\sigma_{g\to g}^i}\sum_{g'=1}^{g-1}\sigma_{g'\to g}^i \mathrm{J}_{gg'}^{*i}(\nu,x_{i-1},x_i) \;- \\
&\quad -\frac{\sigma_g^i e^{-\frac{\sigma_g^i x_i}{\nu}}}{\nu\sigma_{g\to g}^i}\mathrm{S}_g^*(-\nu,x_{i-1},x_i).
\end{aligned} \tag{2.18b}$$

where, z_1 and z_2 are defined at the slab boundaries, x_{i-1} and x_i, and Δ_g^i is defined as the dimensionless slab width $\sigma_g^i(x_i - x_{i-1})$. A similar set of integral equations are generated for the interior slab points as shown in Appendix Section A.4

2.2.3.2 The F_N Approximation. For the integral equations specified in the last section, various solution methods could be used to determine $\phi_g(x,\mu)$. The solution method chosen for this treatment is a basis function expansion. At the

slab boundaries, the basis function expansions are defined as

$$\phi_g(x_i,-\nu) \;=\; \mathrm{F}_{\mathrm{R}}^{g,i}(\nu)e^{-\frac{\Delta_g^i}{\nu}} \;+\; \frac{\sigma_{g\to g}^i}{2\sigma_g^i}\sum_{\alpha=0}^{N-1}\mathrm{a}_\alpha^{g,i}\psi_\alpha(\nu), \tag{2.19a}$$

and

$$\phi_g(x_{i-1},\nu) \;=\; \mathrm{F}_{\mathrm{L}}^{g,i}(\nu)e^{-\frac{\Delta_g^i}{\nu}} \;+\; \frac{\sigma_{g\to g}^i}{2\sigma_g^i}\sum_{\alpha=0}^{N-1}\mathrm{b}_\alpha^{g,i}\psi_\alpha(\nu). \tag{2.19b}$$

The basis function expansions for interior slab points are defined as

$$\phi_g(x_j,-\nu) \;=\; \mathrm{F}_{\mathrm{R}}^{g,i}(\nu)e^{-\frac{\sigma_g^i}{\nu}(x_i-x_j)} \;+\; \frac{\sigma_{g\to g}^i}{2\sigma_g^i}\sum_{\alpha=0}^{N-1}\mathrm{c}_\alpha^{g,j}\psi_\alpha(\nu), \tag{2.19c}$$

and

$$\phi_g(x_j,\nu) \;=\; \mathrm{F}_{\mathrm{L}}^{g,i}(\nu)e^{-\frac{\sigma_g^i}{\nu}(x_j-x_{i-1})} \;+\; \frac{\sigma_{g\to g}^i}{2\sigma_g^i}\sum_{\alpha=0}^{N-1}\mathrm{d}_\alpha^{g,j}\psi_\alpha(\nu), \tag{2.19d}$$

where,

x_i - Boundary slab points,

x_j - Interior slab points,

$\mathrm{a}_\alpha^{g,i}$ - Boundary expansion coefficients,

$\mathrm{b}_\alpha^{g,i}$ - Boundary expansion coefficients,

$\mathrm{c}_\alpha^{g,j}$ - Interior expansion coefficients,

$\mathrm{d}_\alpha^{g,j}$ - Interior expansion coefficients,

$\psi_\alpha(\nu)$ - Basis functions to be selected.

When the basis function expansions are substituted into the singular integral equations, after much algebra, a set of equations is generated that specify the relations between the expansion coefficients and the various source terms for the slab boundary points

$$\sum_{\alpha=0}^{N-1}\left[a_\alpha^{g,i}B_\alpha^g(\nu) + b_\alpha^{g,i}A_\alpha^g(\nu)e^{-\frac{\Delta_g^i}{\nu}}\right] = R1_g^i(\nu,x_{i-1}) + \\ + \frac{1}{\sigma_{g\to g}^i}T1_g^i(\nu,x_{i-1},x_i) + \frac{1}{\sigma_{g\to g}^i}S1_g^i(\nu,x_{i-1},x_i), \tag{2.20a}$$

$$\sum_{\alpha=0}^{N-1}\left[b_\alpha^{g,i}B_\alpha^g(\nu) + a_\alpha^{g,i}A_\alpha^g(\nu)e^{-\frac{\Delta_g^i}{\nu}}\right] = R2_g^i(\nu,x_i) + \\ + \frac{1}{\sigma_{g\to g}^i}T2_g^i(\nu,x_{i-1},x_i) + \frac{1}{\sigma_{g\to g}^i}S2_g^i(\nu,x_{i-1},x_i). \tag{2.20b}$$

For the interior, the integral equations become

$$\sum_{\alpha=0}^{N-1}\left[c_\alpha^{g,j}B_\alpha^g(\nu) - d_\alpha^{g,j}A_\alpha^g(\nu)\right] = R1_g^i(\nu,x_j) + \frac{1}{\sigma_{g\to g}^i}T1_g^i(\nu,x_j,x_i) + \\ + \frac{1}{\sigma_{g\to g}^i}S1_g^i(\nu,x_j,x_i) - e^{-\frac{\sigma_g^i}{\nu}(x_i-x)}\sum_{\alpha=0}^{N-1}b_\alpha^{g,i}A_\alpha^g(\nu), \tag{2.20c}$$

$$\sum_{\alpha=0}^{N-1}\left[d_\alpha^{g,j}B_\alpha^g(\nu) - c_\alpha^{g,j}A_\alpha^g(\nu)\right] = R2_g^i(\nu,x_j) + \frac{1}{\sigma_{g\to g}^i}T2_g^i(\nu,x_{i-1},x_j) + \\ + \frac{1}{\sigma_{g\to g}^i}S2_g^i(\nu,x_{i-1},x_j) - e^{-\frac{\sigma_g^i}{\nu}(x_j-x_{i-1})}\sum_{\alpha=0}^{N-1}a_\alpha^{g,i}A_\alpha^g(\nu), \tag{2.20d}$$

where,

$$A_\alpha^g(\nu) = \frac{\sigma_{g\to g}^i}{2\sigma_g^i}\int_0^1 d\eta\,\frac{\eta}{\eta+\nu}\psi_\alpha(\eta), \tag{2.21a}$$

$$B_\alpha^g(\nu) = \lambda_{gg}(\nu)\psi_\alpha(\nu) - \frac{\sigma_{g\to g}^i}{2\sigma_g^i}\int_0^1 d\eta\,\frac{\eta}{\eta-\nu}\psi_\alpha(\eta), \tag{2.21b}$$

with

$$\lambda_{gg}(\nu) = 1+\nu\,\frac{\sigma_{g\to g}^i}{2\sigma_g^i}\int_{-1}^{+1}d\eta\,\frac{1}{\eta-\nu} = 1+\nu\,\frac{\sigma_{g\to g}^i}{2\sigma_g^i}\ln\left|\frac{1-\nu}{1+\nu}\right|. \tag{2.21c}$$

The inhomogeneous boundary terms that specify the source from adjacent slabs and the boundary conditions are

$$\begin{aligned} \mathrm{R1}_g^i(\nu,x) \;=\; & \int_0^1 \mathrm{d}\eta \;\Big[\mathrm{F}_{\mathrm{R}}^{g,i}(\eta)\;\mathrm{C}(\sigma_g^i(x_i-x),\eta,\nu) + \\ & + e^{-\frac{\sigma_g^i}{\eta}(x-x_{i-1})}\;\mathrm{F}_{\mathrm{L}}^{g,i}(\eta)\;\mathrm{S}(\sigma_g^i(x_i-x),\eta,\nu)\Big], \end{aligned} \tag{2.22a}$$

$$\begin{aligned} \mathrm{R2}_g^i(\nu,x) \;=\; & \int_0^1 \mathrm{d}\eta \;\Big[\mathrm{F}_{\mathrm{L}}^{g,i}(\eta)\;\mathrm{C}(\sigma_g^i(x-x_{i-1}),\eta,\nu) + \\ & + e^{-\frac{\sigma_g^i}{\eta}(x_i-x)}\;\mathrm{F}_{\mathrm{R}}^{g,i}(\eta)\;\mathrm{S}(\sigma_g^i(x-x_{i-1},\eta,\nu)\Big], \end{aligned} \tag{2.22b}$$

where,

$$\mathrm{C}(\xi,\eta,\nu) \;=\; \begin{cases} \dfrac{\xi}{\nu^2}e^{-\xi/\nu} & \eta=\nu \\ \dfrac{e^{-\xi/\eta}\;-\;e^{-\xi/\nu}}{\eta-\nu} & \eta\neq\nu, \end{cases} \tag{2.22c}$$

$$\mathrm{S}(\xi,\eta,\nu) \;=\; \frac{1-e^{-\xi\frac{\nu\eta}{\eta+\nu}}}{\eta+\nu}, \tag{2.22d}$$

and x is defined as the slab boundary and interior points, or $x \in \{x_i, x_j\}$.

The down scatter terms that specify the source scattering from higher energy groups are

$$\mathrm{T1}_g^i(\nu,x,x_i) \;=\; \sigma_g^i \sum_{g'=1}^{g-1} \sigma_{g'\to g}^i\;\mathrm{I}_{gg'}^{*i}(\nu,x,x_i), \tag{2.23a}$$

and

$$\mathrm{T2}_g^i(\nu,x_{i-1},x) \;=\; \sigma_g^i \sum_{g'=1}^{g-1} \sigma_{g'\to g}^i\;\mathrm{J}_{gg'}^{*i}(\nu,x_{i-1},x). \tag{2.23b}$$

As shown in Appendix Section A.3.3, relationships for the integrals $\mathrm{I}_{gg'}^{*i}(\nu,x,x_i)$ and $\mathrm{J}_{gg'}^{*i}(\nu,x_{i-1},x)$ are derived for two ranges of the angular variable.

When these integrals are singular, $\mu = \frac{\sigma^i_{g'}}{\sigma^i_g}\xi = s_{gg'}\xi < 1$, then the relationships are

$$\sigma^i_{g'\to g'}\mathrm{I}^{*i}_{gg'}(\xi,x,x_i) = \frac{\sigma^i_{g'\to g'}}{\sigma^i_g}\sum_{\alpha=0}^{N-1}\mathcal{K}\psi_\alpha(s_{gg'}\xi) - \frac{1}{\sigma^i_g}\mathrm{S1}^i_{g'}(s_{gg'}\xi,x,x_i) - \\ - \sum_{g''=1}^{g'-1}\sigma^i_{g''\to g'}\mathrm{I}^{*i}_{gg''}(\xi,x,x_i), \tag{2.24a}$$

and

$$\sigma^i_{g'\to g'}\mathrm{J}^{*i}_{gg'}(\xi,x_{i-1},x) = \frac{\sigma^i_{g'\to g'}}{\sigma^i_g}\sum_{\alpha=0}^{N-1}\mathcal{F}\psi_\alpha(s_{gg'}\xi) - \frac{1}{\sigma^i_g}\mathrm{S2}^i_{g'}(s_{gg'}\xi,x_{i-1},x) - \\ - \sum_{g''=1}^{g'-1}\sigma^i_{g''\to g'}\mathrm{J}^{*i}_{gg''}(\xi,x_{i-1},x), \tag{2.24b}$$

where,

$$\mathcal{K} = \begin{cases} \mathrm{a}^{g',i}_\alpha & x = x_{i-1} \\ \mathrm{c}^{g',j}_\alpha & x \neq x_{i-1}, \end{cases} \qquad \mathcal{F} = \begin{cases} \mathrm{b}^{g',i}_\alpha & x = x_i \\ \mathrm{d}^{g',j}_\alpha & x \neq x_i. \end{cases} \tag{2.24c}$$

If $s_{gg'}\xi > 1$, then the integrals are no longer singular, and the relationships are

$$\sigma^i_g\Lambda_{g'g'}(s_{gg'}\xi)\mathrm{I}^{*i}_{gg'}(\xi,x,x_i) = \sum_{\alpha=0}^{N-1}\left[\mathcal{K}\mathrm{A}^{g'}_\alpha(-s_{gg'}\xi) + \mathcal{K}_1\mathrm{A}^{g'}_\alpha(s_{gg'}\xi)\right] + \\ + \mathrm{R1}^i_{g'}(s_{gg'}\xi,x) - \frac{(s_{gg'}\xi)\mathrm{L}(s_{gg'}\xi)}{\sigma^i_{g'}}\mathrm{S1}^i_{g'}(s_{gg'}\xi,x,x_i) - \\ - \sigma^i_g\sum_{g''=1}^{g'-1}\Lambda_{g''g'}(s_{gg'}\xi)\mathrm{I}^{*i}_{gg''}(\xi,x,x_i), \tag{2.25a}$$

and

$$\sigma^i_g\Lambda_{g'g'}(s_{gg'}\xi)\mathrm{J}^{*i}_{gg'}(\xi,x_{i-1},x) = \sum_{\alpha=0}^{N-1}\left[\mathcal{F}\mathrm{A}^{g'}_\alpha(-s_{gg'}\xi) + \mathcal{F}_1\mathrm{A}^{g'}_\alpha(s_{gg'}\xi)\right] + \\ + \mathrm{R2}^i_{g'}(s_{gg'}\xi,x) - \frac{(s_{gg'}\xi)\mathrm{L}(s_{gg'}\xi)}{\sigma^i_{g'}}\mathrm{S2}^i_{g'}(s_{gg'}\xi,x_{i-1},x) - \\ - \sigma^i_g\sum_{g''=1}^{g'-1}\Lambda_{g''g'}(s_{gg'}\xi)\mathrm{J}^{*i}_{gg''}(\xi,x_{i-1},x), \tag{2.25b}$$

where,

$$\mathcal{K}_1 = \begin{cases} -\mathrm{b}_\alpha^{g',i} e^{-\frac{\sigma_g^i}{s_{gg'\xi}}(x_i - x_{i-1})} & x = x_{i-1} \\ \mathrm{d}_\alpha^{g',j} - \mathrm{b}_\alpha^{g',i} e^{-\frac{\sigma_g^i}{s_{gg'\xi}}(x_i - x)} & x \neq x_{i-1}, \end{cases} \tag{2.25c}$$

and

$$\mathcal{F}_1 = \begin{cases} -\mathrm{a}_\alpha^{g',i} e^{-\frac{\sigma_g^i}{s_{gg'\xi}}(x_i - x_{i-1})} & x = x_i \\ \mathrm{c}_\alpha^{g',j} - \mathrm{a}_\alpha^{g',i} e^{-\frac{\sigma_g^i}{s_{gg'\xi}}(x - x_{i-1})} & x \neq x_i. \end{cases} \tag{2.25d}$$

The terms that specify the distributed isotropic source for $x_{i-1} \leq x \leq x_i$ are

$$\mathrm{S1}_g^i(\nu, x, x_i) = \begin{cases} \frac{\sigma_g^i}{\nu} \int_x^{x_i} \mathrm{d}z \, e^{-\frac{\sigma_g^i}{\nu}(z-x)} \mathrm{S}_g^i(z) & \nu \neq 0 \\ \mathrm{S}_g^i(x) & \nu = 0, \end{cases} \tag{2.26a}$$

and

$$\mathrm{S2}_g^i(\nu, x_{i-1}, x) = \begin{cases} \frac{\sigma_g^i}{\nu} \int_{x_{i-1}}^{x} \mathrm{d}z \, e^{-\frac{\sigma_g^i}{\nu}(x-z)} \mathrm{S}_g^i(z) & \nu \neq 0 \\ \mathrm{S}_g^i(x) & \nu = 0. \end{cases} \tag{2.26b}$$

At this point, the source, $\mathrm{S}_g^i(x)$, is a general function. Thus, the above integrals cannot be performed analytically in general. A numerical method of integration can be used to calculate values for this term. As an example, if a set of abscissas and source values is available that describes the source in the media, then an interpolation scheme coupled to a numerical integration routine can be constructed to evaluate the source terms.

2.2.3.3 The Post Processor Associated with the $\mathrm{F_N}$ Method. It has been shown by calculation that the $\mathrm{F_N}$ approximations, equations (2.19), converge

slowly with N. The convergence rate can be increased if the basis function summation term in the F_N approximations are modified with the integral equations, equations (2.20). The first task is to regularize the singular $B^g_\alpha(\mu)$ term.

The non-singular formulation of $B^g_\alpha(\nu)$ is determined from the original definition

$$\begin{aligned} B^g_\alpha(\nu) &= \lambda_{gg}(\nu)\psi_\alpha(\nu) - \frac{\sigma^i_{g\to g}}{2\sigma^i_g} \fint_0^1 d\eta \, \frac{\eta}{\eta-\nu}\psi_\alpha(\eta) \\ &= \left(1 + \nu\frac{\sigma^i_{g\to g}}{2\sigma^i_g} \fint_{-1}^{+1} d\eta \, \frac{1}{\eta-\nu}\right)\psi_\alpha(\nu) - \frac{\sigma^i_{g\to g}}{2\sigma^i_g} \fint_0^1 d\eta \, \frac{\eta}{\eta-\nu}\psi_\alpha(\eta). \end{aligned} \tag{2.27}$$

If

$$\nu\psi_\alpha(\nu)\frac{\sigma^i_{g\to g}}{2\sigma^i_g} \fint_{-1}^{+1} d\eta \, \frac{1}{\eta-\nu}$$

is added to the second term and subtracted from the first term, then $B^g_\alpha(\nu)$ becomes

$$\begin{aligned} B^g_\alpha(\nu) &= \left(1 + \nu\frac{\sigma^i_{g\to g}}{2\sigma^i_g}\ln\left|\frac{\nu}{1+\nu}\right|\right)\psi_\alpha(\nu) - \frac{\sigma^i_{g\to g}}{2\sigma^i_g}\int_0^1 d\eta \, \frac{\eta\psi_\alpha(\eta) - \nu\psi_\alpha(\nu)}{\eta-\nu} \\ &= \lambda^*_{gg}(\nu)\psi_\alpha(\nu) - B^{*g}_\alpha(\nu), \end{aligned} \tag{2.28}$$

where, $\lambda^*_{gg}(\nu)$ and $B^{*g}_\alpha(\nu)$ are no longer singular at $\nu = \eta$. L'Hospital's rule is used to determine the integrand for $B^{*g}_\alpha(\nu)$

$$B^{*g}_\alpha(\nu) = \frac{\sigma^i_{g\to g}}{2\sigma^i_g}\int_0^1 d\eta \begin{cases} \left(\eta\dfrac{d}{d\eta}\psi_\alpha(\eta) + \psi_\alpha(\eta)\right) & \eta = \nu \\ \dfrac{\eta\psi_\alpha(\eta) - \nu\psi_\alpha(\nu)}{\eta-\nu} & \eta \neq \nu. \end{cases} \tag{2.29}$$

The singular $B^g_\alpha(\mu)$ term is eliminated in equations (2.20) by substituting in equation (2.28) to obtain

$$\begin{aligned} &\sum_{\alpha=0}^{N-1}\left[a^{g,i}_\alpha\left(\lambda^*_{gg}(\nu)\psi_\alpha(\nu) - B^{*g}_\alpha(\nu)\right) + b^{g,i}_\alpha A^g_\alpha(\nu)e^{-\frac{\Delta^i_g}{\nu}}\right] = \\ &= R1^i_g(\nu, x_{i-1}) + \frac{1}{\sigma^i_{g\to g}}T1^i_g(\nu, x_{i-1}, x_i) + \frac{1}{\sigma^i_{g\to g}}S1^i_g(\nu, x_{i-1}, x_i), \end{aligned} \tag{2.30a}$$

$$\sum_{\alpha=0}^{N-1}\left[b_{\alpha}^{g,i}\left(\lambda_{gg}^{*}(\nu)\psi_{\alpha}(\nu)-B_{\alpha}^{*g}(\nu)\right)+a_{\alpha}^{g,i}A_{\alpha}^{g}(\nu)e^{-\frac{\Delta_g^i}{\nu}}\right] = \\ = R2_g^i(\nu,x_i)+\frac{1}{\sigma_{g\to g}^i}T2_g^i(\nu,x_{i-1},x_i)+\frac{1}{\sigma_{g\to g}^i}S2_g^i(\nu,x_{i-1},x_i). \tag{2.30b}$$

These equations are solved for $\sum_{\alpha=0}^{N-1} a_{\alpha}^{g,i}\psi_{\alpha}(\mu)$ and $\sum_{\alpha=0}^{N-1} b_{\alpha}^{g,i}\psi_{\alpha}(\mu)$ and substituted into the original F_N approximations, equations (2.19), to obtain

$$\phi_g(x_{i-1},-\mu) = F_R^{g,i}(\mu)e^{-\frac{\Delta_g^i}{\mu}}+ \\ +\frac{1}{2\sigma_g^i\lambda_{gg}^{*}(\mu)}\left[\sigma_{g\to g}^i R1_g^i(\mu,x_{i-1}) + S1_g^i(\mu,x_{i-1},x_i)+\right. \\ \left.+T1_g^i(\mu,x_{i-1},x_i) + \sigma_{g\to g}^i\sum_{\alpha=0}^{N-1}\left\{a_{\alpha}^{g,i}B_{\alpha}^{*g}(\mu)-b_{\alpha}^{g,i}A_{\alpha}^{g}(\mu)e^{-\frac{\Delta_g^i}{\mu}}\right\}\right], \tag{2.31a}$$

and

$$\phi_g(x_i,\mu) = F_L^{g,i}(\mu)e^{-\frac{\Delta_g^i}{\mu}}+ \\ +\frac{1}{2\sigma_g^i\lambda_{gg}^{*}(\mu)}\left[\sigma_{g\to g}^i R2_g^i(\mu,x_i) + S2_g^i(\mu,x_{i-1},x_i)+\right. \\ \left.+T2_g^i(\mu,x_{i-1},x_i) + \sigma_{g\to g}^i\sum_{\alpha=0}^{N-1}\left\{b_{\alpha}^{g,i}B_{\alpha}^{*g}(\mu)-a_{\alpha}^{g,i}A_{\alpha}^{g}(\mu)e^{-\frac{\Delta_g^i}{\mu}}\right\}\right]. \tag{2.31b}$$

The same procedure can be performed with the interior slab formulation to obtain

$$\phi_g(x_j,-\mu) = F_R^{g,i}(\mu)e^{-\frac{\sigma_g^i}{\mu}(x_i-x_j)}+\frac{1}{2\sigma_g^i\lambda_{gg}^{*}(\mu)}\times \\ \times\left[\sigma_{g\to g}^i R1_g^i(\mu,x_j) + S1_g^i(\mu,x_j,x_i) + T1_g^i(\mu,x_j,x_i)+\right. \\ \left.+\sigma_{g\to g}^i\sum_{\alpha=0}^{N-1}\left\{c_{\alpha}^{g,j}B_{\alpha}^{*g}(\mu)+\left(d_{\alpha}^{g,j}-b_{\alpha}^{g,i}e^{-\frac{\sigma_g^i}{\mu}(x_i-x_j)}\right)A_{\alpha}^{g}(\mu)\right\}\right], \tag{2.31c}$$

and

$$\phi_g(x_j,\mu) = F_L^{g,i}(\mu)e^{-\frac{\sigma_g^i}{\mu}(x_j-x_{i-1})}+\frac{1}{2\sigma_g^i\lambda_{gg}^{*}(\mu)}\times \\ \times\left[\sigma_{g\to g}^i R2_g^i(\mu,x_j) + S2_g^i(\mu,x_{i-1},x_j) + T2_g^i(\mu,x_{i-1},x_j)+\right. \\ \left.+\sigma_{g\to g}^i\sum_{\alpha=0}^{N-1}\left\{d_{\alpha}^{g,j}B_{\alpha}^{*g}(\mu)+\left(c_{\alpha}^{g,j}-a_{\alpha}^{g,i}e^{-\frac{\sigma_g^i}{\mu}(x_j-x_{i-1})}\right)A_{\alpha}^{g}(\mu)\right\}\right]. \tag{2.31d}$$

Equations (2.31) are used to determine the final values of the angular flux. The derivation for the interior slab points can be found in Appendix Section A.5.1.

2.2.3.4 Extension of the F_N Method to Multiple Slabs. At this point, the incoming slab boundary flux values, $F_R^{g,i}(\mu)$ and $F_L^{g,i}(\mu)$, are general functions. To determine the fluxes for multiple slabs, the general functions $F_R^{g,i}(\mu)$ and $F_L^{g,i}(\mu)$ must represent specific functions at the boundaries of the slabs. For the method being employed in this treatment, the rightmost incoming boundary flux, $F_R^{g,NS}(\mu)$, is zero. The leftmost incoming boundary flux for group g is

$$F_L^{g,1}(\mu) = S_0^g \, \delta(\mu - \mu_0^g), \tag{2.32a}$$

for a beam source, and

$$F_L^{g,1}(\mu) = S_0^g, \tag{2.32b}$$

for an isotropic source. The same source, either a beam or isotropic, is used for every group. To connect multiple slabs together, the i^{th} slab's incoming boundary flux is the outgoing boundary flux of the adjacent slab, or

$$F_L^{g,i}(\mu) = \phi_g(x_{i-1}, \mu) \tag{2.33a}$$

$$F_R^{g,i}(\mu) = \phi_g(x_i, -\mu) \tag{2.33b}$$

This connection is realized in the inhomogeneous boundary terms, equations (2.22). For a beam source incident on the leftmost face canted at the

angle μ_0^g, the terms are

$$\begin{aligned} \mathrm{R1}_g^i(\mu,x) \;=\; & \int_0^1 \mathrm{d}\eta \;\; \eta \left[\mathrm{C}(\sigma_g^i(x_i - x),\eta,\mu)\phi_g(x_i,-\eta) + \right. \\ & \left. + \, e^{-\frac{\sigma_g^i}{\eta}(x-x_{i-1})} \mathrm{S}(\sigma_g^i(x_i - x),\eta,\mu)\phi_g(x_{i-1},\eta) \right] \; + \\ & + \, \mu_0^g \; S_0^g \; e^{-\frac{1}{\mu_0^g}\left(\sum_{k=1}^{i-1} \Delta_g^k + \sigma_g^i(x-x_{i-1})\right)} \; \mathrm{S}(\sigma_g^i(x_i - x),\mu_0^g,\mu), \end{aligned} \tag{2.34a}$$

and

$$\begin{aligned} \mathrm{R2}_g^i(\mu,x) \;=\; & \int_0^1 \mathrm{d}\eta \;\; \eta \left[\mathrm{C}(\sigma_g^i(x - x_{i-1}),\eta,\mu)\phi_g(x_{i-1},\eta) + \right. \\ & \left. + \, e^{-\frac{\sigma_g^i}{\eta}(x_i - x)} \mathrm{S}(\sigma_g^i(x - x_{i-1}),\eta,\mu)\phi_g(x_i,-\eta) \right] \; + \\ & + \, \mu_0^g \; S_0^g \; e^{-\frac{1}{\mu_0^g}\sum_{k=1}^{i-1} \Delta_g^k} \mathrm{C}(\sigma_g^i(x - x_{i-1}),\mu_0^g,\mu). \end{aligned} \tag{2.34b}$$

For an isotropic source incident on the leftmost face, the terms are

$$\begin{aligned} \mathrm{R1}_g^i(\mu,x) \;=\; & \int_0^1 \mathrm{d}\eta \;\; \eta \left[\mathrm{C}(\sigma_g^i(x_i - x),\eta,\mu)\phi_g(x_i,-\eta) + \right. \\ & \left. + \, e^{-\frac{\sigma_g^i}{\eta}(x-x_{i-1})} \mathrm{S}(\sigma_g^i(x_i - x),\eta,\mu)\phi_g(x_{i-1},\eta) \right] \; + \\ & + \, S_0^g \int_0^1 \mathrm{d}\eta \;\; \eta e^{-\frac{1}{\eta}\left(\sum_{k=1}^{i-1} \Delta_g^k + \sigma_g^i(x-x_{i-1})\right)} \mathrm{S}(\sigma_g^i(x_i - x),\eta,\mu), \end{aligned} \tag{2.35a}$$

and

$$\begin{aligned} \mathrm{R2}_g^i(\mu,x) \;=\; & \int_0^1 \mathrm{d}\eta \;\; \eta \left[\mathrm{C}(\sigma_g^i(x - x_{i-1}),\eta,\mu)\phi_g(x_{i-1},\eta) + \right. \\ & \left. + \, e^{-\frac{\sigma_g^i}{\eta}(x_i - x)} \mathrm{S}(\sigma_{g\to g}^i(x - x_{i-1}),\eta,\mu)\phi_g(x_i,-\eta) \right] \; + \\ & + \, S_0^g \int_0^1 \mathrm{d}\eta \;\; \eta e^{-\frac{1}{\eta}\sum_{k=1}^{i-1} \Delta_g^k} \mathrm{C}(\sigma_g^i(x - x_{i-1}),\eta,\mu). \end{aligned} \tag{2.35b}$$

The flux at the leftmost slab boundary, $\phi_g(x_0,\eta)$, represents the flux without the source, so

$$\phi_g(x_0,\eta) \;=\; 0. \tag{2.36a}$$

Since there is no source on the rightmost slab boundary, the flux at that boundary is

$$\phi_g(x_{NS}, -\eta) \;=\; 0. \tag{2.36b}$$

These formulations are valid for slab boundary and interior points.

2.2.3.5 Scalar Flux Determination. Two methods are available for calculation of the scalar fluxes. The transport equation can be solved at $\mu = 0$, or the angular flux can be integrated over μ. Both methods have approximations. The first method cannot use an exact value of zero for μ. A value of 1.0×10^{-20} is used as an approximation. The second method uses numerical integration for the basis functions. The direct integration method is the preferred method because it does not stress the post processor when calculating angular fluxes. The extra stress on the post processor, created when calculating the angular flux at a small μ, could keep the F_N method from converging on an answer.

The original transport equation can be used to determine the scalar fluxes

$$\left[\mu\frac{\partial}{\partial x} \;+\; \sigma_g^i\right] \phi_g(x,\mu) \;=\; \frac{1}{2}\sum_{g'=1}^{g} \sigma_{g'\to g}^i \int_{-1}^{+1} d\mu'\, \phi_{g'}(x,\mu') \;+\; \frac{1}{2}S_g^i(x). \tag{2.37}$$

If μ is set to zero and the group scalar flux is defined as

$$\phi_g(x) \;=\; \int_{-1}^{+1} d\mu'\, \phi_g(x,\mu'), \tag{2.38}$$

then the transport equations becomes

$$\sigma_g^i \phi_g(x,0) \;=\; \frac{1}{2}\sum_{g'=1}^{g} \sigma_{g'\to g}^i \phi_{g'}(x) \;+\; \frac{1}{2}S_g^i(x). \tag{2.39}$$

Solving this equation for $\phi_g(x)$ obtains

$$\phi_g(x) = \frac{2\sigma_g^i}{\sigma_{g\to g}^i}\phi_g(x,0) - \frac{1}{\sigma_{g\to g}^i}\sum_{g'=1}^{g-1}\sigma_{g'\to g}^i\phi_{g'}(x) - \frac{1}{\sigma_{g\to g}^i}\mathrm{S}_g^i(x). \tag{2.40}$$

This is implemented by first calculating the scalar flux for group one, then group two, etc.... However, the angular flux value for $\mu = 0$, $\phi_g(x,0)$, must be determined and that poses a problem as shown in equation (2.31). The denominator of some terms contain μ, so an approximation of setting μ close, but not equal to, zero is imposed and the resultant scalar flux value could be inaccurate or the $\mathrm{F_N}$ method could have problems converging while trying to calculate the angular flux at a small μ.

The integration of the original $\mathrm{F_N}$ approximations, equations (2.19), over μ is the preferred method to obtain a scalar flux because most of the integrals are evaluated analytically. To obtain the scalar flux, $\mathrm{F_L^{g,i}}(\mu)$ and $\mathrm{F_R^{g,i}}(\mu)$ are expressed in terms of known quantities at the slab boundaries

$$\mathrm{F_L^{g,i}}(\mu) = \sum_{l=1}^{i-1}\frac{\sigma_{g\to g}^l}{\sigma_g^l}\sum_{\alpha=0}^{N-1}\mathrm{b}_\alpha^{g,l}\psi_\alpha(\mu)e^{-\frac{1}{\mu}\sum_{k=l+1}^{i-1}\Delta_g^k}, \tag{2.41a}$$

and

$$\mathrm{F_R^{g,i}}(\mu) = \sum_{l=i+1}^{\mathrm{NS}}\frac{\sigma_{g\to g}^l}{\sigma_g^l}\sum_{\alpha=0}^{N-1}\mathrm{a}_\alpha^{g,l}\psi_\alpha(\mu)e^{-\frac{1}{\mu}\sum_{k=i+1}^{l-1}\Delta_g^k}. \tag{2.41b}$$

These functions are substituted into the $\mathrm{F_N}$ approximations, and integrated over μ from $[0,1]$. The result of this procedure is

$$\begin{aligned}\phi_g(x_0) &= \int_0^1 d\eta\,\mathcal{U}(\eta) + \sum_{l=1}^{\mathrm{NS}}\frac{\sigma_{g\to g}^l}{\sigma_g^l}\sum_{\alpha=0}^{N-1}\mathrm{a}_\alpha^{g,l}\times \\ &\times\int_0^1 d\eta\,\psi_\alpha(\eta)e^{-\frac{1}{\eta}\sum_{k=1}^{l-1}\Delta_g^k},\end{aligned} \tag{2.42a}$$

$$\phi_g(x_{\rm NS}) = \int_0^1 d\eta\, \mathcal{U}(\eta) e^{-\frac{1}{\eta}\sum_{k=1}^{\rm NS}\Delta_g^k} + \sum_{l=1}^{\rm NS}\frac{\sigma_{g\to g}^l}{\sigma_g^l}\sum_{\alpha=0}^{N-1} b_\alpha^{g,l} \times$$
$$\times \int_0^1 d\eta\, \psi_\alpha(\eta) e^{-\frac{1}{\eta}\sum_{k=l+1}^{\rm NS}\Delta_g^k}, \tag{2.42b}$$

$$\phi_g(x_i) = \int_0^1 d\eta\, \mathcal{U}(\eta) e^{-\frac{1}{\eta}\sum_{k=1}^{i}\Delta_g^k} + \sum_{\alpha=0}^{N-1}\left[\frac{\sigma_{g\to g}^i}{\sigma_g^i} b_\alpha^{g,i} + \frac{\sigma_{g\to g}^{i+1}}{\sigma_g^{i+1}} a_\alpha^{g,i+1}\right] \times$$
$$\times \int_0^1 d\eta\, \psi_\alpha(\eta) + \sum_{l=1}^{i}\frac{\sigma_{g\to g}^l}{\sigma_g^l}\sum_{\alpha=0}^{N-1} b_\alpha^{g,l}\int_0^1 d\eta\, \psi_\alpha(\eta) e^{-\frac{1}{\eta}\sum_{k=l+1}^{i}\Delta_g^k} + \tag{2.42c}$$
$$+ \sum_{l=i+2}^{\rm NS}\frac{\sigma_{g\to g}^l}{\sigma_g^l}\sum_{\alpha=0}^{N-1} a_\alpha^{g,l}\int_0^1 d\eta\, \psi_\alpha(\eta) e^{-\frac{1}{\eta}\sum_{k=i+1}^{l-1}\Delta_g^k},$$

and

$$\phi_g(x_j) = \int_0^1 d\eta\, \mathcal{U}(\eta) e^{-\frac{1}{\eta}\left[\sum_{k=1}^{i}\Delta_g^k + \sigma_g^i(x_j - x_{i-1})\right]} +$$
$$\frac{\sigma_{g\to g}^i}{\sigma_g^i}\sum_{\alpha=0}^{N-1}\left(d_\alpha^{g,j} + c_\alpha^{g,j}\right)\int_0^1 d\eta\, \psi_\alpha(\eta) + \sum_{l=1}^{i-1}\frac{\sigma_{g\to g}^l}{\sigma_g^l}\sum_{\alpha=0}^{N-1} b_\alpha^{g,l} \times$$
$$\times \int_0^1 d\eta\, \psi_\alpha(\eta) e^{-\frac{1}{\eta}\left[\sum_{k=l+1}^{i-1}\Delta_g^k + \sigma_g^i(x_j - x_{i-1})\right]} + \tag{2.42d}$$
$$+ \sum_{l=i+1}^{\rm NS}\frac{\sigma_{g\to g}^l}{\sigma_g^l}\sum_{\alpha=0}^{N-1} a_\alpha^{g,l}\int_0^1 d\eta\, \psi_\alpha(\eta) e^{-\frac{1}{\eta}\left[\sum_{k=i+1}^{l-1}\Delta_g^k + \sigma_g^i(x_i - x_j)\right]},$$

where,

$$\mathcal{U}(\eta) = \begin{cases} S_0\, \delta(\eta - \mu_0^g) & \text{Beam Source} \\ S_0 & \text{Isotropic Source.} \end{cases} \tag{2.42e}$$

All integrations over the basis functions are performed numerically using the standard shifted Gauss-Legendre quadrature scheme.

2.2.4 Coupling of the F_N and Galactic Cosmic Ray Cascade Models

From the physical model, a distributed monodirectional source due to the galactic cosmic ray cascade exists within the slab. The F_N algorithm, as derived, allows for a distributed isotropic source. Since a direct substitution of the cascade

source into the F_N algorithm cannot be performed, generation of an isotropic source from the monodirectional cascade source is used as an alternative. This is accomplished by determining the collided flux from the cascade source and setting the F_N source to be this collided flux. This derivation is performed for a single slab only.

2.2.4.1 Generation of the F_N Isotropic Source. The formulation of the isotropic F_N source term in equations (2.9) starts with the uncollided and collided solutions to the transport equation with a monodirectional source ($0 < \mu_{GIT} \leq 1$)

$$\left[\mu\frac{\partial}{\partial x} + \sigma_g\right]\phi_g(x,\mu) = \frac{1}{2}\sum_{g'=1}^{g}\sigma_{g'\to g}\int_{-1}^{+1}d\mu'\,\phi_{g'}(x,\mu') + \\ + \Psi_g(x)\delta(\mu-\mu_{GIT}), \tag{2.43a}$$

with boundary conditions of

$$\phi_g(x_0,\mu) = 0 \tag{2.43b}$$

where, $\Psi_g(x)$ is the neutron flux found from the galactic cosmic ray cascade model as described in Section 2.2.4.2.

Let the angular flux be composed of the uncollided and collided angular fluxes

$$\phi_g(x,\mu) = \phi_g^u(x,\mu) + \phi_g^c(x,\mu). \tag{2.44}$$

Substituting into equations (2.43) yields

$$\left[\mu\frac{\partial}{\partial x} + \sigma_g\right]\phi_g^u(x,\mu) = \Psi_g(x)\delta(\mu-\mu_{GIT}), \tag{2.45a}$$

$$\phi_g^u(x_0,\mu) \;=\; 0, \tag{2.45b}$$

and

$$\left[\mu\frac{\partial}{\partial x} \;+\; \sigma_g\right]\phi_g^c(x,\mu) \;=\; \frac{1}{2}\sum_{g'=1}^{g}\sigma_{g'\to g}\int_{-1}^{+1}\mathrm{d}\mu'\;\phi_{g'}^c(x,\mu') \;+ \\ +\;\frac{1}{2}\sum_{g'=1}^{g}\sigma_{g'\to g}\int_{-1}^{+1}\mathrm{d}\mu'\;\phi_{g'}^u(x,\mu'). \tag{2.45c}$$

Equation (2.45c) is the transport equation used in the F_N method for a single slab if

$$S_g(x) \;=\; \sum_{g'=1}^{g}\sigma_{g'\to g}\int_{-1}^{+1}\mathrm{d}\mu'\;\phi_{g'}^u(x,\mu'). \tag{2.46}$$

Therefore, to obtain the F_N source term, equation (2.45a) is solved for the uncollided flux, $\phi_g^u(x,\mu)$, which is then substituted into equation (2.46).

A solution to equation (2.45a) for a single slab is

$$\phi_g^u(x,\mu) \;=\; \int_{x_0}^{x}\mathrm{d}z\;\frac{e^{-\frac{\sigma_g}{\mu}(x-z)}}{\mu}\Psi_g(z)\delta(\mu-\mu_{\mathrm{GIT}}). \tag{2.47}$$

Substituting equation (2.47) into equation (2.46) yields

$$S_g(x) \;=\; \sum_{g'=1}^{g}\sigma_{g'\to g}\int_{-1}^{+1}\mathrm{d}\mu'\;\int_{x_0}^{x}\mathrm{d}z\;\frac{e^{-\frac{\sigma_{g'}(x-z)}{\mu'}}}{\mu'}\Psi_{g'}(z)\delta(\mu'-\mu_{\mathrm{GIT}}). \tag{2.48}$$

The integral on μ is easily performed to obtain

$$S_g(x) \;=\; \sum_{g'=1}^{g}\sigma_{g'\to g}\int_{x_0}^{x}\mathrm{d}z\;\frac{e^{-\frac{\sigma_{g'}(x-z)}{\mu_{\mathrm{GIT}}}}}{\mu_{\mathrm{GIT}}}\Psi_{g'}(z). \tag{2.49}$$

This formulation can then be placed into equations (2.26) to determine terms required for the F_N method for a single slab. The next task is to determine $\Psi_g(x)$.

2.2.4.2 The Galactic Cosmic Ray Cascade Formulation for the F_N Source.

The flux found from the galactic cosmic ray cascade transport equation, equation (2.5), is the flux of particle j based on the particle fragmentation and transport through the medium. The flux that must be used as the F_N source is for neutrons which is found by setting j to 0. Because the neutrons are acting as a source, the transport part of equation (2.5) is set to zero so that particles are not transported in space and energy by the galactic cosmic ray equations when created. The resultant algebraic transport equation is solved for the neutron flux

$$\Psi_g(\tau) \;=\; \psi_0(\tau, \mathrm{E}_g) \;=\; \frac{1}{\sigma_0} \sum_{k=2}^{J} \mathrm{M}_{0,k}\, \sigma_k\, \psi_k(\tau, \mathrm{E}_g), \tag{2.50}$$

where, E_g represents the energy of the group being calculated.

When the general Green's function solution, equation (2.6), is introduced into the above equation, the result is

$$\begin{aligned} \Psi_g(\tau) \;=\; & \frac{1}{\mathrm{S}_P(\mathrm{E}_g)} \sum_{l=1}^{J-2} \mathrm{M}_{1,J-l} \frac{\sigma_{J-l}}{\sigma_0} \sum_{r=1}^{N_l} e^{-\frac{a_r}{b_r} s_g - (\sigma_{J-i_1} - \frac{a_r}{b_r} \overline{\nu}_{J-i_1})\tau} \;\times \\ & \times\; \tilde{\mathrm{Y}}^{J-l}_{i_1,r} \left[\theta(s_g - \overline{\nu}_{J-i_1}\tau) - \theta(s_g - \overline{\nu}_{J-i_2}\tau)\right], \end{aligned} \tag{2.51}$$

where, s_g is the path length evaluated at E_g.

To convert from the optical path length, τ, to a physical space dimension, z, this differential relation must be satisfied

$$\Psi_g(\tau)\,|\mathrm{d}\tau| \;=\; \Psi_g(z)\,|\mathrm{d}z|\,. \tag{2.52}$$

If $\tau = \rho z$, where ρ is the density of the target material, then

$$\Psi_g(z) \;=\; \rho \Psi_g(\tau). \tag{2.53}$$

To complete the variable change, these definitions must be specified

$$\sigma_{J-l} \equiv \rho\sigma_{J-l}, \tag{2.54a}$$

$$S_P(E_g) \equiv \rho S_P(E_g), \tag{2.54b}$$

and

$$s_g \equiv \int_{E_g}^{E_0} dE' \frac{1}{\rho S_P(E_{g'})} = \frac{1}{\rho} s_g. \tag{2.54c}$$

Therefore, the final expression for the galactic cosmic ray cascade source used in the F_N source is

$$\begin{aligned}\Psi_g(z) &= \frac{\rho}{S_P(E_g)} \sum_{l=1}^{J-2} M_{0,J-l} \frac{\sigma_{J-l}}{\sigma_0} \sum_{r=1}^{N_l} e^{-\frac{a_r}{b_r} s_g - (\sigma_{J-i_1} - \frac{a_r}{b_r}\overline{\nu}_{J-i_1})z} \times \\ &\times \tilde{Y}_{i_1,r}^{J-l} \left[\theta(\frac{s_g}{\overline{\nu}_{J-i_1}} - z) - \theta(\frac{s_g}{\overline{\nu}_{J-i_2}} - z) \right].\end{aligned} \tag{2.55}$$

This result is used in equation (2.49) to generate a source of neutrons from the galactic cosmic ray cascade.

2.2.4.3 F_N Distributed Source. In the last two sections, an F_N neutron source is derived from the galactic cosmic ray cascade. This section places the result in the F_N context.

The cascade neutron source in equation (2.55) is substituted into the F_N source term in equation (2.49) to obtain

$$\begin{aligned}S_g(x) &= \frac{\rho}{\sigma_0 \mu_{GIT}} \sum_{l=1}^{J-2} M_{0,J-l} \sigma_{J-l} \sum_{r=1}^{N_l} \tilde{Y}_{i_1,r}^{J-l} \times \\ &\times \sum_{g'=1}^{g} \frac{\sigma_{g' \to g}}{S_P(E_{g'})} \left[I_{g'}(\overline{\nu}_{J-i_1}, x) - I_{g'}(\overline{\nu}_{J-i_2}, x) \right],\end{aligned} \tag{2.56a}$$

where,

$$I_{g'}(\xi,x) \;=\; \int_{x_0}^{x} \mathrm{d}z\, e^{-\left[\frac{\sigma_{g'}}{\mu_{\mathrm{GIT}}}(x-z)+(\sigma_{J-i_1}-\frac{a_r}{b_r}\overline{\nu}_{J-i_1})z+\frac{a_r}{b_r}s_{g'}\right]}\theta(\frac{s_{g'}}{\xi}-z). \tag{2.56b}$$

To complete the analysis, equations (2.56) are substituted into the $\mathrm{F_N}$ source term, equations (2.26), for a single slab to obtain

$$\begin{aligned}\mathrm{S1}_g(\nu,x,x_1) \;&=\; \frac{\rho\sigma_g}{\sigma_0\mu_{\mathrm{GIT}}\nu}\sum_{l=1}^{J-2}\mathrm{M}_{0,J-l}\sigma_{J-l}\sum_{r=1}^{N_l}\times \\ &\times\; \tilde{\mathrm{Y}}_{i_1,r}^{J-l}\sum_{g'=1}^{g}\frac{\sigma_{g'\to g}}{\mathrm{S}_P(\mathrm{E}_{g'})}\mathrm{IP1},\end{aligned} \tag{2.57a}$$

$$\begin{aligned}\mathrm{S2}_g(\nu,x_0,x) \;&=\; \frac{\rho\sigma_g}{\sigma_0\mu_{\mathrm{GIT}}\nu}\sum_{l=1}^{J-2}\mathrm{M}_{0,J-l}\sigma_{J-l}\sum_{r=1}^{N_l}\times \\ &\times\; \tilde{\mathrm{Y}}_{i_1,r}^{J-l}\sum_{g'=1}^{g}\frac{\sigma_{g'\to g}}{\mathrm{S}_P(\mathrm{E}_{g'})}\mathrm{IP2},\end{aligned} \tag{2.57b}$$

where,

$$\mathrm{IP1} \;=\; \int_{x}^{x_1}\mathrm{d}z\, e^{-\frac{\sigma_g}{\nu}(z-x)}\left[I_{g'}(\overline{\nu}_{J-i_1},z)-I_{g'}(\overline{\nu}_{J-i_2},z)\right], \tag{2.57c}$$

and

$$\mathrm{IP2} \;=\; \int_{x_0}^{x}\mathrm{d}z\, e^{-\frac{\sigma_g}{\nu}(x-z)}\left[I_{g'}(\overline{\nu}_{J-i_1},z)-I_{g'}(\overline{\nu}_{J-i_2},z)\right]. \tag{2.57d}$$

For $\nu = 0$, the term in equations (2.26) is the source value in equations (2.56).

The integrals in equations (2.56b), and (2.57) have been evaluated using the MAPLE symbolic manipulation routines in MATHCAD (Reference [23]). However, the integrals in equations (2.57) must be partially evaluated to allow evaluation in MATHCAD. The full integrals are

$$\begin{aligned}\mathrm{IP1} \;&=\; \int_{x}^{x_1}\mathrm{d}z\, e^{-\frac{\sigma_g}{\nu}(z-x)}\int_{x_0}^{z}\mathrm{d}w\, e^{-\frac{\sigma_{g'}}{\mu_{\mathrm{GIT}}}(z-w)-(\sigma_{J-i_1}-\frac{a_r}{b_r}\overline{\nu}_{J-i_1})w-\frac{a_r}{b_r}s_{g'}}\times \\ &\times\; \left[\theta\left(\frac{s_{g'}}{\overline{\nu}_{J-i_1}}-w\right)-\theta\left(\frac{s_{g'}}{\overline{\nu}_{J-i_2}}-w\right)\right],\end{aligned} \tag{2.58a}$$

and

$$\begin{aligned} \mathrm{IP2} \;=\; & \int_{x_0}^{x} \mathrm{d}z\, e^{-\frac{\sigma_g}{\nu}(x-z)} \int_{x_0}^{z} \mathrm{d}w\, e^{-\frac{\sigma_{g'}}{\mu_{\mathrm{GIT}}}(z-w)-(\sigma_{J-i_1}-\frac{a_r}{b_r}\overline{\nu}_{J-i_1})w-\frac{a_r}{b_r}s_{g'}} \times \\ & \times \left[\theta\left(\frac{s_{g'}}{\overline{\nu}_{J-i_1}}-w\right)-\theta\left(\frac{s_{g'}}{\overline{\nu}_{J-i_2}}-w\right)\right]. \end{aligned} \tag{2.58b}$$

The partially evaluated integrals are

$$\begin{aligned} \mathrm{IP1} \;=\; & -\int_{q_1}^{p_1} \mathrm{d}w\, e^{-(\sigma_{J-i_1}-\frac{a_r}{b_r}\overline{\nu}_{J-i_1})w-\frac{a_r}{b_r}s_{g'}} \int_{x}^{x_1} \mathrm{d}z\, e^{-\frac{\sigma_g}{\nu}(z-x)-\frac{\sigma_{g'}}{\mu_{\mathrm{GIT}}}(z-w)} - \\ & -\int_{q_2}^{p_2} \mathrm{d}w\, e^{-(\sigma_{J-i_1}-\frac{a_r}{b_r}\overline{\nu}_{J-i_1})w-\frac{a_r}{b_r}s_{g'}} \int_{w}^{x_1} \mathrm{d}z\, e^{-\frac{\sigma_g}{\nu}(z-x)-\frac{\sigma_{g'}}{\mu_{\mathrm{GIT}}}(z-w)}, \end{aligned} \tag{2.59a}$$

and

$$\mathrm{IP2} \;=\; -\int_{q_1}^{p_1} \mathrm{d}w\, e^{-(\sigma_{J-i_1}-\frac{a_r}{b_r}\overline{\nu}_{J-i_1})w-\frac{a_r}{b_r}s_{g'}} \int_{w}^{x} \mathrm{d}z\, e^{-\frac{\sigma_g}{\nu}(x-z)-\frac{\sigma_{g'}}{\mu_{\mathrm{GIT}}}(z-w)}, \tag{2.59b}$$

where,

$$p_1 \;=\; \min\left(\frac{s_{g'}}{\overline{\nu}_{J-i_2}}, x\right) \qquad\qquad q_1 \;=\; \max\left(\frac{s_{g'}}{\overline{\nu}_{J-i_1}}, x_0\right), \tag{2.59c}$$

and

$$p_2 \;=\; \min\left(\frac{s_{g'}}{\overline{\nu}_{J-i_2}}, x_1\right) \qquad\qquad q_2 \;=\; \max\left(\frac{s_{g'}}{\overline{\nu}_{J-i_1}}, x\right). \tag{2.59d}$$

These are the integrals symbolically evaluated by MATHCAD.

CHAPTER 3

NUMERICAL IMPLEMENTATION

The numerical methods required to solve the F_N equations are simple and straight-forward. The tasks that require some form of numerical method are determination of the expansion coefficients, collocation points, Legendre polynomials, general source function, basis function, and various integrals. The following numerical algorithms are required: matrix inversion, cubic spline interpolation, and Gauss-Legendre integration. Also, two iterations are required to complete the algorithm.

3.1 Evaluation of Expansion Coefficients

The integral equations, equations (2.18), are in the form of the inhomogeneous Fredholm equation

$$\phi(x) - \lambda \int_a^b \mathrm{d}\xi \; k(x,\xi)\phi(\xi) - f(x) \;=\; r(x). \tag{3.1}$$

If the solution, $\phi(x)$, is replaced with a basis function expansion

$$\phi(x) \;=\; \sum_{j=0}^{n} a_j u_j(x), \tag{3.2}$$

then the resultant equation is

$$\sum_{j=0}^{n} a_j u_j(x) - \lambda \sum_{j=0}^{n} a_j \int_a^b \mathrm{d}\xi \; k(x,\xi)u_j(\xi) - f(x) \;=\; r(x), \tag{3.3}$$

where, the kernel, $k(x,\xi)$, is singular but can be regularized.

To determine the coefficients, equation (3.3) is multiplied by a set of test functions $v_i(x)$, $i = 0, 1, \ldots, N$. The inner product of $v_i(x)$ and $r(x)$ is then required to be zero for each value of i

$$\int_0^\infty \mathrm{d}x\, v_i(x) r(x) \;=\; 0 \qquad i = 0, 1, \ldots, n. \tag{3.4}$$

If $v_i(x)$ is equal to $\delta(x - x_i)$, then the process is called the *collocation method*. If $v_i(x)$ is equal to x^i, then the process is called the *method of moments*. A more general method called the *Galerkin method* uses a general weight for $v_i(x)$. The collocation method was chosen for this problem because the above integrals can be performed analytically. The matrix elements are the integrals with the rows representing the order of the basis function expansion j and the columns representing the basis of the delta functions i. The solution vector is the basis function expansion coefficients. The inhomogeneous vector is composed of the terms associated with the boundary conditions, external sources, down scatter sources, and slab interfaces.

From experience, the choice of the collocation points, x_i in the above formulation and ν_β in the $\mathrm{F_N}$ notation, has not greatly affected the solution or its rate of convergence, as long as the positive root of the infinite medium dispersion relation or constraint, ν_0^g, is included. Three sets of collocation points have been used extensively in $\mathrm{F_N}$ calculations. The first set is $N - 1$ evenly spaced points over the interval $[0, 1]$. The second set is formed by the zeros of the Legendre

polynomials $\nu_\beta \in \{P_{N-1}(2\nu - 1) = 0\}$. These are determined from a subprogram in Reference [24]. The third set is formed by the zeros of the Chebyshev polynomials $\nu_\beta \in \{T_{N-1}(2\nu - 1) = 0\}$. These are determined from

$$\nu_\beta = \frac{1}{2} + \frac{1}{2}\cos\left(\frac{2\beta - 1}{2N}\pi\right). \tag{3.5}$$

Recall that ν_0^g is the positive real root of the infinite medium dispersion relation

$$\Lambda_{gg}(\nu_0^g) = 0 = 1 - \nu_0^g \frac{\sigma_{g\to g}^i}{2\sigma_g^i} \ln\left|\frac{1-\nu_0^g}{1+\nu_0^g}\right|. \tag{3.6}$$

The behavior of this function is well known. In the interval $[1, \infty)$, the function monotonically decreases; therefore, there is one real root. The function is symmetric about zero, so it has another real root in the interval $(-\infty, -1]$. To determine the positive root, a routine is used that is based on the bisection root finding technique. The condition number of the collocation matrices is very sensitive to the precession of ν_0^g, thus, a relative error equal to the machine precession is required. This appears to give acceptable results over all ranges of operation.

The use of the collocation method transforms equations (2.20) into two matrix equations of the form

$$\sum_{\alpha=0}^{N-1} [a_\alpha \Xi_{\alpha\beta} + b_\alpha \Psi_{\alpha\beta}] = \Upsilon_\beta, \tag{3.7a}$$

and

$$\sum_{\alpha=0}^{N-1} [a_\alpha \Psi_{\alpha\beta} + b_\alpha \Xi_{\alpha\beta}] = \Gamma_\beta, \tag{3.7b}$$

where,

$$\Psi_{\alpha\beta} = A_{\alpha}^{g}(\nu_{\beta}), \tag{3.7c}$$

and

$$\Xi_{\alpha\beta} = B_{\alpha}^{g}(\nu_{\beta}). \tag{3.7d}$$

These matrix equations could be solved directly, but $\Psi\alpha\beta$ goes to zero as α increases. This creates an ill-conditioned matrix equation. A change in the form of the matrix equations not only side steps the ill-conditioned matrix problem, but reduces the computer storage requirements by a factor of two. To reformulate the matrix equations, equation (3.7a) and equation (3.7b) are added to obtain

$$\sum_{\alpha=0}^{N-1} \left[(a_{\alpha} + b_{\alpha}) (\Xi_{\alpha\beta} + \Psi_{\alpha\beta}) \right] = (\Upsilon_{\beta} + \Gamma_{\beta}). \tag{3.8a}$$

The same equations are subtracted to obtain

$$\sum_{\alpha=0}^{N-1} \left[(a_{\alpha} - b_{\alpha}) (\Xi_{\alpha\beta} - \Psi_{\alpha\beta}) \right] = (\Upsilon_{\beta} - \Gamma_{\beta}). \tag{3.8b}$$

The new matrix equations are solved for g_{α}^{+} and g_{α}^{-} by letting

$$g_{\alpha}^{+} = a_{\alpha} + b_{\alpha}, \tag{3.9a}$$

and

$$g_{\alpha}^{-} = a_{\alpha} - b_{\alpha}. \tag{3.9b}$$

The original coefficients can be recovered from

$$a_{\alpha} = \frac{1}{2} \left(g_{\alpha}^{+} + g_{\alpha}^{-} \right), \tag{3.10a}$$

and

$$b_\alpha = \frac{1}{2}\left(g_\alpha^+ - g_\alpha^-\right). \tag{3.10b}$$

The matrix equations are solved using LU decomposition as found in Reference [24], which is based on Crout's algorithm with partial pivoting. The coefficients are determined using the companion back-substitution algorithm. The matrices only need to be decomposed when the number of terms used in the basis function expansion changes.

The QR and Singular Value Decomposition (SVD) algorithms from Reference [24] were used instead of the LU decomposition algorithm when F_N algorithm did not converge; however, the QR and SVD algorithms did not make the F_N algorithm converge either. Therefore, the matrices created in this algorithm are not ill-conditioned. Since the LU decomposition algorithm is a fast and convenient algorithm, it is the algorithm of choice.

3.2 General Function Integration

The terms containing integrals that must be evaluated either analytically or numerically are the matrix terms $A_\alpha^g(\nu)$, $B_\alpha^g(\nu)$, and $B_\alpha^{*g}(\nu)$, the inhomogeneous terms $R1_g^i(\nu, x)$ and $R2_g^i(\nu, x)$, and the source terms $S1_g^i(\nu, x, x_i)$ and $S2_g^i(\nu, x_{i-1}, x)$. Due to the generality of the functions involved, the Gauss-Legendre quadrature is used. The quadrature points and weights are found with the **GAULEG** subprogram from Reference [24].

An alternative method to determine $A_\alpha^g(\nu)$ and $B_\alpha^g(\nu)$ can be found using the Legendre polynomial as the basis function. The Legendre polynomial recursion relation is used to determine a recursion relation for these terms. Therefore, numerical integrations need not be performed. The derivation for these relations are found in Reference [12].

The recursion relation for $A_\alpha^g(\xi)$ with $\alpha \geq 1$ is

$$\begin{aligned} A_\alpha^g(\xi) &= -\left(\frac{2\alpha-1}{\alpha}\right)(2\xi-1)\,A_{\alpha-1}^g(\xi) - \left(\frac{\alpha-1}{\alpha}\right)A_{\alpha-2}^g(\xi) + \\ &+ \frac{1}{2}\delta_{\alpha,2} + \delta_{\alpha,1}, \end{aligned} \tag{3.11a}$$

and

$$A_0^g(\xi) = 1 - \xi \ln\left|1 + \frac{1}{\xi}\right|. \tag{3.11b}$$

The forward recursion is stable only for $\xi \in [-1, 0]$, and the backward recursion is stable for $\xi \notin [-1, 0]$ which can be evaluated with Miller's algorithm (Reference [24]).

The recursion relation for $B_\alpha^g(\xi)$ with $\alpha \geq 1$ is

$$\begin{aligned} B_\alpha^g(\xi) &= \left(\frac{2\alpha-1}{\alpha}\right)(2\xi-1)\,B_{\alpha-1}^g(\xi) - \left(\frac{\alpha-1}{\alpha}\right)B_{\alpha-2}^g(\xi) + \\ &- \frac{\sigma_{g\to g}^i}{2\sigma_g^i}\delta_{\alpha,2} - \frac{\sigma_{g\to g}^i}{\sigma_g^i}\delta_{\alpha,1}, \end{aligned} \tag{3.12a}$$

and

$$B_0^g(\xi) = 2 - \frac{\sigma_{g\to g}^i}{\sigma_g^i}\left[1 + \xi \ln\left|1 + \frac{1}{\xi}\right|\right]. \tag{3.12b}$$

The forward recursion is stable only for $\xi \in [0, 1]$, and the backward recursion with Miller's algorithm must be used when $\xi = \nu_0^g$.

To evaluate $B_\alpha^{*g}(\mu)$, equation (2.28) gives

$$B_\alpha^{*g}(\mu) = \lambda_{gg}^{*}(\mu)\psi_\alpha(\mu) - B_\alpha^{g}(\mu), \tag{3.13}$$

where, $B_\alpha^{g}(\mu)$ and $\psi_\alpha(\mu)$ are determined from the appropriate recurrence relations.

3.3 Determination of the Legendre Polynomials

The standard recursion relation is used to determine the value of the Legendre polynomials for any value of x. This function is used for determination of the basis functions

$$P_n(x) = x\frac{(2n-1)}{n}P_{n-1}(x) - \frac{(n-1)}{n}P_{n-2}(x), \tag{3.14a}$$

$$P_0(x) = 1 \quad \text{and} \quad P_1(x) = x. \tag{3.14b}$$

This formulation provides a stable calculation of the Legendre polynomials over all orders, n, and all values of x being used in the F_N algorithm.

3.4 Cubic Spline Function Interpolation

The F_N formulation contains a general isotropic source distribution as shown in equations (2.26). This source is specified with two vectors for each energy group with a source. The first vector contains the slab positions of the source values. The second vector contains the source value at the slab positions. Since this source must be integrated at various Gauss-Legendre quadrature points, a natural cubic spline is fit to the source values. The algorithms that determine and store the second derivative values and interpolate the source values are from

Reference [24]. The Gauss-Legendre integration algorithm for equations (2.26) uses pre-calculated source values interpolated at the quadrature points.

3.5 Basis Functions

In contrast to the choice of collocation points, the choice of the basis functions, $\psi_\alpha(\mu)$, is crucial to the convergence of the F_N method. The use of monomials, μ^α and $(2\mu^\gamma - 1)^\alpha$, where γ is a value between 0 and 1, has been shown to generate ill-conditioned matrices (condition number $||A||_\infty >> 1$), and therefore, unstable convergence properties. The use of shifted Legendre polynomials, $P_\alpha(2\mu - 1)$, has been shown to have fairly stable convergence properties. However, modified Legendre polynomials, $P_\alpha(2\mu^\gamma - 1)$, when they converge, tend to converge faster than the shifted Legendre polynomials.

The derivative of the basis functions is required in equation (2.29). The table below shows some examples of basis functions and their corresponding derivatives.

3.6 Iteration Schemes

Two iterations are required to facilitate the F_N algorithm. The first (Iteration 1) is an iteration to converge the fluxes over the number of basis expansion terms, N. The second (Iteration 2) adjusts the interior slab boundary fluxes with constant N to accelerate the first iteration.

3.6.1 Iteration 1

As the number of expansion terms is increased, the relative error between the fluxes calculated from the current and previous expansion terms is determined for each boundary point and angle. If the maximum relative error is smaller than a prescribed value, then the boundary problem is deemed converged. If the maximum relative error is larger than the prescribed value, the number of expansion terms is increased, and new fluxes are calculated.

Since the interior integral equations depend on the boundary expansion coefficients, the following algorithm is imposed. All slab boundary expansion coefficients must be determined for every iteration in N. If the boundary fluxes do not converged, then computer time is not wasted computing interior fluxes with inaccurate boundary coefficients. Once the boundary fluxes converge, then all the fluxes are determined, and the convergence of all points is tested as described above.

3.6.2 Iteration 2

To solve for the fluxes in slab i, the right boundary incoming flux from slab $i+1$, $\phi_g(x_i, -\mu)$, is needed. But it has not yet been determined. Therefore the i^{th} slab's boundary fluxes are inaccurate. If multiple calculational passes are made through the slabs, then the inaccuracies are diminished. There are three methods that could be used to perform these passes. The first is to create a slab based matrix and use a solution matrix iteration technique, such as Gauss-Sidel, or a

simultaneous technique, such as LU decomposition, to solve for the resultant boundary fluxes. The next method determines the fluxes using multiple passes until the difference between successive passes is less than a prescribed tolerance value. The final method calculates the fluxes for a specified number of passes.

The first and second methods obtain the best answer for the chosen number of expansion terms. However, in the iteration over expansion terms, the most accurate interior boundary fluxes are not necessary. A balance must be obtained between the time of calculation of the most accurate slab boundary fluxes for a certain number of expansion terms and the determination of the number of expansion terms that converge the boundary fluxes. The third method achieves a sufficient balance by estimating the interior slab boundary fluxes and allows the iteration over the number of expansion terms to drive the final boundary fluxes.

With these numerical methods and considerations, a computer program has been written to implement the F_N algorithm. In Chapter 4, the program is verified by performing internal consistency checks and comparisons to standard codes.

Table 3.1: List of Basis Functions and Derivatives

Number	$\psi_\alpha(\nu)$	$\frac{\mathrm{d}}{\mathrm{d}\nu}\psi_\alpha(\nu)$
1	$P_\alpha(2\nu-1)$	$\frac{2\alpha}{1-(2\nu-1)^2}\left[\psi_{\alpha-1}(\nu)-(2\nu-1)\psi_\alpha(\nu)\right]$
2	$P_\alpha(2\nu^\gamma-1)$	$\frac{2\nu^{\gamma-1}\alpha\gamma}{1-(2\nu^\gamma-1)^2}\left[\psi_{\alpha-1}(\nu)-(2\nu^\gamma-1)\psi_\alpha(\nu)\right]$
3	ν^α	$\alpha\psi_{\alpha-1}(\nu)$
4	$(2\nu^\gamma-1)^\alpha$	$2\nu^{\gamma-1}\alpha\gamma\psi_{\alpha-1}(\nu)$

CHAPTER 4

PROGRAM VERIFICATION

Three separate programs are available for application of the F_N algorithm. The MGSLAB program is for heterogeneous media and a single slab for the galactic cosmic ray cascade source. The MGSEMI program is for a homogeneous semi-infinite media. The FNCRIT program, for verification only, determines the critical slab thickness and fluxes for a single slab and energy group. Even though the FNCRIT program is not applied to the galactic cosmic ray cascade problem, it is included in the F_N algorithm package created. These programs must be verified internally and against other verified and accepted programs. Section 4.1 describes the internal verifications performed and associated results. Section 4.2 describes the external verifications performed and associated results.

In this chapter, it will be shown that the MGSLAB, MGSEMI, and FNCRIT programs are internally consistent and any discrepancies between these programs and ANISN/PC (the program used for external verification) are well understood and fully explained. Therefore, the programs are viable tools that can be used to analyze the galactic cosmic ray cascade and other problems.

4.1 Internal Verification

Various measures are used to verify that the heterogeneous finite and homogeneous semi-infinite mathematical models are programmed properly in MGSLAB and MGSEMI. FNCRIT is not internally verified because it is the MGSLAB program with modifications necessary for inclusion of the critical slab calculation. The first and most important internal verification is the proper compilation of the programs. In this and all other sections, it is assumed that the programs are compiled and linked properly.

Six measures are used to verify proper programming. The first measure is verification of faster convergence rates and more accurate fluxes for increasingly accurate computed integral terms. When the integrals in equations (2.20) are computed with higher accuracy, the F_N algorithm should converge with fewer expansion terms and the fluxes calculated should be more precise. The next measure is more accurate and consistent fluxes for a decrease in convergence tolerance. As the precision of the converged fluxes is increased, by decreasing the convergence tolerance, the fluxes should approach the same value. The third measure is a consistent number of expansion terms for convergence with variation in the initial number of expansion terms. The problem should converge with the same number of expansion terms without regard to the initial number of expansion terms. The next measure is consistent fluxes with variation in basis functions. The resultant fluxes should be the same no matter what basis function are used. The

next measure is verification of a faster convergence rate for an increase in the number of passes for the internal slab boundaries. As the internal slab boundary fluxes approach their true values, the number of expansion terms for convergence should decrease. The last measure is consistent fluxes when slab boundary flux calculations are compared to slab interior flux edits. The algorithm should calculate the same fluxes whether the interior or boundary formulation is used.

4.1.1 Variation of the Number of Points Used in Quadrature Integrations

As the number of quadrature points is increased for the matrix element integral evaluations, the fluxes should become more accurate, and the F_N algorithm should converge faster because fewer expansion terms are required. This is investigated by increasing the number of quadratures points for the matrix element integrals, and noting the number of expansion terms required for convergence.

The physical problem being analyzed for MGSLAB and MGSEMI is a single energy group problem with a beam source of unit strength normally incident on the left face of the slab. For MGSLAB, a single slab one centimeter thick is used. The total cross section is 1.0 cm^{-1} and the scattering cross section is 0.99 $cm - steradian^{-1}$. Shifted Legendre polynomials, $P_\alpha(2\mu - 1)$, are the basis functions. The convergence tolerance is 10^{-6}.

The number of quadrature points is increased from five to ninety as shown in Tables 4.1 and 4.2 for the MGSLAB and MGSEMI programs, respectively. From these tables, as the integral evaluation becomes more accurate, fewer expansion

terms are required for convergence of the problem and the fluxes become more accurate.

4.1.2 Variation of the Convergence Tolerance

The iteration scheme which determines the final number of expansion terms used in the F_N algorithm is controlled by the convergence tolerance. A relative flux is calculated between successive iterations and compared to this tolerance at every edited spatial and angular point. As this tolerance is decreased, the fluxes should approach the same value. This is investigated by decreasing the convergence tolerance and comparing fluxes at three different spatial points and one angular point.

The same physical model is analyzed as above. The number of quadrature points used for the matrix elements integrals is thirty-five. The reported fluxes are converted to units of flux per steradian.

The convergence tolerance is decreased from 10^{-2} to 2×10^{-8} and compared at $\mu = 0.5$ for $x = 0.25$, 0.50, and 0.75 centimeters as shown in Tables 4.3 and 4.4 for the MGSLAB and MGSEMI programs, respectively. From these tables, as the convergence tolerance is decreased, the fluxes converge to the same number.

4.1.3 Variation of the Initial Number of Expansion Terms

The iteration scheme which determines the final number of expansion terms used in the F_N algorithm must start with an initial number of expansion terms.

For a single slab, the convergence properties should not be a function of the number of terms used to start the iteration. This is investigated by varying the initial number of expansion terms and noting the number of terms required for convergence.

Using the same physical model as described in the sections above, the initial number of expansion terms is increased from three to twenty-one as shown in Tables 4.5 and 4.6 for the MGSLAB and MGSEMI programs, respectively. From these tables, as the initial number of expansion terms is varied, the number of terms required for problem convergence does not vary.

4.1.4 Variation of the Basis Functions

As the basis functions are changed, the fluxes should remain the same. This is investigated by varying the basis functions and comparing the resultant fluxes. The basis functions being varied are the modified Legendre polynomials, $P_\alpha(2\mu^\gamma - 1)$, where γ is a value between 0 and 1. The same physical problem above is being analyzed.

The adjustable parameter, γ, is varied from 0.70 to 1.0 for MGSLAB and 0.65 to 1.0 for MGSEMI as shown in Tables 4.7 and 4.8 for the MGSLAB and MGSEMI programs, respectively. From these tables, the fluxes are the same no matter what basis function is used. The number of expansion terms required to converge the problem however, varied depending on the basis function used. This is an expected result.

4.1.5 Variation of the Number of Inner Slab Boundary Iterations

For multiple slabs, an inner iteration which estimates the interior slab interface fluxes is used to accelerate convergence in N. With each execution of the F_N algorithm over the slabs without changing the number of expansion terms, the interior slab interface fluxes approach the true fluxes. Therefore, as the number of inner iterations is increased, the F_N algorithm should converge faster by requiring fewer number of expansion terms for problem convergence. This is investigated by increasing the number of inner iterations and noting the number of expansion terms required for convergence.

The physical problem being analyzed for MGSLAB is a single energy group problem with a beam source of unit strength normally incident on the left media face. Four, one centimeter thick slabs of the same material used in the previous verifications is specified. The convergence tolerance is 10^{-4}.

The number inner iterations is increased from one to five as shown in Table 4.9. From this table, as the number of inner iterations is increased, fewer expansion terms are required for problem convergence.

4.1.6 Variation of the Number of Slabs and Interior Points

Whether the F_N algorithm determines the fluxes at interior slab (edit) points or at slab interfaces, the final flux value should be the same. This is investigated by executing MGSLAB with one energy group and four slabs of the same material with no interior points and with one slab with three interior points.

The same physical problem analyzed above is used.

The results are shown in Table 4.10. From this table, the flux values are identical whether calculated as slab interface points or interior slab points.

4.2 External Verifications

In the last section, it was shown that the mathematical model is programmed properly. This section shows some of the verifications used to compare the F_N algorithm to ANISN/PC (Reference [25]) which is a one dimensional, anisotropic, multigroup, S_N transport code for the PC computing environment. ANISN/PC has been modified to execute on a VAX/VMS machine, a DEC ALPHA machine with the OPENVMS operating system, and all UNIX machines.

4.2.1 Finite Slab Comparison

The MGSLAB and ANISN/PC programs are used to determine the fluxes for all combinations of one to three energy groups and one to three slabs for an incident beam of unit strength and an exponential distributed source of the form e^{-x}. The exponentially source is fit with a cubic spline and the source term integrals evaluated with a Gauss-Legendre quadrature order of fifty-six. For all cases, the transport media is one centimeter thick. For two slabs, the slab thicknesses are 0.4 cm and 0.6 cm. For three slabs, the slab thicknesses are 0.2 cm, 0.4 cm, and 0.4 cm. The convergence tolerance is 10^{-4}. The number of quadrature

points for the matrix elements and the boundary terms is thirty-five. The ANISN/PC program is executed with sixteen discrete angles and 100 mesh cells. The number of direction edit points in MGSLAB are thirty-two and the number of slab position edit points is forty for a single slab, fifty for two slabs, and sixty for three slabs. The beam source incident on the left side of the transport media is directed along the closest discrete angle represented in ANISN/PC to the normal at the slab face. A slim, 10^{-6} cm, vacuum slab is constructed in the ANISN/PC model to contain the shell source which models the delta function source used in MGSLAB.

The cross section sets used are consistent for all cases. For the first region or slab, the cross sections are

g	σ_g^1	$\sigma_{1\to g}^1$	$\sigma_{2\to g}^1$	$\sigma_{3\to g}^1$
1	2.0	1.0	0.0	0.0
2	5.0	1.0	3.0	0.0
3	3.0	0.1	0.2	1.5

For the second region or slab, the cross sections are

g	σ_g^2	$\sigma_{1\to g}^2$	$\sigma_{2\to g}^2$	$\sigma_{3\to g}^2$
1	5.0	3.0	0.0	0.0
2	2.0	0.5	1.0	0.0
3	3.0	0.4	0.1	1.0

For the third region or slab, the cross sections are

g	σ_g^3	$\sigma_{1\to g}^3$	$\sigma_{2\to g}^3$	$\sigma_{3\to g}^3$
1	3.0	2.8	0.0	0.0
2	2.0	0.1	0.9	0.0
3	5.0	0.9	0.9	1.0

To transform the angular fluxes into consistent units of particles per square centimeter per second per steradian for comparison, the ANISN/PC values are divided by 4π, and the F_N values are divided by 2π.

The comparison between ANISN/PC and MGSLAB angular and scalar fluxes for three groups and three slabs with a beam source are shown as an example in Figures 4.1 and 4.2. Figures 4.3 and 4.4 show the example comparison plots for the distributed source. The lines represent the MGSLAB fluxes, and the symbols are the ANISN/PC fluxes. For each group, the slab boundary fluxes at 0.0 cm, 0.2 cm, 0.6 cm, and 1.0 cm along with the fluxes at the slab centers of 0.1 cm, 0.4 cm, and 0.8 cm are shown on the angular flux plots. The MGSLAB angular fluxes match the ANISN/PC angular fluxes except along the direction of the beam source. This is because ANISN/PC prints the collided and uncollided angular fluxes added together, whereas, theoretically, the uncollided flux along the beam at the left slab face is infinite and exponentially decreases inside the slab. This effects the scalar flux in group one because ANISN/PC is trying to model the delta function source. Figure 4.2 shows this discrepancy. When a distributed source is used, as in Figure 4.4, this problem is not encountered.

From the example plots shown and those not shown, MGSLAB and ANISN/PC generate the same fluxes for the same physical problem. This verifies that MGSLAB can be used as a tool for solving heterogeneous slab neutral particle transport problems.

4.2.2 Semi-infinite Media Comparisons

The MGSEMI and ANISN/PC programs are used to determine the fluxes for a semi-infinite slab with the same beam source used in the finite slab comparison. Only one region is used, but one to three energy groups are compared. The same cross sections are used as in the finite slab case. The ANISN/PC and MGSEMI angular flux values are compared only at the slab boundary. The scalar flux values are not compared. The limited comparison is due to the ANISN/PC program generating results that are influenced by the rightmost boundary and the beam source. To overcome this limitation, the slab thickness in ANISN/PC is greatly increased. Figure 4.5 shows an example comparison plot for three groups. The group one fluxes are not identical, but have the same shape. The group two and three fluxes are approximately the same. The discrepancy in group one is mainly due to the beam source delta function problems as seen in the finite slab case. The delta function is smeared out over all angles because of the infinite extent of the slab for the scattering process, unlike the finite slab case.

From the example plots shown and those not shown, MGSEMI and ANISN/PC generate the same fluxes for the same physical problem. This verifies that MGSEMI can be used as a tool for solving homogeneous semi-infinite media neutral particle transport problems.

4.2.3 Critical Slab Comparisons

The FNCRIT and ANISN/PC programs are used to determine critical slab thicknesses and resultant angular and scalar fluxes for two different cross sections and various discrete ordinates, S_N. The physical problem being analyzed is a single energy group, single finite slab whose thickness is determined by the amount of material necessary to achieve a self-sustaining neutron population. The material is defined by the total to scatter plus fission cross section ratio, c.

Table 4.11 shows the critical slab thickness as calculated by the programs. Figures 4.6 through 4.9 show example angular and scalar comparison plots for the S_{32} and cross sections of 1.6 and 1.1.

A normalization scheme is required to enable comparison between FNCRIT and ANISN/PC. The normalization is performed in FNCRIT and sets its scalar flux at $x = 0$ equal to the ANISN/PC scalar flux. The normalization parameter in FNCRIT is the a_0 parameter as discussed in Section A.8.2. The analytical scalar flux at $x = 0$ for the F_N method is

$$\phi_{\text{fn}}(0) \;=\; \frac{c}{2} a_0 \;\equiv\; \phi_{\text{anisn}}(0) \tag{4.1a}$$

The scale parameter, a_0, is solved for and used in the FNCRIT program. This requires the ANISN/PC problem to be executed before the FNCRIT program.

From the example plots shown and those not shown, FNCRIT and ANISN/PC generate the same fluxes, for discrete ordinates of large order, for the same physical problem. This verifies that FNCRIT can be used as a tool for solving

critical thickness problems which is realized, will not be part of a spacecraft shielding problem.

4.2.4 Scientific Literature Comparisons

The last comparison is with calculations in the scientific literature. In Reference [12], two problems are analyzed with the F_N method. The first problem contains pathological cross sections. The cross sections contain a degenerate eigenvalue and a self scatter cross section of zero. A degenerate eigenvalue is a singularity problem encountered in the energy group particle transfer equations, equations (2.25), when $s_{gg'\nu} = \nu_0^g$. The self scatter cross section being equal to zero creates another singularity in the energy group particle transfer equations, equations (2.24). The forerunner to MGSLAB is used to generate the fluxes for this cross section set. Because the degenerate eigenvalue derivation is dependent on a special case that will not manifest itself in most real material cross sections, the algorithm was not included in the current version of MGSLAB. The second problem is an analysis of gamma rays interacting with an iron slab. The original literature only included the angular fluxes at the slab boundaries; therefore, only these values are shown. Tables 4.12 through 4.15 show the pathological cross section boundary fluxes. Tables 4.16 through 4.19 show the iron slab boundary fluxes. These tables compare exactly, to a specified tolerance, with the fluxes in Reference [12]. This verifies that F_N method as implemented in this dissertation is proper and can be used to solve neutral particle transport problems like the

galactic cosmic ray cascade.

Table 4.1: Variation of Matrix Element Integral Quadrature to Determine the Number of Expansion Terms for Convergence for MGSLAB

Integral Quadrature	Expansion Terms	Flux at $\mu = 0.5$		
		$x = 0.25$ cm	$x = 0.50$ cm	$x = 0.75$ cm
5	51	3.63639E-1	5.70638E-1	6.48887E-1
10	47	3.63458E-1	5.70738E-1	6.49061E-1
15	47	3.83459E-1	5.70738E-1	6.49060E-1
25	41	3.63459E-1	5.70738E-1	6.49060E-1
50	41	3.63459E-1	5.70738E-1	6.49060E-1
90	41	3.63459E-1	5.70738E-1	6.49060E-1

Table 4.2: Variation of Matrix Element Integral Quadrature to Determine the Number of Expansion Terms for Convergence for MGSEMI

Integral Quadrature	Expansion Terms	Flux at $\mu = 0.5$		
		$x = 0.25$ cm	$x = 0.50$ cm	$x = 0.75$ cm
5	47	1.29453	2.26721	2.98061
10	45	1.29428	2.26730	2.98071
15	39	1.29428	2.26730	2.98072
25	39	1.29428	2.26730	2.98072
50	39	1.29428	2.26730	2.98071
90	39	1.29428	2.26730	2.98071

Table 4.3: Variation of Convergence Tolerance and the Resultant Fluxes for MGSLAB

Convergence Tolerance	Expansion Terms	Flux at $\mu = 0.5$		
		$x = 0.25$ cm	$x = 0.50$ cm	$x = 0.75$ cm
1.0e-2	13	5.7864393E-02	9.0835148E-02	1.0329645E-01
1.0e-3	15	5.7834357E-02	9.0839556E-02	1.0330132E-01
1.0e-4	23	5.7847281E-02	9.0836134E-02	1.0330116E-01
1.0e-5	31	5.7846122E-02	9.0835786E-02	1.0330109E-01
1.0e-6	41	5.7846242E-02	9.0835738E-02	1.0330110E-01
1.0e-7	59	5.7846255E-02	9.0835744E-02	1.0330110E-01
2.0e-8	81	5.7846256E-02	9.0835744E-02	1.0330110E-01

Table 4.4: Variation of Convergence Tolerance and the Resultant Fluxes for MGSEMI

Convergence Tolerance	Expansion Terms	Flux at $\mu = 0.5$		
		$x = 0.25$ cm	$x = 0.50$ cm	$x = 0.75$ cm
1.0e-2	9	2.0583760E-01	3.6091514E-01	4.7444385E-01
1.0e-3	13	2.0601616E-01	3.6085225E-01	4.7438955E-01
1.0e-4	21	2.0598931E-01	3.6085700E-01	4.7439580E-01
1.0e-5	29	2.0599167E-01	3.6085168E-01	4.7439558E-01
1.0e-6	39	2.0599147E-01	3.6085199E-01	4.7439553E-01
1.0e-7	49	2.0599145E-01	3.6085198E-01	4.7439552E-01
2.0e-8	81	2.0599145E-01	3.6085198E-01	4.7439552E-01

Table 4.5: Variation of the Initial Number of Expansion Terms and the Number of Expansion Terms for Convergence for MGSLAB

Initial Number of Expansion Terms	Number of Expansion Terms for Convergence
3	29
7	29
11	29
15	29
21	29

Table 4.6: Variation of the Initial Number of Expansion Terms and the Number of Expansion Terms for Convergence for MGSEMI

Initial Number of Expansion Terms	Number of Expansion Terms for Convergence
3	29
7	29
11	29
15	29
21	29

Table 4.7: Variation of Basis Functions in Determining the Fluxes for MGSLAB

$P_\alpha(2\mu^\gamma - 1)$ γ	Expansion Terms	Flux at $\mu = 0.5$		
		$x = 0.25$ cm	$x = 0.50$ cm	$x = 0.75$ cm
0.70	33	3.63459E-1	5.70738E-1	6.49060E-1
0.75	29	3.63459E-1	5.70738E-1	6.49060E-1
0.80	31	3.63459E-1	5.70738E-1	6.49060E-1
0.85	31	3.63459E-1	5.70738E-1	6.49060E-1
0.90	31	3.63459E-1	5.70738E-1	6.49060E-1
0.95	35	3.63459E-1	5.70738E-1	6.49060E-1
1.00	41	3.63459E-1	5.70738E-1	6.49060E-1

Table 4.8: Variation of Basis Functions in Determining the Fluxes for MGSEMI

$P_\alpha(2\mu^\gamma - 1)$ γ	Expansion Terms	Flux at $\mu = 0.5$		
		$x = 0.25$ cm	$x = 0.50$ cm	$x = 0.75$ cm
0.65	33	1.29428	2.26730	2.98071
0.70	27	1.29428	2.26730	2.98071
0.75	29	1.29428	2.26730	2.98071
0.80	27	1.29428	2.26730	2.98071
0.85	27	1.29428	2.26730	2.98071
0.90	31	1.29428	2.26730	2.98071
0.95	33	1.29428	2.26730	2.98071
1.00	39	1.29428	2.26730	2.98071

Table 4.9: Variation of the Number of Iterations on Interior Slab Interfaces and the Number of Expansion Terms for Convergence

Number of Inner Iterations	Expansion Terms for Convergence	Flux at $\mu = 0.5$		
		$x = 1.0$ cm	$x = 2.0$ cm	$x = 3.0$ cm
1	31	1.0247E-1	1.5446E-2	2.3006E-2
2	27	1.0247E-1	1.5446E-2	2.3006E-2
3	25	1.0247E-1	1.5446E-2	2.3006E-2
4	25	1.0247E-1	1.5446E-2	2.3006E-2
5	23	1.0247E-1	1.5446E-2	2.3006E-2

Table 4.10: Comparison of Fluxes from a Four Slab Geometry versus a Single Slab with Three Interior Points at a Tolerance of 1.0×10^{-6}

Geometry	Flux at $\mu = 0.5$			
	$x = 0.25$cm	$x = 0.50$cm	$x = 0.75$cm	$x = 1.00$cm
4 Slabs	3.63459E-1	5.70738E-1	6.49060E-1	6.24782E-1
1 Slab	3.63459E-1	5.70738E-1	6.49060E-1	6.24782E-1

Table 4.11: Critical Slab Thickness for the FNCRIT and ANISN/PC Programs

Quadrature and Cross Section	FNCRIT in cm	ANISN/PC in cm
S_8 and $c = 1.6$	1.02392597657862	1.04069
S_{16} and $c = 1.6$	1.02392597657862	1.02701
S_{32} and $c = 1.6$	1.02392597657862	1.02476
S_{32} and $c = 1.1$	4.22661933230336	4.22834

Table 4.12: Left Boundary Angular Flux Values for the Pathological Cross Section Problem

	μ					
g	0.05	0.1	0.2	0.3	0.4	0.5
1	1.2813(-1)[1]	1.1660(-1)	1.0041(-1)	8.8866(-2)	7.9986(-2)	7.2858(-2)
2	7.7363(-2)	7.1154(-2)	6.2123(-2)	5.5490(-2)	5.0281(-2)	4.6037(-2)
3	5.6265(-2)	5.2399(-2)	4.6539(-2)	4.2071(-2)	3.8471(-2)	3.5481(-2)
4	4.5318(-2)	4.2624(-2)	3.8381(-2)	3.5035(-2)	3.2276(-2)	2.9946(-2)
5	3.8517(-2)	3.6527(-2)	3.3272(-2)	3.0621(-2)	2.8389(-2)	2.6473(-2)
6	3.3837(-2)	3.2315(-2)	2.9729(-2)	2.7556(-2)	2.5689(-2)	2.4062(-2)
7	3.0396(-2)	2.9207(-2)	2.7105(-2)	2.5284(-2)	2.3687(-2)	2.2276(-2)
8	2.7746(-2)	2.6806(-2)	2.5072(-2)	2.3521(-2)	2.2134(-2)	2.0891(-2)
9	2.5634(-2)	2.4886(-2)	2.3442(-2)	2.2106(-2)	2.0887(-2)	1.9779(-2)
10	2.3904(-2)	2.3310(-2)	2.2099(-2)	2.0939(-2)	1.9859(-2)	1.8864(-2)
11	2.2458(-2)	2.1988(-2)	2.0970(-2)	1.9957(-2)	1.8994(-2)	1.8094(-2)
12	2.1228(-2)	2.0861(-2)	2.0004(-2)	1.9116(-2)	1.8253(-2)	1.7435(-2)
13	2.0166(-2)	1.9885(-2)	1.9166(-2)	1.8385(-2)	1.7609(-2)	1.6862(-2)
14	1.9238(-2)	1.9031(-2)	1.8430(-2)	1.7743(-2)	1.7042(-2)	1.6359(-2)
15	1.7895(-5)	1.7895(-5)	1.7895(-5)	1.7895(-5)	1.7894(-5)	1.7894(-5)
16	9.1193(-3)	9.1021(-3)	8.9941(-3)	8.8398(-3)	8.6638(-3)	8.4777(-3)

[1] Read as 1.2813×10^{-1}

Table 4.13: Left Boundary Angular Flux Values for the Pathological Cross Section Problem — *Continued*

	μ				
g	0.6	0.7	0.8	0.9	1.0
1	6.6973(-2)	6.2013(-2)	5.7767(-2)	5.4084(-2)	5.0857(-2)
2	4.2494(-2)	3.9480(-2)	3.6881(-2)	3.4613(-2)	3.2615(-2)
3	3.2946(-2)	3.0763(-2)	2.8861(-2)	2.7186(-2)	2.5699(-2)
4	2.7943(-2)	2.6199(-2)	2.4666(-2)	2.3306(-2)	2.2090(-2)
5	2.4806(-2)	2.3341(-2)	2.2042(-2)	2.0881(-2)	1.9838(-2)
6	2.2631(-2)	2.1361(-2)	2.0226(-2)	1.9206(-2)	1.8284(-2)
7	2.1021(-2)	1.9897(-2)	1.8886(-2)	1.7971(-2)	1.7140(-2)
8	1.9773(-2)	1.8764(-2)	1.7850(-2)	1.7019(-2)	1.6260(-2)
9	1.8773(-2)	1.7858(-2)	1.7023(-2)	1.6259(-2)	1.5558(-2)
10	1.7951(-2)	1.7113(-2)	1.6344(-2)	1.5637(-2)	1.4985(-2)
11	1.7260(-2)	1.6488(-2)	1.5775(-2)	1.5116(-2)	1.4506(-2)
12	1.6669(-2)	1.5954(-2)	1.5290(-2)	1.4673(-2)	1.4100(-2)
13	1.6156(-2)	1.5492(-2)	1.4871(-2)	1.4291(-2)	1.3749(-2)
14	1.5705(-2)	1.5086(-2)	1.4503(-2)	1.3956(-2)	1.3441(-2)
15	1.7894(-5)	1.7894(-5)	1.7893(-5)	1.7893(-5)	1.7893(-5)
16	8.2879(-3)	8.0983(-3)	7.9110(-3)	7.7276(-3)	7.5489(-3)

Table 4.14: Right Boundary Angular Flux Values for the Pathological Cross Section Problem

g	μ					
	0.05	0.1	0.2	0.3	0.4	0.5
1	4.5701(-7)	4.8998(-7)	5.6471(-7)	6.5894(-7)	7.8516(-7)	9.6666(-7)
2	7.3831(-7)	7.9749(-7)	9.2983(-7)	1.0958(-6)	1.3185(-6)	1.6409(-6)
3	9.6077(-7)	1.0392(-6)	1.2115(-6)	1.4230(-6)	1.7003(-6)	2.0893(-6)
4	1.1809(-6)	1.2788(-6)	1.4910(-6)	1.7477(-6)	2.0786(-6)	2.5330(-6)
5	1.4023(-6)	1.5200(-6)	1.7726(-6)	2.0744(-6)	2.4585(-6)	2.9771(-6)
6	1.6263(-6)	1.7641(-6)	2.0575(-6)	2.4046(-6)	2.8416(-6)	3.4235(-6)
7	1.8529(-6)	2.0112(-6)	2.3460(-6)	2.7385(-6)	3.2281(-6)	3.8724(-6)
8	2.0822(-6)	2.2612(-6)	2.6377(-6)	3.0759(-6)	3.6177(-6)	4.3236(-6)
9	2.3135(-6)	2.5137(-6)	2.9322(-6)	3.4160(-6)	4.0098(-6)	4.7762(-6)
10	2.5465(-6)	2.7679(-6)	3.2287(-6)	3.7581(-6)	4.4034(-6)	5.2293(-6)
11	2.7806(-6)	3.0234(-6)	3.5265(-6)	4.1013(-6)	4.7976(-6)	5.6820(-6)
12	3.0152(-6)	3.2794(-6)	3.8250(-6)	4.4449(-6)	5.1916(-6)	6.1333(-6)
13	3.2497(-6)	3.5354(-6)	4.1232(-6)	4.7880(-6)	5.5843(-6)	6.5821(-6)
14	3.4835(-6)	3.7907(-6)	4.4206(-6)	5.1297(-6)	5.9749(-6)	7.0275(-6)
15	2.3398(-9)	2.3402(-9)	2.3410(-9)	2.3419(-9)	2.3427(-9)	2.3435(-9)
16	1.2655(-6)	1.3423(-6)	1.4865(-6)	1.6302(-6)	1.7799(-6)	1.9399(-6)

Table 4.15: Right Boundary Angular Flux Values for the Pathological Cross Section Problem — *Continued*

	μ				
g	0.6	0.7	0.8	0.9	1.0
1	1.2644(-6)	1.9188(-6)	3.8488(-6)	9.6935(-6)	2.5162(-5)
2	2.1567(-6)	3.0745(-6)	4.7969(-6)	7.9539(-6)	1.3354(-5)
3	2.6827(-6)	3.6719(-6)	5.4072(-6)	8.4198(-6)	1.3377(-5)
4	3.2046(-6)	4.2769(-6)	6.0732(-6)	9.0719(-6)	1.3866(-5)
5	3.7257(-6)	4.8834(-6)	6.7563(-6)	9.7887(-6)	1.4525(-5)
6	4.2475(-6)	5.4902(-6)	7.4451(-6)	1.0532(-5)	1.5262(-5)
7	4.7704(-6)	6.0965(-6)	8.1350(-6)	1.1287(-5)	1.6036(-5)
8	5.2938(-6)	6.7014(-6)	8.8230(-6)	1.2045(-5)	1.6828(-5)
9	5.8170(-6)	7.3039(-6)	9.5070(-6)	1.2799(-5)	1.7625(-5)
10	6.3390(-6)	7.9030(-6)	1.0185(-5)	1.3548(-5)	1.8421(-5)
11	6.8589(-6)	8.4974(-6)	1.0857(-5)	1.4288(-5)	1.9209(-5)
12	7.3754(-6)	9.0859(-6)	1.1519(-5)	1.5018(-5)	1.9985(-5)
13	7.8876(-6)	9.6676(-6)	1.2172(-5)	1.5734(-5)	2.0749(-5)
14	8.3944(-6)	1.0241(-5)	1.2813(-5)	1.6437(-5)	2.1495(-5)
15	2.3443(-9)	2.3450(-9)	2.3458(-9)	2.3466(-9)	2.3474(-9)
16	2.1142(-6)	2.3070(-6)	2.5235(-6)	2.7700(-6)	3.0545(-6)

Table 4.16: Left Boundary Angular Flux Values for the Iron Slab Problem

	μ					
g	0.05	0.1	0.2	0.3	0.4	0.5
1	2.6676(-2)	2.3995(-2)	2.0336(-2)	1.7801(-2)	1.5889(-2)	1.4378(-2)
2	5.2111(-2)	4.7223(-2)	4.0437(-2)	3.5657(-2)	3.2006(-2)	2.9093(-2)
3	3.7432(-2)	3.4273(-2)	2.9767(-2)	2.6511(-2)	2.3980(-2)	2.1931(-2)
4	3.6376(-2)	3.3630(-2)	2.9604(-2)	2.6618(-2)	2.4253(-2)	2.2312(-2)
5	3.5820(-2)	3.3465(-2)	2.9892(-2)	2.7159(-2)	2.4947(-2)	2.3100(-2)
6	3.6063(-2)	3.4070(-2)	3.0917(-2)	2.8411(-2)	2.6329(-2)	2.4556(-2)
7	2.4795(-2)	2.3650(-2)	2.1757(-2)	2.0194(-2)	1.8861(-2)	1.7704(-2)
8	2.6132(-2)	2.5122(-2)	2.3376(-2)	2.1882(-2)	2.0576(-2)	1.9421(-2)
9	2.8500(-2)	2.7614(-2)	2.5995(-2)	2.4547(-2)	2.3245(-2)	2.2069(-2)
10	3.2597(-2)	3.1830(-2)	3.0318(-2)	2.8889(-2)	2.7560(-2)	2.6330(-2)
11	3.9796(-2)	3.9167(-2)	3.7765(-2)	3.6333(-2)	3.4940(-2)	3.3610(-2)
12	5.1910(-2)	5.1584(-2)	5.0494(-2)	4.9168(-2)	4.7762(-2)	4.6346(-2)
13	1.5781(-2)	1.6779(-2)	1.7971(-2)	1.8609(-2)	1.8935(-2)	1.9064(-2)
14	1.3336(-2)	1.4244(-2)	1.5458(-2)	1.6229(-2)	1.6731(-2)	1.7049(-2)
15	8.8737(-3)	9.4910(-3)	1.0406(-2)	1.1073(-2)	1.1575(-2)	1.1959(-2)
16	2.3930(-3)	2.5592(-3)	2.8282(-3)	3.0458(-3)	3.2278(-3)	3.3821(-3)
17	6.0379(-4)	6.4190(-4)	7.0559(-4)	7.5958(-4)	8.0700(-4)	8.4932(-4)
18	4.0769(-5)	4.3372(-5)	4.7756(-5)	5.1532(-5)	5.4913(-5)	5.7999(-5)
19	6.1145(-6)	6.4725(-6)	7.0782(-6)	7.6032(-6)	8.0771(-6)	8.5134(-6)

Table 4.17: Left Boundary Angular Flux Values for the Iron Slab Problem — *Continued*

	μ				
g	0.6	0.7	0.8	0.9	1.0
1	1.3145(-2)	1.2117(-2)	1.1244(-2)	1.0492(-2)	9.8369(-3)
2	2.6698(-2)	2.4687(-2)	2.2970(-2)	2.1485(-2)	2.0185(-2)
3	2.0228(-2)	1.8784(-2)	1.7541(-2)	1.6459(-2)	1.5507(-2)
4	2.0679(-2)	1.9282(-2)	1.8071(-2)	1.7008(-2)	1.6067(-2)
5	2.1526(-2)	2.0165(-2)	1.8972(-2)	1.7918(-2)	1.6979(-2)
6	2.3021(-2)	2.1676(-2)	2.0485(-2)	1.9422(-2)	1.8467(-2)
7	1.6688(-2)	1.5785(-2)	1.4978(-2)	1.4251(-2)	1.3592(-2)
8	1.8392(-2)	1.7468(-2)	1.6633(-2)	1.5874(-2)	1.5183(-2)
9	2.1004(-2)	2.0035(-2)	1.9150(-2)	1.8338(-2)	1.7592(-2)
10	2.5194(-2)	2.4144(-2)	2.3173(-2)	2.2273(-2)	2.1437(-2)
11	3.2352(-2)	3.1167(-2)	3.0054(-2)	2.9009(-2)	2.8027(-2)
12	4.4954(-2)	4.3603(-2)	4.2303(-2)	4.1057(-2)	3.9867(-2)
13	1.9060(-2)	1.8967(-2)	1.8810(-2)	1.8608(-2)	1.8376(-2)
14	1.7237(-2)	1.7329(-2)	1.7348(-2)	1.7312(-2)	1.7235(-2)
15	1.2252(-2)	1.2473(-2)	1.2636(-2)	1.2753(-2)	1.2832(-2)
16	3.5139(-3)	3.6268(-3)	3.7236(-3)	3.8067(-3)	3.8779(-3)
17	8.8743(-4)	9.2194(-4)	9.5330(-4)	9.8188(-4)	1.0080(-3)
18	6.0844(-5)	6.3487(-5)	6.5953(-5)	6.8263(-5)	7.0432(-5)
19	8.9197(-6)	9.3012(-6)	9.6613(-6)	1.0003(-5)	1.0327(-5)

Table 4.18: Right Boundary Angular Flux Values for the Iron Slab Problem

	μ					
g	0.05	0.1	0.2	0.3	0.4	0.5
1	4.6286(-5)	4.9431(-5)	5.7083(-5)	6.7649(-5)	8.9146(-5)	1.7505(-4)
2	9.8793(-5)	1.0537(-4)	1.2091(-4)	1.4138(-4)	1.7025(-4)	2.1330(-4)
3	8.3317(-5)	8.8923(-5)	1.0170(-4)	1.1787(-4)	1.3969(-4)	1.7073(-4)
4	9.3154(-5)	9.9491(-5)	1.1351(-4)	1.3070(-4)	1.5305(-4)	1.8364(-4)
5	1.0571(-4)	1.1298(-4)	1.2863(-4)	1.4722(-4)	1.7059(-4)	2.0138(-4)
6	1.2265(-4)	1.3119(-4)	1.4907(-4)	1.6967(-4)	1.9472(-4)	2.2656(-4)
7	9.4413(-5)	1.0103(-4)	1.1460(-4)	1.2983(-4)	1.4790(-4)	1.7019(-4)
8	1.0859(-4)	1.1624(-4)	1.3167(-4)	1.4865(-4)	1.6836(-4)	1.9212(-4)
9	1.2831(-4)	1.3739(-4)	1.5538(-4)	1.7478(-4)	1.9680(-4)	2.2274(-4)
10	1.5735(-4)	1.6847(-4)	1.9015(-4)	2.1301(-4)	2.3840(-4)	2.6758(-4)
11	2.0326(-4)	2.1750(-4)	2.4478(-4)	2.7287(-4)	3.0332(-4)	3.3740(-4)
12	2.8111(-4)	3.0041(-4)	3.3661(-4)	3.7286(-4)	4.1102(-4)	4.5244(-4)
13	1.6780(-4)	1.8023(-4)	2.0290(-4)	2.2480(-4)	2.4706(-4)	2.7036(-4)
14	1.5666(-4)	1.6825(-4)	1.8907(-4)	2.0873(-4)	2.2820(-4)	2.4801(-4)
15	1.1581(-4)	1.2400(-4)	1.3847(-4)	1.5181(-4)	1.6465(-4)	1.7733(-4)
16	3.6635(-5)	3.9089(-5)	4.3366(-5)	4.7232(-5)	5.0873(-5)	5.4381(-5)
17	9.5847(-6)	1.0174(-5)	1.1189(-5)	1.2093(-5)	1.2930(-5)	1.3722(-5)
18	6.6624(-7)	7.0823(-7)	7.7968(-7)	8.4231(-7)	8.9961(-7)	9.5318(-7)
19	1.0024(-7)	1.0606(-7)	1.1596(-7)	1.2461(-7)	1.3249(-7)	1.3983(-7)

Table 4.19: Right Boundary Angular Flux Values for the Iron Slab Problem — *Continued*

	μ				
g	0.6	0.7	0.8	0.9	1.0
1	4.8010(-4)	1.2490(-3)	2.7431(-3)	5.1717(-3)	8.6617(-3)
2	2.7680(-4)	3.6438(-4)	4.7562(-4)	6.0693(-4)	7.5306(-4)
3	2.1516(-4)	2.7581(-4)	3.5305(-4)	4.4501(-4)	5.4851(-4)
4	2.2618(-4)	2.8350(-4)	3.5647(-4)	4.4389(-4)	5.4319(-4)
5	2.4288(-4)	2.9791(-4)	3.6772(-4)	4.5175(-4)	5.4802(-4)
6	2.6810(-4)	3.2208(-4)	3.9012(-4)	4.7223(-4)	5.6704(-4)
7	1.9848(-4)	2.3455(-4)	2.7964(-4)	3.3408(-4)	3.9731(-4)
8	2.2158(-4)	2.5850(-4)	3.0422(-4)	3.5935(-4)	4.2364(-4)
9	2.5414(-4)	2.9272(-4)	3.3996(-4)	3.9671(-4)	4.6309(-4)
10	3.0202(-4)	3.4340(-4)	3.9329(-4)	4.5287(-4)	5.2261(-4)
11	3.7652(-4)	4.2228(-4)	4.7635(-4)	5.4016(-4)	6.1467(-4)
12	4.9844(-4)	5.5048(-4)	6.1015(-4)	6.7904(-4)	7.5855(-4)
13	2.9526(-4)	3.2232(-4)	3.5212(-4)	3.8526(-4)	4.2228(-4)
14	2.6857(-4)	2.9022(-4)	3.1330(-4)	3.3815(-4)	3.6512(-4)
15	1.9006(-4)	2.0300(-4)	2.1628(-4)	2.3004(-4)	2.4440(-4)
16	5.7808(-5)	6.1193(-5)	6.4563(-5)	6.7942(-5)	7.1348(-5)
17	1.4483(-5)	1.5219(-5)	1.5937(-5)	1.6641(-5)	1.7335(-5)
18	1.0039(-6)	1.0525(-6)	1.0992(-6)	1.1445(-6)	1.1885(-6)
19	1.4675(-7)	1.5333(-7)	1.5965(-7)	1.6573(-7)	1.7161(-7)

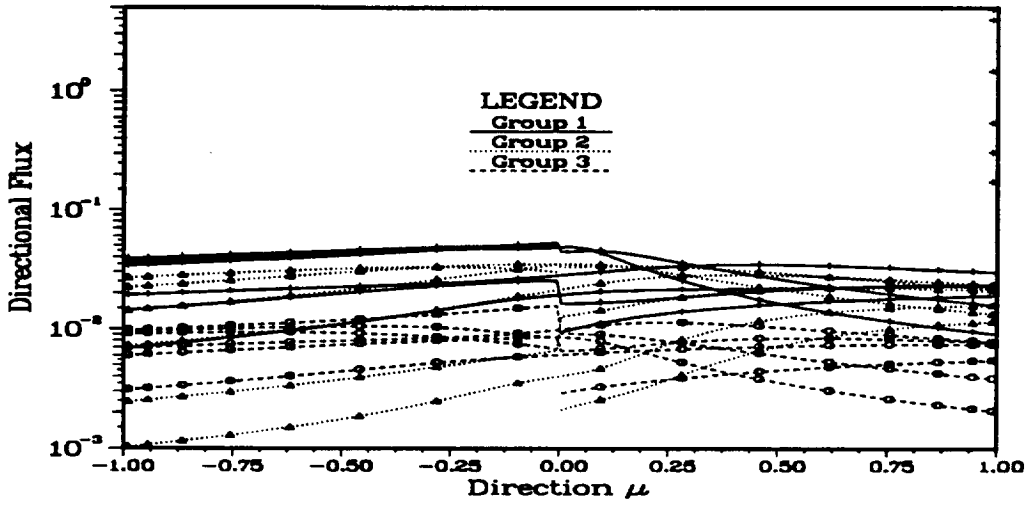

Figure 4.1: ANISN/PC versus MGSLAB Angular Fluxes for Three Regions and Three Energy Groups with a Beam Source at Slab Positions of 0.0 cm, 0.1 cm, 0.2 cm, 0.4 cm, 0.6 cm, 0.8 cm, and 1.0 cm

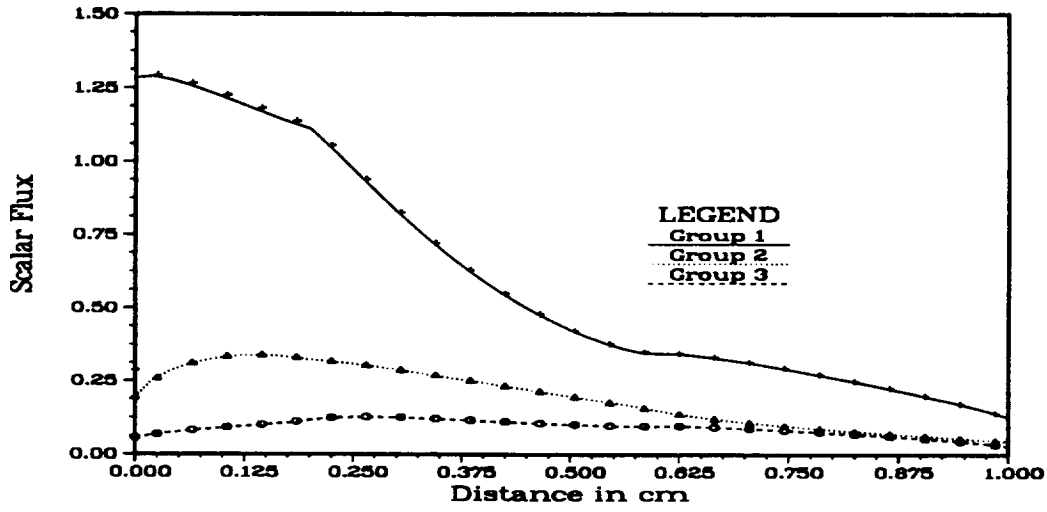

Figure 4.2: ANISN/PC versus MGSLAB Scalar Fluxes for Three Regions and Three Energy Groups with a Beam Source

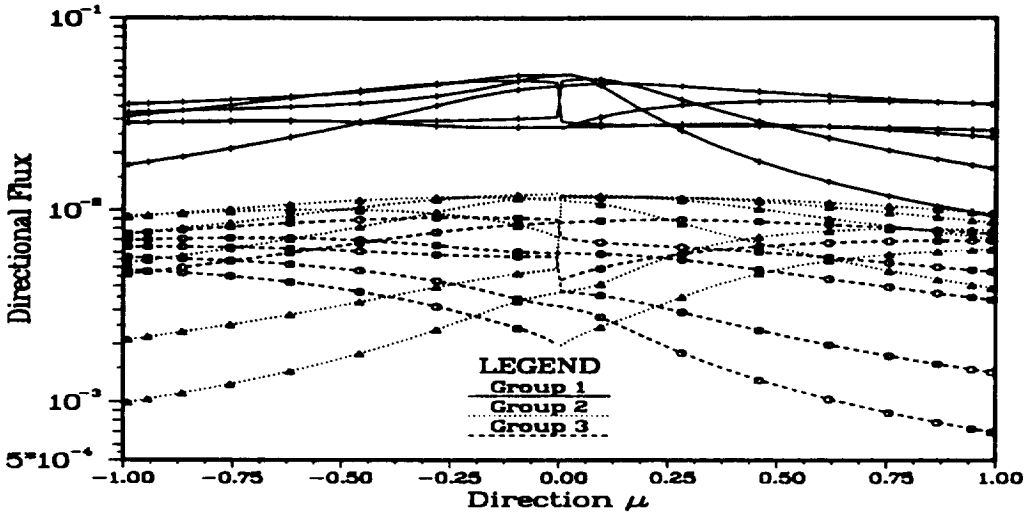

Figure 4.3: ANISN/PC versus MGSLAB Angular Fluxes for Three Regions and Three Energy Groups with a Cubic Spline Fit Distributed Source at Slab Positions of 0.0 cm, 0.1 cm, 0.2 cm, 0.4 cm, 0.6 cm, 0.8 cm, and 1.0 cm

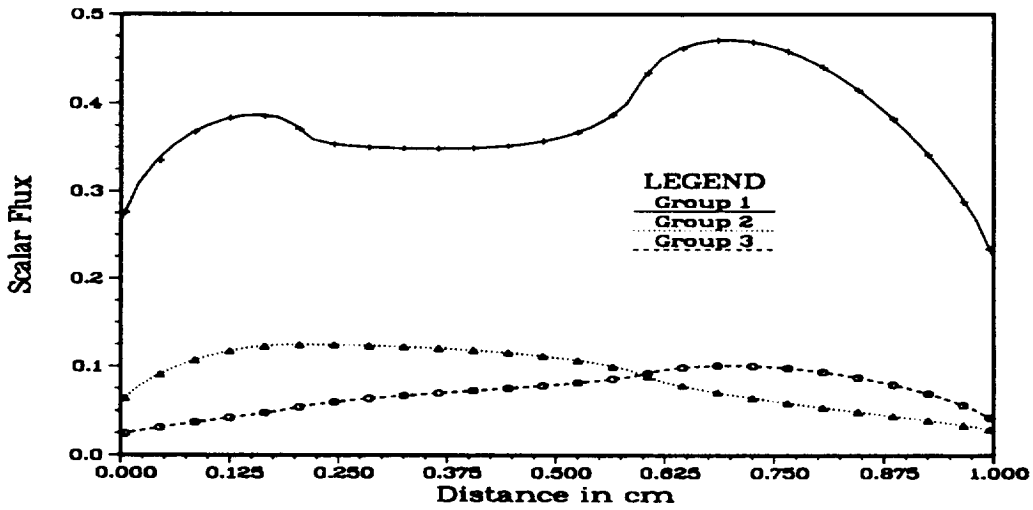

Figure 4.4: ANISN/PC versus MGSLAB Scalar Fluxes for Three Regions and Three Energy Groups with a Cubic Spline Fit Distributed Source

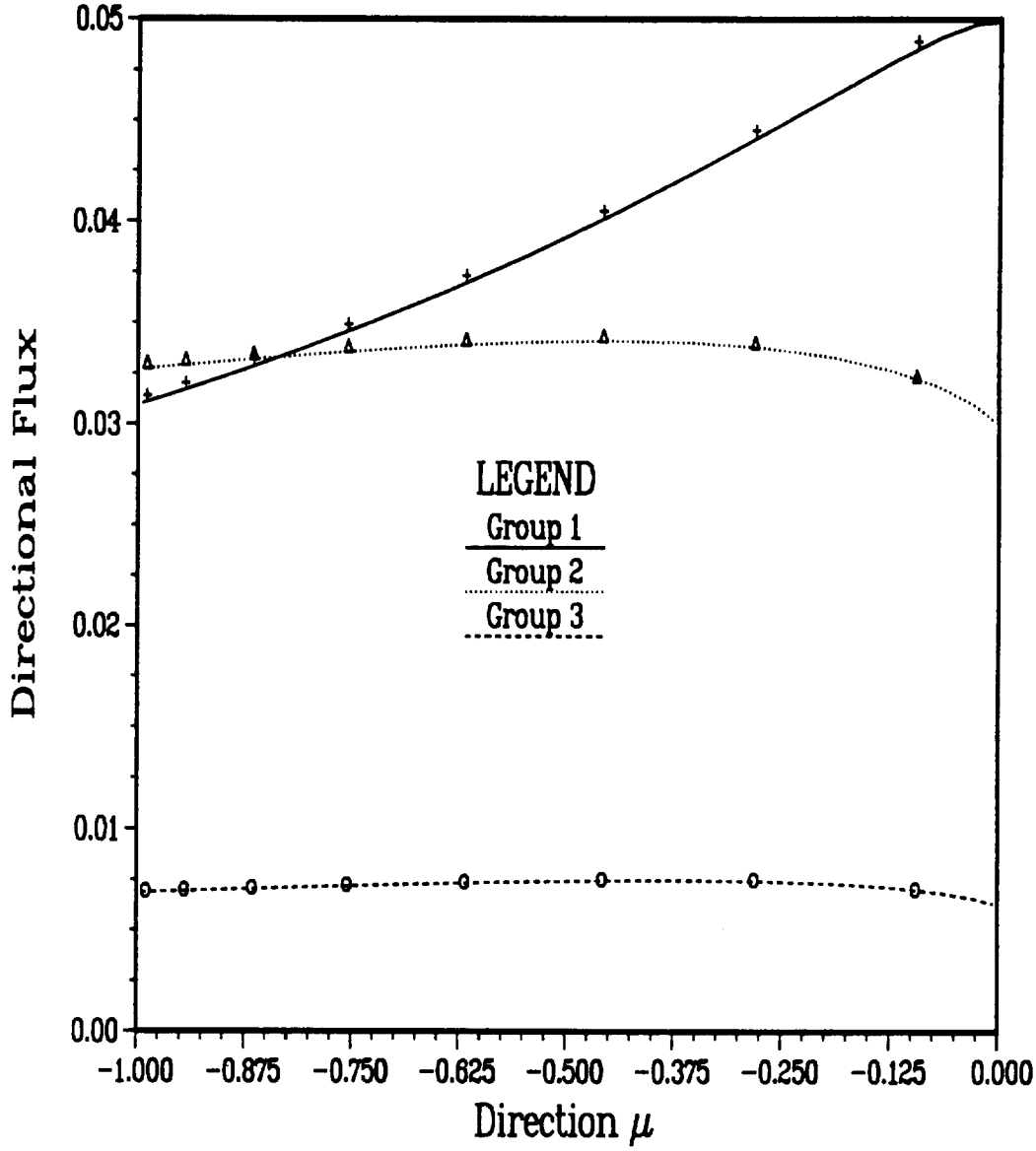

Figure 4.5: ANISN/PC versus MGSEMI Boundary Angular Fluxes for Three Energy Group with a Beam Source at the Boundary

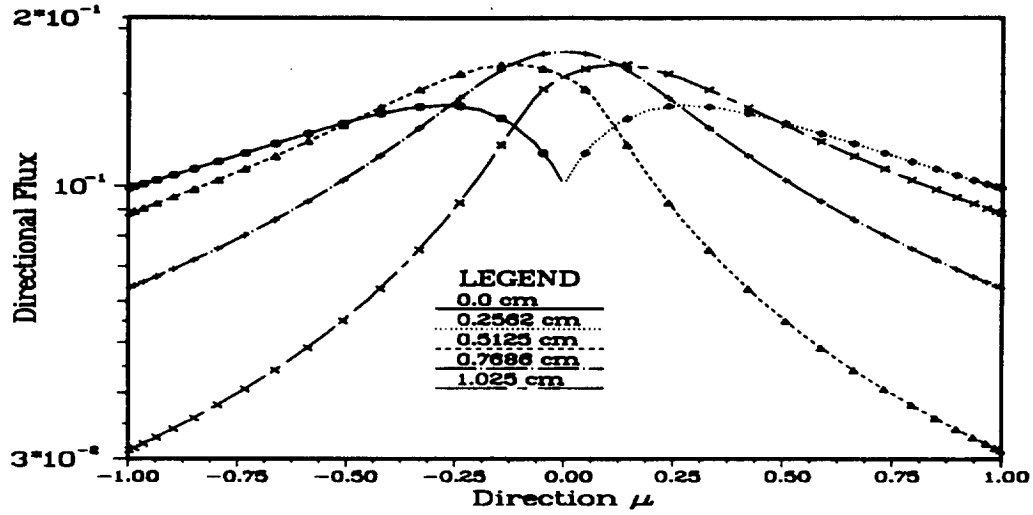

Figure 4.6: ANISN/PC versus FNCRIT Angular Flux Values for an S_{32} Problem and $c = 1.6$

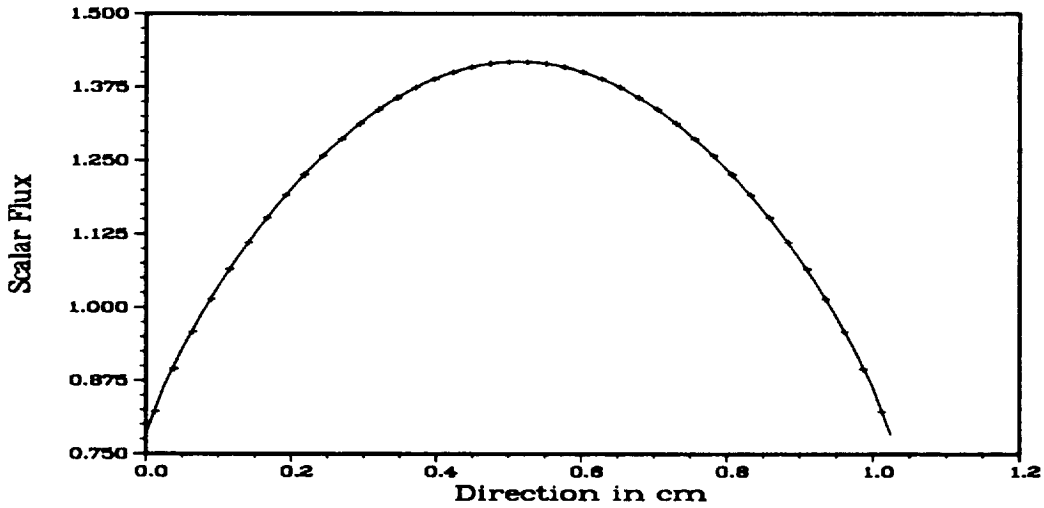

Figure 4.7: ANISN/PC versus FNCRIT Scalar Flux Values for an S_{32} Problem and $c = 1.6$

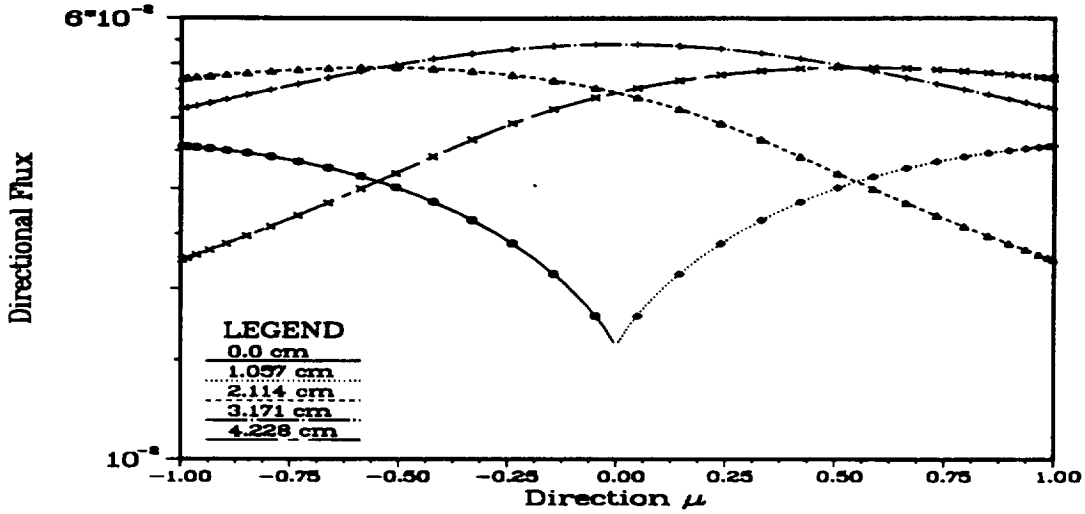

Figure 4.8: ANISN/PC versus FNCRIT Angular Flux Values for an S_{32} Problem and $c = 1.1$

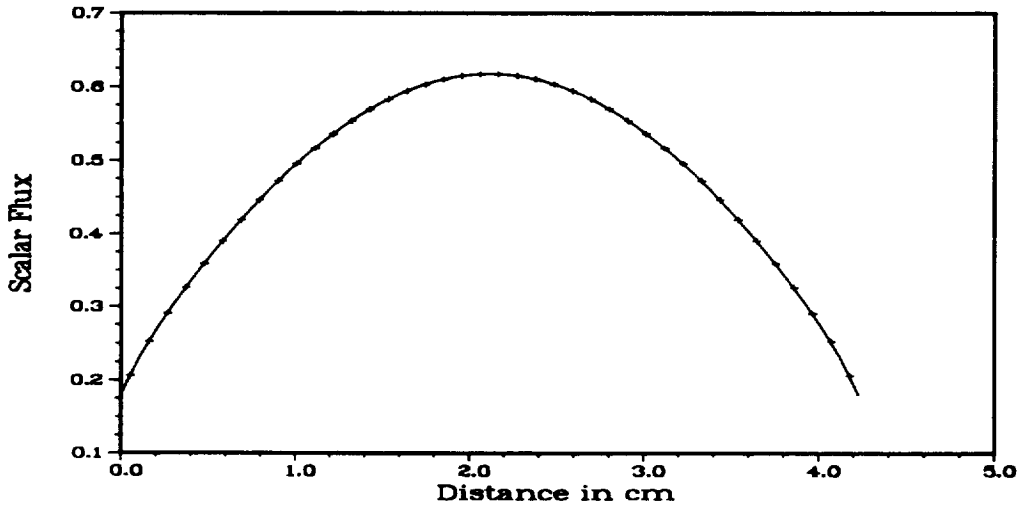

Figure 4.9: ANISN/PC versus FNCRIT Scalar Flux Values for an S_{32} Problem and $c = 1.1$

CHAPTER 5

RESULTS

In Chapter 4, it was shown that the MGSLAB, MGSEMI, and FNCRIT programs generate verifiable results for beam, isotropic, distributed source, and critical slab problems. The MGSEMI and MGSLAB programs are coupled to the galactic ion transport program, GIT, and applied to the galactic cosmic ray cascade problem. The specific cross section, multiplicity, path length, and stopping power models used in the coupled programs are discussed. For all calculations, the target material is aluminum which is composed of 100% Al-27 with a density of 2.696 $\frac{g}{cm^3}$.

5.1 Cross Section and Multiplicity Models

Two cross section models are used in the galactic cosmic ray cascade problem: a nuclear liquid drop model for the GIT program and the ENDF/B V cross sections for the MGSEMI and MGSLAB programs. The liquid drop model can be used in the GIT program because the speed of the interacting ions is assumed to be large.

5.1.1 GIT Cross Sections

In the nuclear liquid drop model, it is assumed that the total nuclear charge is spread uniformly throughout the entire spherical nuclear volume and the nuclear density is constant. From these assumptions, the nuclear volume is proportional to the atomic mass, or $V \propto A$. Therefore, the nuclear radius is proportional to the cube root of the atomic mass, or $R = R_0 \times A^{\frac{1}{3}}$. The speed of the ions is assumed large; therefore, the cross sectional area of the ion nucleus is the cross section of interaction because resonance and quantum effects are negligible. The cross sectional area of the target nucleus is assumed identical for all target nuclei and is not included explicitly in the interaction cross section, but is included in the proportionality constant, R_0. For the liquid drop model, the cross sectional area is proportional to the square of the radius, or $\sigma_j \propto A^{\frac{2}{3}}$. In the GIT model, it is assumed that all ions contain only protons. Thus, A is defined as the charge number, j. The cross section can then be written as

$$\sigma_j = \overline{\sigma} j^{\frac{2}{3}}, \tag{5.1}$$

where, $\overline{\sigma}$ is the proportionality constant or the cross section normalization parameter. From Reference [6], the value of $\overline{\sigma}$ representative of an air shield is $0.01247 \frac{\text{cm}^2}{\text{g}}$. This value accounts for the cross sectional area of the target nuclei and the proportionality constant, R_0, specified above.

To use these cross sections in the MGSEMI and MGSLAB programs, the values are multiplied by the density of the target material. In addition, $\overline{\sigma}$ must be

computed for the target material. The cross section normalization parameter is proportional to the cross sectional area of the target material, $A_{\mathbf{target}}^{\frac{2}{3}}$. The normalization parameter of the new target material can be related to that of an air shield

$$\overline{\sigma}_{\mathbf{target}} = \overline{\sigma}_{\mathbf{air}} \left[\frac{A_{\mathbf{target}}}{A_{\mathbf{air}}} \right]^{\frac{2}{3}}. \tag{5.2}$$

Therefore, the value for $\overline{\sigma}_{\mathrm{Al}}$ is

$$\overline{\sigma}_{\mathrm{Al}} = 0.01247 \left[\frac{27}{14.4} \right]^{\frac{2}{3}} = 0.1896 \frac{\mathrm{cm}^2}{\mathrm{g}}.$$

The above constants are used in the GIT, MGSEMI, and MGSLAB programs to simulate the galactic cosmic ray cascade.

5.1.2 GIT Multiplicities

The GIT cross section model represents the ion interaction probability for the target nuclei. The multiplicity, $\mathrm{M}_{j,k}$, describes the number of j^{th} ions coming from each fragmentation of the k^{th} ion. The charge number of the k^{th} ion must be conserved after the interaction; therefore

$$\mathrm{M}_{j,k} = \begin{cases} \dfrac{2}{k-1} & k > j \\ 0 & k \leq j. \end{cases} \tag{5.3}$$

If the resultant ion charge number is multiplied by the multiplicity term and summed for all resultant ions, the outcome is equal to the charge number of the incoming ion; that is, charge is conserved.

As previously noted, the GIT model does not account for neutrons; however, all ions except hydrogen contain neutrons. The GIT model is modified through the multiplicity term to accept neutrons. This is accomplished by defining a fraction, f_n, of all particles created with a charge of one as neutrons. These neutrons are then given a charge of zero. The value of f_n for the analyses in this dissertation is set at 0.5.

The new multiplicity term for the creation of protons from the fragmentation of ion k is

$$M_{1,k} = (1 - f_n)\frac{2}{k-1}. \tag{5.3b}$$

For neutrons, the multiplicity term is

$$M_{0,k} = f_n\frac{2}{k-1}. \tag{5.4a}$$

The importance of the f_n fraction will be discussed in the conclusions; however, it allows the original GIT model to be used as a starting point for the source used in the neutral particle transport model.

5.1.3 MGSEMI and MGSLAB Cross Sections

A simple and accurate analytical model does not exist for neutron cross sections in Al-27. However, extensive experimental data do exist up to neutron energies of 20 MeV and are provided in the ENDF/B V database. This database is used to generate eleven energy group neutron cross sections for Al-27 with down scattering only. The NJOY program (Reference [26]) accessed and collapsed the

database to create the desired cross sections. Initial ion beams of 20 MeV per nucleon are not typical for the galactic cosmic ray cascade. A typical value is 1000 MeV per nucleon. In order to create a cross section set to match the problem, the ENDF/B V energy group of 10 MeV to 20 MeV is extended to 100 MeV. To create a twelfth energy group, 100 MeV to 1000 MeV, the 20 MeV cross sections were decreased slightly and used. For high energies, these extended cross sections do not represent anything physical, but the point here is to demonstrate behavior, not generate accurate numbers. Table 5.1 shows the energy groups and macroscopic cross sections generated. The eleven group cross section will be referred to as the limited cross section set and the twelve group cross section set will be referred to as the extend cross section set.

5.2 Path Length and Proton Stopping Power Model

The path length and proton stopping power model used in the galactic cosmic ray cascade is based on a parametric form of the proton range, $R_p(E)$, (Reference [27])

$$R_p(E) = \alpha'_0 \ln\left(1 + \alpha'_1 E^{n'_0}\right), \tag{5.5a}$$

where, the parametric constants are

$$\alpha'_0 = 500, \quad \alpha'_1 = 3.66 \times 10^{-6}, \quad \text{and} \quad n'_0 = 1.79. \tag{5.5b}$$

Therefore, from the definition of path length

$$s = s(E_0, E) = R_p(E_0) - R_p(E), \tag{5.6}$$

where, E_0 is the energy of a proton in the initial beam of ions. From this path length, a stopping power can be determined (called the Wilson stopping power),

$$S_P^w(E) = -\frac{dE}{ds} = \frac{1 + \alpha_1' E^{n_0'}}{\alpha_0' \alpha_1' n_0' E^{n_0'-1}}. \tag{5.7}$$

For ease in computation, the Wilson stopping power can be simplified to a linear function of energy by setting n_0' to one and changing the two parametric constants, α_0' and α_1', to reflect the original function value.

The form of this new simplified stopping power, S_P^s, is

$$S_P^s(E) = aE + b \tag{5.8a}$$

where, a and b are to be determined. Because the simplified stopping power is linear, the slope, a, can be extracted from two values of the stopping power known at two different energies. The two stopping powers are determined using the more accurate Wilson stopping power in equation (5.7). Therefore, the slope is

$$a = \frac{S_P^w(E_1) - S_P^w(E_2)}{E_1 - E_2}. \tag{5.8b}$$

A simplified proton range function can be specified for the condition of linearity using the form of equation (5.5a)

$$R_p^s(E) = \alpha_0 \ln(1 + \alpha_1 E), \tag{5.9}$$

where, α_0 and α_1 are the new parametric constants with values that must reflect the original function.

Using this new proton range, the simplified path length is

$$s = R_p(E_0) - \alpha_0 \ln(1 + \alpha_1 E). \tag{5.10}$$

The simplified stopping power is determined from the simplified path length and compared with equation (5.8a)

$$S_p^s(E) = -\frac{dE}{ds} = \frac{1}{\alpha_0} E + \frac{1}{\alpha_0 \alpha_1}; \tag{5.11a}$$

therefore,

$$\alpha_0 = \frac{1}{a} \qquad \text{and} \qquad b = \frac{1}{\alpha_0 \alpha_1}. \tag{5.11b}$$

To determine α_1, the simplified proton range function is evaluated at E_0

$$R_p(E_0) = \alpha_0 \ln(1 + \alpha_1 E_0). \tag{5.12a}$$

If the proton range at E_0 is evaluated using the more accurate formulation in equation (5.5a), then the above equation can be solved for α_1

$$\alpha_1 = -\frac{1 - e^{R_p(E_0)\beta}}{E_0}. \tag{5.12b}$$

To extend this model so it can be used in the MGSEMI and MGSLAB programs, the energy and path length variables must be discretized as explained in Section 5.1.3. This only affects the nomenclature used in the above equations. The variable changes are

$$E \Rightarrow E_g \qquad \text{and} \qquad s \Rightarrow s_g.$$

The simplified stopping power and path length models described above are used in the GIT, MGSEMI, and MGSLAB programs.

5.3 Application to the Galactic Cosmic Ray Cascade

The galactic cosmic ray cascade algorithm will be demonstrated in two ways. The first will be to show examples of the algorithm. A beam of fluorine ions incident on a finite and semi-infinite aluminum slab will be analyzed. The second demonstration will show a study of the transmitted scalar flux for varying thickness of aluminum slabs.

The specific format of the results are the neutron angular, $\phi_g(x,\mu)$, and scalar, $\phi_g(x)$, flux profiles, ion flux profiles, $\psi_j(x,\mathrm{E}_g)$, and GIT source values, $\Psi_g(x)$, for each energy group.

The neutron flux profiles, both angular and scalar, are the primary results for this work. From these profiles, new low energy neutron models can be added to BRYNTRN and verified. Once a suitable model exists for BRYNTRN, the neutron dose rates can then be calculated. The GIT, MGSEMI, and MGSLAB programs have been verified separately (Reference [6] and Chapter 4); therefore, these results are within a specified numerical tolerance within the given physical assumptions.

5.3.1 Demonstration of the Coupled Algorithms

To demonstrate the coupled programs, analyses of a 1000 MeV per nucleon fluorine beam incident on semi-infinite and finite aluminum slabs are performed. To determine the importance of the neutrons with energies above 20 MeV, the extended cross section set is replaced with the limited cross section set and the same analyses are performed again.

5.3.1.1 Semi-infinite and Finite Slab Analysis for the Extended Cross Section Set. A beam of fluorine ions at an energy of 1000 MeV per nucleon are normally incident on a semi-infinite aluminum slab. The resultant ion flux profiles for energies of 999 MeV per nucleon, 100 MeV per nucleon, and 10 MeV per nucleon are shown in Figures 5.1 through 5.3. There is no change in the energy group profiles below 10 MeV per nucleon, therefore they are not shown. The reason they are identical is that the path length or penetration depth, $s(E_0, E)$, is logarithmic with respect to energy and the small energy values, compared to 1000 MeV, do not alter the path length enough to change the flux profiles. The next set of profiles, Figures 5.4 through 5.6, show the neutron source used in the F_N algorithm.

For this example, the F_N algorithm's convergence tolerance is 5.0×10^{-3} to allow group six to converge. To compensate for the low convergence tolerance, the initial number of expansion terms is set to forty-one so that all the other groups converged with a maximum relative error approximately 1.0×10^{-6}. Only two points are slow to converge in group six. This is deemed unimportant to the overall problem allowing the convergence tolerance and initial number of expansion terms fix mentioned above. The reason for the slow convergence rate is due to the formulation of the integral in equation (2.58b). When the interior edit point nears $\frac{s_1}{\rho \bar{\nu}_j}$, the integral value is small and the resultant source is not large enough to let the F_N algorithm converge. The basis functions are modified Legendre polynomials

with γ equal to 0.95. The number of direction edit points is eight which are set to the zeros of the Legendre polynomials. With these parameters, the angular neutron flux profiles at the slab boundary, 100 centimeters, and 200 centimeters are shown in Figures 5.7 through 5.10.

Figure 5.11 shows a three dimensional surface profile of the scalar flux by energy group and position. Forty, evenly spaced internal positions to a depth of 200 centimeters allow a fine enough grid to see the behavior of the neutrons well into the media.

The same set of profiles shown for the semi-infinite media are also shown for a finite slab. Figures 5.12 through 5.14 are the ion flux profiles from 1000 Mev, 100 MeV, and 10 MeV per nucleon. Figures 5.15 through 5.17 show the neutron source used in the F_N algorithm. Some of the parameters are changed for the finite slab case. The slab thickness is 120 centimeters and only twenty internal slab positions are used to determine the scalar flux. The basis functions are the shifted Legendre polynomials. The convergence tolerance is lowered to 2.0×10^{-4} and the initial number of expansion terms is lowered to thirty-one. From these parameters, the angular neutron flux profiles are shown in Figures 5.18 through 5.21. The three dimensional surface profile of the scalar flux is shown in Figure 5.22.

5.3.1.2 Semi-infinite and Finite Slab Analysis for the Limited Cross Section Set. To determine if the created cross sections for energy group twelve are important, the same problems as described above are executed for the limited cross section set

created by NJOY. The first energy group now only represents neutrons with energies between 10 MeV and 20 MeV. The results for the semi-infinite media are shown in Figures 5.23 through 5.33. The results for the finite slab are shown in Figures 5.34 through 5.44.

5.3.1.3 Discussion. This section describes and discusses the profiles identified above. Also, the differences between the limited and extended cross section sets are discussed.

A detailed discussion of the ion flux profiles in Figures 5.1 through 5.3, Figures 5.12 through 5.14, Figures 5.23 through 5.25, and Figures 5.34 through 5.36, is given in Reference [6]; however, several important features of the profiles are highlighted here. Based on the continuous slowing down approximation, as an ion in the incident beam loses a given amount of energy, $(E_0 - E_1)$, the ion traverses a known path length, $s(E_0, E_1)$ or s_1. If the ion has not collided with a target nuclei, the ion travels a distance of $x_J = \frac{s_1}{\rho \bar{\nu}_J}$. The number of ions from the initial beam that have not collided with the target and have slowed down to an energy of E_1 is $e^{-\sigma_J x_J}$. The number of E_1 ions that have fragmented into lighter ions $(0 \leq j \leq J-1)$ at x_J is $\sigma_J \psi_J(x_J, E_1)$ or $\sigma_J e^{-\sigma_J x_J}$. These secondary ions travel a maximum distance of $x_j = \frac{s_1}{\rho \bar{\nu}_j}$ at an energy of E_1. The source of $J-1$ ions can only begin to generate these ions at x_J. Because there is only a point source for $J-1$ ions, the flux profile at energy E_1 decays in the range x_J to x_{J-1}. In this region, the $J-1$ ions continuously generate lighter

ions. As the $J-1$ ion flux decays, the number of $J-2$ ions increases. However, when the source of the $J-2$ ions abates, the $J-2$ ion flux profile decays like the $J-1$ ion profile until it reaches its maximum range. At x_{J-1}, the flux profile for $J-2$ ions has an infinite slope change. This indicates that the source of $J-2$ ions (i.e., those produced by $J-1$ ions only) has gone abruptly to zero. This discontinuity occurs in all flux profiles, but the flux profiles become smoother[1] for the lighter ions because the discontinuous source at ion J (the original cause of the discontinuity) is a smaller fraction of the total source of the lighter ions. These features can be seen in varying detail in all of the ion flux profile plots.

The neutron source profiles in Figures 5.4 through 5.6, Figures 5.15 through 5.17, Figures 5.26 through 5.28, and Figures 5.37 through 5.39, have the same discontinuity as the ion flux profiles except the discontinuities are superimposed on one another throughout the slab because the neutron source at a certain energy is the summation of all higher energy ion sources. If the leading edge of the neutron source profile from Figure 5.4 is magnified, as in Figure 5.45, then the discontinuities can be seen in detail. The discontinuities still occur at $\frac{s_g}{\rho \bar{\nu}_J}$, but the discontinuities for all ions at energy levels above and including group g are superimposed upon one another. The smoothing of the source profiles, as seen in the ion profiles, is also a feature of the neutron source profiles, and is enhanced for the larger energy groups. This enhancement is a result of adding the source from

[1]The discontinuity manifests itself in higher and higher derivatives of the ion flux.

all ions and all higher energy groups together. In the regions of the slab where ions are generating neutrons, the number of neutrons increases. As the source of neutrons stops, the neutrons then start to decrease due to scattering and absorption.

The neutron angular flux profiles in Figures 5.7 through 5.10, Figures 5.18 through 5.21, Figures 5.29 through 5.32, and Figures 5.40 through 5.43, show that the angular fluxes are fairly constant with angle in the slab interiors. If there is a direction preference, then it is in the forward direction, the original direction of the ion beam. The transmitted boundary fluxes for the finite slabs show this forward peak preference to an even greater extent than the interior fluxes. The boundary fluxes for the semi-infinite slabs and the left face reflective fluxes for the finite slabs show a backward peaked flux because of the relative size difference between the aluminum nucleus and the neutron. For the finite slabs, the transmitted fluxes within each energy group are approximately the same value. This is due to the isotropic scattering assumption.

The neutron scalar flux profiles in Figures 5.11, 5.22, 5.33, and 5.44 show that the scalar neutron flux peaks at about fifty centimeters into the slabs in the energy group that represents 0.1 MeV. The placement of the flux peaks within the slab matches that of the source; however, the source is largest in group three.

There is a difference between the fluxes for semi-infinite and finite slabs. The angular fluxes are generally larger within the finite slabs which is due to the

size of the semi-infinite slab. The neutrons have more region to fill, so the numbers of a neutrons at each angle and position is smaller than if a boundary is present.

Upon comparison of the limited cross section fluxes to the extended cross section fluxes (ignoring the first group), the limited fluxes are smaller by a factor of two in the interior and a factor of ten at the boundaries. This emphasizes the need for higher energy cross sections. This will discussed in detail in the conclusions.

5.3.2 Slab Thickness Study

As a practical example in using this algorithm, a study of aluminum slab thickness versus transmitted scalar flux, which can be related to exposure or dose, is undertaken. A convergence tolerance of 10^{-4} is used for the extended cross section set to generate scalar fluxes at the transmission boundary for slabs ranging from thirty-five centimeters to 150 centimeters. Figure 5.46 shows the transmitted fluxes versus slab thickness. It shows an atypical peak around eighty centimeters. Common sense would dictate that as the slab gets thicker, the flux would decrease; however, the physics of the galactic cosmic ray cascade dictates that neutrons are created within the slab instead of at the slab boundary. If the slab is thin, then not enough material exists to create neutrons. If the slab is thick, then enough material exists to shield the neutrons created inside it. If the slab is as thick as where the neutron source peaks, then the transmitted neutron flux is at its highest. The implications to spacecraft design are very important. Certain wall thicknesses could produce larger neutron doses that thinner or thicker walls. The

thickness and material of the shield wall is a critical component to occupant safety which is the reason for the interest in this topic.

Table 5.1: Twelve Group, Extended, Down Scatter Al-27 Macroscopic Neutron Cross Sections Generated from ENDF/B V and NJOY

g	Energy MeV	Total σ_g	$\sigma_{k\to g}$				
			$k=1$	$k=2$	$k=3$	$k=4$	$k=5$
1	1E+3	1.03095-1[1]	4.40101-2				
2	1E+2	1.05095-1	4.06120-2	4.40101-2			
3	1E+1	1.74551-1	8.35890-3	4.06120-2	1.59178-1		
4	1E+0	2.47382-1	6.14990-4	8.35890-3	1.47600-2	2.43442-1	
5	1E-1	2.80333-1	6.85712-6	6.14990-4	2.70893-4	3.89500-3	2.77977-1
6	1E-2	8.97516-2	9.72033-8	6.85712-6	2.98519-6	1.11336-8	2.10545-3
7	1E-3	8.13180-2	1.97605-9	9.72033-8	5.29865-8	1.29161-10	0.0
8	1E-4	8.15770-2	0.0	1.97605-9	1.92298-9	0.0	0.0
9	1E-5	8.24746-2	0.0	0.0	0.0	0.0	0.0
10	1E-6	8.61492-2	0.0	0.0	0.0	0.0	0.0
11	1E-7	9.23780-2	0.0	0.0	0.0	0.0	0.0
12	1E-8	1.17601-1	0.0	0.0	0.0	0.0	0.0

g	Energy MeV	$\sigma_{k\to g}$				
		$k=6$	$k=7$	$k=8$	$k=9$	$k=10$
6	1E-2	8.68781-2				
7	1E-3	2.42815-3	7.87578-2			
8	1E-4	0.0	2.39954-3	7.87638-2		
9	1E-5	0.0	0.0	2.39966-3	7.87698-2	
10	1E-6	0.0	0.0	0.0	2.40032-3	7.67518-2
11	1E-7	0.0	0.0	0.0	0.0	4.58806-3
12	1E-8	0.0	0.0	0.0	0.0	0.0

g	Energy MeV	$\sigma_{k\to g}$	
		$k=11$	$k=12$
11	1E-7	8.17276-2	
12	1E-8	3.58753-4	8.84142-2

[1] Read as 1.03095×10^{-1}

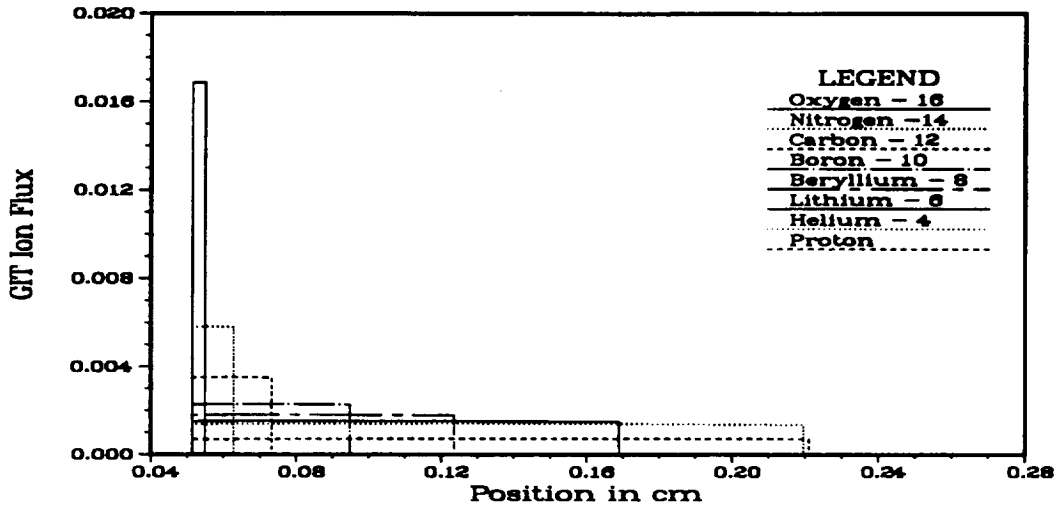

Figure 5.1: GIT Ion Flux Profile for a Fluorine Beam of 1000 MeV per Nucleon at an Energy of 999.0 MeV (Energy Group 1) for a Semi-infinite Aluminum Media using the Extended Cross Section Set

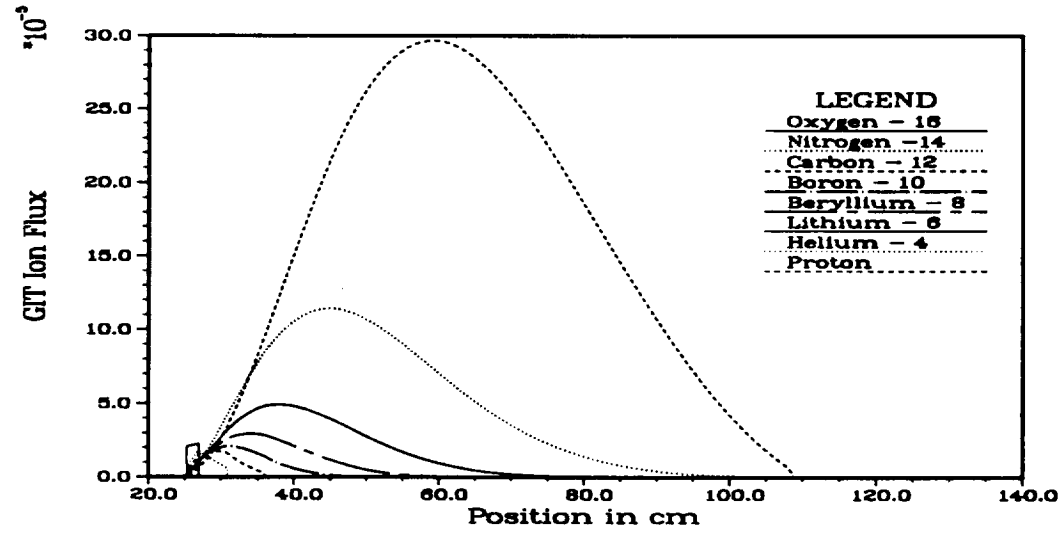

Figure 5.2: GIT Ion Flux Profile for a Fluorine Beam of 1000 MeV per Nucleon at an Energy of 100.0 MeV (Energy Group 2) for a Semi-infinite Aluminum Media using the Extended Cross Section Set

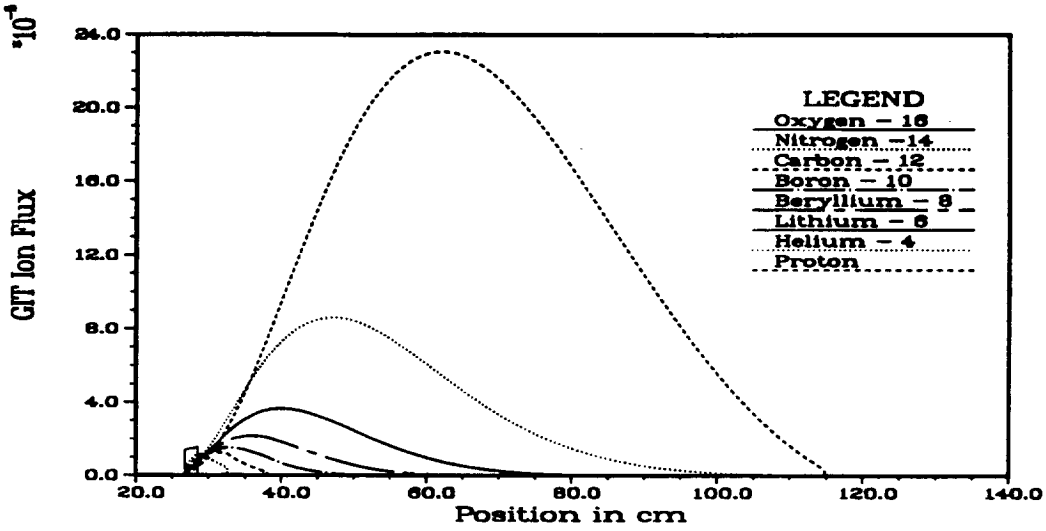

Figure 5.3: GIT Ion Flux Profile for a Fluorine Beam of 1000 MeV per Nucleon at an Energy of 10.0 MeV (Energy Group 3) for a Semi-infinite Aluminum Media using the Extended Cross Section Set

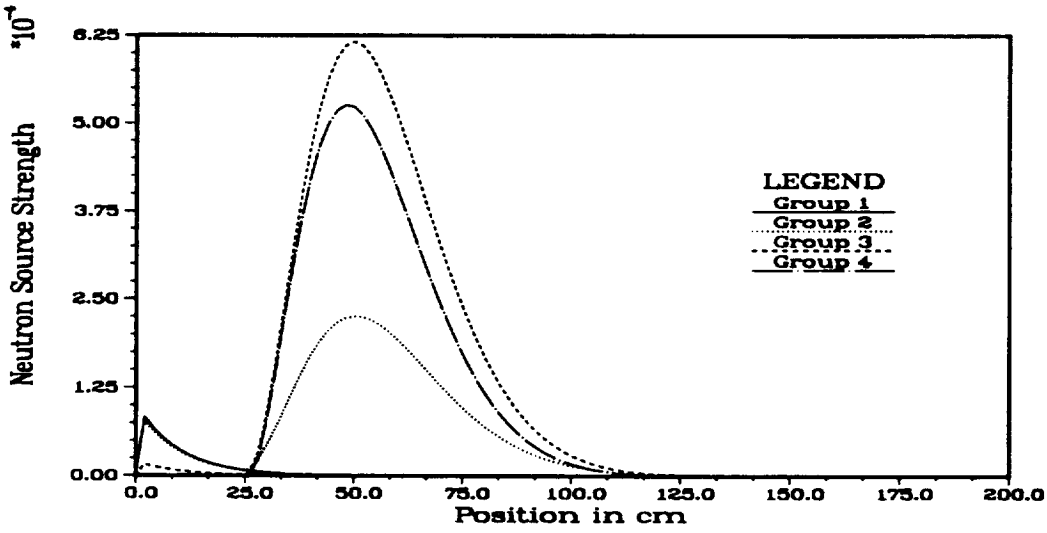

Figure 5.4: GIT Neutron Source Profile for Energy Groups One through Four for a Fluorine Beam of 1000 MeV per Nucleon and a Semi-infinite Aluminum Media using the Extended Cross Section Set

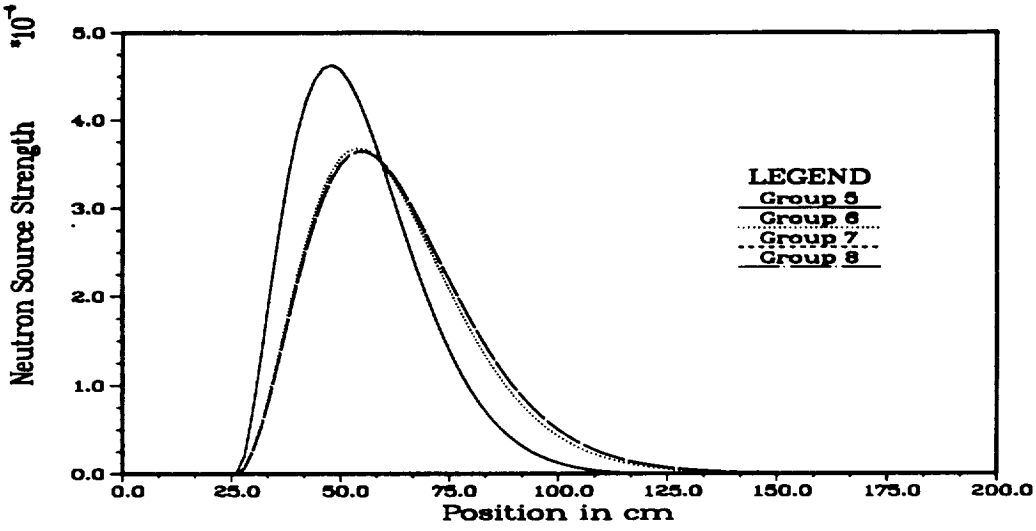

Figure 5.5: GIT Neutron Source Profile for Energy Groups Five through Eight for a Fluorine Beam of 1000 MeV per Nucleon and a Semi-infinite Aluminum Media using the Extended Cross Section Set

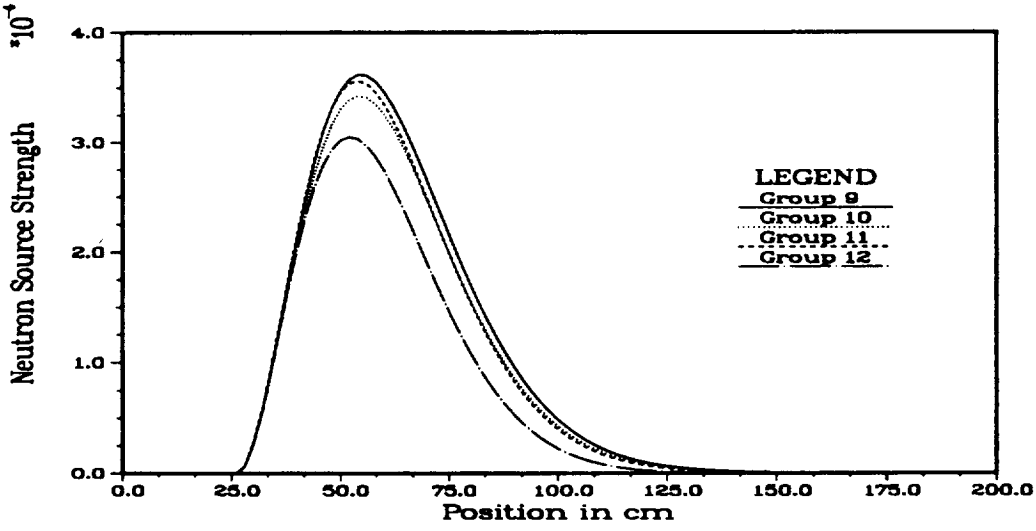

Figure 5.6: GIT Neutron Source Profile for Energy Groups Nine through Twelve for a Fluorine Beam of 1000 MeV per Nucleon and a Semi-infinite Aluminum Media using the Extended Cross Section Set

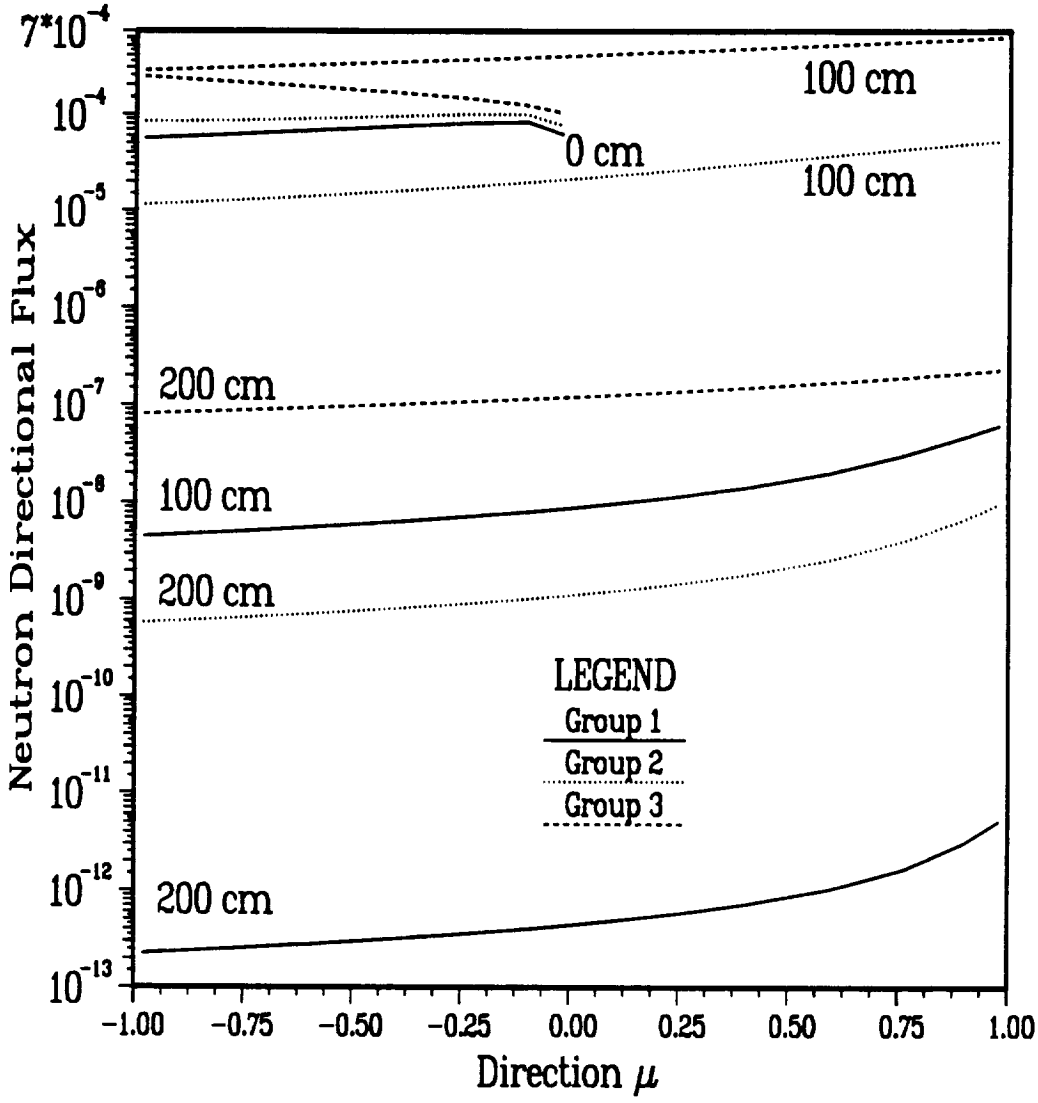

Figure 5.7: Angular Neutron Flux Profile for $x = 0$ cm, $x = 100$ cm, and $x = 200$ cm for Energy Groups One through Three, a Fluorine Beam of 1000 MeV per Nucleon, and a Semi-infinite Aluminum Media using the Extended Cross Section Set

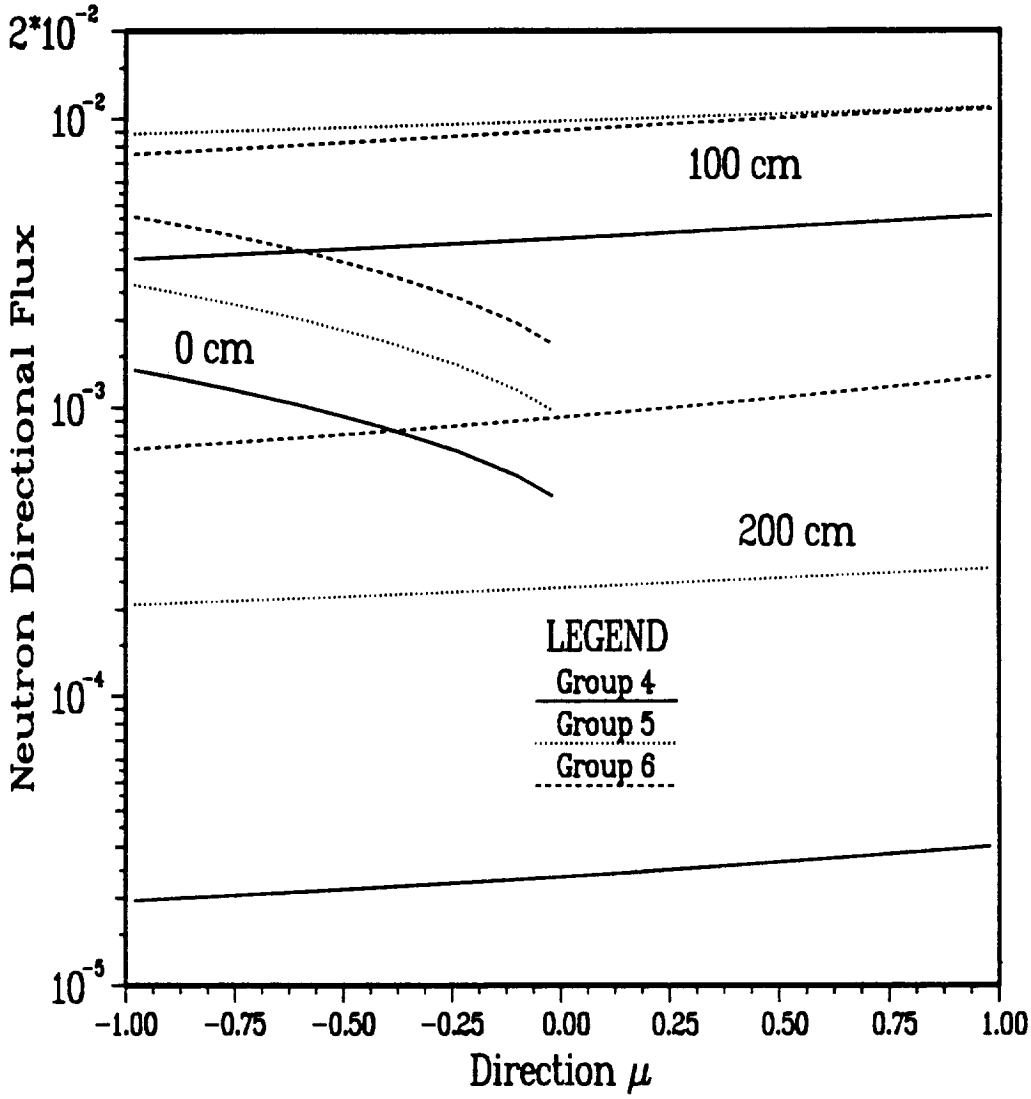

Figure 5.8: Angular Neutron Flux Profile for $x = 0$ cm, $x = 100$ cm, and $x = 200$ cm for Energy Groups Four through Six, a Fluorine Beam of 1000 MeV per Nucleon, and a Semi-infinite Aluminum Media using the Extended Cross Section Set

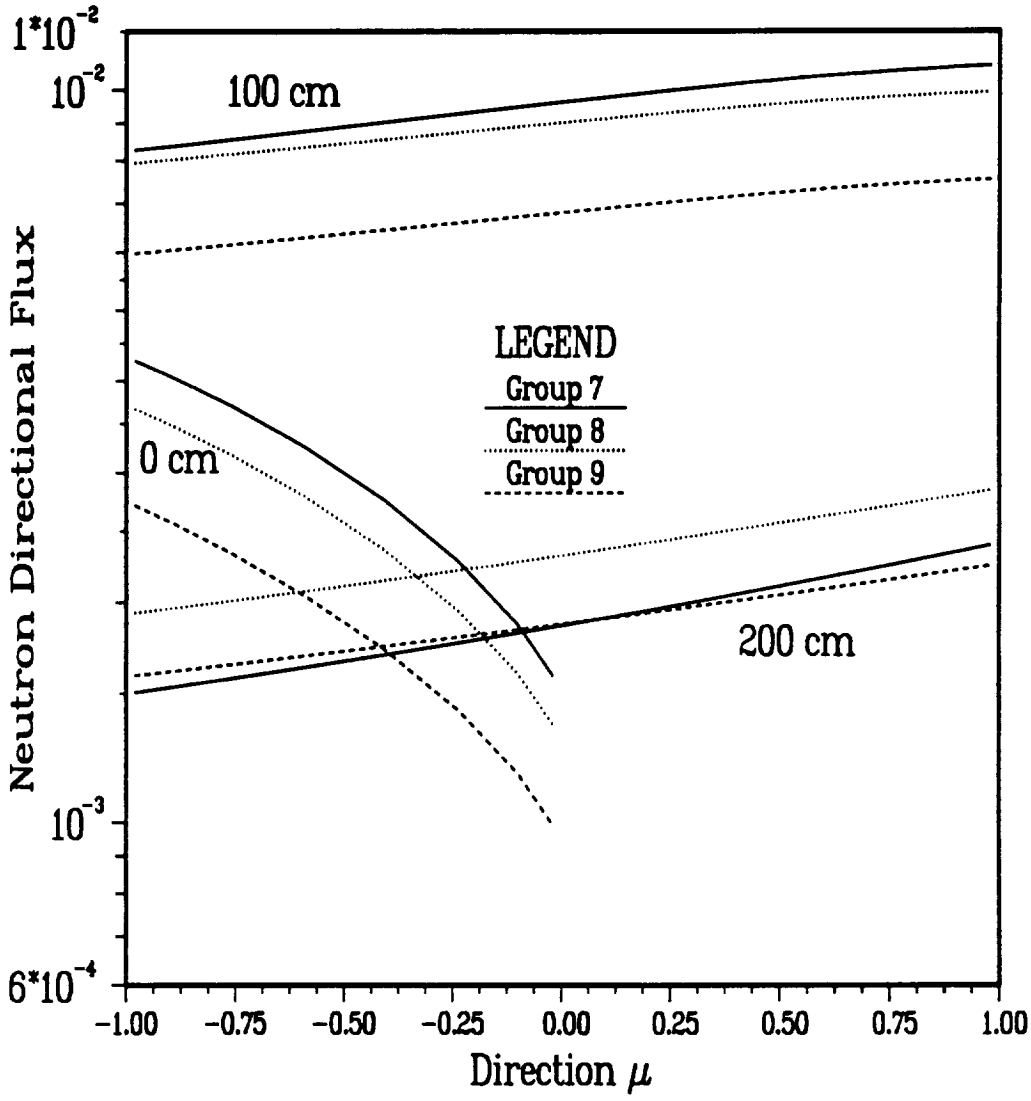

Figure 5.9: Angular Neutron Flux Profile for $x = 0$ cm, $x = 100$ cm, and $x = 200$ cm for Energy Groups Seven through Nine, a Fluorine Beam of 1000 MeV per Nucleon, and a Semi-infinite Aluminum Media using the Extended Cross Section Set

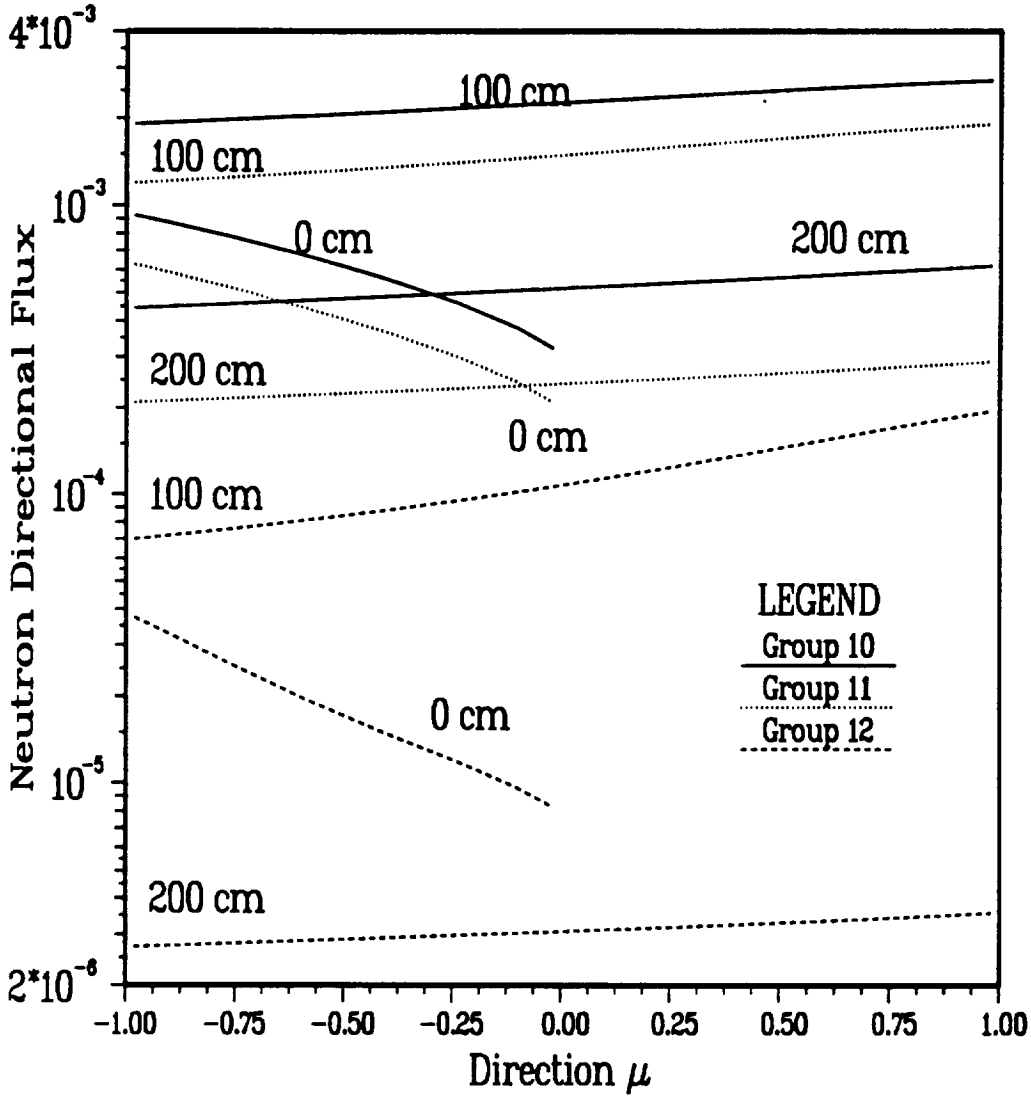

Figure 5.10: Angular Neutron Flux Profile for $x = 0$ cm, $x = 100$ cm, and $x = 200$ cm for Energy Groups Ten through Twelve, a Fluorine Beam of 1000 MeV per Nucleon, and a Semi-infinite Aluminum Media using the Extended Cross Section Set

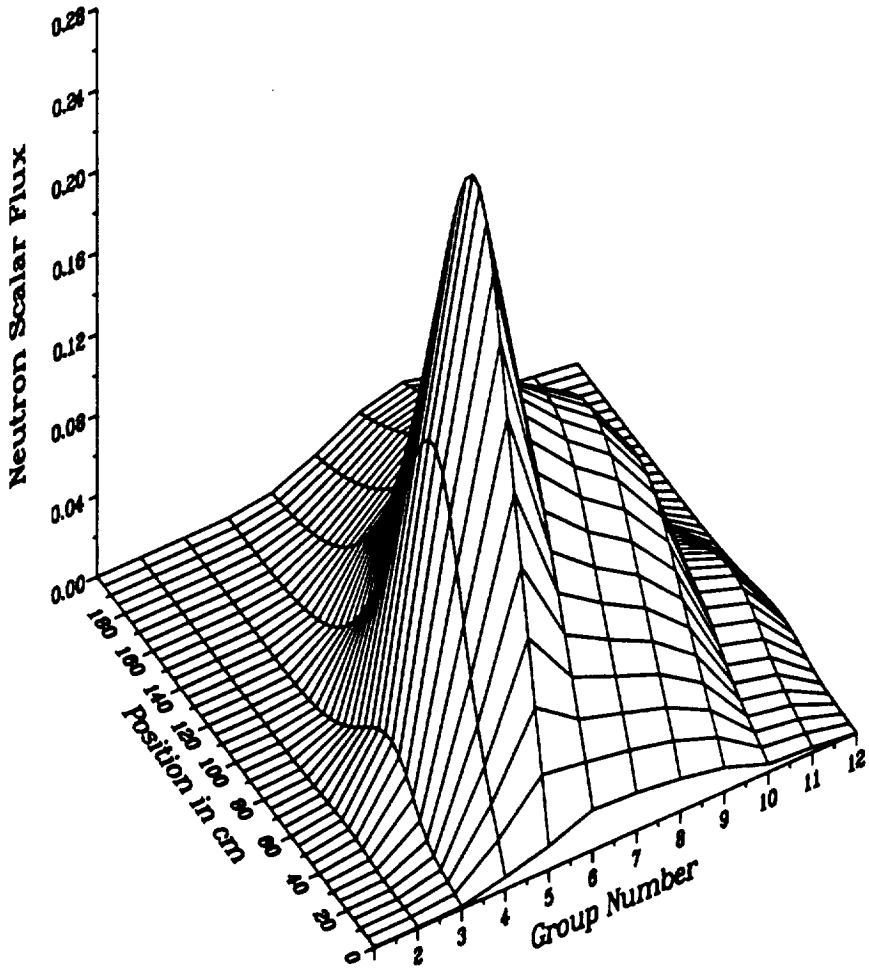

Figure 5.11: Scalar Neutron Flux Profile by Energy Group with a Fluorine Beam of 1000 MeV per Nucleon and a Semi-infinite Aluminum Media using the Extended Cross Section Set

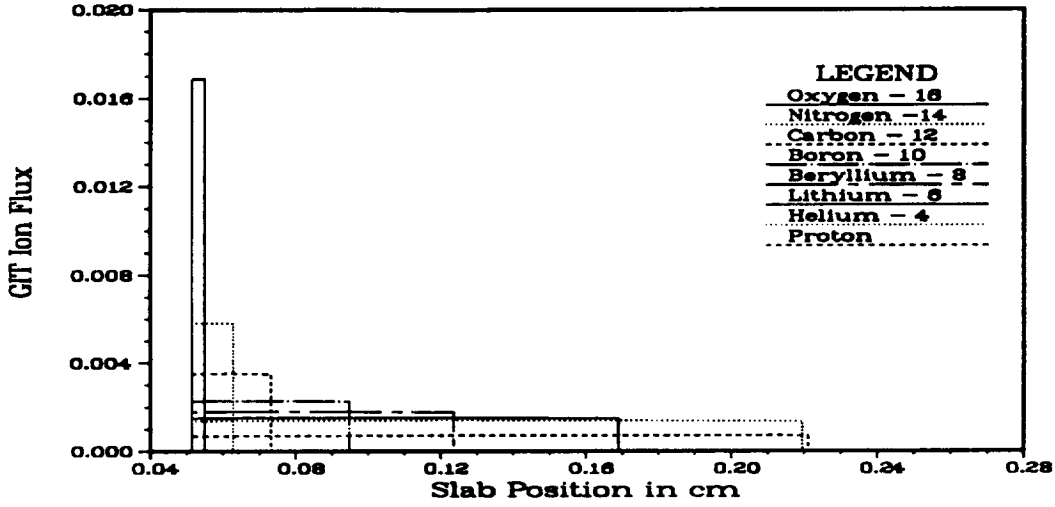

Figure 5.12: GIT Ion Flux Profile for a Fluorine Beam of 1000 MeV per Nucleon at an Energy of 999.0 MeV (Energy Group 1) for a Finite Aluminum Slab using the Extended Cross Section Set

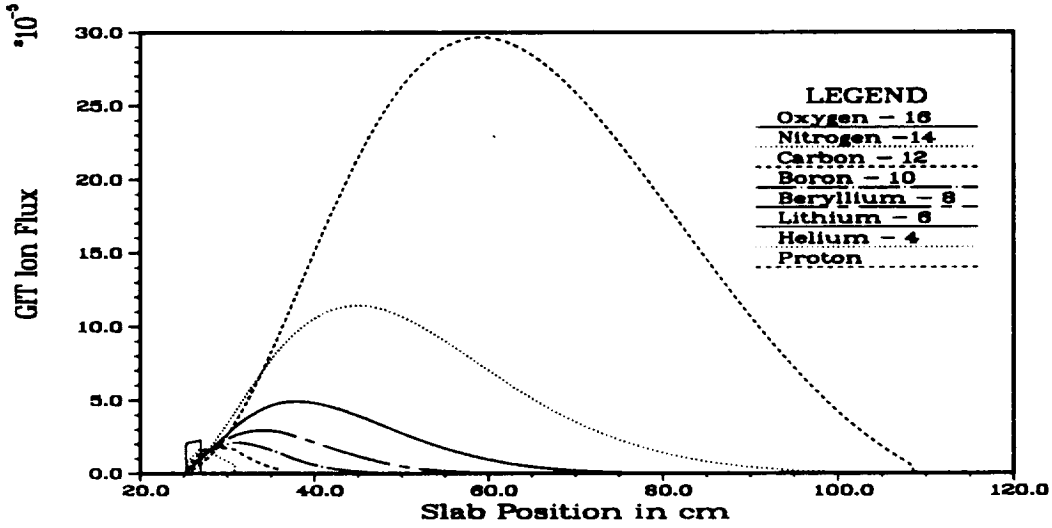

Figure 5.13: GIT Ion Flux Profile for a Fluorine Beam of 1000 MeV per Nucleon at an Energy of 100.0 MeV (Energy Group 2) for a Finite Aluminum Slab using the Extended Cross Section Set

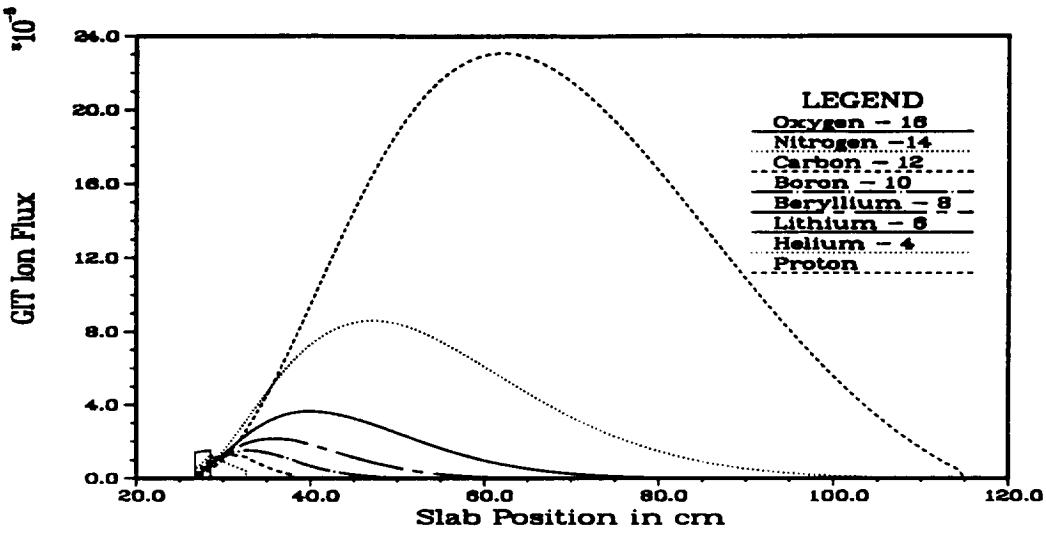

Figure 5.14: GIT Ion Flux Profile for a Fluorine Beam of 1000 MeV per Nucleon at an Energy of 10.0 MeV (Energy Group 3) for a Finite Aluminum Slab using the Extended Cross Section Set

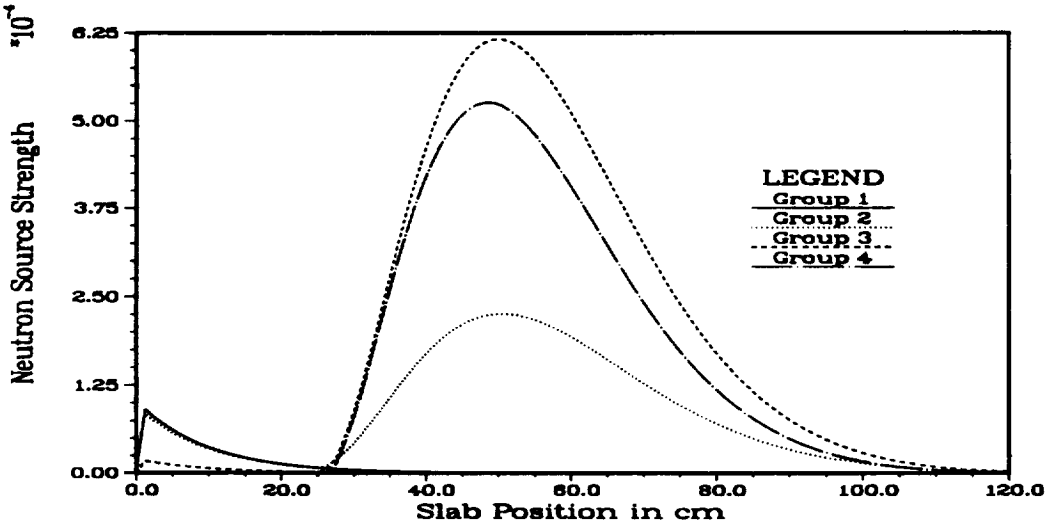

Figure 5.15: GIT Neutron Source Profile for Energy Groups One through Four for a Fluorine Beam of 1000.0 MeV per Nucleon and a Finite Aluminum Slab using the Extended Cross Section Set

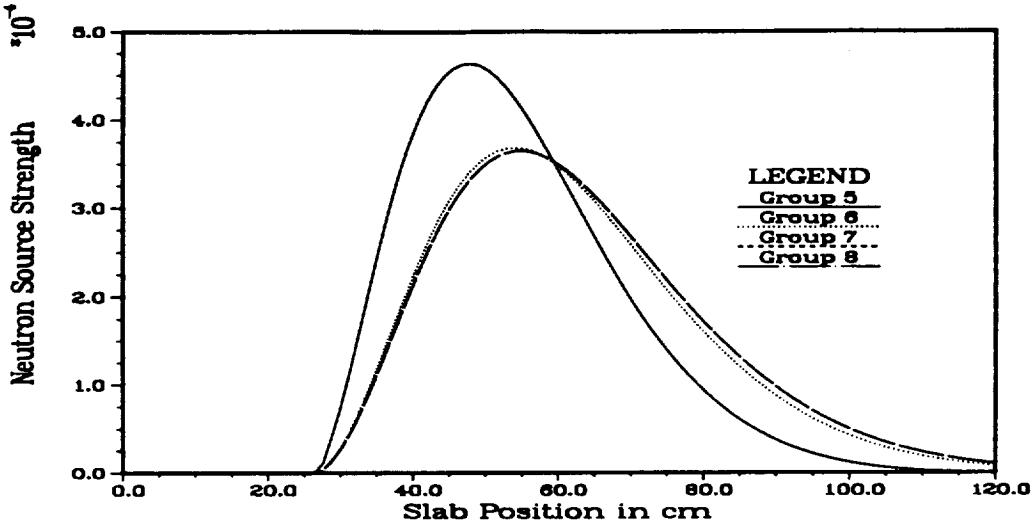

Figure 5.16: GIT Neutron Source Profile for Energy Groups Five through Eight for a Fluorine Beam of 1000 MeV per Nucleon and a Finite Aluminum Slab using the Extended Cross Section Set

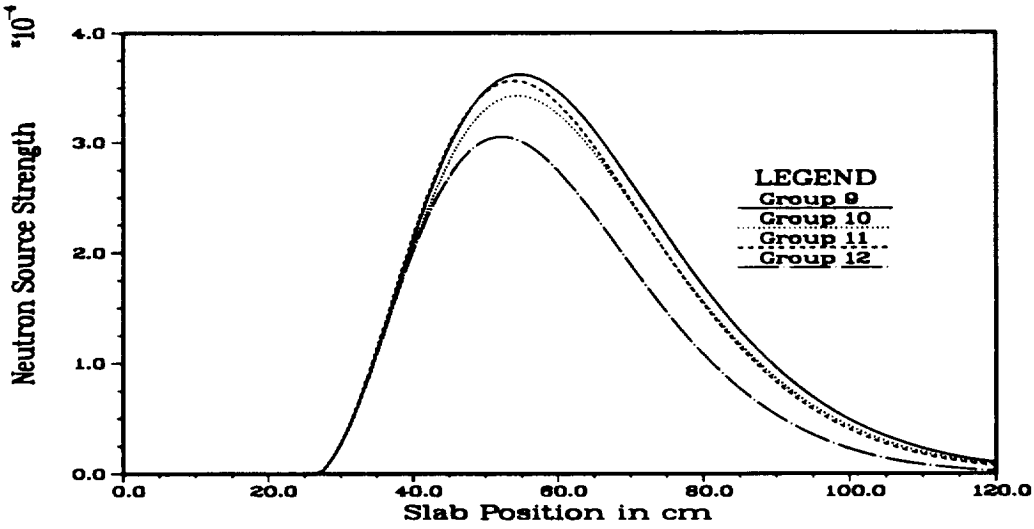

Figure 5.17: GIT Neutron Source Profile for Energy Groups Nine through Twelve for a Fluorine Beam of 1000 MeV per Nucleon and a Finite Aluminum Slab using the Extended Cross Section Set

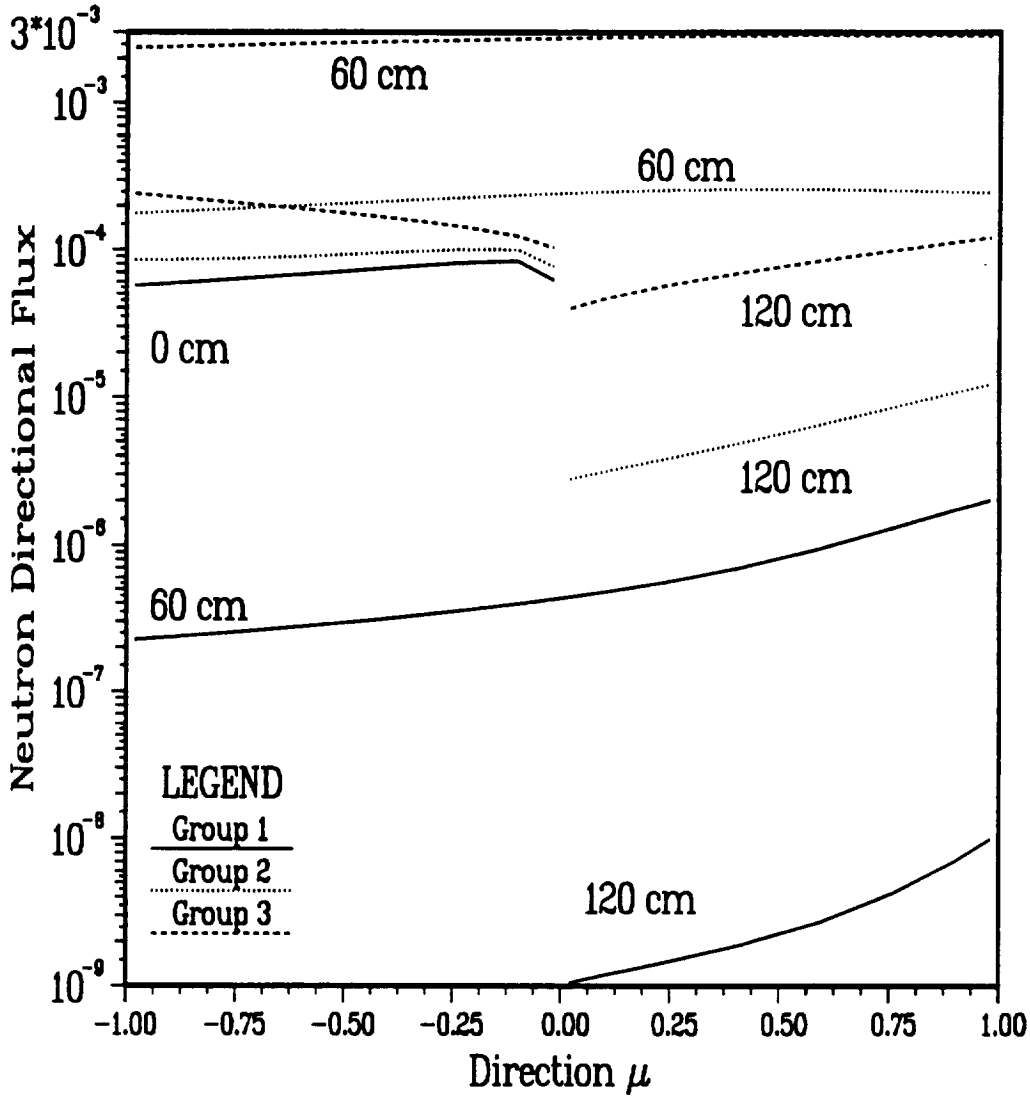

Figure 5.18: Angular Neutron Flux Profile for $x = 0$ cm, $x = 60$ cm, and $x = 120$ cm for Energy Groups One through Three, a Fluorine Beam of 1000 MeV per Nucleon, and a Finite Aluminum Slab using the Extended Cross Section Set

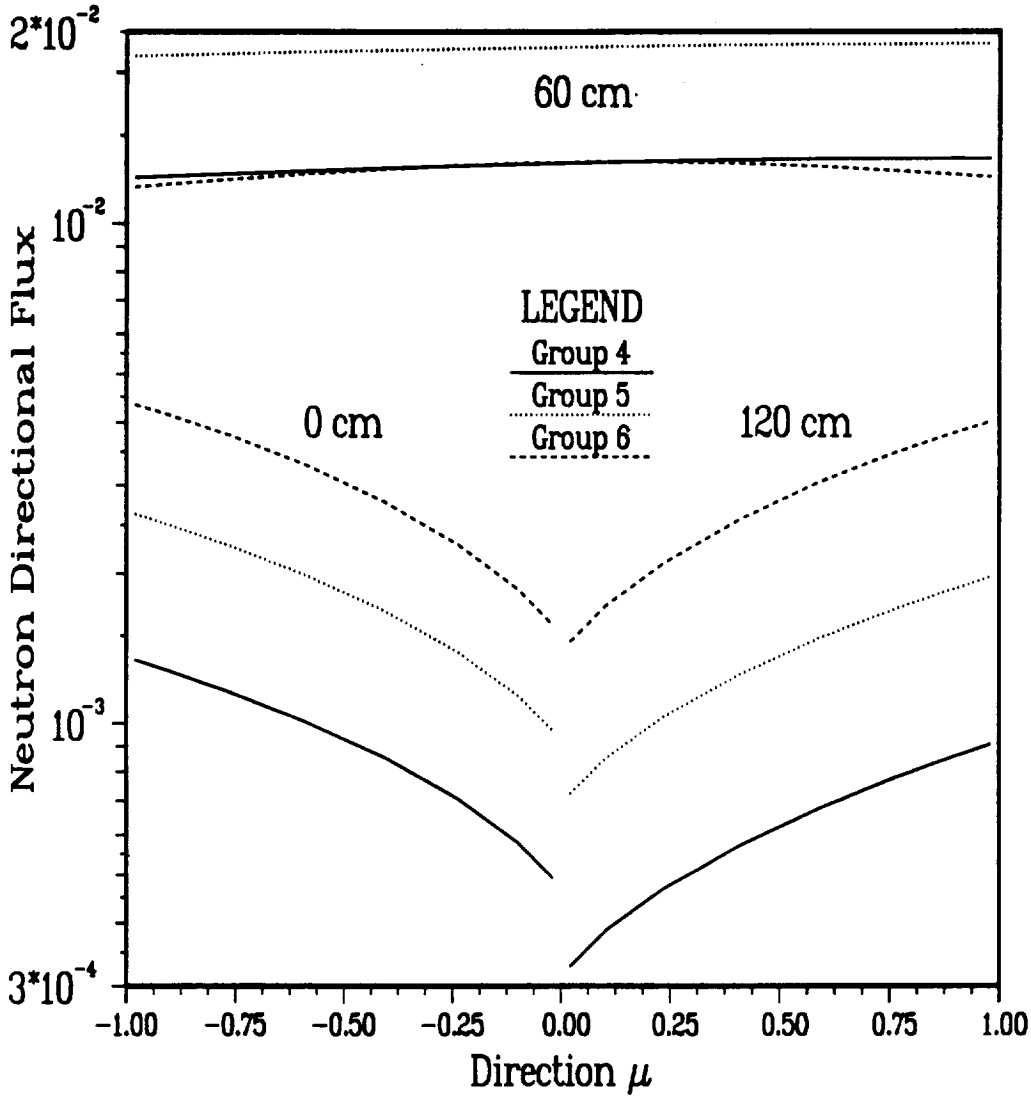

Figure 5.19: Angular Neutron Flux Profile for $x = 0$ cm, $x = 60$ cm, and $x = 120$ cm for Energy Groups Four through Six, a Fluorine Beam of 1000 MeV per Nucleon, and a Finite Aluminum Slab using the Extended Cross Section Set

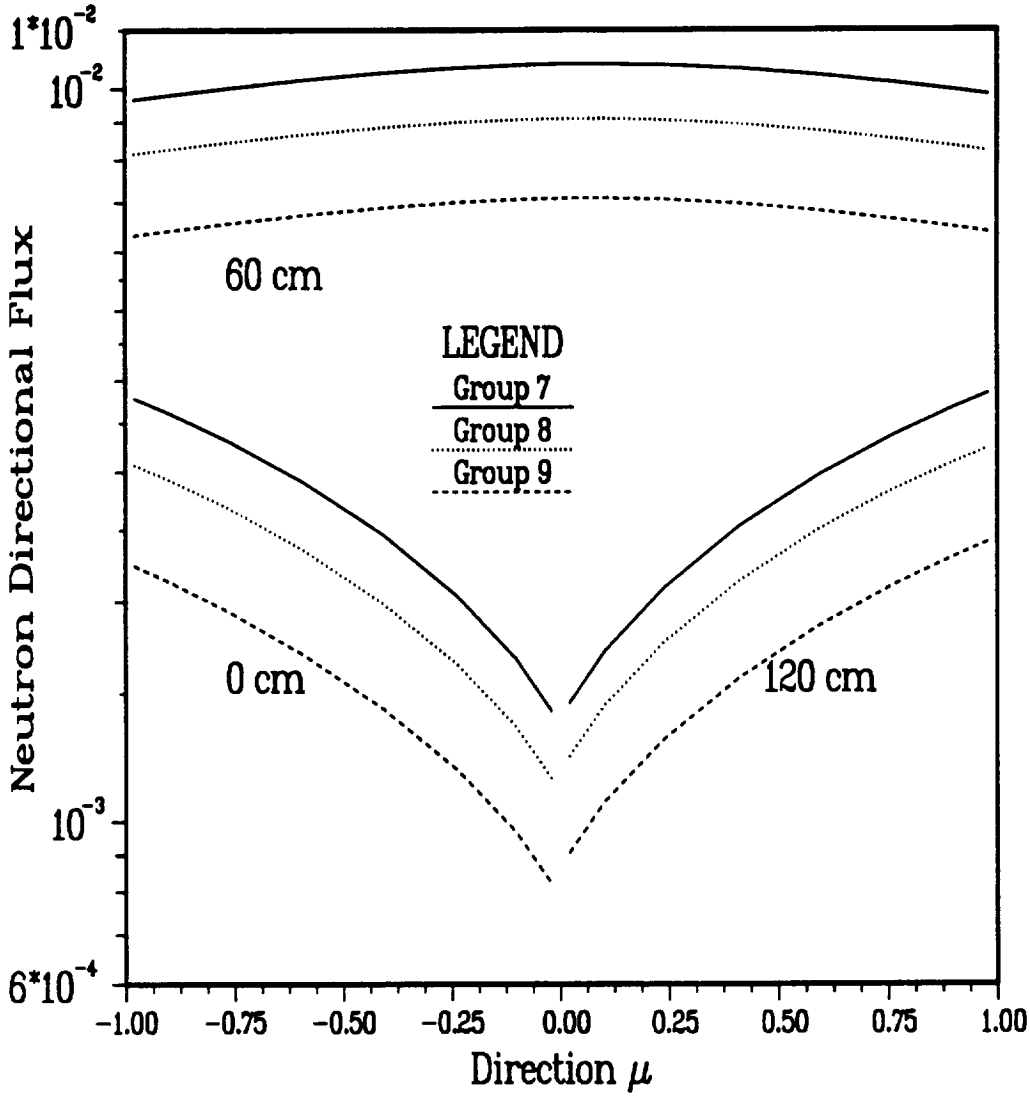

Figure 5.20: Angular Neutron Flux Profile for $x = 0$ cm, $x = 60$ cm, and $x = 120$ cm for Energy Groups Seven through Nine, a Fluorine Beam of 1000 MeV per Nucleon, and a Finite Aluminum Slab using the Extended Cross Section Set

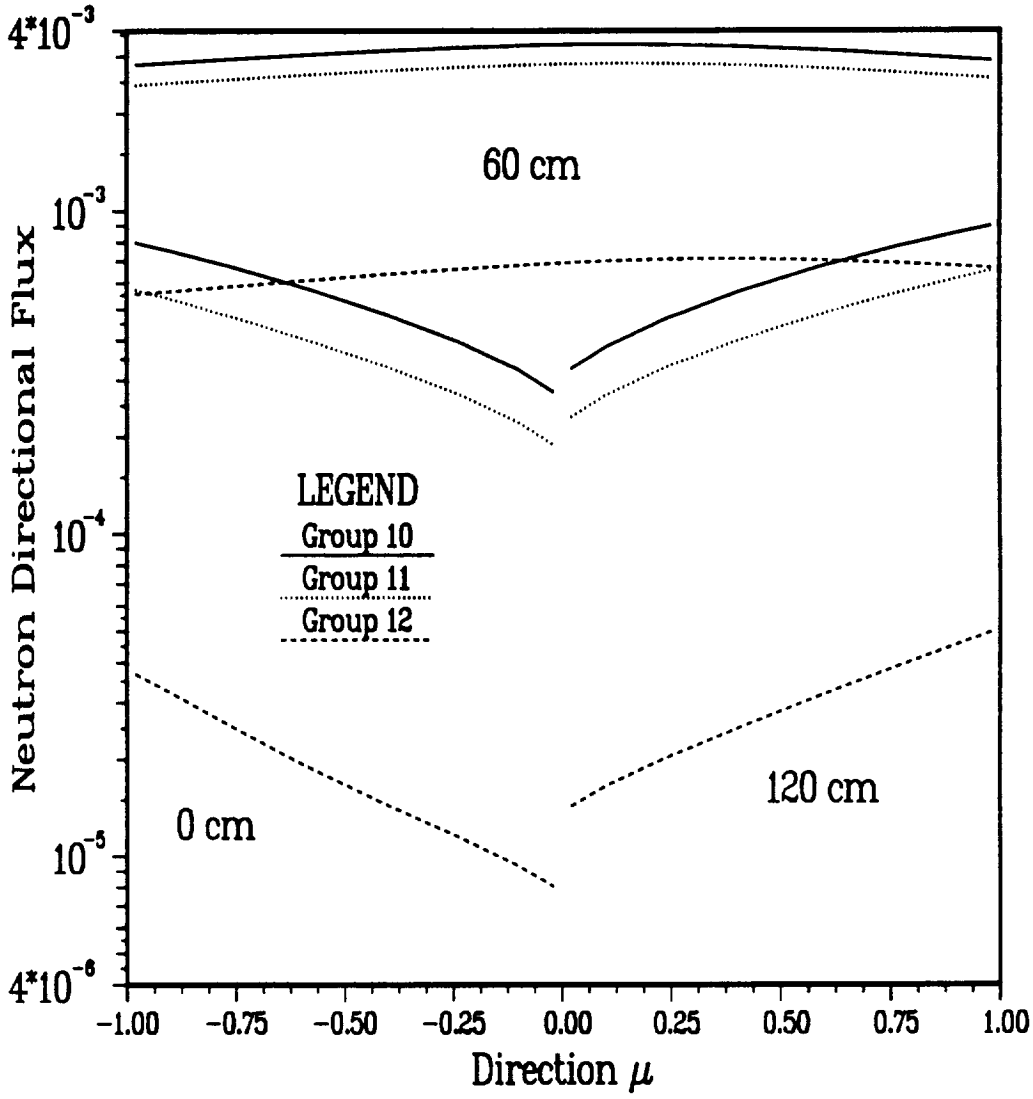

Figure 5.21: Angular Neutron Flux Profile for $x = 0$ cm, $x = 60$ cm, and $x = 120$ cm for Energy Groups Ten through Twelve, a Fluorine Beam of 1000 MeV per Nucleon, and a Finite Aluminum Slab using the Extended Cross Section Set

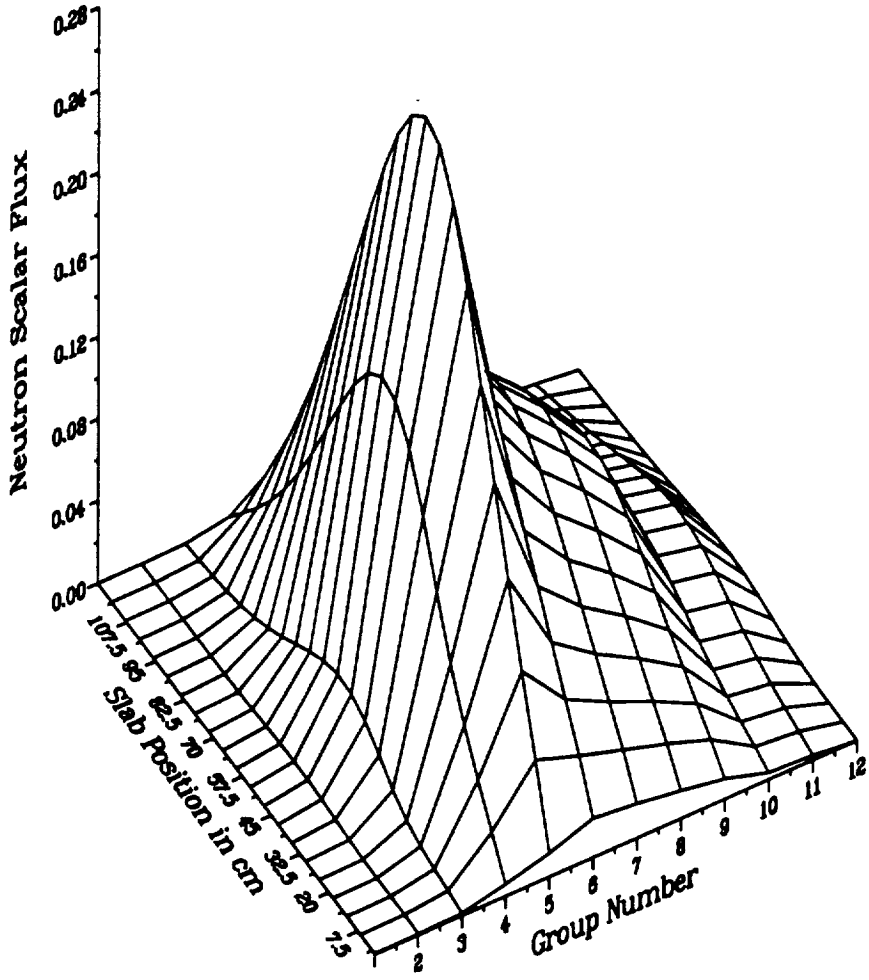

Figure 5.22: Scalar Neutron Flux Profile by Energy Group with a Fluorine Beam of 1000 MeV per Nucleon and a Finite Aluminum Slab using the Extended Cross Section Set

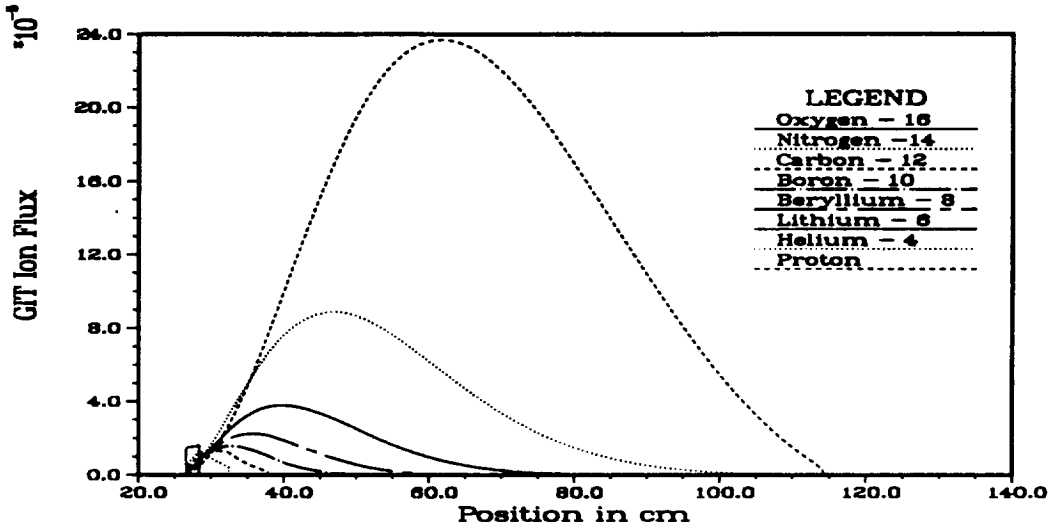

Figure 5.23: GIT Ion Flux Profile for a Fluorine Beam of 1000 MeV per Nucleon at an Energy of 20.0 MeV (Energy Group 1) for a Semi-infinite Aluminum Media using the Limited Cross Section Set

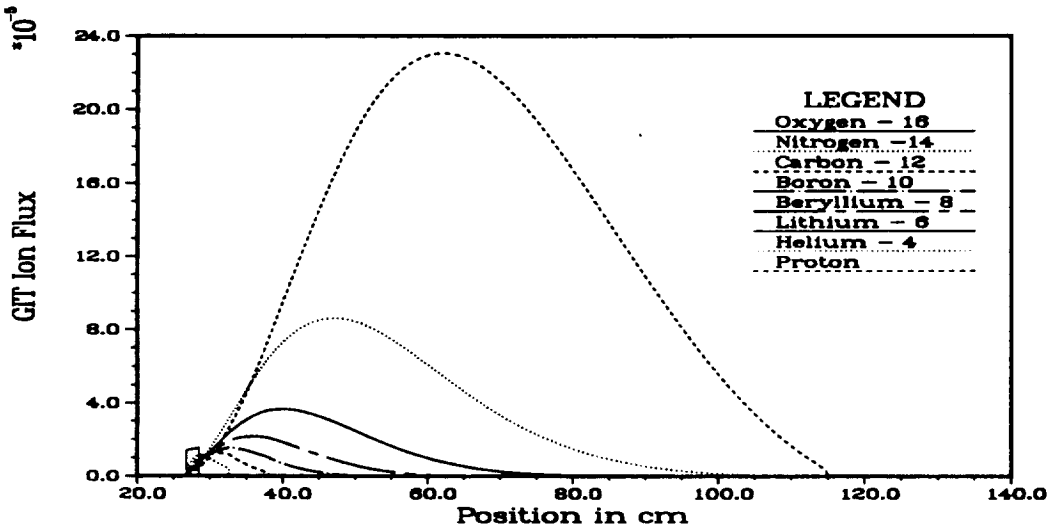

Figure 5.24: GIT Ion Flux Profile for a Fluorine Beam of 1000 MeV per Nucleon at an Energy of 10.0 MeV (Energy Group 2) for a Semi-infinite Aluminum Media using the Limited Cross Section Set

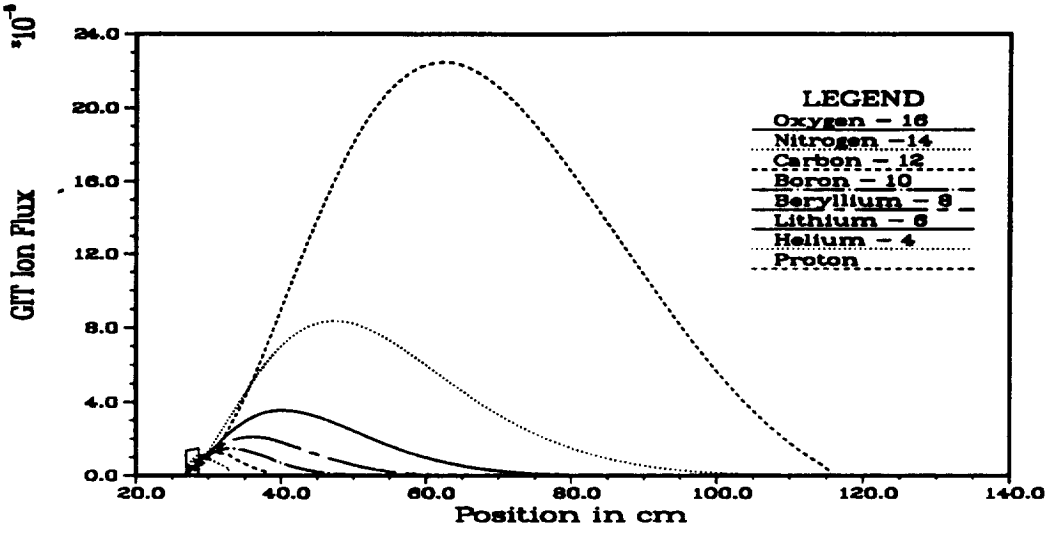

Figure 5.25: GIT Ion Flux Profile for a Fluorine Beam of 1000 MeV per Nucleon at an Energy of 1.0 MeV (Energy Group 3) for a Semi-infinite Aluminum Media using the Limited Cross Section Set

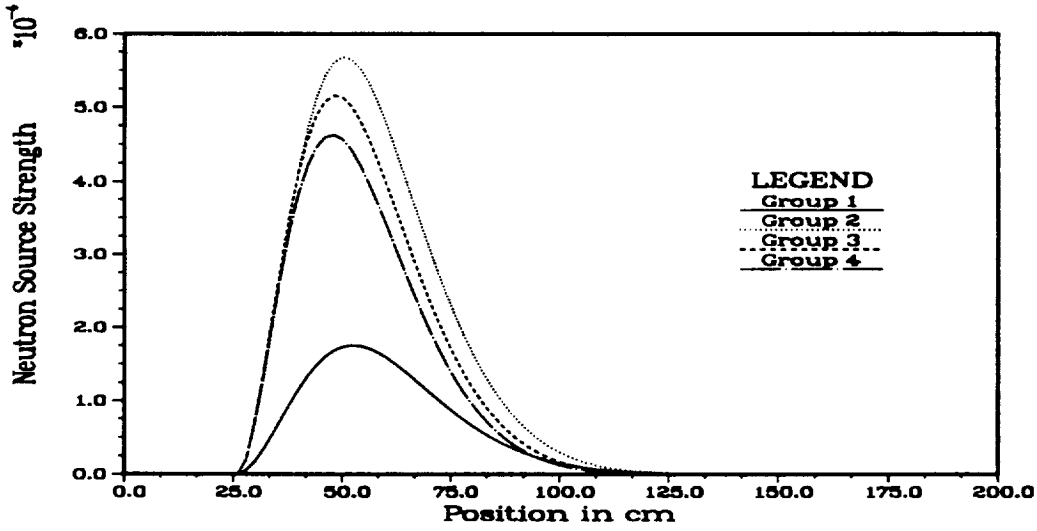

Figure 5.26: GIT Neutron Source Profile for Energy Groups One through Four for a Fluorine Beam of 1000 MeV per Nucleon and a Semi-infinite Aluminum Media using the Limited Cross Section Set

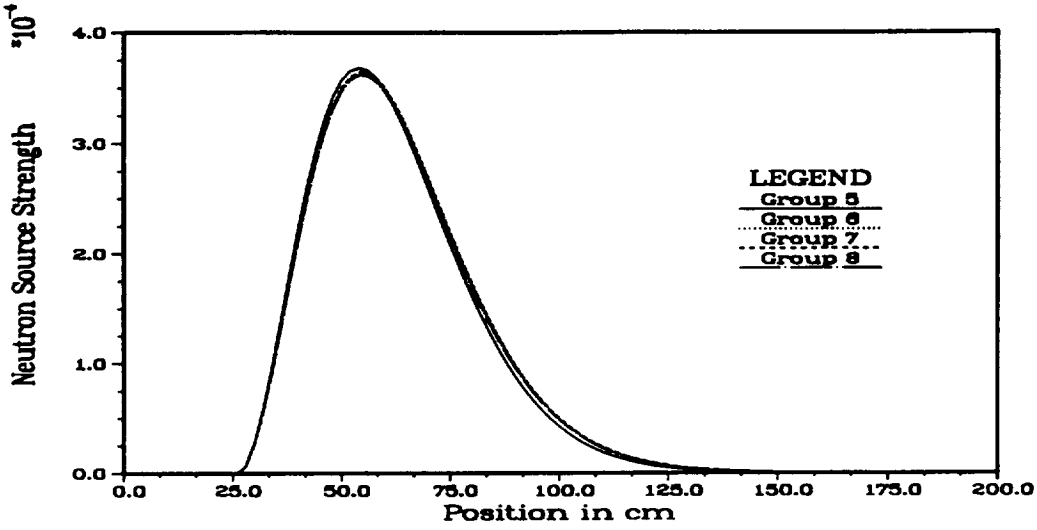

Figure 5.27: GIT Neutron Source Profile for Energy Groups Five through Eight for a Fluorine Beam of 1000 MeV per Nucleon and a Semi-infinite Aluminum Media using the Limited Cross Section Set

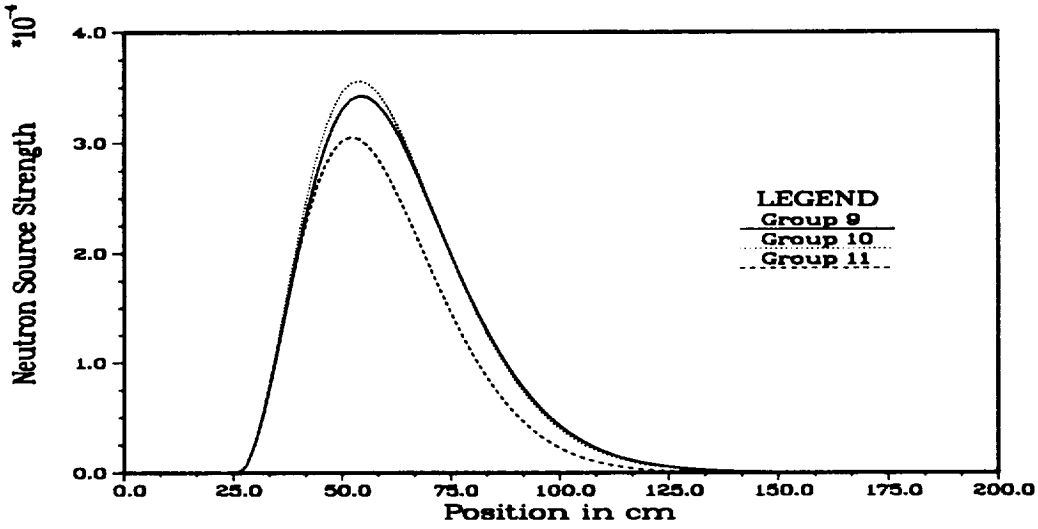

Figure 5.28: GIT Neutron Source Profile for Energy Groups Nine through Eleven or a Fluorine Beam of 1000 MeV per Nucleon and a Semi-infinite Aluminum Media using the Limited Cross Section Set

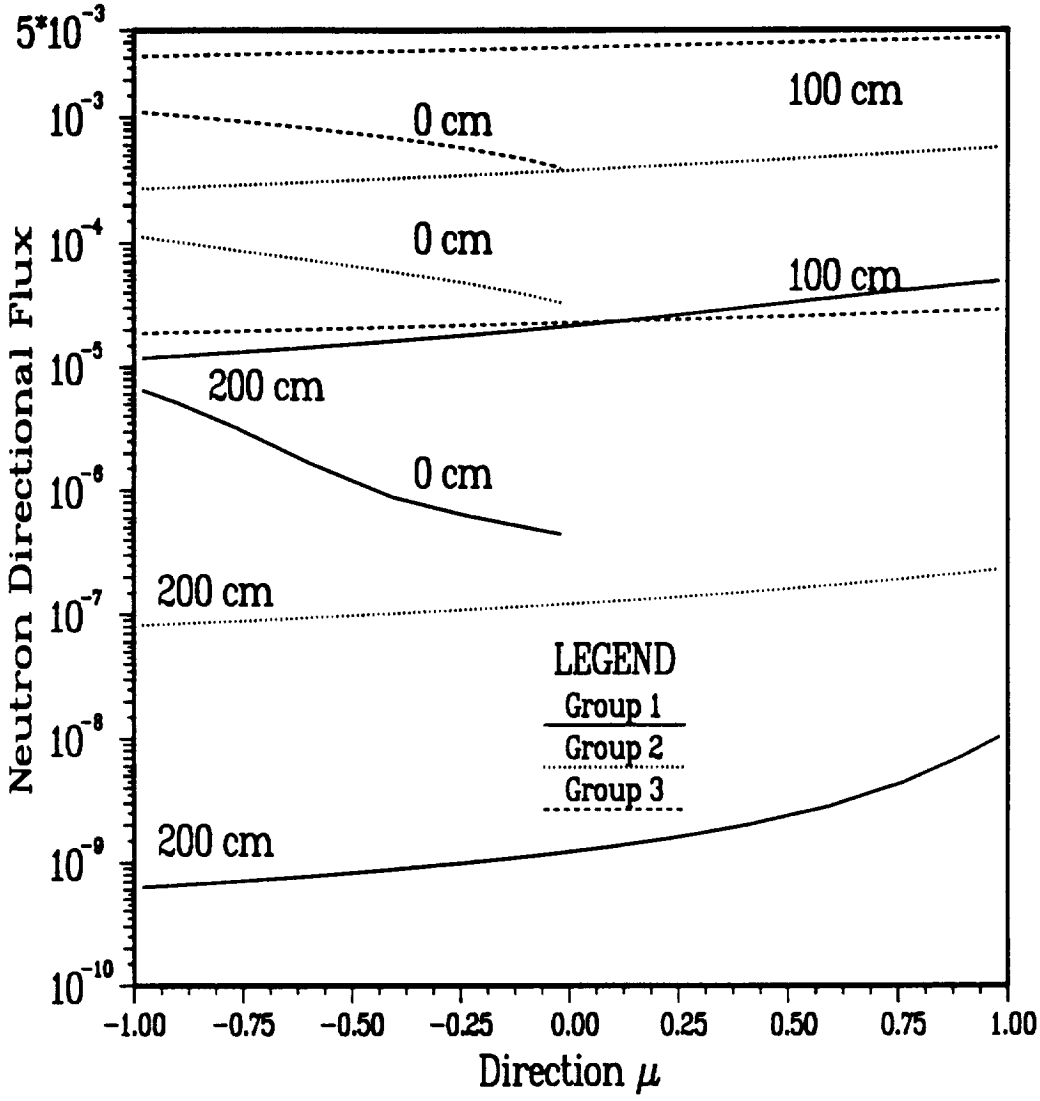

Figure 5.29: Angular Neutron Flux Profile for $x = 0$ cm, $x = 100$ cm, and $x = 200$ cm for Energy Groups One through Three, a Fluorine Beam of 1000 MeV per Nucleon, and a Semi-infinite Aluminum Media using the Limited Cross Section Set

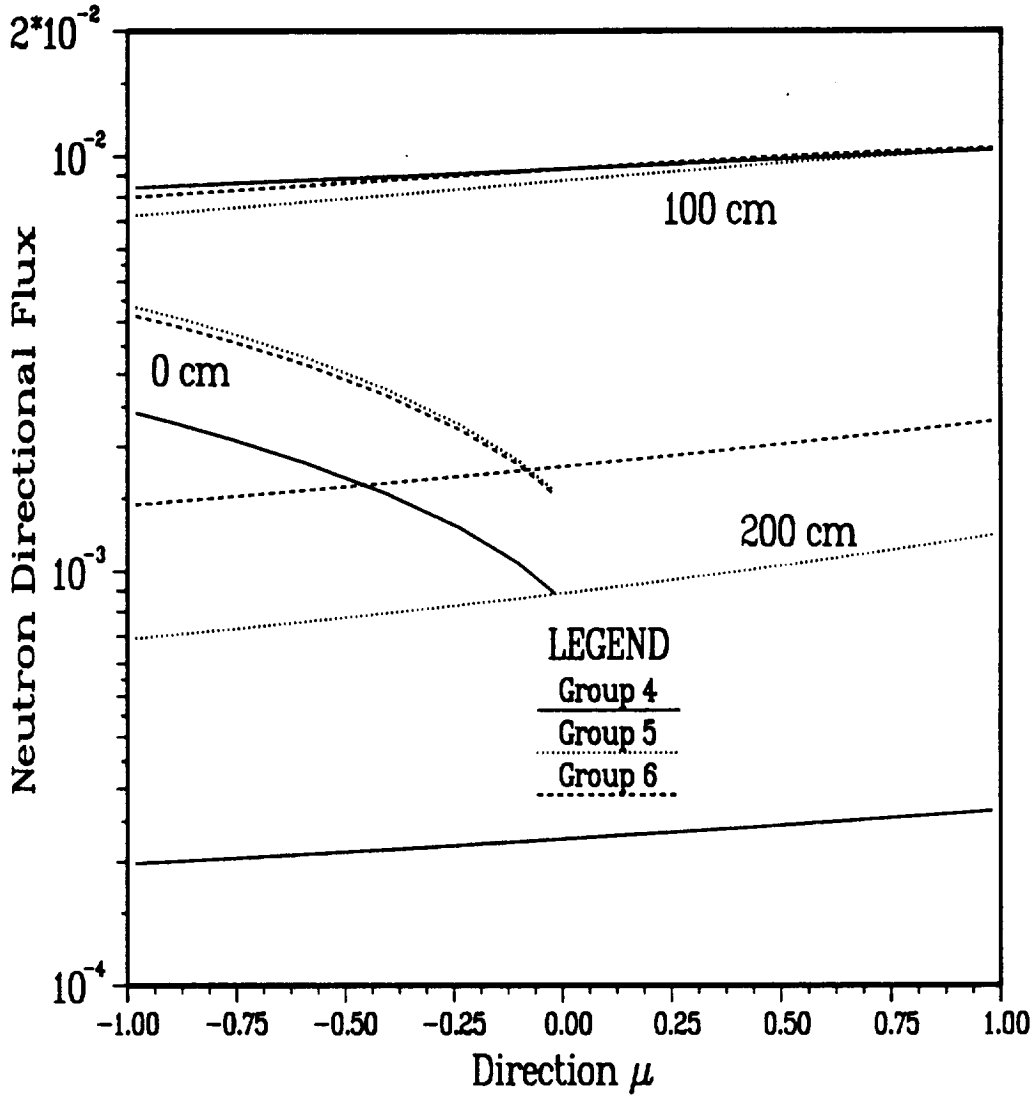

Figure 5.30: Angular Neutron Flux Profile for $x = 0$ cm, $x = 100$ cm, and $x = 200$ cm for Energy Groups Four through Six, a Fluorine Beam of 1000 MeV per Nucleon, and a Semi-infinite Aluminum Media using the Limited Cross Section Set

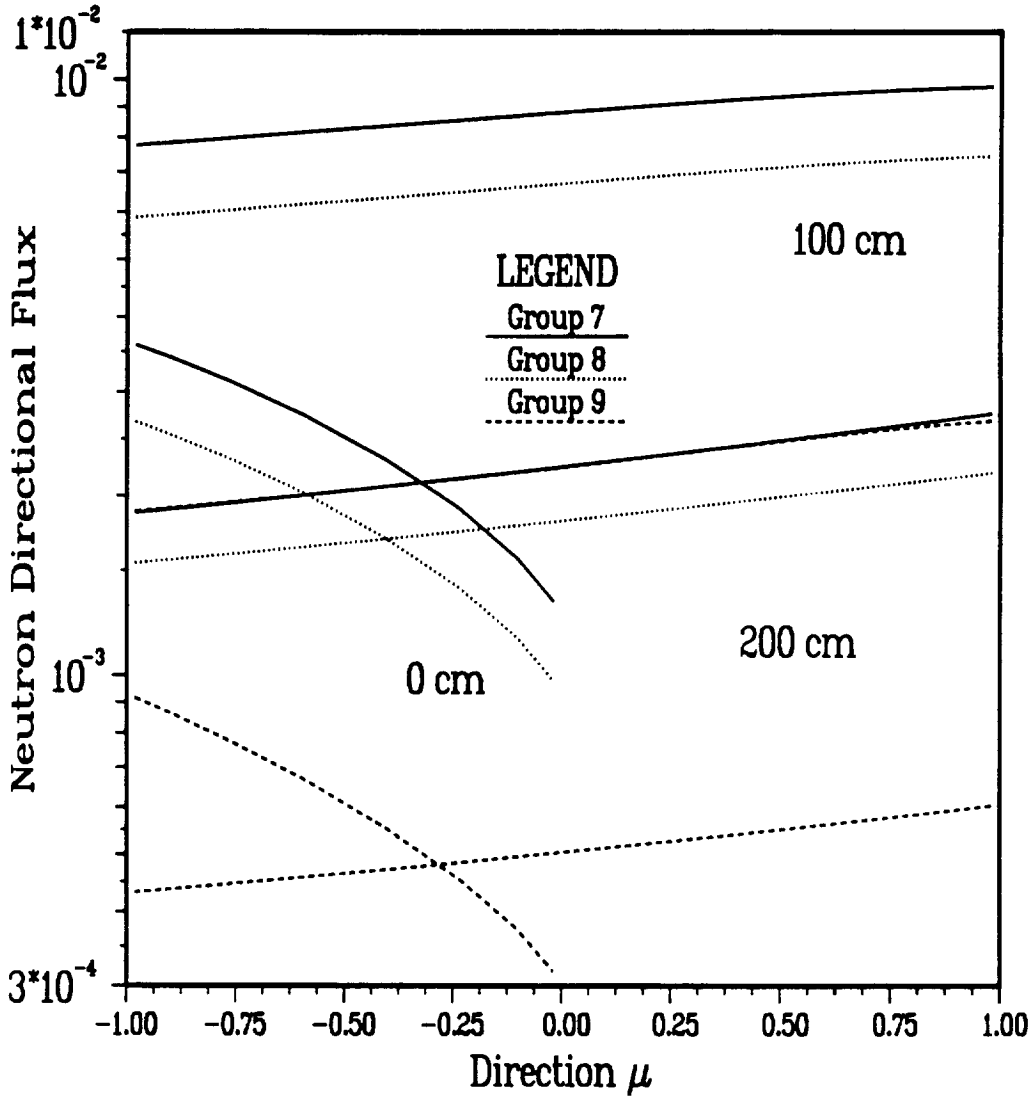

Figure 5.31: Angular Neutron Flux Profile for $x = 0$ cm, $x = 100$ cm, and $x = 200$ cm for Energy Groups Seven through Nine, a Fluorine Beam of 1000 MeV per Nucleon, and a Semi-infinite Aluminum Media using the Limited Cross Section Set

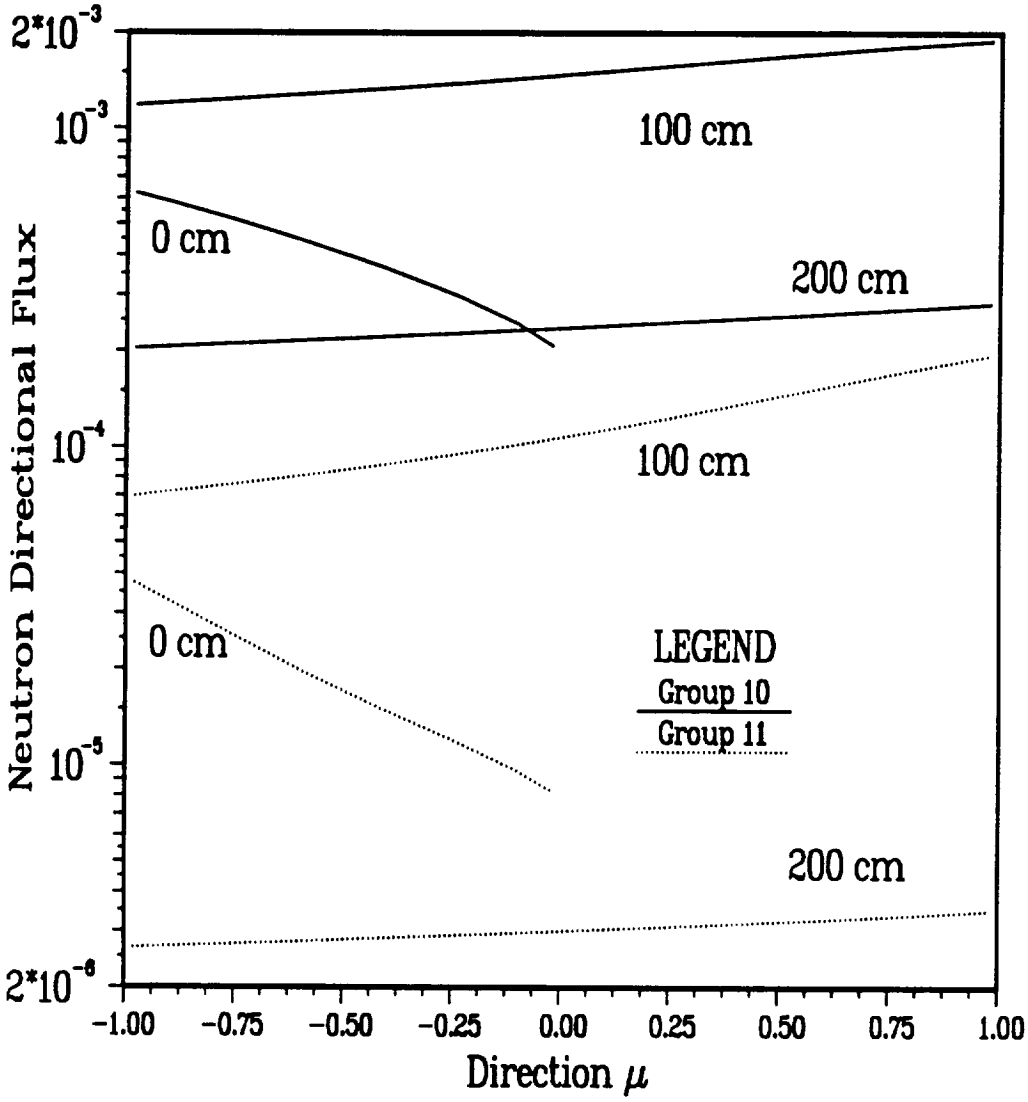

Figure 5.32: Angular Neutron Flux Profile for $x = 0$ cm, $x = 100$ cm, and $x = 200$ cm for Energy Groups Ten and Eleven, a Fluorine Beam of 1000 MeV per Nucleon, and a Semi-infinite Aluminum Media using the Limited Cross Section Set

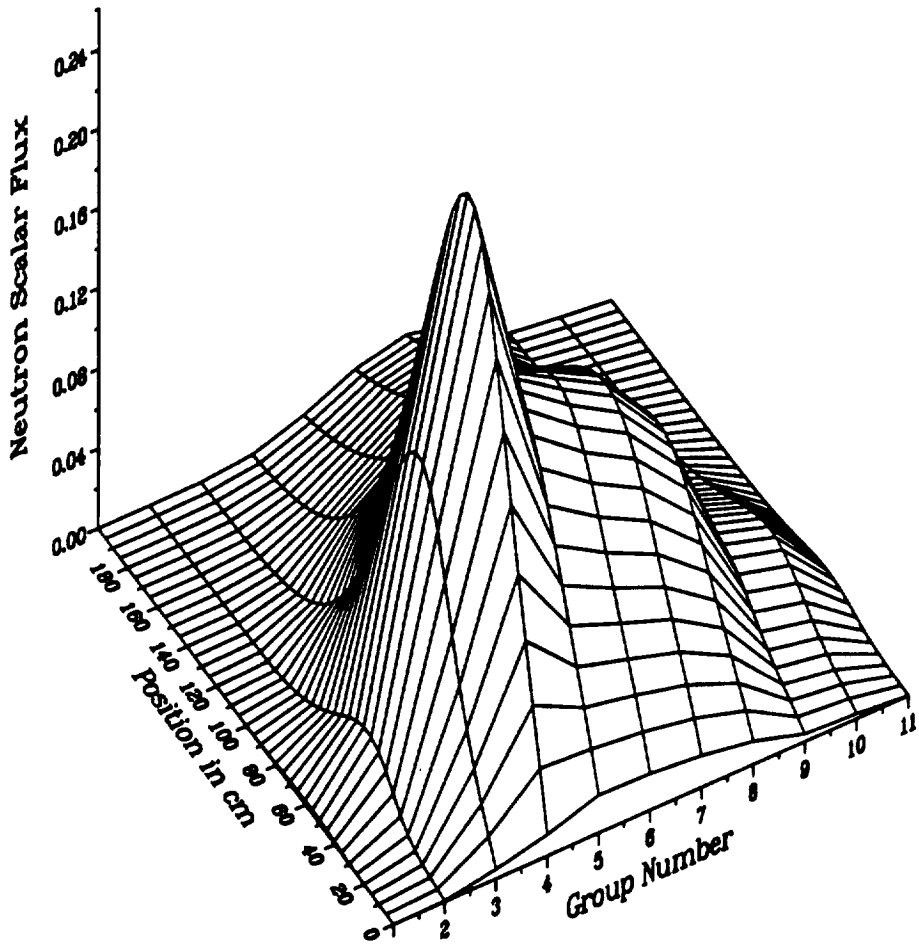

Figure 5.33: Scalar Neutron Flux Profile by Energy Group with a Fluorine Beam of 1000 MeV per Nucleon and a Semi-infinite Aluminum Media using the Limited Cross Section Set

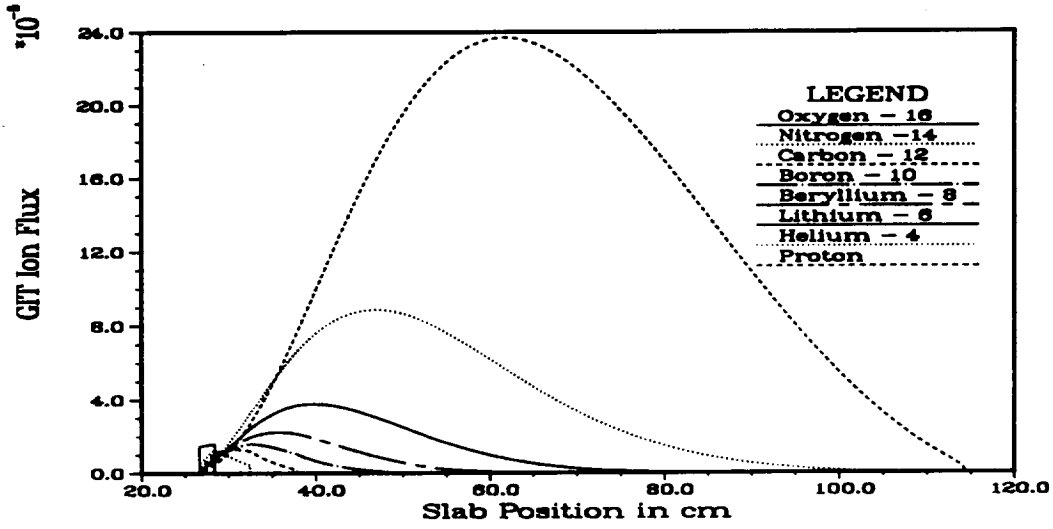

Figure 5.34: GIT Ion Flux Profile for a Fluorine Beam of 1000 MeV per Nucleon at an Energy of 20.0 MeV (Energy Group 1) for a Finite Aluminum Slab using the Limited Cross Section Set

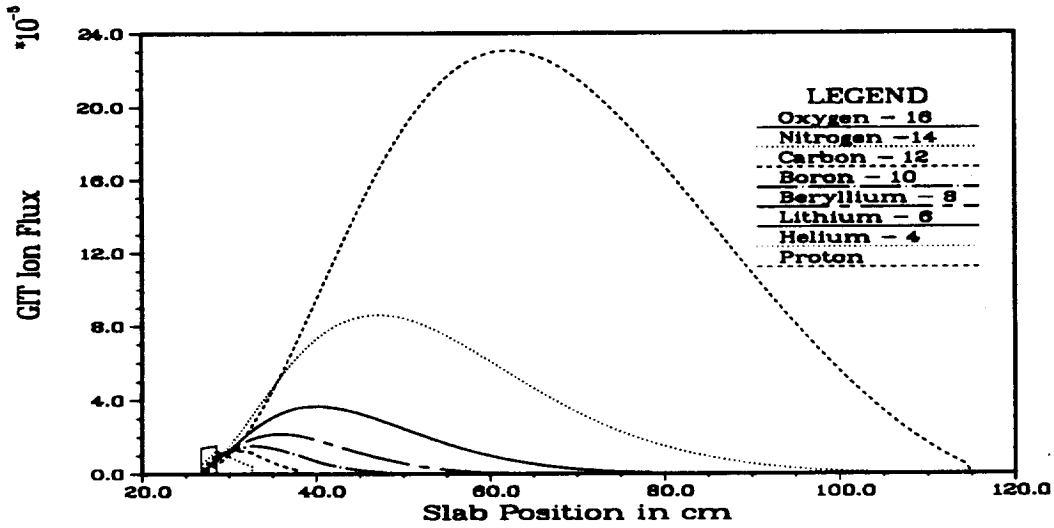

Figure 5.35: GIT Ion Flux Profile for a Fluorine Beam of 1000 MeV per Nucleon at an Energy of 10.0 MeV (Energy Group 2) for a Finite Aluminum Slab using the Limited Cross Section Set

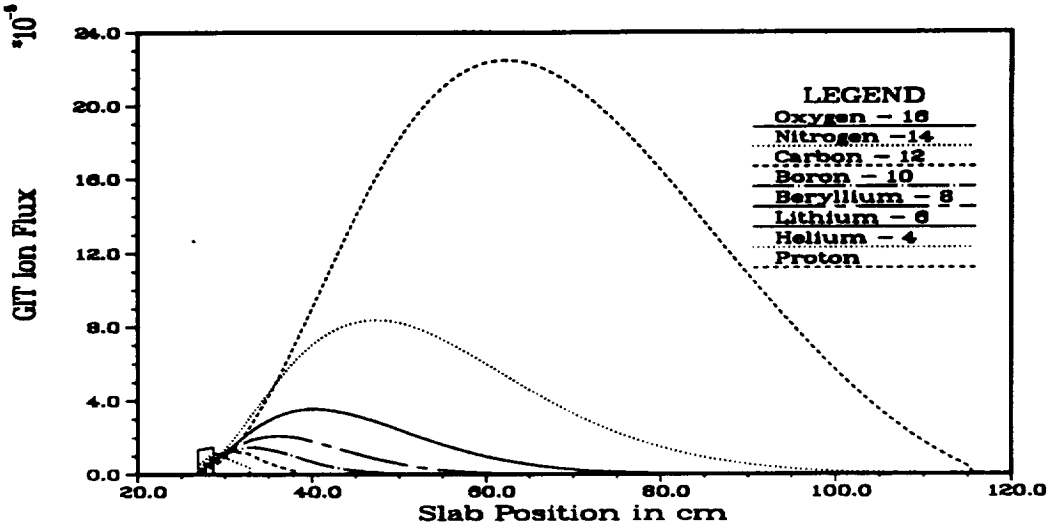

Figure 5.36: GIT Ion Flux Profile for a Fluorine Beam of 1000 MeV per Nucleon at an Energy of 1.0 MeV (Energy Group 3) for a Finite Aluminum Slab using the Limited Cross Section Set

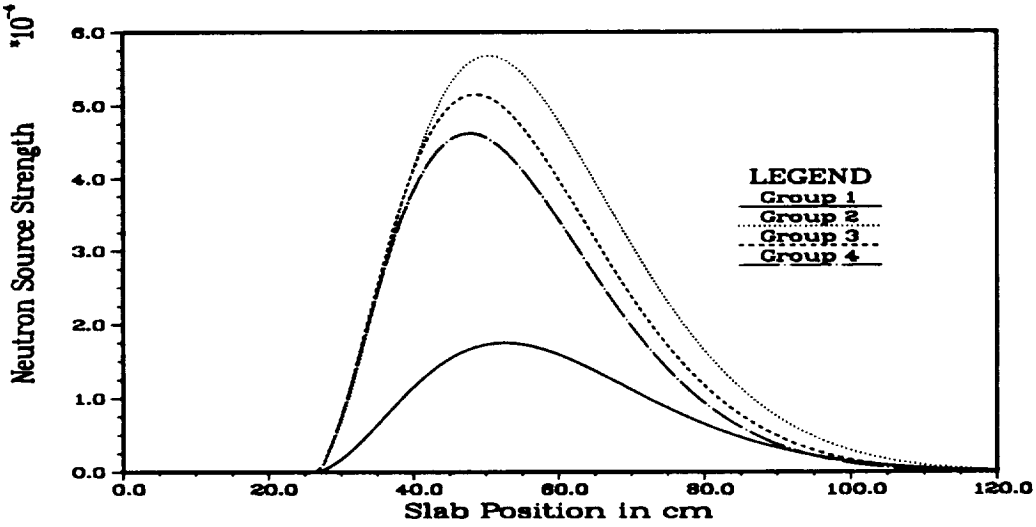

Figure 5.37: GIT Neutron Source Profile for Energy Groups One through Four for a Fluorine Beam of 1000 MeV per Nucleon and a Finite Aluminum Slab using the Limited Cross Section Set

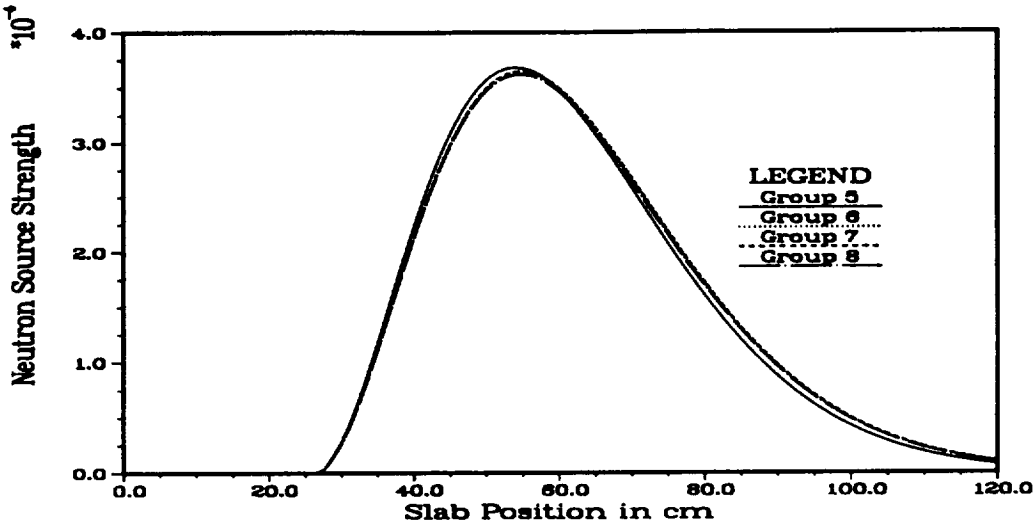

Figure 5.38: GIT Neutron Source Profile for Energy Groups Five through Eight for a Fluorine Beam of 1000 MeV per Nucleon and a Finite Aluminum Slab using the Limited Cross Section Set

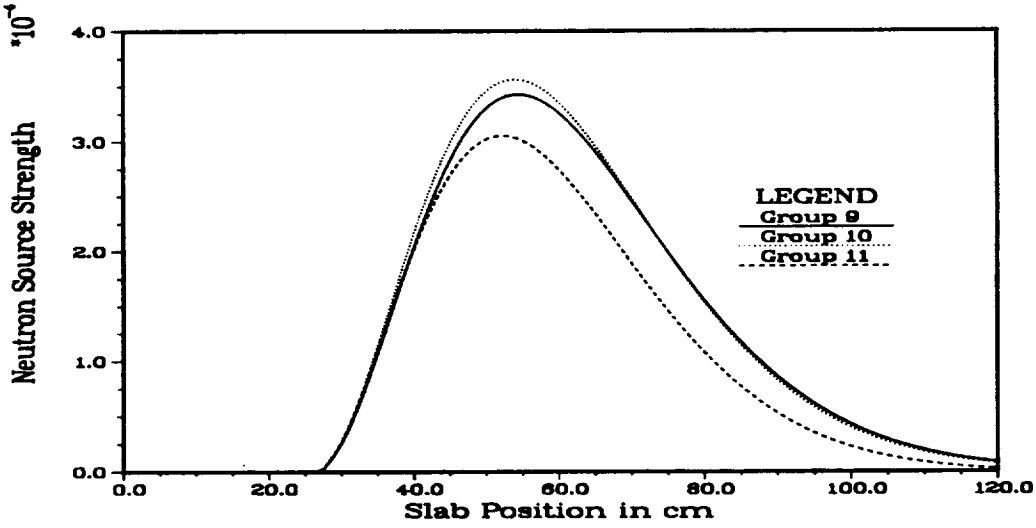

Figure 5.39: GIT Neutron Source Profile for Energy Groups Nine through Eleven for a Fluorine Beam of 1000 MeV per Nucleon and a Finite Aluminum Slab using the Limited Cross Section Set

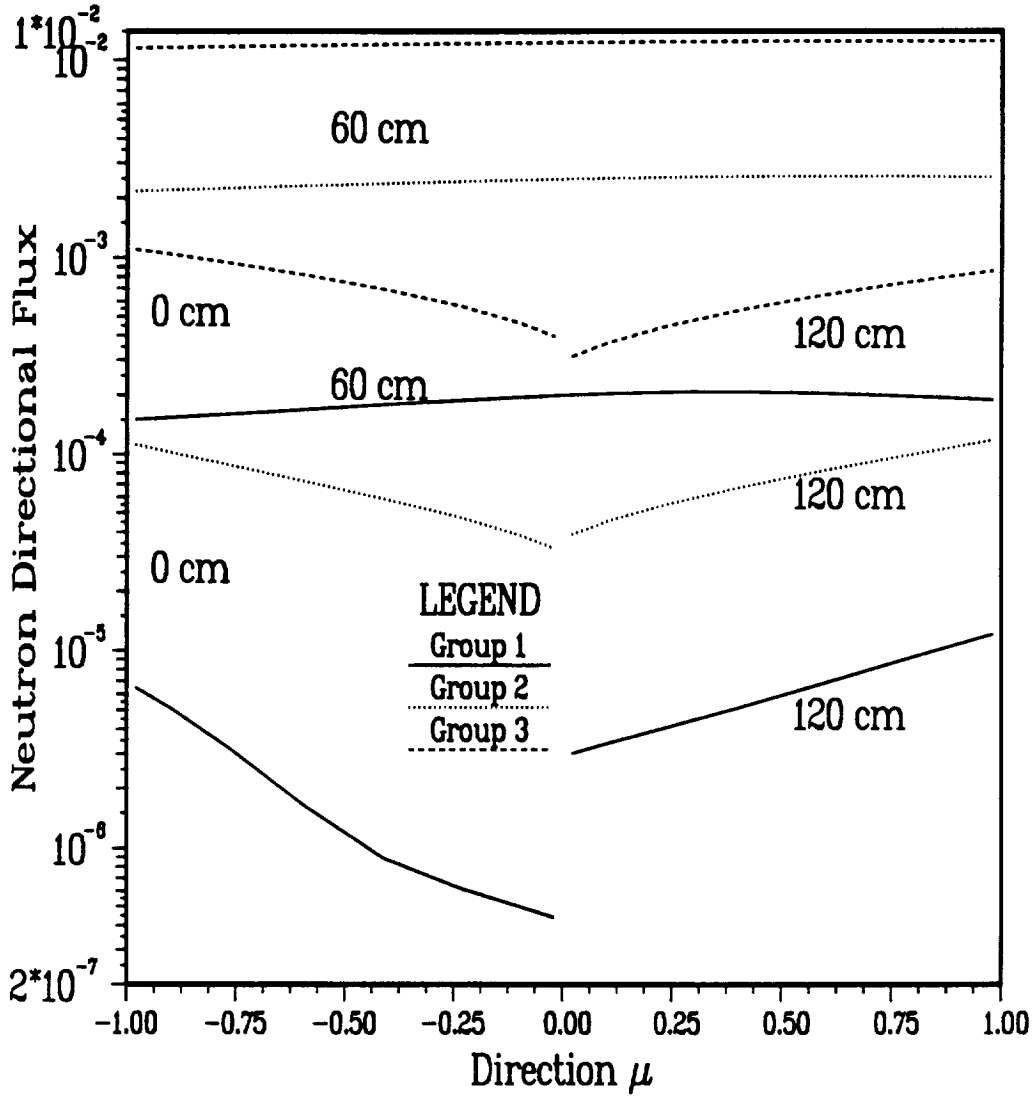

Figure 5.40: Angular Neutron Flux Profile for $x = 0$ cm, $x = 60$ cm, and $x = 120$ cm for Energy Groups One through Three, a Fluorine Beam of 1000 MeV per Nucleon, and a Finite Aluminum Slab using the Limited Cross Section Set

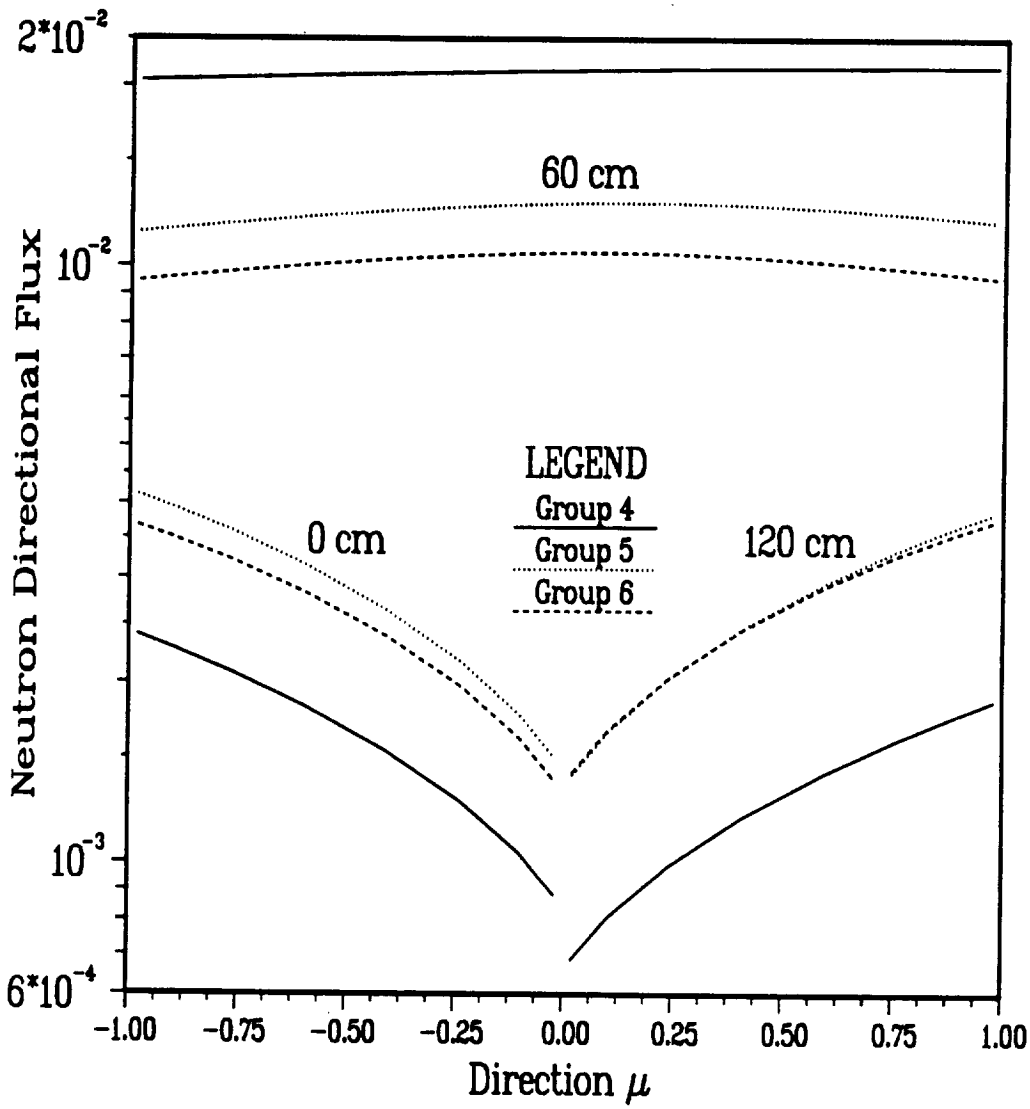

Figure 5.41: Angular Neutron Flux Profile for $x = 0$ cm, $x = 60$ cm, and $x = 120$ cm for Energy Groups Four through Six, a Fluorine Beam of 1000 MeV per Nucleon, and a Finite Aluminum Slab using the Limited Cross Section Set

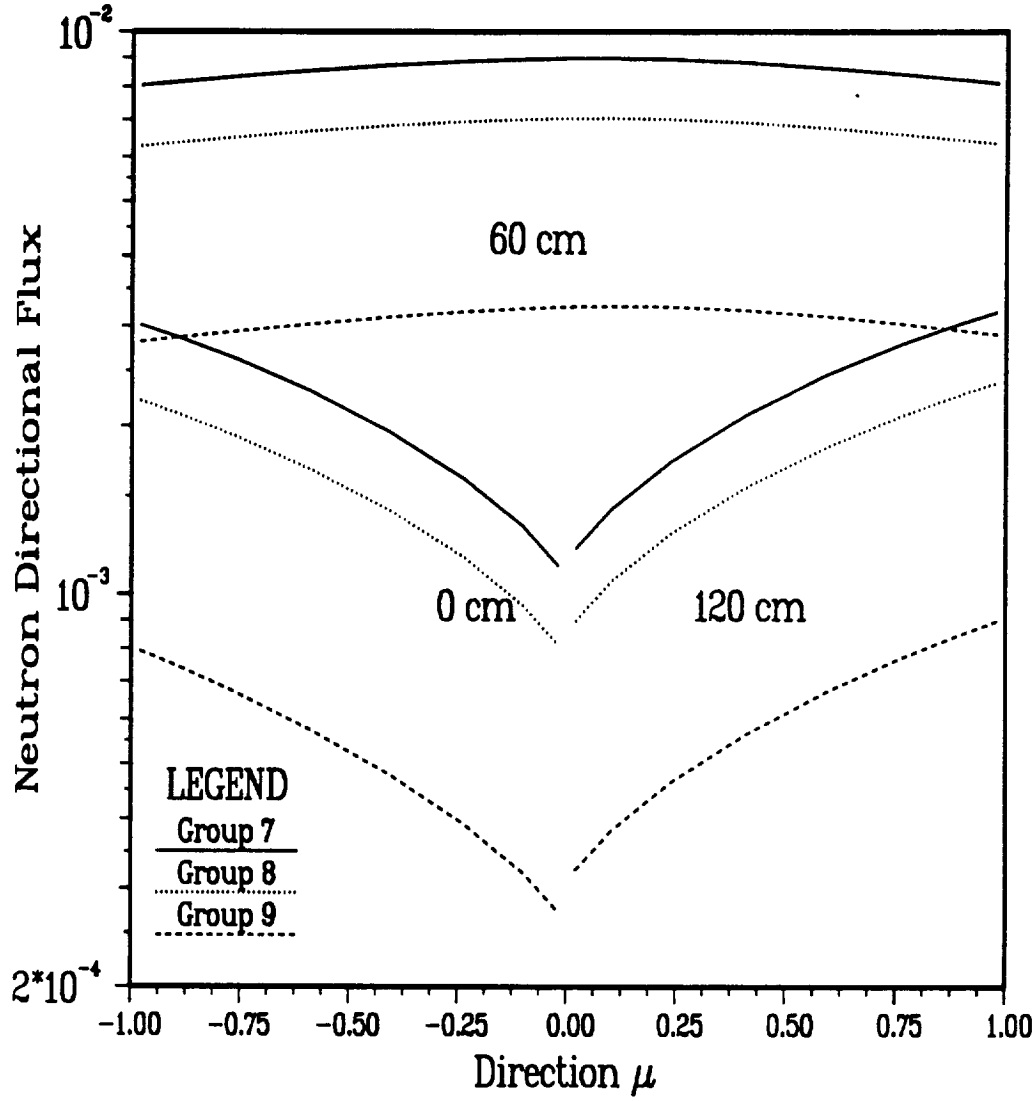

Figure 5.42: Angular Neutron Flux Profile for $x = 0$ cm, $x = 60$ cm, and $x = 120$ cm for Energy Groups Seven through Nine, a Fluorine Beam of 1000 MeV per Nucleon, and a Finite Aluminum Slab using the Limited Cross Section Set

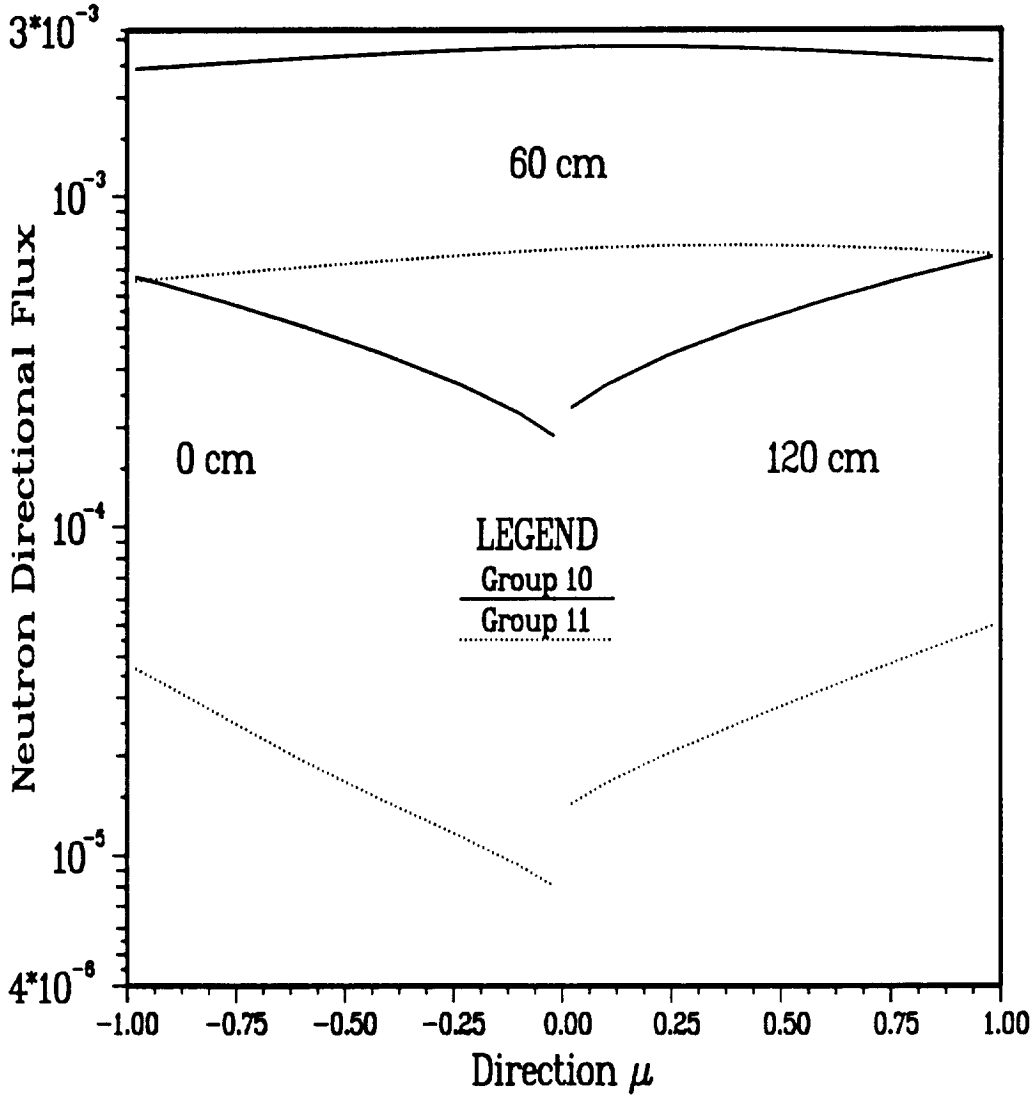

Figure 5.43: Angular Neutron Flux Profile for $x = 0$ cm, $x = 60$ cm, and $x = 120$ cm for Energy Groups Ten and Eleven, a Fluorine Beam of 1000 MeV per Nucleon, and a Finite Aluminum Slab using the Limited Cross Section Set

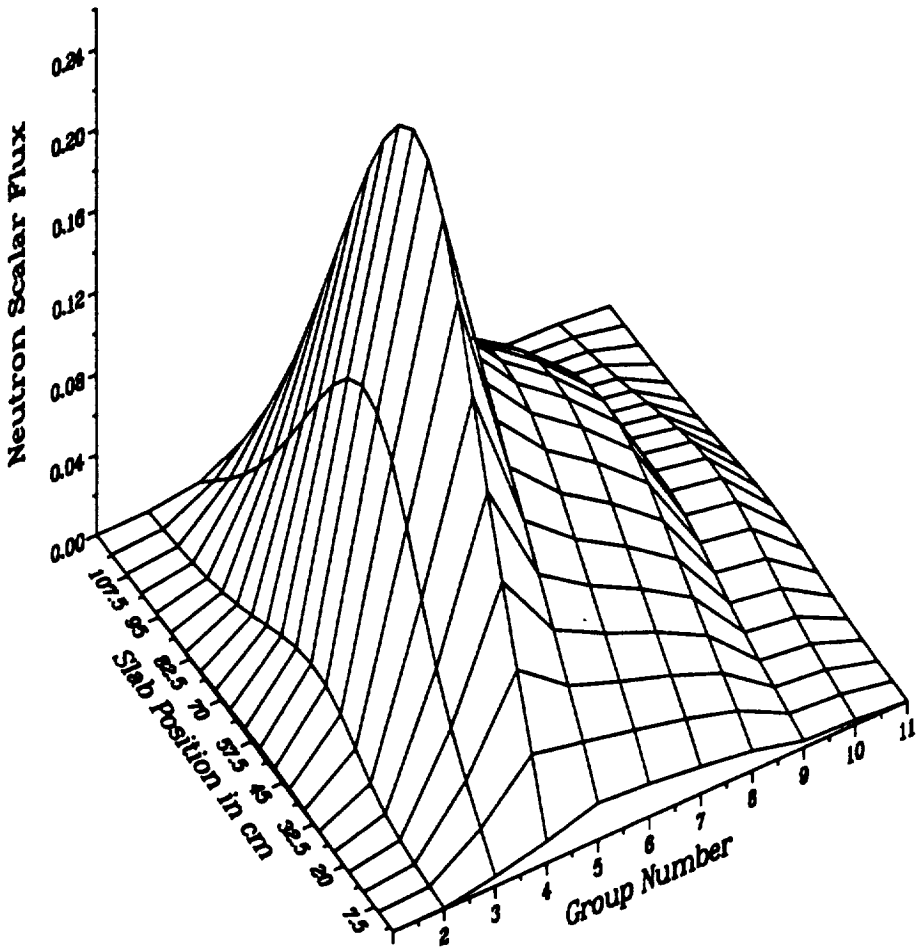

Figure 5.44: Scalar Neutron Flux Profile by Energy Group with a Fluorine Beam of 1000 MeV per Nucleon and a Finite Aluminum Slab using the Limited Cross Section Set

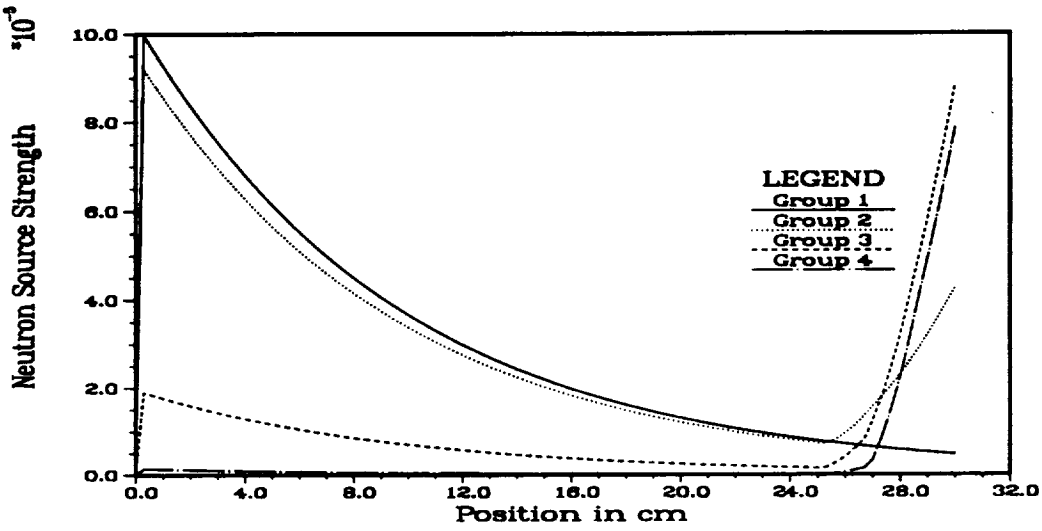

Figure 5.45: Magnified Neutron Source Profile of Energy Groups One through Four for a Fluorine Beam of 1000 MeV per Nucleon in a Semi-infinite Aluminum Media

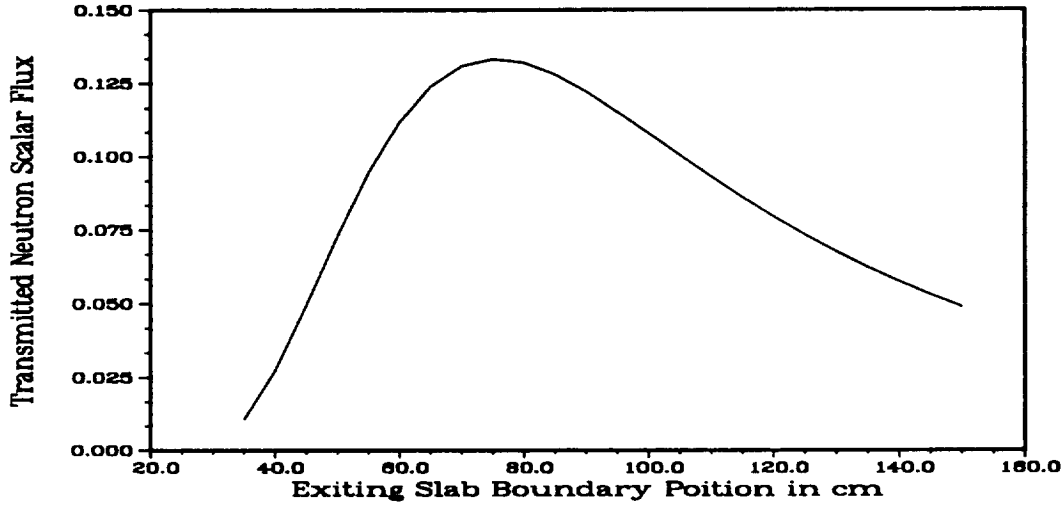

Figure 5.46: Transmitted Neutron Total Scalar Flux versus Aluminum Slab Thickness using the Extended Cross Section Set

CHAPTER 6

RECOMMENDATIONS AND CONCLUSIONS

A multigroup, isotropic scatter, neutral particle F_N transport solver for semi-infinite and heterogenous slabs has been created and coupled to a closed-form analytical solution to the galactic cosmic ray cascade, GIT, to determine the behavior of low energy neutrons in the cascade. This is a first step in creating a neutron benchmark to be used with BRYNTRN.

The formulation uses a closed-form representation for the neutron source in a basis function expansion for the neutron transport solution. Therefore, truncation errors are limited to the number of terms used in the expansion. These errors are under program control and secondary to the round-off errors caused by the discretization of the real numbers by the computer. The round-off error for a 64-bit floating point representation becomes important when the incident ion charge is twelve or higher for the GIT algorithm and ten or higher for the F_N algorithm. For a 128-bit floating point representation, the charge number can be extended to twenty-three for the GIT algorithm. The problem manifests itself in the recurrence relation used to determine the partial fraction coefficients, $\tilde{Y}^{J-l}_{i_1,r}$. The potential for other round-off errors can also be a problem in the F_N algorithm, e.g., numerous matrices are inverted, large summations are made, and numerical

integrations are performed. These problems can be mitigated, but not avoided, by using sound and proven numerical solution techniques, such as Crout's Algorithm with partial pivoting and back-substitution for solution of all matrix equations.

The MGSLAB, MGSEMI, and FNCRIT programs created for this dissertation can also be used without accessing the GIT algorithm. The programs can be used to obtain answers to problems in themselves, or can be used as an accurate benchmark. Also, the F_N algorithm treats some problems that would be difficult for an S_N based code, in particular, deep particle penetration problems. Since the spatial variable is not discretized, there are no discretization errors. Therefore, the flux at the spatial point of interest can be determined in one calculation using the F_N method. In contrast, the S_N method contains inherent discretization errors with every spatial step in the slab until the point of interest is reached. For deep penetration problems with many spatial steps, the errors can accumulate until the resultant fluxes are meaningless.

The major problem with the F_N algorithm is the choice of the basis functions used in the expansion. The closer the lower order basis functions fit the solution, the more accurate the F_N algorithm becomes, and the number of terms needed to represent the solution is reduced; thus, the potential for truncation error is avoided. This can be overcome in part by allowing various basis functions to be available to the user. The initial basis function may not solve the problem, but trial and error should converge on the best set of basis functions to use for the

particular problem being studied.

This dissertation is the starting point for a comprehensive benchmark for the galactic cosmic ray cascade. The major issue that still requires addressing is the reformulation of the GIT closed-form solution to allow for isotopes of the ions being created by fragmentation; that is, the inclusion of neutrons in the formulation. The approximation that allows a fraction of particles with a charge of one to represent neutrons, the f_n parameter, destroys the charge conservation of the multiplicities and is *ad hoc*. In addition, more extensive cross section sets should be used. The 20 MeV limitation of the ENDF/B V database hinders this benchmark and is inconvenient for normal use. If the initial ion energy is raised without adding the requisite cross sections, the high energy neutrons scattered below 20 MeV are not considered, and invalid answers are produced as has been shown.

Only the Green's function formulation of the GIT solution is used in this work. This allows verification of the techniques used to solve the galactic cosmic ray cascade. Other formulations of the GIT solution exist for an energy distributed source and a composite ion beam source. The basis function expansion method used in the F_N algorithm can also be used on the anisotropic scattering transport equation. In addition, a simultaneous method or a source iteration can be incorporated to include flux dependent sources such as upscatter or fission. These utilities could be incorporated into this benchmark.

To determine the coupled charged particle and neutron fluxes another method can be used. This method is based on the S_N solution to the three dimensional neutral particle and Spencer-Lewis charged particle transport equations utilizing SMART scattering (References [2] and [3]). Whether this method is used as a benchmark for BRYNTRN or as a replacement, it should be investigated when a production version of the program is released.

The algorithm and programs presented in this dissertation generate results that can be verified and explained. An example and application are presented and the results are well understood within the physical assumptions. Therefore, this work, assuming the use of proper cross sections, will generate a benchmark quality solution to the galactic cosmic ray cascade and other transport problems of import.

APPENDIX A

DERIVATION OF THE ANALYTICAL SOLUTION TO THE NEUTRAL PARTICLE TRANSPORT EQUATION

In this appendix, the steps involved in deriving the simplified Boltzmann equation used in the F_N method and the manipulations needed to generate the resultant equations used in the various programs are shown.

The full Boltzmann transport equation is

$$\left[\frac{1}{v}\frac{\partial}{\partial t} + \mathbf{\Omega}\cdot\nabla_{\mathbf{r}} + \mathbf{a}\cdot\nabla_{\mathbf{v}} + \sigma(\mathbf{r},\mathrm{E})\right]\Phi(\mathbf{r},\mathbf{\Omega},\mathrm{E},t) =$$
$$= \int_0^\infty \mathrm{dE}' \int_{4\pi} \mathrm{d}\mathbf{\Omega}'\,\sigma(\mathbf{r},\mathrm{E}')\,\mathrm{f}(\mathbf{r};\mathbf{\Omega}',\mathrm{E}'\rightarrow\mathbf{\Omega},\mathrm{E})\,\Phi(\mathbf{r},\mathbf{\Omega}',\mathrm{E}',t) + \qquad (A.1)$$
$$+ \mathrm{Q}(\mathbf{r},\mathbf{\Omega},\mathrm{E},t).$$

The sections below use various assumptions and approximations to reduce this equation to a form that describes the physical situation being studied and can be solved using analytical techniques.

A.1 Creation of a One Dimensional Transport Equation

These steps transform the Boltzmann equation in to a one dimensional, multiple group, multiple region transport equation suitable for the F_N method.

1. Assume

   - Steady State.

- No external forces acting on the particle

$$\mathbf{a} \cdot \nabla_{\mathbf{v}} \; = \; 0. \tag{A.2}$$

- Plane geometry

$$\mathbf{\Omega} \cdot \mathbf{r} \; = \; \cos\theta = \mu, \tag{A.3a}$$

$$\mathbf{\Omega} \cdot \nabla \Phi(\mathbf{r}, \mathbf{\Omega}, \mathrm{E}) = \mu \frac{\partial}{\partial z} \Phi(x, \mu, \mathrm{E}), \tag{A.3b}$$

$$\sigma(\mathbf{r}, \mathrm{E}) \Phi(\mathbf{r}, \mathbf{\Omega}, \mathrm{E}) = \sigma(x, \mathrm{E}) \Phi(x, \mu, \mathrm{E}), \tag{A.3c}$$

$$\begin{aligned} \int_0^\infty \mathrm{dE}' \int_{4\pi} \mathrm{d}\mathbf{\Omega}' \, \sigma(\mathbf{r}, \mathrm{E}) \mathrm{f}(\mathbf{r}; \mathbf{\Omega}', \mathrm{E}' \rightarrow \mathbf{\Omega}, \mathrm{E}) \Phi(x, \mu', \mathrm{E}') = \\ \int_0^\infty \mathrm{dE}' \int_{4\pi} \mathrm{d}\mathbf{\Omega}' \, \sigma(x, \mathrm{E}') \mathrm{f}(x; \mathbf{\Omega}', \mathrm{E}' \rightarrow \mathbf{\Omega}, \mathrm{E}) \Phi(x, \mu, \mathrm{E}), \end{aligned} \tag{A.3d}$$

$$\mathrm{Q}(\mathbf{r}, \mathbf{\Omega}, \mathrm{E}) \; = \; \mathrm{Q}(x, \mu, \mathrm{E}). \tag{A.3e}$$

- f depends only on $\mathbf{\Omega}' \cdot \mathbf{\Omega} = \mu_0$

$$\sigma(x, \mathrm{E}') \; \mathrm{f}(x; \mathbf{\Omega}', \mathrm{E}' \rightarrow \mathbf{\Omega}, \mathrm{E}) \; = \; \sigma(x, \mathrm{E}') \; \mathrm{f}(x; \mathrm{E}' \rightarrow \mathrm{E}; \mu_0). \tag{A.4}$$

2. Expand $\sigma(x, \mathrm{E}') \; \mathrm{f}(x; \mathrm{E}' \rightarrow \mathrm{E}; \mu_0)$ in Legendre polynomials

$$\sigma(x, \mathrm{E}') \; \mathrm{f}(x; \mathrm{E}' \rightarrow \mathrm{E}; \mu_0) \; = \sum_{l=0}^{\infty} \frac{2l+1}{4\pi} \; \sigma_l(x; \mathrm{E}' \rightarrow \mathrm{E}) \; P_l(\mu_0), \tag{A.5a}$$

where,

$$\sigma_l(x; \mathrm{E}' \rightarrow \mathrm{E}) \; = \; 2\pi \int_{-1}^{+1} \mathrm{d}\mu_0 \, \sigma(x, \mathrm{E}) \; f(x; \mathrm{E}' \rightarrow \mathrm{E}; \mu_0) P_l(\mu_0), \tag{A.5b}$$

and assume isotropic scattering by truncating the series at $l = 0$

$$\int_{-1}^{+1} \mathrm{d}\mu_0 \, \sigma(x, \mathrm{E}') \; \mathrm{f}(x; \mathrm{E}' \rightarrow \mathrm{E}; \mu_0) \; = \; \frac{1}{2\pi} \sigma_0(x, \mathrm{E}' \rightarrow \mathrm{E}). \tag{A.6}$$

3. Expand $Q(x, \mu, E)$ in Legendre polynomials

$$Q(x, \mu, E) = \sum_{l=0}^{\infty} \frac{2l+1}{4\pi} Q_l(x, E) P_l(\mu), \tag{A.7a}$$

where,

$$Q_l(x, E) = 2\pi \int_{-1}^{+1} d\mu \, Q(x, \mu, E) P_l(\mu), \tag{A.7b}$$

and assume an isotropic source by truncating the series at $l = 0$

$$Q(x, \mu, E) = \frac{1}{2\pi} Q_0(x, E) = \frac{1}{2} S(x, E). \tag{A.8a}$$

4. Substitute these assumptions into equation (A.1) to obtain

$$\begin{aligned} &\left[\mu \frac{\partial}{\partial z} + \sigma(x, E)\right] \Phi(x, \mu, E) = \\ &\quad = \frac{1}{2} \int_0^{\infty} dE' \, \sigma_0(x; E' \rightarrow E) \int_{-1}^{+1} d\mu' \, \Phi(x, \mu', E') + \frac{1}{2} S(x, E). \end{aligned} \tag{A.9}$$

5. Specify the standard multigroup procedure

$$\int_0^{\infty} dE' \, (\cdot) = \sum_{g'=1}^{G} \int_{E_{g'}}^{E_{g'-1}} dE' \, (\cdot). \tag{A.10}$$

Substituting this into the transport equation gives

$$\begin{aligned} &\left[\mu \frac{\partial}{\partial z} + \sigma(z, E)\right] \Phi(x, \mu, E) = \\ &\quad = \frac{1}{2} \sum_{g'=1}^{G} \int_{E_{g'}}^{E_{g'-1}} dE' \, \sigma_0(x; E' \rightarrow E) \int_{-1}^{+1} d\mu' \, \Phi(x, \mu', E') + \\ &\quad + \frac{1}{2} S(x, E). \end{aligned} \tag{A.11}$$

6. Integrate the transport equation over $\mathrm{E} \in [\mathrm{E}_g, \mathrm{E}_{g-1}]$ and define

$$\phi_g(x,\mu) \equiv \int_{\mathrm{E}_g}^{\mathrm{E}_{g-1}} \mathrm{dE}\, \Phi(x,\mu,\mathrm{E}), \tag{A.12a}$$

$$\mathrm{S}_g^{\mathrm{i}}(x) \equiv \int_{\mathrm{E}_g}^{\mathrm{E}_{g-1}} \mathrm{dE}\, \mathrm{S}(x,\mathrm{E}), \tag{A.12b}$$

$$\sigma_g(x) \int_{\mathrm{E}_g}^{\mathrm{E}_{g-1}} \mathrm{dE}\, \Phi(x,\mu,\mathrm{E}) \equiv \int_{\mathrm{E}_g}^{\mathrm{E}_{g-1}} \mathrm{dE}\, \sigma(x,\mathrm{E})\Phi(x,\mu,\mathrm{E}). \tag{A.12c}$$

The resulting set of transport equations for $g = 1, 2, \ldots, G$ are

$$\begin{aligned} &\left[\mu\frac{\partial}{\partial z} + \sigma_g(z)\right]\phi_g(x,\mu) = \\ &\quad = \frac{1}{2}\int_{\mathrm{E}_g}^{\mathrm{E}_{g-1}} \mathrm{dE} \sum_{g'=1}^{G} \int_{\mathrm{E}_{g'}}^{\mathrm{E}_{g'-1}} \mathrm{dE}'\, \sigma_0(x;\mathrm{E}' \to \mathrm{E}) \times \\ &\quad \times \int_{-1}^{+1} \mathrm{d}\mu'\, \Phi(x,\mu,\mathrm{E}) + \frac{1}{2}\mathrm{S}_g^{\mathrm{i}}(x). \end{aligned} \tag{A.13}$$

7. Assume the scattering term can be rewritten as

$$\frac{1}{2}\int_{-1}^{+1} \mathrm{d}\mu' \sum_{g'=1}^{G} \left[\int_{\mathrm{E}_{g'}}^{\mathrm{E}_{g'-1}} \mathrm{dE}'\, \Phi(x,\mu',\mathrm{E}') \int_{\mathrm{E}_g}^{\mathrm{E}_{g-1}} \mathrm{dE}\, \sigma_0(x;\mathrm{E}' \to \mathrm{E})\right], \tag{A.14a}$$

then define

$$\begin{aligned} &\sigma_{g'\to g}(x) \int_{\mathrm{E}_{g'}}^{\mathrm{E}_{g'-1}} \mathrm{dE}'\, \Phi(x,\mu',\mathrm{E}') \equiv \\ &\quad \equiv \int_{\mathrm{E}_{g'}}^{\mathrm{E}_{g'-1}} \mathrm{dE}'\, \Phi(x,\mu',\mathrm{E}') \int_{\mathrm{E}_g}^{\mathrm{E}_{g-1}} \mathrm{dE}\, \sigma_0(x;\mathrm{E} \to \mathrm{E}), \end{aligned} \tag{A.14b}$$

to give

$$\begin{aligned} &\left[\mu\frac{\partial}{\partial z} + \sigma_g(x)\right]\phi_g(x,\mu) = \\ &\quad = \frac{1}{2}\sum_{g'=1}^{G} \sigma_{g'\to g}(x) \int_{-1}^{+1} \mathrm{d}\mu'\, \phi_{g'}(x,\mu') + \frac{1}{2}\mathrm{S}_g^{\mathrm{i}}(x). \end{aligned} \tag{A.15}$$

8. Assume constant cross sections across slab i

$$\left[\mu\frac{\partial}{\partial z} + \sigma_g^i\right]\phi_g(x,\mu) = \\ = \frac{1}{2}\sum_{g'=1}^{G}\sigma_{g'\to g}^i\int_{-1}^{+1}\mathrm{d}\mu'\,\phi_{g'}(x,\mu') + \frac{1}{2}\mathrm{S}_g^i(x). \tag{A.16a}$$

9. Use these boundary conditions, where $\mathrm{F}_{\mathrm{L}}^{g,i}(\mu)$ and $\mathrm{F}_{\mathrm{R}}^{g,i}(\mu)$ are known functions

$$\phi_g(x_{i-1},\mu) = \mathrm{F}_{\mathrm{L}}^{g,i}(\mu) \qquad \mu > 0, \tag{A.16b}$$

$$\phi_g(x_i,-\mu) = \mathrm{F}_{\mathrm{R}}^{g,i}(\mu) \qquad \mu > 0. \tag{A.16c}$$

A.2 Creation of a Set of Integral Equations on a Slab Boundary

These steps create a set of complex integral equations from the transport equation, equations (A.16). The complex integrals are evaluated on the real axis by use of the Plemelj relations.

1. Replace μ by $-\mu$, multiply by $e^{-\frac{\sigma_g^i x}{s}}$, and integrate x on $[z_1,z_2]$

$$\frac{s\mu}{\mu-s}B_g(\mu,s) - \sigma_g^i\int_{z_1}^{z_2}\mathrm{d}x\,e^{-\frac{\sigma_g^i x}{s}}\phi_g(x,-\mu) = \\ = \sum_{g'=1}^{G}\frac{\sigma_{g'}^i}{2}\,\frac{s}{\mu-s}\,\rho_{gg'}^*(s) + \frac{1}{2}\frac{s}{\mu-s}\,\mathrm{S}_g^*(s,z_1,z_2), \tag{A.17a}$$

where,

$$B_g(\mu,s) = e^{-\frac{\sigma_g^i z_1}{s}}\phi_g(z_1,-\mu) - e^{-\frac{\sigma_g^i z_2}{s}}\phi_g(z_2,-\mu), \tag{A.17b}$$

$$\rho_{gg'}^*(s) = \int_{z_1}^{z_2}\mathrm{d}x\,e^{-\frac{\sigma_g^i x}{s}}\int_{-1}^{+1}\mathrm{d}\mu'\,\phi_{g'}(x,-\mu'), \tag{A.17c}$$

$$\mathrm{S}_g^*(s,z_1,z_2) = \int_{z_1}^{z_2}\mathrm{d}x\,e^{-\frac{\sigma_g^i x}{s}}\mathrm{S}_g^i(x). \tag{A.17d}$$

2. Divide by s and integrate μ on $[-1,+1]$

$$\int_{-1}^{+1} \mathrm{d}\mu \, \frac{\mu}{\mu - s} B_g(\mu, s) \;=\; \sigma_g^i \sum_{g'=1}^{G} \frac{\rho_{gg'}^*(s)}{s} \Lambda_{g'g}(s) + \\ + \mathrm{L}(s) \mathrm{S}_g^*(s, z_1, z_2), \tag{A.18a}$$

where,

$$\Lambda_{g'g}(s) \;=\; \delta_{g'g} \;+\; \frac{s\sigma_{g'\to g}^i}{\sigma_g^i} \mathrm{L}(s), \tag{A.18b}$$

$$\mathrm{L}(s) \;=\; \frac{1}{2} \int_{-1}^{+1} \mathrm{d}\mu \, \frac{1}{\mu - s}. \tag{A.18c}$$

3. Multiply by $e^{\frac{\sigma_g^i z_1}{s}}$

$$\int_{-1}^{+1} \mathrm{d}\mu \, \frac{\mu}{\mu - s} C_g(\mu, s) \;=\; \sigma_g^i \sum_{g'=1}^{G} \mathrm{I}_{gg'}^{*i}(s, z_1, z_2) \Lambda_{g'g}(s) + \\ + \mathrm{L}(s) \mathrm{S}_g^*(s, z_1, z_2) e^{\frac{\sigma_g^i z_1}{s}}, \tag{A.19a}$$

where,

$$\begin{aligned} C_g(\mu, s) \;&=\; e^{\frac{\sigma_g^i z_1}{s}} B_g(\mu, s) \\ &=\; \phi_g(z_1, -\mu) \;-\; e^{-\frac{\sigma_g^i (z_2 - z_1)}{s}} \phi_g(z_2, -\mu), \end{aligned} \tag{A.19b}$$

$$\begin{aligned} \mathrm{I}_{gg'}^{*i}(s, z_1, z_2) \;&=\; \frac{e^{\frac{\sigma_g^i z_1}{s}}}{s} \rho_{gg'}^*(s) \\ &=\; \frac{1}{s} \int_{z_1}^{z_2} \mathrm{d}x \, e^{-\frac{\sigma_g^i (x - z_1)}{s}} \int_{-1}^{+1} \mathrm{d}\mu \, \phi_{g'}(x, -\mu). \end{aligned} \tag{A.19c}$$

4. Change $s = -s$ and $\mu = -\mu$ in equation (A.18a), and multiply by $e^{-\frac{\sigma_g^i z_2}{s}}$

$$\int_{-1}^{+1} \mathrm{d}\mu \, \frac{\mu}{\mu - s} D_g(\mu, s) \;=\; \sigma_g^i \sum_{g'=1}^{G} \mathrm{J}_{gg'}^{*i}(s, z_1, z_2) \Lambda_{g'g}(s) + \\ + \mathrm{L}(s) \mathrm{S}_g^*(-s, z_1, z_2) e^{-\frac{\sigma_g^i z_2}{s}}, \tag{A.20a}$$

where,

$$\begin{aligned} D_g(\mu,s) &= -e^{-\frac{\sigma_g^i x_2}{s}} B_g(-\mu,-s) \\ &= \phi_g(z_2,\mu) - e^{-\frac{\sigma_g^i(x_2-z_1)}{s}} \phi_g(z_1,\mu), \end{aligned} \tag{A.20b}$$

$$\begin{aligned} \mathrm{J}^{*i}_{gg'}(s,z_1,z_2) &= \frac{e^{-\frac{\sigma_g^i x_2}{s}}}{s} \rho^*_{gg'}(s) \\ &= \frac{1}{s}\int_{z_1}^{z_2} \mathrm{d}x\, e^{-\frac{\sigma_g^i(x_2-x)}{s}} \int_{-1}^{+1} \mathrm{d}\mu\, \phi_{g'}(x,-\mu). \end{aligned} \tag{A.20c}$$

5. Define ν_0^g to be the zero of the infinite medium dispersion relation, $\Lambda_{gg}(s)$ (Note: if $\frac{\sigma_{g\to g}^i}{\sigma_g^i} < 1$ then $|\nu_0^g| > 1$ and real). Then $\mathrm{L}(\nu_0^g)$ becomes

$$\mathrm{L}(\nu_0^g) = -\frac{\sigma_g^i}{\sigma_{g\to g}^i\, \nu_0^g}. \tag{A.21}$$

The integral equations, equations (A.19a) and (A.20a), become a set of constraints (related to the concept of boundary conditions for differential equations)

$$\int_{-1}^{+1} \mathrm{d}\mu\, \frac{\mu}{\mu-\nu_0^g} C_g(\mu,\nu_0^g) = -\frac{\sigma_g^i}{\nu_0^g \sigma_{g\to g}^i} \mathrm{S}^*_g(\nu_0^g,z_1,z_2) e^{\frac{\sigma_g^i z_1}{\nu_0^g}}, \tag{A.22a}$$

$$\int_{-1}^{+1} \mathrm{d}\mu\, \frac{\mu}{\mu-\nu_0^g} D_g(\mu,\nu_0^g) = -\frac{\sigma_g^i}{\nu_0^g \sigma_{g\to g}^i} \mathrm{S}^*_g(-\nu_0^g,z_1,z_2) e^{-\frac{\sigma_g^i z_2}{\nu_0^g}}. \tag{A.22b}$$

6. Use the Plemelj relation (Reference [22])

$$\lim_{\epsilon\to 0} \frac{1}{\eta-(\nu\pm i\epsilon)} = \wp\left[\frac{1}{\eta-\nu}\right] \pm i\pi\delta(\eta-\nu), \tag{A.23a}$$

to restrict the integrals to the real axis. If the Cauchy type integral

$$\chi(s) = \int_{-1}^{+1} \mathrm{d}\eta\, \frac{f(\eta)}{\eta-s}, \tag{A.23b}$$

is evaluated using the Plemelj relations, the new formulation is

$$\lim_{\epsilon \to 0} \chi(\nu \pm i\epsilon) = \chi^{\pm}(\nu) = \fint_{-1}^{+1} d\eta \, \frac{f(\eta)}{\eta - \nu} \pm i\pi f(\nu). \tag{A.23c}$$

Apply these rules of integration to the integral equations to obtain

$$\begin{aligned} &\fint_{-1}^{+1} d\eta \, \frac{\eta}{\eta - \nu} C_g(\eta, \nu) \; \pm \; i\pi\nu C_g(\nu, \nu) \; = \\ &\quad = \; \sigma_g^i \sum_{g'=1}^{G} \Lambda_{g'g}^{\pm}(\nu) \; I_{gg'}^{*i}(\nu, z_1, z_2) \; + \; e^{\frac{\sigma_g^i z_1}{\nu}} S_g^*(\nu, z_1, z_2) L^{\pm}(\nu), \end{aligned} \tag{A.24a}$$

$$\begin{aligned} &\fint_{-1}^{+1} d\eta \, \frac{\eta}{\eta - \nu} D_g(\eta, \nu) \; \pm \; i\pi\nu D_g(\nu, \nu) \; = \\ &\quad = \sigma_g^i \sum_{g'=1}^{G} \Lambda_{g'g}^{\pm}(\nu) \; J_{gg'}^{*i}(\nu, z_1, z_2) + e^{-\frac{\sigma_g^i z_2}{\nu}} S_g^*(-\nu, z_1, z_2) L^{\pm}(\nu), \end{aligned} \tag{A.24b}$$

where,

$$L^{\pm}(\nu) \; = \; \frac{1}{2} \fint_{-1}^{+1} d\eta \, \frac{1}{\eta - \nu} \; \pm \; \frac{i\pi}{2}, \tag{A.24c}$$

$$\Lambda_{g'g}^{\pm}(\nu) \; = \; \lambda_{g'g}(\nu) \; \pm \; \frac{i\pi\nu\sigma_{g' \to g}^i}{2\sigma_g^i}, \tag{A.24d}$$

$$\lambda_{g'g}(\nu) \; = \; \delta_{g'g} \; + \; \frac{\nu\sigma_{g' \to g}^i}{2\sigma_g^i} \fint_{-1}^{+1} d\eta \, \frac{1}{\eta - \nu} \; = \; \delta_{g'g} \; + \; \frac{\nu\sigma_{g' \to g}^i}{2\sigma_g^i} \ln \left| \frac{1 - \nu}{1 + \nu} \right| . \tag{A.24e}$$

(note: all integration variables have been changed to η and $\nu \in [0, 1] \cup \nu_0^g$)

7. Eliminate $I_{gg}^{*i}(\nu, z_1, z_2)$ and $J_{gg}^{*i}(\nu, z_1, z_2)$ by adding and subtracting the positive and negative branches of the equations and combining, there results

$$\begin{aligned}
&\int_{-1}^{+1} d\eta \, \frac{\eta}{\eta-\nu} C_g(\eta,\nu) - \frac{2\sigma_g^i}{\sigma_{g\to g}^i} \lambda_{gg}(\nu) C_g(\nu,\nu) \; = \\
&\quad = \; -\frac{\sigma_g^i e^{\frac{\sigma_g^i x_1}{\nu}}}{\nu \sigma_{g\to g}^i} \mathrm{S}_g^*(\nu, z_1, z_2) \; + \\
&\quad + \; \frac{\sigma_{g\to g}^i}{\sigma_g^i} \sum_{\substack{g'=1 \\ g'\neq g}}^{G} \sigma_{g'\to g}^i \; \mathrm{I}_{gg'}^{*i}(\nu, z_1, z_2),
\end{aligned} \tag{A.25a}$$

$$\begin{aligned}
&\int_{-1}^{+1} d\eta \, \frac{\eta}{\eta-\nu} D_g(\eta,\nu) - \frac{2\sigma_g^i}{\sigma_{g\to g}^i} \lambda_{gg}(\nu) D_g(\nu,\nu) \; = \\
&\quad = \; -\frac{\sigma_g^i e^{-\frac{\sigma_g^i x_2}{\nu}}}{\nu \sigma_{g\to g}^i} \mathrm{S}_g^*(-\nu, z_1, z_2) \; + \\
&\quad + \; \frac{\sigma_{g\to g}^i}{\sigma_g^i} \sum_{\substack{g'=1 \\ g'\neq g}}^{G} \sigma_{g'\to g}^i \; \mathrm{J}_{gg'}^{*i}(\nu, z_1, z_2).
\end{aligned} \tag{A.25b}$$

8. Rewrite the integral equations in terms of the fluxes by changing the integration variables so they are evaluated on the interval $[0,1]$ to obtain

$$\begin{aligned}
&\int_0^1 d\eta \, \frac{\eta}{\eta-\nu} \phi_g(x_{i-1}, -\eta) \; + \; \int_0^1 d\eta \, \frac{\eta}{\eta+\nu} \phi_g(x_{i-1}, \eta) \; - \\
&\quad - e^{-\frac{\Delta_g^i}{\nu}} \left[\int_0^1 d\eta \, \frac{\eta}{\eta-\nu} \phi_g(x_i, -\eta) + \int_0^1 d\eta \, \frac{\eta}{\eta+\nu} \phi_g(x_i, \eta) \right] - \\
&\quad - \; \frac{2\sigma_g^i}{\sigma_{g\to g}^i} \lambda_{gg}(\nu) \left[\phi_g(x_{i-1}, -\nu) \; - \; \phi_g(x_i, -\nu) e^{-\frac{\Delta_g^i}{\nu}} \right] \; = \\
&\quad = \; -\frac{\sigma_g^i}{\sigma_{g\to g}^i} \sum_{\substack{g'=1 \\ g'\neq g}}^{G} \sigma_{g'\to g}^i \mathrm{I}_{gg'}^{*i}(\nu, x_{i-1}, x_i) \; - \\
&\quad - \; \frac{\sigma_g^i e^{\frac{\sigma_g^i x_{i-1}}{\nu}}}{\nu \sigma_{g\to g}^i} \mathrm{S}_g^*(\nu, x_{i-1}, x_i),
\end{aligned} \tag{A.26a}$$

$$
\begin{aligned}
&\int_0^1 d\eta \, \frac{\eta}{\eta-\nu}\phi_g(x_i,\eta) \; + \; \int_0^1 d\eta \, \frac{\eta}{\eta+\nu}\phi_g(x_i,-\eta) \; - \\
&\quad -e^{-\frac{\Delta_g^i}{\nu}}\left[\int_0^1 d\eta \, \frac{\eta}{\eta-\nu}\phi_g(x_{i-1},\eta) + \int_0^1 d\eta \, \frac{\eta}{\eta+\nu}\phi_g(x_{i-1},-\eta)\right] - \\
&\quad - \frac{2\sigma_g^i}{\sigma_{g\to g}^i}\lambda_{gg}(\nu)\left[\phi_g(x_i,\nu) \; - \; \phi_g(x_{i-1},\nu)e^{-\frac{\Delta_g^i}{\nu}}\right] \; = \\
&\quad = \; -\frac{\sigma_g^i}{\sigma_{g\to g}^i}\sum_{\substack{g'=1 \\ g'\neq g}}^{G}\sigma_{g'\to g}^i \mathrm{J}_{gg'}^{*i}(\nu,x_{i-1},x_i) \; - \\
&\quad - \frac{\sigma_g^i e^{-\frac{\sigma_g^i x_i}{\nu}}}{\nu\sigma_{g\to g}^i}\mathrm{S}_g^*(-\nu,x_{i-1},x_i),
\end{aligned}
\tag{A.26b}
$$

where, z_1 and z_2 are defined as the slab boundaries, x_{i-1} and x_i and $\Delta_g^i = \sigma_g^i\,(x_i - x_{i-1})$ is the dimensionless slab width.

These integral equations are in the form of an inhomogeneous Fredholm equation. Various methods of solution are available. The one chosen for this work is a basis function expansion and a collocation method for determination of the expansion coefficients.

A.3 Application of the F_N Approximation to the Slab Boundary Integral Equations

The method used to solve equations (A.26) is a basis function expansion called the F_N approximation first developed by C. E. Siewert. The basis functions can be any set of functions; however, orthogonal functions on the interval $[0,1]$ create matrices that are not ill-conditioned as with the matrices generated by non-orthogonal functions.

Substitute these boundary conditions and F_N approximations into the

integral equations

$$\phi_g(x_{i-1},\nu) \;=\; \mathrm{F}_{\mathrm{L}}^{g,i}(\nu), \tag{A.27a}$$

$$\phi_g(x_i,-\nu) \;=\; \mathrm{F}_{\mathrm{R}}^{g,i}(\nu), \tag{A.27b}$$

$$\phi_g(x_{i-1},\nu) \;=\; \mathrm{F}_{\mathrm{L}}^{g,i}(\nu)e^{-\frac{\Delta_g^i}{\nu}} \;+\; \frac{\sigma_{g\to g}^i}{2\sigma_g^i}\sum_{\alpha=0}^{N-1}\mathrm{b}_\alpha^{g,i}\psi_\alpha(\nu), \tag{A.28a}$$

$$\phi_g(x_i,-\nu) \;=\; \mathrm{F}_{\mathrm{R}}^{g,i}(\nu)e^{-\frac{\Delta_g^i}{\nu}} \;+\; \frac{\sigma_{g\to g}^i}{2\sigma_g^i}\sum_{\alpha=0}^{N-1}\mathrm{a}_\alpha^{g,i}\psi_\alpha(\nu), \tag{A.28b}$$

to generate a related set of singular integral equations that are solved for the expansion coefficients using a collocation procedure. The resultant integral equations are

$$\begin{aligned}\sum_{\alpha=0}^{N-1}\left[\mathrm{a}_\alpha^{g,i}\mathrm{B}_\alpha^g(\nu) \;+\mathrm{b}_\alpha^{g,i}\mathrm{A}_\alpha^g(\nu)e^{-\frac{\Delta_g^i}{\nu}}\right] \;&=\; \mathrm{R1}_g^i(\nu,x_{i-1}) \;+\\ +\;\frac{1}{\sigma_{g\to g}^i}\mathrm{T1}_g^i(\nu,x_{i-1},x_i) \;&+\; \frac{1}{\sigma_{g\to g}^i}\mathrm{S1}_g^i(\nu,x_{i-1},x_i),\end{aligned} \tag{A.29a}$$

$$\begin{aligned}\sum_{\alpha=0}^{N-1}\left[\mathrm{b}_\alpha^{g,i}\mathrm{B}_\alpha^g(\nu) \;+\; \mathrm{a}_\alpha^{g,i}\mathrm{A}_\alpha^g(\nu)e^{-\frac{\Delta_g^i}{\nu}}\right] \;&=\; \mathrm{R2}_g^i(\nu,x_i) \;+\\ +\;\frac{1}{\sigma_{g\to g}^i}\mathrm{T2}_g^i(\nu,x_{i-1},x_i) \;&+\; \frac{1}{\sigma_{g\to g}^i}\mathrm{S2}_g^i(\nu,x_{i-1},x_i),\end{aligned} \tag{A.29b}$$

where,

$$\mathrm{A}_\alpha^g(\nu) \;=\; \frac{\sigma_{g\to g}^i}{2\sigma_g^i}\int_0^1 \mathrm{d}\eta\,\frac{\eta}{\eta+\nu}\psi_\alpha(\eta), \tag{A.29c}$$

$$\mathrm{B}_\alpha^g(\nu) \;=\; \lambda_{gg}(\nu)\psi_\alpha(\nu) \;-\; \frac{\sigma_{g\to g}^i}{2\sigma_g^i}\int_0^1 \mathrm{d}\eta\,\frac{\eta}{\eta-\nu}\psi_\alpha(\eta), \tag{A.29d}$$

$$\mathrm{R1}_g^i(\nu,x_{i-1}) \;=\; \int_0^1 \mathrm{d}\eta\,\eta\left[\mathrm{F}_{\mathrm{R}}^{g,i}(\eta)\mathrm{C}(\Delta_g^i,\nu,\eta) \;+\; \mathrm{F}_{\mathrm{L}}^{g,i}(\eta)\mathrm{S}(\Delta_g^i,\nu,\eta)\right], \tag{A.29e}$$

$$R2_g^i(\nu, x_i) = \int_0^1 d\eta\, \eta \left[F_L^{g,i}(\eta) C(\Delta_g^i, \nu, \eta) + F_R^{g,i}(\eta) S(\Delta_g^i, \nu, \eta) \right], \tag{A.29f}$$

$$C(\Delta_g^i, \nu, \eta) = \frac{e^{-\frac{\Delta_g^i}{\nu}} - e^{-\frac{\Delta_g^i}{\eta}}}{\nu - \eta}, \tag{A.29g}$$

$$S(\Delta_g^i, \nu, \eta) = \frac{1 - e^{-\Delta_g^i \left[\frac{1}{\nu} + \frac{1}{\eta}\right]}}{\eta + \nu}, \tag{A.29h}$$

$$T1_g^i(\nu, x_{i-1}, x_i) = \sigma_g^i \sum_{\substack{g'=1 \\ g' \neq g}}^{G} \sigma_{g' \to g}^i I_{gg'}^{*i}(\nu, x_{i-1}, x_i), \tag{A.29i}$$

$$T2_g^i(\nu, x_{i-1}, x_i) = \sigma_g^i \sum_{\substack{g'=1 \\ g' \neq g}}^{G} \sigma_{g' \to g}^i J_{gg'}^{*i}(\nu, x_{i-1}, x_i), \tag{A.29j}$$

$$S1_g^i(\nu, x_{i-1}, x_i) = \frac{\sigma_g^i}{\nu} \int_{x_{i-1}}^{x_i} dz\, e^{-\frac{\sigma_g^i (z - x_{i-1})}{\nu}} S_g^i(z), \tag{A.29k}$$

$$S2_g^i(\nu, x_{i-1}, x_i) = \frac{\sigma_g^i}{\nu} \int_{x_{i-1}}^{x_i} dz\, e^{-\frac{\sigma_g^i (x_i - z)}{\nu}} S_g^i(z). \tag{A.29l}$$

These equations are changed into matrix equations using the collocation procedure and the expansion coefficients $a_\alpha^{g,i}$ and $b_\alpha^{g,i}$ are determined using a matrix decomposition scheme as described in Chapter 3.

A.3.1 Singularities Encountered in the F_N Equations

The integral term $B_\alpha^g(\nu)$, the exponential term $C(\Delta_g^i, \nu, \eta)$, and the source terms $S1_g^i(\nu, x_{i-1}, x_i)$ and $S2_g^i(\nu, x_{i-1}, x_i)$ have singularities which must be carefully handled.

For the $B_\alpha^g(\nu)$ term, the original definition is

$$B_\alpha^g(\nu) = \lambda_{gg}(\nu)\psi_\alpha(\nu) - \frac{\sigma_{g \to g}^i}{2\sigma_g^i} \int_0^1 d\eta\, \frac{\eta}{\eta - \nu} \psi_\alpha(\eta), \tag{A.30a}$$

where,

$$\lambda_{gg}(\nu) \;=\; 1 \;+\; \frac{\sigma^i_{g\to g}\nu}{2\sigma^i_g} \fint_{-1}^{+1} \mathrm{d}\eta \, \frac{1}{\eta - \nu}. \tag{A.30b}$$

To regularize this term, if

$$\nu\psi_\alpha(\nu)\frac{\sigma^i_{g\to g}}{2\sigma^i_g} \fint_{-1}^{+1} \mathrm{d}\eta \, \frac{1}{\eta - \nu}$$

is added to the second term and subtracted from the first term, then $\mathrm{B}^g_\alpha(\nu)$ becomes

$$\mathrm{B}^g_\alpha(\nu) \;=\; \lambda^*_{gg}(\nu)\psi_\alpha(\nu) \;-\; \mathrm{B}^{*g}_\alpha(\nu), \tag{A.31a}$$

where,

$$\lambda^*_{gg}(\nu) \;=\; 1 - \frac{\sigma^i_{g\to g}\nu}{2\sigma^i_g} \int_0^1 \mathrm{d}\eta \, \frac{1}{\eta + \nu} \;=\; 1 + \frac{\sigma^i_{g\to g}\nu}{1\sigma^i_g} \ln\left|\frac{\nu}{1+\nu}\right|, \tag{A.31b}$$

$$\mathrm{B}^{*g}_\alpha(\nu) \;=\; \frac{\sigma^i_{g\to g}}{2\sigma^i_g} \int_0^1 \mathrm{d}\eta \, \frac{\eta\psi_\alpha(\eta) \;-\; \nu\psi_\alpha(\nu)}{\eta - \nu}. \tag{A.31c}$$

When $\nu = \eta$, L'Hospital's rule is used to find a new integrand for $\mathrm{B}^{*g}_\alpha(\nu)$, or

$$\mathrm{B}^{*g}_\alpha(\nu) \;=\; \frac{\sigma^i_{g\to g}}{2\sigma^i_g} \int_0^1 \mathrm{d}\eta \begin{cases} \nu \dfrac{\mathrm{d}}{\mathrm{d}\nu}\psi_\alpha(\nu) \;+\; \psi_\alpha(\nu) & \eta = \nu \\ \dfrac{\eta\psi_\alpha(\eta) \;-\; \nu\psi_\alpha(\nu)}{\eta - \nu} & \eta \neq \nu. \end{cases} \tag{A.31d}$$

For the $\mathrm{C}(\Delta^i_g, \nu, \eta)$ term, when $\nu = \eta$, use L'Hospital's rule to obtain

$$\mathrm{C}(\Delta^i_g, \nu, \nu) \;=\; \frac{\Delta^i_g}{\nu^2} \, e^{-\frac{\Delta^i_g}{\nu}}. \tag{A.32}$$

The source terms encounter a singularity as $\nu \to 0$. This problem is solved by structuring the terms to conform to a delta function definition

$$\mathrm{S1}^i_g(\nu, x_{i-1}, x_i) \;=\; \sigma^i_g \int_{x_{i-1}}^{x_i} \mathrm{d}z \, \left[\frac{e^{-\frac{\sigma^i_g(z - x_{i-1})}{\nu}}}{\nu}\right] \mathrm{S}^i_g(z), \tag{A.33a}$$

$$S2_g^i(\nu, x_{i-1}, x_i) \;=\; \sigma_g^i \int_{x_{i-1}}^{x_i} dz \left[\frac{e^{-\frac{\sigma_g^i(x_i - z)}{\nu}}}{\nu}\right] S_g^i(z). \tag{A.33b}$$

As $\nu \rightarrow 0$, the functions in the brackets behave as the delta functions $\delta(\sigma_g^i(z - x_{i-1}))$ and $\delta(\sigma_g^i(x_i - z))$. When the delta functions are placed in the source terms and evaluated, there results

$$S1_g^i(\nu, x_{i-1}, x_i) \;=\; \begin{cases} S_g^i(x_{i-1}) & \nu = 0 \\ \dfrac{\sigma_g^i}{\nu} \displaystyle\int_{x_{i-1}}^{x_i} dz\, e^{-\frac{\sigma_g^i(z - x_{i-1})}{\nu}} S_g^i(z) & \nu \neq 0, \end{cases} \tag{A.33c}$$

$$S2_g^i(\nu, x_{i-1}, x_i) \;=\; \begin{cases} S_g^i(x_i) & \nu = 0 \\ \dfrac{\sigma_g^i}{\nu} \displaystyle\int_{x_{i-1}}^{x_i} dz\, e^{-\frac{\sigma_g^i(x_i - z)}{\nu}} S_g^i(z) & \nu \neq 0. \end{cases} \tag{A.33d}$$

A.3.2 Post Processor

With the regularized $B_\alpha^g(\nu)$ term, the F_N approximations can be rewritten to achieve a faster convergence rate (fewer number of expansion terms required to converge). These equations comprise the post processor and are used to determine the final values of the flux.

If the non-singular expression for $B_\alpha^g(\mu)$ is substituted into the integral equations, equations (A.29), the results are

$$\sum_{\alpha=0}^{N-1} \left[a_\alpha^{g,i} \left(\lambda_{gg}^*(\mu)\psi_\alpha(\mu) \;-\; B_\alpha^{*g}(\mu) \right) + b_\alpha^{g,i} A_\alpha^g(\mu) e^{-\frac{\Delta_g^i}{\mu}} \right] \;=$$
$$=\; R1_g^i(\mu, x_{i-1}) + \frac{1}{\sigma_{g\to g}^i} T1_g^i(\mu, x_{i-1}, x_i) + \frac{1}{\sigma_{g\to g}^i} S1_g^i(\mu, x_{i-1}, x_i), \tag{A.34a}$$

$$\sum_{\alpha=0}^{N-1} \left[b_\alpha^{g,i} \left(\lambda_{gg}^*(\mu)\psi_\alpha(\mu) \;-\; B_\alpha^{*g}(\mu) \right) + a_\alpha^{g,i} A_\alpha^g(\mu) e^{-\frac{\Delta_g^i}{\mu}} \right] \;=$$
$$=\; R2_g^i(\mu, x_i) + \frac{1}{\sigma_{g\to g}^i} T2_g^i(\mu, x_{i-1}, x_i) + \frac{1}{\sigma_{g\to g}^i} S2_g^i(\mu, x_{i-1}, x_i). \tag{A.34b}$$

These equations can be solve for the basis functions to obtain

$$\sum_{\alpha=0}^{N-1} a_\alpha^{g,i}\psi_\alpha(\mu) = \frac{1}{\lambda_{gg}^*(\mu)}\left\{\left[\sum_{\alpha=0}^{N-1} a_\alpha^{g,i}B_\alpha^{*g}(\mu) - b_\alpha^{g,i}A_\alpha^g(\mu)e^{-\frac{\Delta_g^i}{\mu}}\right] + \right.$$
$$\left. +R1_g^i(\mu,x_{i-1}) + \frac{1}{\sigma_{g\to g}^i}T1_g^i(\mu,x_{i-1},x_i) + \frac{1}{\sigma_{g\to g}^i}S1_g^i(\mu,x_{i-1},x_i)\right\}, \tag{A.35a}$$

$$\sum_{\alpha=0}^{N-1} b_\alpha^{g,i}\psi_\alpha(\mu) = \frac{1}{\lambda_{gg}^*(\mu)}\left\{\left[\sum_{\alpha=0}^{N-1} b_\alpha^{g,i}B_\alpha^{*g}(\mu) - a_\alpha^{g,i}A_\alpha^g(\mu)e^{-\frac{\Delta_g^i}{\mu}}\right] + \right.$$
$$\left. +R2_g^i(\mu,x_i) + \frac{1}{\sigma_{g\to g}^i}T2_g^i(\mu,x_{i-1},x_i) + \frac{1}{\sigma_{g\to g}^i}S2_g^i(\mu,x_{i-1},x_i)\right\}. \tag{A.35b}$$

These equations are substituted into the F_N approximations, equations (A.28), to obtain the post processor

$$\phi_g(x_{i-1},-\mu) = F_R^{g,i}(\mu)e^{-\frac{\Delta_g^i}{\mu}} + \frac{1}{2\sigma_g^i\lambda_{gg}^*(\mu)}\left\{\sigma_{g\to g}^i R1_g^i(\mu,x_{i-1}) + \right.$$
$$+\sigma_{g\to g}^i\sum_{\alpha=0}^{N-1}\left[a_\alpha^{g,i}B_\alpha^{*g}(\mu) - b_\alpha^{g,i}A_\alpha^g(\mu)e^{-\frac{\Delta_g^i}{\mu}}\right] + \tag{A.36a}$$
$$\left. +S1_g^i(\mu,x_{i-1},x_i) + T1_g^i(\mu,x_{i-1},x_i)\right\},$$

$$\phi_g(x_i,\mu) = F_L^{g,i}(\mu)e^{-\frac{\Delta_g^i}{\mu}} + \frac{1}{2\sigma_g^i\lambda_{gg}^*(\mu)}\left\{\sigma_{g\to g}^i R2_g^i(\mu,x_i) + \right.$$
$$+\sigma_{g\to g}^i\sum_{\alpha=0}^{N-1}\left[b_\alpha^{g,i}B_\alpha^{*g}(\mu) - a_\alpha^{g,i}A_\alpha^g(\mu)e^{-\frac{\Delta_g^i}{\mu}}\right] + \tag{A.36b}$$
$$\left. +S2_g^i(\mu,x_{i-1},x_i) + T2_g^i(\mu,x_{i-1},x_i)\right\}.$$

A.3.3 Scattering Terms

In this section, the expressions for $I_{gg'}^{*i}(\nu,x_{i-1},x_i)$ and $J_{gg'}^{*i}(\nu,x_{i-1},x_i)$ in the equations

$$T1_g^i(\nu,x_{i-1},x_i) = \sigma_g^i\sum_{\substack{g'=1\\g'\neq g}}^{G}\sigma_{g'\to g}^i I_{gg'}^{*i}(\nu,x_{i-1},x_i), \tag{A.37a}$$

$$T2_g^i(\nu,x_{i-1},x_i) = \sigma_g^i\sum_{\substack{g'=1\\g'\neq g}}^{G}\sigma_{g'\to g}^i J_{gg'}^{*i}(\nu,x_{i-1},x_i), \tag{A.37b}$$

for the scattering terms are derived.

Since the particle group transfer functions $I^{*i}_{gg'}(\nu, x_{i-1}, x_i)$ and $J^{*i}_{gg'}(\nu, x_{i-1}, x_i)$ are dependent on the spatial integral of the scalar flux for all other groups, the scalar flux must be known at all points in the slab. The numerical scheme used to solve the F_N equations dictates that the boundary values must be determined before the interior values. These steps show how the transfer functions are reformulated in terms of the other group angular fluxes at the boundary.

1. The transport equation for group g' can be rewritten with a integrating factor as

$$\mu \frac{\partial}{\partial z}\left[\phi_{g'}(x,\mu)e^{\frac{\sigma^i_{g'}x}{\mu}}\right] = \frac{e^{\frac{\sigma^i_{g'}x}{\mu}}}{2}\sum_{g''=1}^{G}\sigma^i_{g''\to g'}\phi_{g''}(x) + + \frac{e^{-\frac{\sigma^i_{g'}x}{-\mu}}}{2}S^i_{g'}(x), \tag{A.38}$$

which can be integrated on $x \in [z_1, z_2]$ to obtain

$$2\left[\phi_{g'}(z_2,\mu)e^{\frac{\sigma^i_{g'}z_2}{\mu}} - \phi_{g'}(z_1,\mu)e^{\frac{\sigma^i_{g'}z_1}{\mu}}\right] = \frac{1}{\mu}S^*_{g'}(-\mu, z_1, z_2) + + \frac{1}{\mu}\sum_{g''=1}^{G}\sigma^i_{g''\to g'}\int_{z_1}^{z_2}dx\,\phi_{g''}(x)e^{\frac{\sigma^i_{g'}x}{\mu}}. \tag{A.39}$$

2. For a second equation, let $\mu = -\mu$ in the transport equation and integrate on $x \in [z_1, z_2]$ to obtain

$$2\left[\phi_{g'}(z_1,-\mu)e^{-\frac{\sigma^i_{g'}z_1}{\mu}} - \phi_{g'}(z_2,-\mu)e^{-\frac{\sigma^i_{g'}z_2}{\mu}}\right] = = \frac{1}{\mu}S^*_{g'}(\mu, z_1, z_2) + \frac{1}{\mu}\sum_{g''=1}^{G}\sigma^i_{g''\to g'}\int_{z_1}^{z_2}dx\,\phi_{g''}(x)e^{-\frac{\sigma^i_{g'}x}{\mu}}. \tag{A.40}$$

3. Multiply equation (A.39) by $e^{-\frac{\sigma^i_{g'} z_2}{\mu}}$ and equation (A.40) by $e^{\frac{\sigma^i_{g'} z_1}{\mu}}$ to obtain

$$2\left[\phi_{g'}(z_2,\mu) - \phi_{g'}(z_1,\mu)e^{-\frac{\sigma^i_{g'}(z_2-z_1)}{\mu}}\right] =$$
$$= \frac{e^{-\frac{\sigma^i_{g'} z_2}{\mu}}}{\mu} S^*_{g'}(-\mu, z_1, z_2) + \tag{A.41a}$$
$$+ \frac{1}{\mu}\sum_{g''=1}^{G} \sigma^i_{g''\to g'} \int_{z_1}^{z_2} \mathrm{d}x\, \phi_{g''}(x) e^{\frac{\sigma^i_{g'}(z_2-x)}{\mu}},$$

$$2\left[\phi_{g'}(z_1,-\mu) - \phi_{g'}(z_2,-\mu)e^{-\frac{\sigma^i_{g'}(z_2-z_1)}{\mu}}\right] =$$
$$= \frac{e^{\frac{\sigma^i_{g'} z_1}{\mu}}}{\mu} S^*_{g'}(\mu, z_1, z_2) + \tag{A.41b}$$
$$+ \frac{1}{\mu}\sum_{g''=1}^{G} \sigma^i_{g''\to g'} \int_{z_1}^{z_2} \mathrm{d}x\, \phi_{g''}(x) e^{-\frac{\sigma^i_{g'}(x-z_1)}{\mu}}.$$

4. Transform the exponential in the scalar flux integral to be a function of g and not g', by letting $\mu = \frac{\sigma^i_{g'}}{\sigma^i_g}\xi = s_{gg'}\xi < 1$ so that $\xi \in [0, \frac{1}{s_{gg'}}]$ to obtain

$$2\left[\phi_{g'}(z_2, s_{gg'}\xi) - \phi_{g'}(z_1, s_{gg'}\xi)e^{-\frac{\sigma^i_{g'}(z_2-z_1)}{s_{gg'}\xi}}\right] =$$
$$= \frac{e^{-\frac{\sigma^i_{g'} z_2}{s_{gg'}\xi}}}{s_{gg'}\xi} S^*_{g'}(-s_{gg'}\xi, z_1, z_2) + \tag{A.42a}$$
$$+ \frac{1}{s_{gg'}\xi}\sum_{g''=1}^{G} \sigma^i_{g''\to g'} \int_{z_1}^{z_2} \mathrm{d}x\, \phi_{g''}(x) e^{\frac{\sigma^i_{g'}(z_2-x)}{s_{gg'}\xi}},$$

$$2\left[\phi_{g'}(z_1, -s_{gg'}\xi) - \phi_{g'}(z_2, -s_{gg'}\xi)e^{-\frac{\sigma^i_{g'}(z_2-z_1)}{s_{gg'}\xi}}\right] =$$
$$\frac{e^{\frac{\sigma^i_{g'} z_1}{s_{gg'}\xi}}}{s_{gg'}\xi} S^*_{g'}(s_{gg'}\xi, z_1, z_2) + \tag{A.42b}$$
$$+ \frac{1}{s_{gg'}\xi}\sum_{g''=1}^{G} \sigma^i_{g''\to g'} \int_{z_1}^{z_2} \mathrm{d}x\, \phi_{g''}(x) e^{-\frac{\sigma^i_{g'}(x-z_1)}{s_{gg'}\xi}}.$$

5. Remember $\frac{\sigma^i_{g'}}{s_{gg'}} = \sigma^i_g$ so that the transfer functions are rewritten as

$$\frac{1}{\xi}\int_{z_1}^{z_2} \mathrm{d}x\, e^{-\frac{\sigma^i_g(z_2-x)}{\xi}}\phi_{g''}(x) \;=\; \mathrm{J}^{*i}_{gg''}(\xi, z_1, z_2), \tag{A.43a}$$

$$\frac{1}{\xi}\int_{z_1}^{z_2} \mathrm{d}x\, e^{-\frac{\sigma^i_g(x-z_1)}{\xi}}\phi_{g''}(x) \;=\; \mathrm{I}^{*i}_{gg''}(\xi, z_1, z_2). \tag{A.43b}$$

Substitution into the transport equation solution gives

$$\begin{aligned} 2\left[\phi_{g'}(z_2, s_{gg'}\xi) \;-\; \phi_{g'}(z_1, s_{gg'}\xi)e^{-\frac{\sigma^i_{g'}(z_2-z_1)}{s_{gg'}\xi}}\right] \;=& \\ =\; \frac{e^{-\frac{\sigma^i_{g'}z_2}{s_{gg'}\xi}}}{s_{gg'}\xi}\mathrm{S}^*_{g'}(-s_{gg'}\xi, z_1, z_2) \;+& \\ +\; \frac{\sigma^i_g}{\sigma^i_{g'}}\sum_{g''=1}^{G}\sigma^i_{g''\to g'}\mathrm{J}^{*i}_{gg''}(\xi, z_1, z_2),& \end{aligned} \tag{A.44a}$$

$$\begin{aligned} 2\left[\phi_{g'}(z_1, -s_{gg'}\xi) \;-\; \phi_{g'}(z_2, -s_{gg'}\xi)e^{-\frac{\sigma^i_{g'}(z_2-z_1)}{s_{gg'}\xi}}\right] \;=& \\ =\; \frac{e^{\frac{\sigma^i_{g'}z_1}{s_{gg'}\xi}}}{s_{gg'}\xi}\mathrm{S}^*_{g'}(s_{gg'}\xi, z_1, z_2) \;+& \\ +\; \frac{\sigma^i_g}{\sigma^i_{g'}}\sum_{g''=1}^{G}\sigma^i_{g''\to g'}\mathrm{I}^{*i}_{gg''}(\xi, z_1, z_2).& \end{aligned} \tag{A.44b}$$

6. Again, let z_1 and z_2 be the slab boundaries x_{i-1} and x_i, then the above equations reduce to

$$\begin{aligned} 2\left[\phi_{g'}(x_i, s_{gg'}\xi) \;-\; \phi_{g'}(x_{i-1}, s_{gg'}\xi)e^{-\frac{\Delta^i_{g'}}{s_{gg'}\xi}}\right] \;=& \\ =\; \frac{e^{-\frac{\sigma^i_{g'}x_i}{s_{gg'}\xi}}}{s_{gg'}\xi}\mathrm{S}^*_{g'}(-s_{gg'}\xi, x_{i-1}, x_i) \;+& \\ +\; \frac{\sigma^i_g}{\sigma^i_{g'}}\sum_{g''=1}^{G}\sigma^i_{g''\to g'}\mathrm{J}^{*i}_{gg''}(\xi, x_{i-1}, x_i),& \end{aligned} \tag{A.45a}$$

$$2\left[\phi_{g'}(x_{i-1},-s_{gg'}\xi) \;-\; \phi_{g'}(x_i,-s_{gg'}\xi)e^{-\frac{\Delta^i_{g'}}{s_{gg'}\xi}}\right] \;=$$

$$= \frac{e^{\frac{\sigma^i_{g'}x_{i-1}}{s_{gg'}\xi}}}{s_{gg'}\xi}\mathrm{S}^*_{g'}(s_{gg'}\xi,x_{i-1},x_i) + \tag{A.45b}$$

$$+ \frac{\sigma^i_g}{\sigma^i_{g'}}\sum_{g''=1}^{G}\sigma^i_{g''\to g'}\mathrm{I}^{*i}_{gg''}(\xi,x_{i-1},x_i).$$

7. Apply the boundary conditions and the $\mathrm{F_N}$ approximation for group g', and solve for $\mathrm{I}^{*i}_{gg'}(\xi,x_{i-1},x_i)$ and $\mathrm{J}^{*i}_{gg'}(\xi,x_{i-1},x_i)$

$$\sigma^i_{g'\to g'}\mathrm{I}^{*i}_{gg'}(\xi,x_{i-1},x_i) \;=\; \frac{\sigma^i_{g'\to g'}}{\sigma^i_g}\sum_{\alpha=0}^{N-1}\mathrm{a}^{g',i}_\alpha\psi_\alpha(s_{gg'}\xi) \;-$$

$$- \frac{1}{\sigma^i_g}\mathrm{S1}^i_{g'}(s_{gg'}\xi,x_{i-1},x_i) \;- \tag{A.46a}$$

$$- \sum_{\substack{g''=1\\ g''\neq g'}}^{G}\sigma^i_{g''\to g'}\mathrm{I}^{*i}_{gg''}(\xi,x_{i-1},x_i),$$

$$\sigma^i_{g'\to g'}\mathrm{J}^{*i}_{gg'}(\xi,x_{i-1},x_i) \;=\; \frac{\sigma^i_{g'\to g'}}{\sigma^i_g}\sum_{\alpha=0}^{N-1}\mathrm{b}^{g',i}_\alpha\psi_\alpha(s_{gg'}\xi) \;-$$

$$- \frac{1}{\sigma^i_g}\mathrm{S2}^i_{g'}(s_{gg'}\xi,x_{i-1},x_i) \;- \tag{A.46b}$$

$$- \sum_{\substack{g''=1\\ g''\neq g'}}^{G}\sigma^i_{g''\to g'}\mathrm{J}^{*i}_{gg''}(\xi,x_{i-1},x_i).$$

These equations can be used directly in $\mathrm{T1}^i_g(\mu,x_{i-1},x_i)$ and $\mathrm{T2}^i_g(\mu,x_{i-1},x_i)$ for $\xi\in[0,\frac{1}{s_{gg'}}]$ as long as $\sigma^i_{g'\to g'}$ is not equal to zero.

8. For $\xi\notin[0,\frac{1}{s_{gg'}}]$, $\nu>1$, the results from equations (A.19a) and (A.20a) for group g' can be used because they no longer generate singular integrals

$$\int_{-1}^{+1}\mathrm{d}\eta\,\frac{\eta}{\eta-\nu}C_{g'}(\eta,\nu) \;=\; \sigma^i_{g'}\sum_{g''=1}^{G}\mathrm{I}^{*i}_{g'g''}(\nu,z_1,z_2)\Lambda_{g''g'}(\nu) + \tag{A.47a}$$

$$+ \mathrm{L}(\nu)\mathrm{S}^*_{g'}(\nu,z_1,z_2)e^{\frac{\sigma^i_{g'}z_1}{\nu}},$$

$$\int_{-1}^{+1} d\eta \frac{\eta}{\eta-\nu} D_{g'}(\eta,\nu) = \sigma_{g'}^{i} \sum_{g''=1}^{G} J_{g'g''}^{*i}(\nu,z_1,z_2)\Lambda_{g''g'}(\nu) + \\ + L(\nu) S_{g'}^{*}(-\nu,z_1,z_2) e^{-\frac{\sigma_{g'}^{i} z_2}{\nu}}, \tag{A.47b}$$

where,

$$C_{g'}(\eta,\nu) = \phi_{g'}(z_1,-\eta) - e^{-\frac{\sigma_{g}^{i}(z_2-z_1)}{\nu}} \phi_{g'}(z_2,-\eta), \tag{A.47c}$$

$$D_{g'}(\eta,\nu) = \phi_{g'}(z_2,\eta) - e^{-\frac{\sigma_{g}^{i}(z_2-z_1)}{\nu}} \phi_{g'}(z_1,\eta), \tag{A.47d}$$

$$I_{g'g''}^{*i}(\nu,z_1,z_2) = \frac{1}{\nu} \int_{z_1}^{z_2} dx\, e^{-\frac{\sigma_{g'}^{i}(x-z_1)}{\nu}} \int_{-1}^{+1} d\eta\, \phi_{g''}(x,-\eta), \tag{A.47e}$$

$$J_{g'g''}^{*i}(\nu,z_1,z_2) = \frac{1}{\nu} \int_{z_1}^{z_2} dx\, e^{-\frac{\sigma_{g'}^{i}(z_2-x)}{\nu}} \int_{-1}^{+1} d\eta\, \phi_{g''}(x,-\eta), \tag{A.47f}$$

$$\Lambda_{g''g'}(\nu) = \delta_{g''g'} + \nu \frac{\sigma_{g''\to g'}^{i}}{\sigma_{g'}^{i}} L(\nu), \tag{A.47g}$$

$$L(\nu) = \frac{1}{2} \int_{-1}^{+1} d\eta \frac{1}{\eta-\nu}, \tag{A.47h}$$

$$S_{g'}^{*}(\nu,z_1,z_2) = \int_{z_1}^{z_2} dx\, e^{-\frac{\sigma_{g}^{i} x}{\nu}} S_{g'}^{i}(x). \tag{A.47i}$$

9. Rewrite the integral equations in terms of the flux values by splitting the integrals over the interval $\eta \in [0,1]$ to obtain

$$\int_{0}^{1} d\eta \frac{\eta}{\eta-\nu} \phi_{g'}(z_1,-\eta) - e^{-\frac{\sigma_{g'}^{i}(z_2-z_1)}{\nu}} \int_{0}^{1} d\eta \frac{\eta}{\eta-\nu} \phi_{g'}(z_2,-\eta) + \\ + \int_{0}^{1} d\eta \frac{\eta}{\eta+\nu} \phi_{g'}(z_1,\eta) - \\ - e^{-\frac{\sigma_{g'}^{i}(z_2-z_1)}{\nu}} \int_{0}^{1} d\eta \frac{\eta}{\eta+\nu} \phi_{g'}(z_2,\eta) = \\ = \sigma_{g'}^{i} \sum_{g''=1}^{G} \Lambda_{g''g'}(\nu) I_{g'g''}^{*i}(\nu,z_1,z_2) + \\ + L(\nu) S_{g'}^{*}(\nu,z_1,z_2) e^{\frac{\sigma_{g}^{i} z_1}{\nu}}, \tag{A.48a}$$

$$\int_0^1 d\eta \frac{\eta}{\eta-\nu}\phi_{g'}(z_2,\eta) - e^{-\frac{\sigma^i_{g'}(z_2-z_1)}{\nu}} \int_0^1 d\eta \frac{\eta}{\eta-\nu}\phi_{g'}(z_1,\eta) +$$
$$+ \int_0^1 d\eta \frac{\eta}{\eta+\nu}\phi_{g'}(z_2,-\eta) -$$
$$- e^{-\frac{\sigma^i_{g'}(z_2-z_1)}{\nu}} \int_0^1 d\eta \frac{\eta}{\eta+\nu}\phi_{g'}(z_1,-\eta) = \quad \text{(A.48b)}$$
$$= \sigma^i_{g'} \sum_{g''=1}^{G} \Lambda_{g''g'}(\nu) J^{*i}_{g'g''}(\nu,z_1,z_2) +$$
$$+ L(\nu) S^*_{g'}(-\nu,z_1,z_2) e^{-\frac{\sigma^i_{g'}z_2}{\nu}}.$$

10. Again, let $z_1 = x_{i-1}$ and $z_2 = x_i$, apply the boundary conditions and the F_N approximation, and substitute in known functions

$$\sum_{\alpha=0}^{N-1} \left[a^{g',i}_\alpha A^{g'}_\alpha(-\nu) - b^{g',i}_\alpha A^{g'}_\alpha(\nu) e^{-\frac{\Delta^i_{g'}}{\nu}} \right] + R1^i_{g'}(\nu,x_{i-1}) -$$
$$- L(\nu) S^*_{g'}(\nu,x_{i-1},x_i) e^{\frac{\sigma^i_{g'}x_{i-1}}{\nu}} = \quad \text{(A.49a)}$$
$$= \sigma^i_{g'} \sum_{g''=1}^{G} \Lambda_{g''g'}(\nu) I^{*i}_{g'g''}(\nu,x_{i-1},x_i),$$

$$\sum_{\alpha=0}^{N-1} \left[b^{g',i}_\alpha A^{g'}_\alpha(-\nu) - a^{g',i}_\alpha A^{g'}_\alpha(\nu) e^{-\frac{\Delta^i_{g'}}{\nu}} \right] + R2^i_{g'}(\nu,x_i) -$$
$$- L(\nu) S^*_{g'}(-\nu,x_{i-1},x_i) e^{-\frac{\sigma^i_{g'}x_i}{\nu}} = \quad \text{(A.49b)}$$
$$= \sigma^i_{g'} \sum_{g''=1}^{G} \Lambda_{g''g'}(\nu) J^{*i}_{g'g''}(\nu,x_{i-1},x_i).$$

11. Let $\nu = \frac{\sigma^i_{g'}}{\sigma^i_g}\xi = s_{gg'}\xi > 1$, then

$$\sigma^i_{g'} I^{*i}_{g'g''}(\nu,x_{i-1},x_i) = \sigma^i_g I^{*i}_{gg''}(\xi,x_{i-1},x_i), \quad \text{(A.50a)}$$

$$\sigma^i_{g'} J^{*i}_{g'g''}(\nu,x_{i-1},x_i) = \sigma^i_g J^{*i}_{gg''}(\xi,x_{i-1},x_i). \quad \text{(A.50b)}$$

12. Solve for $I^{*i}_{gg'}(\xi, x_{i-1}, x_i)$ and $J^{*i}_{gg'}(\xi, x_{i-1}, x_i)$

$$\begin{aligned}\sigma^i_g \Lambda_{g'g'}(s_{gg'}\xi) I^{*i}_{gg'}(\xi, x_{i-1}, x_i) \;=\; & R1^i_{g'}(s_{gg'}\xi, x_{i-1}) - \\ & - \frac{(s_{gg'}\xi) L(s_{gg'}\xi)}{\sigma^i_{g'}} S1^i_{g'}(s_{gg'}\xi, x_{i-1}, x_i) + \\ & + \sum_{\alpha=0}^{N-1} \left[a^{g',i}_\alpha A^{g'}_\alpha(-s_{gg'}\xi) \;-\; e^{-\frac{\Delta^i_{g'}}{s_{gg'}\xi}} b^{g',i}_\alpha A^{g'}_\alpha(s_{gg'}\xi) \right] \;- \\ & - \sigma^i_g \sum_{\substack{g''=1 \\ g'' \neq g'}}^{G} \Lambda_{g''g'}(s_{gg'}\xi) I^{*i}_{gg''}(\xi, x_{i-1}, x_i),\end{aligned} \tag{A.51a}$$

$$\begin{aligned}\sigma^i_g \Lambda_{g'g'}(s_{gg'}\xi) J^{*i}_{gg'}(\xi, x_{i-1}, x_i) \;=\; & R2^i_{g'}(s_{gg'}\xi, x_i) - \\ & - \frac{(s_{gg'}\xi) L(s_{gg'}\xi)}{\sigma^i_{g'}} S2^i_{g'}(s_{gg'}\xi, x_{i-1}, x_i) + \\ & + \sum_{\alpha=0}^{N-1} \left[b^{g',i}_\alpha A^{g'}_\alpha(-s_{gg'}\xi) \;-\; e^{-\frac{\Delta^i_{g'}}{s_{gg'}\xi}} a^{g',i}_\alpha A^{g'}_\alpha(s_{gg'}\xi) \right] \;- \\ & - \sigma^i_g \sum_{\substack{g''=1 \\ g'' \neq g'}}^{G} \Lambda_{g''g'}(s_{gg'}\xi) J^{*i}_{gg''}(\xi, x_{i-1}, x_i).\end{aligned} \tag{A.51b}$$

These equations can be used directly in $T1^i_g(\mu, x_{i-1}, x_i)$ and $T2^i_g(\mu, x_{i-1}, x_i)$ for $\xi \notin [0, \frac{1}{s_{gg'}}]$ as long as $\Lambda_{g'g'}(s_{gg'}\xi)$ is not equal to zero.

A.3.4 Problems Encountered in the Scattering Terms

As noted in Section A.3.3, the terms for $I^{*i}_{gg'}(\xi, x_{i-1}, x_i)$ and $J^{*i}_{gg'}(\xi, x_{i-1}, x_i)$ have singularities at

- For $\xi \in [0, \frac{1}{s_{gg'}}]$ with $\sigma^i_{g' \to g'} = 0$.
- For $\xi \notin [0, \frac{1}{s_{gg'}}]$ with $\Lambda_{g'g'}(s_{gg'}\xi) = 0$ or $s_{gg'}\xi = \nu^g_0$.

The steps below determine the expressions that are used in $\mathrm{T1}_g^i(\mu, x_{i-1}, x_i)$ and $\mathrm{T2}_g^i(\mu, x_{i-1}, x_i)$ for the points indicated above.

1. For $\xi \in [0, \frac{1}{s_{gg'}}]$ with $\sigma^i_{g'\to g'} = 0$, start with the singular equations

$$\begin{aligned}\sigma^i_{g'\to g'}\mathrm{I}^{*i}_{gg'}(\xi, x_{i-1}, x_i) &= \frac{\sigma^i_{g'\to g'}}{\sigma^i_g}\sum_{\alpha=0}^{N-1}\mathrm{a}^{g',i}_\alpha\psi_\alpha(s_{gg'}\xi) - \\ &- \frac{1}{\sigma^i_g}\mathrm{S1}^i_{g'}(s_{gg'}\xi, x_{i-1}, x_i) - \\ &- \sum_{\substack{g''=1\\ g''\neq g'}}^{G}\sigma^i_{g''\to g'}\mathrm{I}^{*i}_{gg''}(\xi, x_{i-1}, x_i),\end{aligned} \tag{A.52a}$$

$$\begin{aligned}\sigma^i_{g'\to g'}\mathrm{J}^{*i}_{gg'}(\xi, x_{i-1}, x_i) &= \frac{\sigma^i_{g'\to g'}}{\sigma^i_g}\sum_{\alpha=0}^{N-1}\mathrm{b}^{g',i}_\alpha\psi_\alpha(s_{gg'}\xi) - \\ &- \frac{1}{\sigma^i_g}\mathrm{S2}^i_{g'}(s_{gg'}\xi, x_{i-1}, x_i) - \\ &- \sum_{\substack{g''=1\\ g''\neq g'}}^{G}\sigma^i_{g''\to g'}\mathrm{J}^{*i}_{gg''}(\xi, x_{i-1}, x_i).\end{aligned} \tag{A.52b}$$

Since $\sigma^i_{g'\to g'} = 0$, the equations above reduce to

$$-\sum_{\substack{g''=1\\ g''\neq g'}}^{G}\sigma^i_{g''\to g'}\mathrm{I}^{*i}_{gg''}(\xi, x_{i-1}, x_i) = \frac{1}{\sigma^i_g}\mathrm{S1}^i_{g'}(s_{gg'}\xi, x_{i-1}, x_i), \tag{A.53a}$$

$$-\sum_{\substack{g''=1\\ g''\neq g'}}^{G}\sigma^i_{g''\to g'}\mathrm{J}^{*i}_{gg''}(\xi, x_{i-1}, x_i) = \frac{1}{\sigma^i_g}\mathrm{S2}^i_{g'}(s_{gg'}\xi, x_{i-1}, x_i). \tag{A.53b}$$

2. Since $\sigma^i_{g'\to g'} = 0$, these terms become

$$\Lambda_{g'g'}(s_{gg'}\xi) = 1, \tag{A.54a}$$

$$\Lambda_{g''g'}(s_{gg'}\xi) = (s_{gg'}\xi)\mathrm{L}(s_{gg'}\xi)\frac{\sigma^i_{g''\to g'}}{\sigma^i_{g'}}, \tag{A.54b}$$

$$A_{\alpha}^{g'}(\xi) \;=\; 0. \tag{A.54c}$$

The above terms are substituted into equations (A.51) to obtain

$$\begin{aligned}\sigma_g^i I_{gg'}^{*i}(\xi, x_{i-1}, x_i) \;=\; & R1_{g'}^i(s_{gg'}\xi, x_{i-1}) - \\ & - \frac{(s_{gg'}\xi)L(s_{gg'}\xi)}{\sigma_{g'}^i} S1_{g'}^i(s_{gg'}\xi, x_{i-1}, x_i) - \\ & - \frac{\sigma_g^i(s_{gg'}\xi)L(s_{gg'}\xi)}{\sigma_{g'}^i} \sum_{\substack{g''=1 \\ g''\neq g'}}^{G} \sigma_{g''\to g'}^i I_{gg''}^{*i}(\xi, x_{i-1}, x_i),\end{aligned} \tag{A.55a}$$

$$\begin{aligned}\sigma_g^i J_{gg'}^{*i}(\xi, x_{i-1}, x_i) \;=\; & R2_{g'}^i(s_{gg'}\xi, x_i) - \\ & - \frac{(s_{gg'}\xi)L(s_{gg'}\xi)}{\sigma_{g'}^i} S2_{g'}^i(s_{gg'}\xi, x_{i-1}, x_i) - \\ & - \frac{\sigma_g^i(s_{gg'}\xi)L(s_{gg'}\xi)}{\sigma_{g'}^i} \sum_{\substack{g''=1 \\ g''\neq g'}}^{G} \sigma_{g''\to g'}^i J_{gg''}^{*i}(\xi, x_{i-1}, x_i).\end{aligned} \tag{A.55b}$$

3. Equations (A.53) can be substituted into the above equations to obtain

$$\sigma_g^i I_{gg'}^{*i}(\xi, x_{i-1}, x_i) \;=\; R1_{g'}^i(s_{gg'}\xi, x_{i-1}), \tag{A.56a}$$

$$\sigma_g^i J_{gg'}^{*i}(\xi, x_{i-1}, x_i) \;=\; R2_{g'}^i(s_{gg'}\xi, x_i). \tag{A.56b}$$

These equations are used directly in $T1_g^i(\mu, x_{i-1}, x_i)$ and $T2_g^i(\mu, x_{i-1}, x_i)$ for $\xi \in [0, \frac{1}{s_{gg'}}]$ when $\sigma_{g'\to g'}^i$ is zero.

4. For $\xi \notin [0, \frac{1}{s_{gg'}}]$ with $\Lambda_{g'g'}(s_{gg'}\xi) = 0$, or $s_{gg'}\xi = \nu_0^g$, start with the singular equations

$$\begin{aligned}\sigma_g^i \mathrm{I}_{gg'}^{*i}(\xi, x_{i-1}, x_i) &= \frac{1}{\Lambda_{g'g'}(s_{gg'}\xi)} \Big\{ \mathrm{R1}_{g'}^i(s_{gg'}\xi, x_{i-1}) - \\ &- \frac{(s_{gg'}\xi)\mathrm{L}(s_{gg'}\xi)}{\sigma_{g'}^i} \mathrm{S1}_{g'}^i(s_{gg'}\xi, x_{i-1}, x_i) + \\ &+ \sum_{\alpha=0}^{N-1} \left[\mathrm{a}_\alpha^{g',i} \mathrm{A}_\alpha^{g'}(-s_{gg'}\xi) - e^{-\frac{\Delta_{g'}^i}{s_{gg'}\xi}} \mathrm{b}_\alpha^{g',i} \mathrm{A}_\alpha^{g'}(s_{gg'}\xi) \right] - \\ &- \sigma_g^i \sum_{\substack{g''=1 \\ g'' \neq g'}}^{G} \Lambda_{g''g'}(s_{gg'}\xi) \mathrm{I}_{gg''}^{*i}(\xi, x_{i-1}, x_i) \Big\},\end{aligned} \tag{A.57a}$$

$$\begin{aligned}\sigma_g^i \mathrm{J}_{gg'}^{*i}(\xi, x_{i-1}, x_i) &= \frac{1}{\Lambda_{g'g'}(s_{gg'}\xi)} \Big\{ \mathrm{R2}_{g'}^i(s_{gg'}\xi, x_i) - \\ &- \frac{(s_{gg'}\xi)\mathrm{L}(s_{gg'}\xi)}{\sigma_{g'}^i} \mathrm{S2}_{g'}^i(s_{gg'}\xi, x_{i-1}, x_i) + \\ &+ \sum_{\alpha=0}^{N-1} \left[\mathrm{b}_\alpha^{g',i} \mathrm{A}_\alpha^{g'}(-s_{gg'}\xi) - e^{-\frac{\Delta_{g'}^i}{s_{gg'}\xi}} \mathrm{a}_\alpha^{g',i} \mathrm{A}_\alpha^{g'}(s_{gg'}\xi) \right] - \\ &- \sigma_g^i \sum_{\substack{g''=1 \\ g'' \neq g'}}^{G} \Lambda_{g''g'}(s_{gg'}\xi) \mathrm{J}_{gg''}^{*i}(\xi, x_{i-1}, x_i) \Big\}.\end{aligned} \tag{A.57b}$$

5. Take the limit as $s_{gg'}\xi \to \nu_0^g$ through the use of L'Hospital's Rule

$$\begin{aligned}\lim_{s_{gg'}\xi \to \nu_0^g} \sigma_g^i \mathrm{I}_{gg'}^{*i}(\xi, x_{i-1}, x_i) &= \frac{1}{\frac{\mathrm{d}}{\mathrm{d}s_{gg'}\xi}\Lambda_{g'g'}(s_{gg'}\xi)} \frac{\mathrm{d}}{\mathrm{d}s_{gg'}\xi} \Big\{ \mathrm{R1}_{g'}^i(s_{gg'}\xi, x_{i-1}) - \\ &- \frac{(s_{gg'}\xi)\mathrm{L}(s_{gg'}\xi)}{\sigma_{g'}^i} \mathrm{S1}_{g'}^i(s_{gg'}\xi, x_{i-1}, x_i) + \\ &+ \sum_{\alpha=0}^{N-1} \left[\mathrm{a}_\alpha^{g',i} \mathrm{A}_\alpha^{g'}(-s_{gg'}\xi) - e^{-\frac{\Delta_{g'}^i}{s_{gg'}\xi}} \mathrm{b}_\alpha^{g',i} \mathrm{A}_\alpha^{g'}(s_{gg'}\xi) \right] - \\ &- \sigma_g^i \sum_{\substack{g''=1 \\ g'' \neq g'}}^{G} \Lambda_{g''g'}(s_{gg'}\xi) \mathrm{I}_{gg''}^{*i}(\xi, x_{i-1}, x_i) \Big\},\end{aligned} \tag{A.58a}$$

$$\lim_{s_{gg'}\xi\to\nu_0^g}\sigma_g^i J_{gg'}^{*i}(\xi,x_{i-1},x_i)=\frac{1}{\frac{d}{ds_{gg'}\xi}\Lambda_{g'g'}(s_{gg'}\xi)}\frac{d}{ds_{gg'}\xi}\Big\{R2_{g'}^i(s_{gg'}\xi,x_i)-$$
$$-\frac{(s_{gg'}\xi)L(s_{gg'}\xi)}{\sigma_{g'}^i}S2_{g'}^i(s_{gg'}\xi,x_{i-1},x_i)+$$
$$+\sum_{\alpha=0}^{N-1}\left[b_\alpha^{g',i}A_\alpha^{g'}(-s_{gg'}\xi)-e^{-\frac{\Delta_{g'}^i}{s_{gg'}\xi}}a_\alpha^{g',i}A_\alpha^{g'}(s_{gg'}\xi)\right]- \tag{A.58b}$$
$$-\sigma_g^i\sum_{\substack{g''=1\\g''\neq g'}}^{G}\Lambda_{g''g'}(s_{gg'}\xi)J_{gg''}^{*i}(\xi,x_{i-1},x_i)\Big\}.$$

6. These differentials are evaluated term by term

$$\frac{d}{ds_{gg'}\xi}A_\alpha^{g'}(s_{gg'}\xi)=\frac{\sigma_{g'\to g'}^i}{2\sigma_{g'}^i}\int_0^1 d\eta\,\frac{\eta}{(\eta+s_{gg'}\xi)^2}\psi_\alpha(\eta). \tag{A.59a}$$

$$\frac{d}{ds_{gg'}\xi}e^{-\frac{\Delta_{g'}^i}{s_{gg'}\xi}}A_\alpha^{g'}(s_{gg'}\xi)=e^{-\frac{\Delta_{g'}^i}{s_{gg'}\xi}}\left[-\frac{d}{ds_{gg'}\xi}A_\alpha^{g'}(s_{gg'}\xi)+\right. \tag{A.59b}$$
$$\left.+\frac{\Delta_{g'}^i}{(s_{gg'}\xi)^2}A_\alpha^{g'}(s_{gg'}\xi)\right].$$

$$\frac{d}{ds_{gg'}\xi}\Lambda_{g''g'}(s_{gg'}\xi)=\frac{\sigma_{g''\to g'}^i}{2\sigma_{g'}^i}\left[\ln\left|\frac{1-s_{gg'}\xi}{1+s_{gg'}\xi}\right|+\frac{2(s_{gg'}\xi)}{(s_{gg'}\xi)^2-1}\right]. \tag{A.59c}$$

$$\frac{d}{ds_{gg'}\xi}R1_{g'}^i(s_{gg'}\xi,x_{i-1})=\int_0^1 d\eta\,\eta\left[F_R^{g',i}(\eta)\times\right.$$
$$\left.\times\frac{d}{ds_{gg'}\xi}C(\Delta_{g'}^i,\eta,s_{gg'}\xi)+F_L^{g',i}(\eta)\frac{d}{ds_{gg'}\xi}S(\Delta_{g'}^i,\eta,s_{gg'}\xi)\right]. \tag{A.59d}$$

$$\frac{d}{ds_{gg'}\xi}R2_{g'}^i(s_{gg'}\xi,x_i)=\int_0^1 d\eta\,\eta\left[F_L^{g',i}(\eta)\times\right.$$
$$\left.\times\frac{d}{ds_{gg'}\xi}C(\Delta_{g'}^i,\eta,s_{gg'}\xi)+F_R^{g',i}(\eta)\frac{d}{ds_{gg'}\xi}S(\Delta_{g'}^i,\eta,s_{gg'}\xi)\right]. \tag{A.59e}$$

$$\frac{d}{ds_{gg'}\xi}C(\Delta_{g'}^i,\eta,s_{gg'}\xi)=\frac{C(\Delta_{g'}^i,\eta,s_{gg'}\xi)-\frac{\Delta_{g'}^i}{(s_{gg'}\xi)^2}e^{-\frac{\Delta_{g'}^i}{s_{gg'}\xi}}}{\eta-s_{gg'}\xi}. \tag{A.59f}$$

$$\frac{\mathrm{d}}{\mathrm{d}s_{gg'}\xi}\mathrm{S}(\Delta^i_{g'},\eta,s_{gg'}\xi) = -\frac{1}{\eta+s_{gg'}\xi}\left[\mathrm{S}(\Delta^i_{g'},\eta,s_{gg'}\xi) + \right. \\ \left. + \frac{\Delta^i_{g'}}{(s_{gg'}\xi)^2}e^{-\Delta^i_{g'}(\frac{1}{\eta}+\frac{1}{s_{gg'}\xi})}\right]. \tag{A.59g}$$

$$\frac{\mathrm{d}}{\mathrm{d}s_{gg'}\xi}(s_{gg'}\xi)\mathrm{L}(s_{gg'}\xi)\frac{\mathrm{S1}^i_{g'}(s_{gg'}\xi,x_{i-1},x_i)}{\sigma^i_{g'}} = \\ = (s_{gg'}\xi)\mathrm{L}(s_{gg'}\xi)\frac{\mathrm{d}}{\mathrm{d}s_{gg'}\xi}\frac{\mathrm{S1}^i_{g'}(s_{gg'}\xi,x_{i-1},x_i)}{\sigma^i_{g'}} + \\ + \mathrm{L}(s_{gg'}\xi)\frac{\mathrm{S1}^i_{g'}(s_{gg'}\xi,x_{i-1},x_i)}{\sigma^i_{g'}} + \\ + \frac{s_{gg'}\xi}{(s_{gg'}\xi)^2-1}\frac{\mathrm{S1}^i_{g'}(s_{gg'}\xi,x_{i-1},x_i)}{\sigma^i_{g'}}. \tag{A.59h}$$

$$\frac{\mathrm{d}}{\mathrm{d}s_{gg'}\xi}(s_{gg'}\xi)\mathrm{L}(s_{gg'}\xi)\frac{\mathrm{S2}^i_{g'}(s_{gg'}\xi,x_{i-1},x_i)}{\sigma^i_{g'}} = \\ = (s_{gg'}\xi)\mathrm{L}(s_{gg'}\xi)\frac{\mathrm{d}}{\mathrm{d}s_{gg'}\xi}\frac{\mathrm{S2}^i_{g'}(s_{gg'}\xi,x_{i-1},x_i)}{\sigma^i_{g'}} + \\ + \mathrm{L}(s_{gg'}\xi)\frac{\mathrm{S2}^i_{g'}(s_{gg'}\xi,x_{i-1},x_i)}{\sigma^i_{g'}} + \\ + \frac{s_{gg'}\xi}{(s_{gg'}\xi)^2-1}\frac{\mathrm{S2}^i_{g'}(s_{gg'}\xi,x_{i-1},x_i)}{\sigma^i_{g'}}. \tag{A.59i}$$

$$\frac{\mathrm{d}}{\mathrm{d}s_{gg'}\xi}\Lambda_{g''g'}(s_{gg'}\xi)\mathrm{I}^{*i}_{gg''}(s_{gg'}\xi,x_{i-1},x_i) = \\ = \mathrm{I}^{*i}_{gg''}(s_{gg'}\xi,x_{i-1},x_i)\frac{\mathrm{d}}{\mathrm{d}s_{gg'}\xi}\Lambda_{g''g'}(s_{gg'}\xi) + \\ + \Lambda_{g''g'}(s_{gg'}\xi)\frac{\mathrm{d}}{\mathrm{d}s_{gg'}\xi}\mathrm{I}^{*i}_{gg''}(s_{gg'}\xi,x_{i-1},x_i). \tag{A.59j}$$

$$\frac{\mathrm{d}}{\mathrm{d}s_{gg'}\xi}\Lambda_{g''g'}(s_{gg'}\xi)\mathrm{J}^{*i}_{gg''}(s_{gg'}\xi,x_{i-1},x_i) = \\ = \mathrm{J}^{*i}_{gg''}(s_{gg'}\xi,x_{i-1},x_i)\frac{\mathrm{d}}{\mathrm{d}s_{gg'}\xi}\Lambda_{g''g'}(s_{gg'}\xi) + \\ + \Lambda_{g''g'}(s_{gg'}\xi)\frac{\mathrm{d}}{\mathrm{d}s_{gg'}\xi}\mathrm{J}^{*i}_{gg''}(s_{gg'}\xi,x_{i-1},x_i). \tag{A.59k}$$

$$\frac{\mathrm{d}}{\mathrm{d}s_{gg'\xi}}\frac{\mathrm{S1}^i_{g'}(s_{gg'\xi},x_{i-1},x_i)}{\sigma^i_{g'}} =$$

$$\begin{cases} 0 & s_{gg'\xi}=0 \\ \dfrac{1}{(s_{gg'\xi})^3}\displaystyle\int_{x_{i-1}}^{x_i}\mathrm{d}z\,\mathrm{S}^i_{g'}(z)e^{-\frac{\sigma^i_{g'}(z-x_{i-1})}{s_{gg'\xi}}}\times & s_{gg'\xi}\neq 0. \\ \times\left(\sigma^i_{g'}(z-x_{i-1})-s_{gg'\xi}\right) & \end{cases} \tag{A.59l}$$

$$\frac{\mathrm{d}}{\mathrm{d}s_{gg'\xi}}\frac{\mathrm{S2}^i_{g'}(s_{gg'\xi},x_{i-1},x_i)}{\sigma^i_{g'}} =$$

$$\begin{cases} 0 & s_{gg'\xi}=0 \\ \dfrac{1}{(s_{gg'\xi})^3}\displaystyle\int_{x_{i-1}}^{x_i}\mathrm{d}z\,\mathrm{S}^i_{g'}(z)e^{-\frac{\sigma^i_{g'}(x_i-z)}{s_{gg'\xi}}}\times & s_{gg'\xi}\neq 0. \\ \times\left(\sigma^i_{g'}(x_i-z)-s_{gg'\xi}\right) & \end{cases} \tag{A.59m}$$

The terms $\frac{\mathrm{d}}{\mathrm{d}s_{gg'\xi}}\mathrm{I}^{*i}_{gg''}(s_{gg'\xi},x_{i-1},x_i)$ and $\frac{\mathrm{d}}{\mathrm{d}s_{gg'\xi}}\mathrm{J}^{*i}_{gg''}(s_{gg'\xi},x_{i-1},x_i)$ can not be evaluated except if there is a limit of strict down scatter and g' only being 1. Then the terms do not need to be determined. This calculation is used only to verify the output in Reference [12] and is only contained in the original non-production version of MGSLAB.

A.4 Creation of a Set of Integral Equations for Interior Slab Points

These steps determine the matrix equations and post processor for the interior flux. Rewrite the integral equations, equations (A.25), in terms of the fluxes by changing the integration variables so that they are evaluated on the interval $[0,1]$. Define z_1 and z_2 as x and x_i for equation (A.25a) and as x_{i-1} and x

for equation (A.25b) to obtain

$$\begin{aligned}
&\int_0^1 d\eta \, \frac{\eta}{\eta-\nu}\phi_g(x,-\eta) \; + \; \int_0^1 d\eta \, \frac{\eta}{\eta+\nu}\phi_g(x,\eta) \; - \\
&\quad - e^{-\frac{\sigma_g^i(x_i-x)}{\nu}} \left[\int_0^1 d\eta \, \frac{\eta\phi_g(x_i,-\eta)}{\eta-\nu} \; + \; \int_0^1 d\eta \, \frac{\eta\phi_g(x_i,\eta)}{\eta+\nu} \right] \; - \\
&\quad - \frac{2\sigma_g^i}{\sigma_{g\to g}^i}\lambda_{gg}(\nu) \left[\phi_g(x,-\nu) \; - \; \phi_g(x_i,-\nu)e^{-\frac{\sigma_g^i(x_i-x)}{\nu}} \right] \; = \\
&\quad = \; -\frac{\sigma_g^i}{\sigma_{g\to g}^i} \sum_{\substack{g'=1 \\ g'\neq g}}^{G} \sigma_{g'\to g}^i I_{gg'}^{*i}(\nu,x,x_i) \; - \\
&\quad - \frac{\sigma_g^i e^{\frac{\sigma_g^i x}{\nu}}}{\nu\sigma_{g\to g}^i} S_g^*(\nu,x,x_i),
\end{aligned} \tag{A.60a}$$

$$\begin{aligned}
&\int_0^1 d\eta \, \frac{\eta}{\eta-\nu}\phi_g(x,\eta) \; + \; \int_0^1 d\eta \, \frac{\eta}{\eta+\nu}\phi_g(x,-\eta) \; - \\
&\quad - e^{-\frac{\sigma_g^i(x-x_{i-1})}{\nu}} \left[\int_0^1 d\eta \, \frac{\eta\phi_g(x_{i-1},\eta)}{\eta-\nu} + \int_0^1 d\eta \, \frac{\eta\phi_g(x_{i-1},-\eta)}{\eta+\nu} \right] \; - \\
&\quad - \frac{2\sigma_g^i}{\sigma_{g\to g}^i}\lambda_{gg}(\nu) \left[\phi_g(x,\nu) \; - \; \phi_g(x_{i-1},\nu)e^{-\frac{\sigma_g^i(x-x_{i-1})}{\nu}} \right] \; = \\
&\quad = \; -\frac{\sigma_g^i}{\sigma_{g\to g}^i} \sum_{\substack{g'=1 \\ g'\neq g}}^{G} \sigma_{g'\to g}^i J_{gg'}^{*i}(\nu,x_{i-1},x) \; - \\
&\quad - \frac{\sigma_g^i e^{-\frac{\sigma_g^i x}{\nu}}}{\nu\sigma_{g\to g}^i} S_g^*(-\nu,x_{i-1},x).
\end{aligned} \tag{A.60b}$$

A.5 Application of the F_N Approximation to the Interior Slab Integral Equations

The same method used on the boundary integral equations is used on the interior equations using different expansion coefficients. The boundary conditions and F_N approximations are

$$\phi_g(x_{i-1},\nu) \; = \; F_L^{g,i}(\nu), \tag{A.61a}$$

$$\phi_g(x_i,-\nu) \; = \; F_R^{g,i}(\nu), \tag{A.61b}$$

$$\phi_g(x,-\nu) \;=\; \mathrm{F}_{\mathrm{R}}^{g,i}(\nu)e^{-\frac{\sigma_g^i(x_i-x)}{\nu}} \;+\; \frac{\sigma_{g\to g}^i}{2\sigma_g^i}\sum_{\alpha=0}^{N-1} c_\alpha^{g,j}\psi_\alpha(\nu), \tag{A.62a}$$

$$\phi_g(x,\nu) \;=\; \mathrm{F}_{\mathrm{L}}^{g,i}(\nu)e^{-\frac{\sigma_g^i(x-x_{i-1})}{\nu}} \;+\; \frac{\sigma_{g\to g}^i}{2\sigma_g^i}\sum_{\alpha=0}^{N-1} d_\alpha^{g,j}\psi_\alpha(\nu). \tag{A.62b}$$

Upon substitution of the boundary conditions and the $\mathrm{F_N}$ approximations into the integral equations, a set of equations is produced that can be solved for the expansion coefficients

$$\begin{aligned}\sum_{\alpha=0}^{N-1}\left[c_\alpha^{g,j}\mathrm{B}_\alpha^g(\nu) \;-\; d_\alpha^{g,j}\mathrm{A}_\alpha^g(\nu)\right] \;&=\; \mathrm{R1}_g^i(\nu,x) \;+\\ &+\; \frac{1}{\sigma_{g\to g}^i}\mathrm{T1}_g^i(\nu,x,x_i) \;+\; \frac{1}{\sigma_{g\to g}^i}\mathrm{S1}_g^i(\nu,x,x_i),\end{aligned} \tag{A.63a}$$

$$\begin{aligned}\sum_{\alpha=0}^{N-1}\left[d_\alpha^{g,j}\mathrm{B}_\alpha^g(\nu) \;-\; c_\alpha^{g,j}\mathrm{A}_\alpha^g(\nu)\right] \;&=\; \mathrm{R2}_g^i(\nu,x) \;+\\ &+\; \frac{1}{\sigma_{g\to g}^i}\mathrm{T2}_g^i(\nu,x_{i-1},x) \;+\; \frac{1}{\sigma_{g\to g}^i}\mathrm{S2}_g^i(\nu,x_{i-1},x),\end{aligned} \tag{A.63b}$$

where,

$$\begin{aligned}\mathrm{R1}_g^i(\nu,x) \;&=\; \int_0^1 d\eta\,\eta\left[\mathrm{F}_{\mathrm{R}}^{g,i}(\eta)\mathrm{C}(\sigma_g^i(x_i-x),\nu,\eta) \;+\right.\\ &\left.+\; e^{-\frac{\sigma_g^i(x-x_{i-1})}{\nu}}\mathrm{F}_{\mathrm{L}}^{g,i}(\eta)\mathrm{S}(\sigma_g^i(x_i-x),\nu,\eta)\right],\end{aligned} \tag{A.63c}$$

$$\begin{aligned}\mathrm{R2}_g^i(\nu,x) \;&=\; \int_0^1 d\eta\,\eta\left[\mathrm{F}_{\mathrm{L}}^{g,i}(\eta)\mathrm{C}(\sigma_g^i(x-x_{i-1}),\nu,\eta) \;+\right.\\ &\left.+\; e^{-\frac{\sigma_g^i(x_i-x)}{\nu}}\mathrm{F}_{\mathrm{R}}^{g,i}(\eta)\mathrm{S}(\sigma_g^i(x-x_{i-1}),\nu,\eta)\right],\end{aligned} \tag{A.63d}$$

$$\mathrm{T1}_g^i(\nu,x,x_i) \;=\; \sigma_g^i\sum_{\substack{g'=1\\ g'\neq g}}^{G}\sigma_{g'\to g}^i\mathrm{I}_{gg'}^{*i}(\nu,x,x_i), \tag{A.63e}$$

$$\mathrm{T2}_g^i(\nu,x_{i-1},x) \;=\; \sigma_g^i\sum_{\substack{g'=1\\ g'\neq g}}^{G}\sigma_{g'\to g}^i\mathrm{J}_{gg'}^{*i}(\nu,x_{i-1},x), \tag{A.63f}$$

$$S1_g^i(\nu, x, x_i) = \frac{\sigma_g^i}{\nu} \int_x^{x_i} dz\, e^{-\frac{\sigma_g^i(z-x_{i-1})}{\nu}} S_g^i(z), \tag{A.63g}$$

$$S2_g^i(\nu, x_{i-1}, x) = \frac{\sigma_g^i}{\nu} \int_{x_{i-1}}^{x} dz\, e^{-\frac{\sigma_g^i(x_i-z)}{\nu}} S_g^i(z), \tag{A.63h}$$

These equations are changed into matrix equations using the collocation procedure and the expansion coefficients $c_\alpha^{g,j}$ and $d_\alpha^{g,j}$ are determined using a matrix decomposition scheme as described in Chapter 3.

A.5.1 Post Processor

To accelerate the convergence rate of the F_N approximations, equations(A.62), the regularized $B_\alpha^g(\mu)$ from equation (A.31) is used in the interior integral equations, equations (A.63), to obtain

$$\begin{aligned} &\lambda_{gg}^*(\mu) \sum_{\alpha=0}^{N-1} c_\alpha^{g,j} \psi_\alpha(\mu) - \sum_{\alpha=0}^{N-1} \left[c_\alpha^{g,j} B_\alpha^{*g}(\mu) + d_\alpha^{g,j} A_\alpha^g(\mu) \right] = \\ &= R1_g^i(\mu, x) + \frac{1}{\sigma_{g\to g}^i} T1_g^i(\mu, x, x_i) + \frac{1}{\sigma_{g\to g}^i} S1_g^i(\mu, x, x_i), \end{aligned} \tag{A.64a}$$

$$\begin{aligned} &\lambda_{gg}^*(\mu) \sum_{\alpha=0}^{N-1} d_\alpha^{g,j} \psi_\alpha(\mu) - \sum_{\alpha=0}^{N-1} \left[d_\alpha^{g,j} B_\alpha^{g}(\mu) + c_\alpha^{g,j} A_\alpha^g(\mu) \right] = \\ &= R2_g^i(\mu, x) + \frac{1}{\sigma_{g\to g}^i} T2_g^i(\mu, x_{i-1}, x) + \frac{1}{\sigma_{g\to g}^i} S2_g^i(\mu, x_{i-1}, x). \end{aligned} \tag{A.64b}$$

These equations are solve for $\sum_{\alpha=0}^{N-1} c_\alpha^{g,j} \psi_\alpha(\mu)$ and $\sum_{\alpha=0}^{N-1} d_\alpha^{g,j} \psi_\alpha(\mu)$ and substituted into the F_N approximations, equations (A.62) to obtain

$$\begin{aligned} \phi_g(x, -\mu) &= F_R^{g,i}(\mu) e^{-\frac{\sigma_g^i(x_i-x)}{\mu}} + \frac{1}{2\sigma_g^i \lambda_{gg}^*(\mu)} \left\{ \sigma_{g\to g}^i R1_g^i(\mu, x) + \right. \\ &+ \sigma_{g\to g}^i \sum_{\alpha=0}^{N-1} \left[c_\alpha^{g,j} B_\alpha^{*g}(\mu) + \left(d_\alpha^{g,j} - b_\alpha^{g,i} e^{-\frac{\sigma_g^i(x_i-x)}{\mu}} \right) A_\alpha^g(\mu) \right] + \\ &\left. + S1_g^i(\mu, x, x_i) + T1_g^i(\mu, x, x_i) \right\}, \end{aligned} \tag{A.65a}$$

$$\phi_g(x,\mu) = \mathrm{F}_{\mathrm{L}}^{g,i}(\mu)e^{-\frac{\sigma_g^i(x-x_{i-1})}{\mu}} + \frac{1}{2\sigma_g^i\lambda_{gg}^*(\mu)}\left\{\sigma_{g\to g}^i \mathrm{R2}_g^i(\mu,x)+\right.$$
$$+\sigma_{g\to g}^i\sum_{\alpha=0}^{N-1}\left[\mathrm{d}_\alpha^{g,j}\mathrm{B}_\alpha^{*g}(\mu)+\left(\mathrm{c}_\alpha^{g,j}-\mathrm{a}_\alpha^{g,i}e^{-\frac{\sigma_g^i(x-x_{i-1})}{\mu}}\right)\mathrm{A}_\alpha^g(\mu)\right]+ \qquad \text{(A.65b)}$$
$$\left.+\mathrm{S2}_g^i(\mu,x_{i-1},x)+\mathrm{T2}_g^i(\mu,x_{i-1},x)\right\}.$$

A.5.2 Scattering Terms

Using the same methodology as for the boundary, derive expressions for

$$\mathrm{T1}_g^i(\nu,x,x_i) = \sigma_g^i\sum_{\substack{g'=1\\g'\neq g}}^{G}\sigma_{g'\to g}^i\mathrm{I}_{gg'}^{*i}(\nu,x,x_i), \qquad \text{(A.66a)}$$

$$\mathrm{T2}_g^i(\nu,x_{i-1},x) = \sigma_g^i\sum_{\substack{g'=1\\g'\neq g}}^{G}\sigma_{g'\to g}^i\mathrm{J}_{gg'}^{*i}(\nu,x_{i-1},x). \qquad \text{(A.66b)}$$

1. From equations (A.44), let z_1 and z_2 equal x_{i-1} and x for equation (A.44a) and x and x_i for equation (A.44b) to obtain

$$2\left[\phi_{g'}(x,s_{gg'}\xi) - \phi_{g'}(x_{i-1},s_{gg'}\xi)e^{-\frac{\sigma_{g'}^i(x-x_{i-1})}{s_{gg'}\xi}}\right] =$$
$$= \frac{e^{-\frac{\sigma_{g'}^i x}{s_{gg'}\xi}}}{s_{gg'}\xi}\mathrm{S}_{g'}^*(-s_{gg'}\xi,x_{i-1},x)+ \qquad \text{(A.67a)}$$
$$+\frac{\sigma_g^i}{\sigma_{g'}^i}\sum_{g''=1}^{G}\sigma_{g''\to g'}^i\mathrm{J}_{gg''}^{*i}(\xi,x_{i-1},x),$$

$$2\left[\phi_{g'}(x,-s_{gg'}\xi) - \phi_{g'}(x_i,-s_{gg'}\xi)e^{-\frac{\sigma_{g'}^i(x_i-x)}{s_{gg'}\xi}}\right] =$$
$$= \frac{e^{\frac{\sigma_{g'}^i x}{s_{gg'}\xi}}}{s_{gg'}\xi}\mathrm{S}_{g'}^*(s_{gg'}\xi,x,x_i)+ \qquad \text{(A.67b)}$$
$$+\frac{\sigma_g^i}{\sigma_{g'}^i}\sum_{g''=1}^{G}\sigma_{g''\to g'}^i\mathrm{I}_{gg''}^{*i}(\xi,x,x_i).$$

2. Apply the boundary conditions and the F_N approximations for group g', and solve for $I^{*i}_{gg'}(\xi, x, x_i)$ and $J^{*i}_{gg'}(\xi, x_{i-1}, x)$

$$\sigma^i_{g'\to g'} I^{*i}_{gg'}(\xi, x, x_i) = \frac{\sigma^i_{g'\to g'}}{\sigma^i_g} \sum_{\alpha=0}^{N-1} c^{g',j}_\alpha \psi_\alpha(s_{gg'}\xi) - \\ - \frac{1}{\sigma^i_g} S1^i_{g'}(s_{gg'}\xi, x, x_i) - \sum_{\substack{g''=1 \\ g''\neq g'}}^{G} \sigma^i_{g''\to g'} I^{*i}_{gg''}(\xi, x, x_i), \tag{A.68a}$$

$$\sigma^i_{g'\to g'} J^{*i}_{gg'}(\xi, x_{i-1}, x) = \frac{\sigma^i_{g'\to g'}}{\sigma^i_g} \sum_{\alpha=0}^{N-1} d^{g',j}_\alpha \psi_\alpha(s_{gg'}\xi) - \\ - \frac{1}{\sigma^i_g} S2^i_{g'}(s_{gg'}\xi, x_{i-1}, x) - \sum_{\substack{g''=1 \\ g''\neq g'}}^{G} \sigma^i_{g''\to g'} J^{*i}_{gg''}(\xi, x_{i-1}, x). \tag{A.68b}$$

These equations are used directly in $T1^i_g(\mu, x, x_i)$ and $T2^i_g(\mu, x_{i-1}, x)$ for $\xi \in [0, \frac{1}{s_{gg'}}]$ as long as $\sigma^i_{g'\to g'}$ is not equal to zero.

3. For $\xi \notin [0, \frac{1}{s_{gg'}}]$, start with equations (A.48) for group g'. Let z_1 and z_2 equal x and x_i for equation (A.48a) and x_{i-1} and x for equation (A.48b). Apply the boundary conditions and the F_N approximations

$$\sum_{\alpha=0}^{N-1} \left[c^{g',j}_\alpha A^{g'}_\alpha(-\nu) + \left(d^{g',j}_\alpha - b^{g',i}_\alpha e^{-\frac{\sigma^i_{g'}(x_i - x)}{\nu}} \right) A^{g'}_\alpha(\nu) \right] + \\ R1^i_{g'}(\nu, x) - L(\nu) S^*_{g'}(\nu, x, x_i) e^{\frac{\sigma^i_{g'} x}{\nu}} = \\ = \sigma^i_{g'} \sum_{g''=1}^{G} \Lambda_{g''g'}(\nu) I^{*i}_{g'g''}(\nu, x, x_i), \tag{A.69a}$$

$$\sum_{\alpha=0}^{N-1} \left[d^{g',j}_\alpha A^{g'}_\alpha(-\nu) + \left(c^{g',j}_\alpha - a^{g',i}_\alpha e^{-\frac{\sigma^i_{g'}(x - x_{i-1})}{\nu}} \right) A^{g'}_\alpha(\nu) \right] + \\ + R2^i_{g'}(\nu, x) - L(\nu) S^*_{g'}(-\nu, x_{i-1}, x) e^{-\frac{\sigma^i_{g'} x}{\nu}} = \\ = \sigma^i_{g'} \sum_{g''=1}^{G} \Lambda_{g''g'}(\nu) J^{*i}_{g'g''}(\nu, x_{i-1}, x). \tag{A.69b}$$

4. Let $\nu = \frac{\sigma^i_{g'}}{\sigma^i_g}\xi = s_{gg'}\xi > 1$, then

$$\sigma^i_{g'} I^{*i}_{g'g''}(\nu, x, x_i) \;=\; \sigma^i_g I^{*i}_{gg''}(\xi, x, x_i), \tag{A.70a}$$

$$\sigma^i_{g'} J^{*i}_{g'g''}(\nu, x_{i-1}, x) \;= \sigma^i_g J^{*i}_{gg''}(\xi, x_{i-1}, x). \tag{A.70b}$$

5. Solve for $I^{*i}_{gg'}(\xi, x, x_i)$ and $J^{*i}_{gg'}(\xi, x_{i-1}, x)$ to obtain

$$\begin{aligned}
\sigma^i_g \Lambda_{g'g'}(s_{gg'}\xi) I^{*i}_{gg'}(\xi, x, x_i) \;=\; & \mathrm{R1}^i_{g'}(s_{gg'}\xi, x) - \\
& - \frac{(s_{gg'}\xi)\mathrm{L}(s_{gg'}\xi)}{\sigma^i_{g'}} \mathrm{S1}^i_{g'}(s_{gg'}\xi, x, x_i) + \\
& + \sum_{\alpha=0}^{N-1} \Bigg[\mathrm{c}^{g',j}_\alpha \mathrm{A}^{g'}_\alpha(-s_{gg'}\xi) + \\
& + \left(\mathrm{d}^{g',j}_\alpha - \mathrm{b}^{g',i}_\alpha e^{-\frac{\sigma^i_{g'}(x_i - x)}{s_{gg'}\xi}} \right) \mathrm{A}^{g'}_\alpha(s_{gg'}\xi) \Bigg] - \\
& - \sigma^i_g \sum_{\substack{g''=1 \\ g'' \neq g'}}^{G} \Lambda_{g''g'}(s_{gg'}\xi) I^{*i}_{gg''}(\xi, x, x_i),
\end{aligned} \tag{A.71a}$$

$$\begin{aligned}
\sigma^i_g \Lambda_{g'g'}(s_{gg'}\xi) J^{*i}_{gg'}(\xi, x_{i-1}, x) \;=\; & \mathrm{R2}^i_{g'}(s_{gg'}\xi, x) - \\
& - \frac{(s_{gg'}\xi)\mathrm{L}(s_{gg'}\xi)}{\sigma^i_{g'}} \mathrm{S2}^i_{g'}(s_{gg'}\xi, x_{i-1}, x) + \\
& + \sum_{\alpha=0}^{N-1} \Bigg[\mathrm{d}^{g',j}_\alpha \mathrm{A}^{g'}_\alpha(-s_{gg'}\xi) + \\
& + \left(\mathrm{c}^{g',j}_\alpha - \mathrm{a}^{g',i}_\alpha e^{-\frac{\sigma^i_{g'}(x - x_{i-1})}{s_{gg'}\xi}} \right) \mathrm{A}^{g'}_\alpha(s_{gg'}\xi) \Bigg] - \\
& - \sigma^i_g \sum_{\substack{g''=1 \\ g'' \neq g'}}^{G} \Lambda_{g''g'}(s_{gg'}\xi) J^{*i}_{gg''}(\xi, x_{i-1}, x).
\end{aligned} \tag{A.71b}$$

These equations are used directly in $\mathrm{T1}^i_g(\mu, x, x_i)$ and $\mathrm{T2}^i_g(\mu, x_{i-1}, x)$ for $\xi \notin [0, \frac{1}{s_{gg'}}]$ as long as $\Lambda_{g'g'}(s_{gg'}\xi)$ is not equal to zero.

A.6 Boundary Conditions for Beam and Isotropic Sources

In this section, the boundary conditions are determined for multiple slabs for a beam or an isotropic source incident on the leftmost face. The slabs are connected through the $F_L^{g,i}(\mu)$ and $F_R^{g,i}(\mu)$ terms in $R1_g^i(\mu, x)$ and $R2_g^i(\mu, x)$ and the post processor.

To obtain the proper relations for a beam source, define the boundary conditions at the slab boundaries as:

Leftmost slab - Beam Source on left face

$$F_L^{g,1}(\mu) = S_0^g \delta(\mu - \mu_0^g), \tag{A.72a}$$

$$F_R^{g,1}(\mu) = \phi_g(x_1, -\mu). \tag{A.72b}$$

Rightmost slab - Vacuum on right face

$$F_L^{g,NS}(\mu) = \phi_g(x_{NS-1}, \mu) + S_0^g e^{-\frac{1}{\mu}\sum_{k=1}^{NS-1}\Delta_g^k} \delta(\mu - \mu_0^g), \tag{A.73a}$$

$$F_R^{g,NS}(\mu) = 0. \tag{A.73b}$$

Non-boundary slabs - Collided plus uncollided flux on both faces

$$F_L^{g,i}(\mu) = \phi_g(x_{i-1}, \mu) + S_0^g e^{-\frac{1}{\mu}\sum_{k=1}^{i-1}\Delta_g^k} \delta(\mu - \mu_0^g), \tag{A.74a}$$

$$F_R^{g,i}(\mu) = \phi_g(x_i, -\mu). \tag{A.74b}$$

A pattern is set up when $F_L^{g,i}(\mu)$ and $F_R^{g,i}(\mu)$ are substituted into $R1_g^i(\mu,x)$ and $R2_g^i(\mu,x)$ which is

$$\begin{aligned} R1_g^i(\mu,x) \;=\; & \int_0^1 d\eta \;\; \eta \left[C(\sigma_g^i(x_i - x),\eta,\mu)\phi_g(x_i,-\eta) + \right. \\ & \left. + \; e^{-\frac{\sigma_g^i(x-x_{i-1})}{\eta}} S(\sigma_g^i(x_i - x),\eta,\mu)\phi_g(x_{i-1},\eta) \right] \; + \\ & + \; \mu_0^g \; S_0^g \; e^{-\frac{1}{\mu_0^g}\left(\sum_{k=1}^{i-1}\Delta_g^k + \sigma_g^i(x-x_{i-1})\right)} \; S(\sigma_g^i(x_i - x),\mu_0^g,\mu), \end{aligned} \tag{A.75a}$$

$$\begin{aligned} R2_g^i(\mu,x) \;=\; & \int_0^1 d\eta \;\; \eta \left[C(\sigma_g^i(x - x_{i-1}),\eta,\mu)\phi_g(x_{i-1},\eta) + \right. \\ & \left. + \; e^{-\frac{\sigma_g^i(x_i-x)}{\eta}} S(\sigma_g^i(x - x_{i-1}),\eta,\mu)\phi_g(x_i,-\eta) \right] \; + \\ & + \; \mu_0^g \; S_0^g \; e^{-\frac{1}{\mu_0^g}\sum_{k=1}^{i-1}\Delta_g^k} C(\sigma_g^i(x - x_{i-1}),\mu_0^g,\mu). \end{aligned} \tag{A.75b}$$

To obtain the proper relations for an isotropic source, define the boundary conditions at the slab boundaries as:

Leftmost slab - Isotropic source on left face

$$F_L^{g,1}(\mu) \;=\; S_0^g, \tag{A.76a}$$

$$F_R^{g,1}(\mu) \;=\; \phi_g(x_1,-\mu). \tag{A.76b}$$

Rightmost slab - Vacuum on right face

$$F_L^{g,NS}(\mu) \;=\; \phi_g(x_{NS-1},\mu) \;+\; S_0^g e^{-\frac{1}{\mu}\sum_{k=1}^{NS-1}\Delta_g^k}, \tag{A.77a}$$

$$F_R^{g,NS}(\mu) \;=\; 0. \tag{A.77b}$$

Middle slabs - Collided plus uncollided on both faces

$$F_L^{g,i}(\mu) = \phi_g(x_{i-1},\mu) + S_0^g e^{-\frac{1}{\mu}\sum_{k=1}^{i-1}\Delta_g^k}, \tag{A.78a}$$

$$F_R^{g,i}(\mu) = \phi_g(x_i,-\mu). \tag{A.78b}$$

A pattern is set up when the boundary values are substituted into $R1_g^i(\mu,x)$ and $R2_g^i(\mu,x)$ which is

$$\begin{aligned} R1_g^i(\mu,x) &= \int_0^1 d\eta\ \eta\left[C(\sigma_g^i(x_i-x),\eta,\mu)\phi_g(x_i,-\eta) + \right. \\ &\left. + e^{-\frac{\sigma_g^i(x-x_{i-1})}{\eta}} S(\sigma_g^i(x_i-x),\eta,\mu)\phi_g(x_{i-1},\eta)\right] + \\ &+ S_0^g \int_0^1 d\eta\ \eta e^{-\frac{1}{\eta}(\sum_{k=1}^{i-1}\Delta_g^k+\sigma_g^i(x-x_{i-1}))} S(\sigma_g^i(x_i-x),\eta,\mu), \end{aligned} \tag{A.79a}$$

$$\begin{aligned} R2_g^i(\mu,x) &= \int_0^1 d\eta\ \eta\left[C(\sigma_g^i(x-x_{i-1}),\eta,\mu)\phi_g(x_{i-1},\eta) + \right. \\ &\left. + e^{-\frac{\sigma_g^i(x_i-x)}{\eta}} S(\sigma_{g\to g}^i(x-x_{i-1}),\eta,\mu)\phi_g(x_i,-\eta)\right] + \\ &+ S_0^g \int_0^1 d\eta\ \eta e^{-\frac{1}{\eta}\sum_{k=1}^{i-1}\Delta_g^k} C(\sigma_g^i(x-x_{i-1},\eta,\mu). \end{aligned} \tag{A.79b}$$

The F_N approximation could be used to put every flux in terms of $F_L^{g,1}(\mu)$ and $F_R^{g,NS}(\mu)$, but the result is a multiplicative recursive relationship or matrix over all the slabs. For any multiple slab analysis, it will be computationally faster to use the post processor to calculate the fluxes at the integration points used for $R1_g^i(\mu,x)$ and $R2_g^i(\mu,x)$.

A.7 Semi-infinite Media

This section is not a detailed derivation of the semi-infinite media F_N method, but the resultant equations are shown for completeness.

A.7.1 Matrix Equations

The boundary matrix equation is

$$\sum_{\alpha=0}^{N-1} a_\alpha^g B_\alpha^g(\nu) = R1_g(\nu, x_0) + \frac{1}{\sigma_{g\to g}} T1_g(\nu, x_0, \infty) + \\ + \frac{1}{\sigma_{g\to g}} S1_g(\nu, x_0, \infty). \tag{A.80a}$$

The interior matrix equations are

$$\sum_{\alpha=0}^{N-1} \left[c_\alpha^{g,j} B_\alpha^g(\nu) - d_\alpha^{g,j} A_\alpha^g(\nu)\right] = R1_g(\nu, x_j) + \frac{1}{\sigma_{g\to g}} T1_g(\nu, x_j, \infty) + \\ + \frac{1}{\sigma_{g\to g}} S1_g(\nu, x_j, \infty), \tag{A.80b}$$

$$\sum_{\alpha=0}^{N-1} \left[d_\alpha^{g,j} B_\alpha^g(\nu) - c_\alpha^{g,j} A_\alpha^g(\nu)\right] = R2_g(\nu, x_j) + \frac{1}{\sigma_{g\to g}} T2_g(\nu, x_0, x_j) + \\ + \frac{1}{\sigma_{g\to g}} S2_g(\nu, x_0, x_j), \tag{A.80c}$$

where,

$$R1_g(\nu, x_j) = \begin{cases} S_0^g \dfrac{\mu_0}{\mu_0 + \nu} e^{-\frac{\sigma_g(x)}{\nu}(x - x_0)}, & \text{BeamSource} \\ S_0^g \displaystyle\int_0^1 d\eta \, \frac{\eta}{\eta + \nu} e^{-\frac{\sigma_g(x)}{\eta}(x - x_0)}, & \text{IsotropicSource,} \end{cases} \tag{A.80d}$$

$$R2_g(\nu, x_j) = \begin{cases} S_0^g \mu_0 C(\sigma_g(x - x_0), \mu_0, \nu), & \text{BeamSource} \\ S_0^g \displaystyle\int_0^1 d\eta \, \eta C(\sigma_g(x - x_0), \eta, \nu), & \text{IsotropicSource,} \end{cases} \tag{A.80e}$$

$$C(\xi, \eta, \nu) = \begin{cases} \dfrac{e^{-\frac{\xi}{\nu}} - e^{-\frac{\xi}{\nu}}}{\eta - \nu} & \eta \neq \nu \\ \dfrac{\xi}{\nu^2} e^{-\frac{\xi}{\nu}} & \eta = \nu, \end{cases} \tag{A.80f}$$

$$T1_g(\nu, x_j, \infty) = \sigma_g \sum_{g'=1}^{g-1} \sigma_{g'\to g} I_{gg}^*(\nu, x_j, \infty), \tag{A.80g}$$

$$T2_g(\nu, x_0, x_j) = \sigma_g \sum_{g'=1}^{g-1} \sigma_{g'\to g} J_{gg}^*(\nu, x_0, x_j), \tag{A.80h}$$

$$\mathrm{S1}_g(\nu, x_j, \infty) = \begin{cases} \mathrm{S}_g(x_j) & \nu = 0 \\ \dfrac{\sigma_g}{\nu} \displaystyle\int_{x_j}^{\infty} \mathrm{d}z\, e^{-\frac{\sigma_g}{\nu}(z-x_j)} \mathrm{S}_g(z) & \nu \neq 0, \end{cases} \tag{A.80i}$$

and

$$\mathrm{S2}_g(\nu, x_0, \infty) = \begin{cases} \mathrm{S}_g(x_j) & \nu = 0 \\ \dfrac{\sigma_g}{\nu} \displaystyle\int_{x_0}^{x_j} \mathrm{d}z\, e^{-\frac{\sigma_g}{\nu}(x_j-z)} \mathrm{S}_g(z) & \nu \neq 0. \end{cases} \tag{A.80j}$$

A.7.2 Post Processor

The boundary post processor is

$$\begin{aligned} \phi_g(x_0, -\mu) &= \frac{1}{2\sigma_g \lambda^*_{gg}(\mu)} \left[\sigma_{g\to g} \sum_{\alpha=0}^{N-1} \mathrm{a}^g_\alpha \mathrm{B}^{*g}_\alpha(\mu) + \right. \\ &\left. + \sigma_{g\to g} \mathrm{R1}_g(\mu, x_0) + \mathrm{T1}_g(\mu, x_0, \infty) + \mathrm{S1}_g(\mu, x_0, \infty) \right]. \end{aligned} \tag{A.81a}$$

The interior post processor is

$$\begin{aligned} \phi_g(x_j, -\mu) &= \frac{1}{2\sigma_g \lambda^*_{gg}(\mu)} \left[\sigma_{g\to g} \sum_{\alpha=0}^{N-1} \left\{ \mathrm{c}^{g,j}_\alpha \mathrm{B}^{*g}_\alpha(\mu) + \mathrm{d}^{g,j}_\alpha \mathrm{A}^g_\alpha(\mu) \right\} + \right. \\ &\left. + \sigma_{g\to g} \mathrm{R1}_g(\mu, x_j) + \mathrm{T1}_g(\mu, x_j, \infty) + \mathrm{S1}_g(\mu, x_j, \infty) \right], \end{aligned} \tag{A.81b}$$

$$\begin{aligned} \phi_g(x_j, \mu) &= \frac{1}{2\sigma_g \lambda^*_{gg}(\mu)} \left[\sigma_{g\to g} \sum_{\alpha=0}^{N-1} \left\{ \mathrm{d}^{g,j}_\alpha \mathrm{B}^g_\alpha(\mu) + \left(\mathrm{c}^{g,j}_\alpha - \right. \right. \right. \\ &\left. \left. \left. - \mathrm{a}^{g,i}_\alpha e^{-\frac{\sigma_g}{\mu}(x_j - x_0)} \right) \mathrm{A}^g_\alpha(\mu) \right\} + \sigma_{g\to g} \mathrm{R2}_g(\mu, x_j) + \right. \\ &\left. + \mathrm{T2}_g(\mu, x_0, x_j) + \mathrm{S2}_g(\mu, x_0, x_j) \right]. \end{aligned} \tag{A.81c}$$

A.7.3 Scattering Terms

The energy group particle transfer terms for $\xi \in [0, s_{gg'}]$ are

$$\begin{aligned} \sigma_g \mathrm{I}^*_{gg'}(\xi, x, \infty) &= \sum_{\alpha=0}^{N-1} \mathcal{K}\psi_\alpha(s_{gg'}\xi) - \frac{1}{\sigma_{g'\to g'}} \mathrm{S1}_{g'}(s_{gg'}\xi, x, \infty) + \\ &+ \frac{\sigma_g}{\sigma_{g'\to g'}} \sum_{g''=1}^{g'-1} \sigma_{g''\to g'} \mathrm{I}^{*i}_{gg''}(\xi, x, \infty), \end{aligned} \tag{A.82a}$$

$$\sigma_g J^*_{gg'}(\xi,x,\infty) = \sum_{\alpha=0}^{N-1} d_\alpha^{g',j}\psi_\alpha(s_{gg'}\xi) - \frac{1}{\sigma_{g'\to g'}} S2_{g'}(s_{gg'}\xi,x,\infty) + \\ + \frac{\sigma_g}{\sigma_{g'\to g'}} \sum_{g''=1}^{g'-1} \sigma_{g''\to g'} J^{*i}_{gg''}(\xi,x,\infty), \tag{A.82b}$$

where,

$$\mathcal{K} = \begin{cases} a_\alpha^g & x = x_0 \\ c_\alpha^{g,j} & x \neq x_0. \end{cases} \tag{A.82c}$$

The energy group particle transfer terms for $\xi \notin [0, s_{gg'}]$ are

$$\sigma_g \Lambda_{g'g'}(s_{gg'}\xi) I^{*i}_{gg'}(\xi,x,\infty) = \sum_{\alpha=0}^{N-1} [\mathcal{K}_1 A_\alpha^g(-s_{gg'}\xi) + \mathcal{K}_2 A_\alpha^g(s_{gg'}\xi)] + \\ + R1_{g'}(s_{gg'}\xi,x) - \frac{(s_{gg'}\xi)L(s_{gg'}\xi)}{\sigma_{g'}} S1_{g'}(s_{gg'}\xi,x,\infty) - \\ - \sigma_g \sum_{g''=1}^{g'-1} \Lambda_{g''g'}(s_{gg'}\xi) I^*_{g'g''}(\xi,x,\infty), \tag{A.83a}$$

$$\sigma_g \Lambda_{g'g'}(s_{gg'}\xi) J^{*i}_{gg'}(\xi,x_0,x) = \sum_{\alpha=0}^{N-1} \left[d_\alpha^{g,j} A_\alpha^g(-s_{gg'}\xi) + \left(c_\alpha^{g,j} - \right.\right. \\ \left.\left. - a_\alpha^g e^{-\frac{\sigma_{g'}}{s_{gg'}\xi}(x-x_0)} \right) A_\alpha^g(s_{gg'}\xi) \right] + \\ + R2_{g'}(s_{gg'}\xi,x) - \frac{(s_{gg'}\xi)L(s_{gg'}\xi)}{\sigma_{g'}} S2_{g'}(s_{gg'}\xi,x_0,x) - \\ - \sigma_g \sum_{g''=1}^{g'-1} \Lambda_{g''g'}(s_{gg'}\xi) J^*_{g'g''}(\xi,x_0,x), \tag{A.83b}$$

where,

$$\mathcal{K}_1 = \begin{cases} a_\alpha^g & x = x_0 \\ c_\alpha^{g,j} & x \neq x_0, \end{cases} \tag{A.83c}$$

$$\mathcal{K}_2 = \begin{cases} 0 & x = x_0 \\ d_\alpha^{g,j} & x \neq x_0. \end{cases} \tag{A.83d}$$

A.7.4 Scalar Flux

The scalar flux is

$$\phi_g(x_0) = \frac{\sigma_{g\to g}}{2\sigma_g}\sum_{\alpha=0}^{N-1} a_\alpha^g \int_0^1 d\eta\, \psi_\alpha(\eta), \tag{A.84a}$$

$$\phi_g(x) = \frac{\sigma_{g\to g}}{2\sigma_g}\sum_{\alpha=0}^{N-1} \left(d_\alpha^{g,j} + c_\alpha^{g,j}\right) \int_0^1 d\eta\, \psi_\alpha(\eta) + \mathcal{I}, \tag{A.84b}$$

where,

$$\mathcal{I} = \begin{cases} S_0^g e^{-\frac{\sigma_g}{\mu_0}(x-x_0)} & \text{BeamSource} \\ S_0^g \int_0^1 d\eta\, e^{-\frac{\sigma_g}{\eta}(x-x_0)} & \text{IsotropicSource.} \end{cases} \tag{A.84c}$$

A.7.5 GIT Neutron Source

The neutron source from the galactic cosmic ray cascade is

$$S_g(x) = \frac{\rho}{\sigma_0 \mu_{GIT}} \sum_{l=1}^{J-2} M_{o,J-l}\sigma_{J-l} \sum_{r=1}^{N_l} \tilde{Y}_{i_1,r}^{J-l} \sum_{g'=1}^{g} \frac{\sigma_{g'\to g}}{S_P(E_{g'})} I(x), \tag{A.85a}$$

where,

$$\begin{aligned} I(x) &= -\int_{x_0}^{\infty} dw\, e^{-\frac{\sigma_g}{\mu_{GIT}}(x-w)-(\sigma_{J-i_1}-\frac{a_r}{b_r}\overline{\nu}_{J-i_1})w-\frac{a_r}{b_r}s_{g'}} \times \\ &\times \left(\theta(\frac{s_{g'}}{\overline{\nu}_{J-i_1}} - w) - \theta(\frac{s_{g'}}{\overline{\nu}_{J-i_2}} - w)\right). \end{aligned} \tag{A.85b}$$

The galactic cosmic ray cascade neutron source in the F_N context is

$$S1_g(\nu, x, \infty) = \frac{\sigma_g(x)\rho}{\nu\sigma_0\mu_{GIT}} \sum_{l=1}^{J-2} M_{0,J-l}\sigma_{J-l} \sum_{r=1}^{N_l} \tilde{Y}_{i_1,r}^{J-l} \sum_{g'=1}^{g} \frac{\sigma_{g'\to g}}{S_P(E_{g'})} I1(x), \tag{A.86a}$$

$$S2_g(\nu, x_0, x) = \frac{\sigma_g(x)\rho}{\nu\sigma_0\mu_{GIT}} \sum_{l=1}^{J-2} M_{0,J-l}\sigma_{J-l} \sum_{r=1}^{N_l} \tilde{Y}_{i_1,r}^{J-l} \sum_{g'=1}^{g} \frac{\sigma_{g'\to g}}{S_P(E_{g'})} I2(x), \tag{A.86b}$$

where,

$$I1(x) = \int_x^{\infty} dz\, e^{-\frac{\sigma_g}{\nu}(z-x)} I(z), \tag{A.86c}$$

$$I2(x) \;=\; \int_{x_0}^{x} \mathrm{d}z\; e^{-\frac{\sigma_s}{\nu}(x-z)} I(z). \tag{A.86d}$$

The integrals are evaluated analytically using MATHCAD.

A.8 Critical Slab Width and Associated Flux

From the F_N formulation, a critical slab width and flux can be determined for the one slab, one energy group, source free problem. The critical problem is defined by the infinite medium dispersion relation with an imaginary root and the specification of the resultant matrix from collocation being equal to zero. Normalization of the angular flux is an input parameter, and the flux is considered to be symmetric about the center of the slab.

A.8.1 Critical Slab Width

The boundary matrix equations with one group, one slab, no source, and flux symmetry ($a_\alpha = b_\alpha$) reduce to

$$\sum_{\alpha=0}^{N-1} a_\alpha \left[B_\alpha(\nu) \;+\; A_\alpha(\nu) e^{-\Delta_c/\nu} \right] \;=\; 0. \tag{A.87}$$

To determine ν_0, use the imaginary root of the infinite medium dispersion relation

$$\Lambda(\nu_0) \;=\; 0 \;=\; 1 - \nu_0 \frac{\sigma_s}{\sigma} \tan^{-1}\left(\frac{1}{\nu_0}\right). \tag{A.88}$$

Since ν_0 is purely imaginary, the first row of the expansion coefficient matrix is complex. To find the critical width, the real and imaginary parts of the determinant of the matrix must be zero at the same value of Δ_c (the critical

width). With $\beta = 1, \ldots, N-1$ and $\alpha = 0, \ldots, N-1$, the determinant equations are

$$\begin{vmatrix} \Re_{\alpha 0} \\ B_\alpha(\nu_\beta) \; + \; A_\alpha(\nu_\beta) e^{-\frac{\Delta_c}{\nu_\beta}} \end{vmatrix} = 0, \tag{A.89a}$$

$$\begin{vmatrix} \Im_{\alpha 0} \\ B_\alpha(\nu_\beta) \; + \; A_\alpha(\nu_\beta) e^{-\frac{\Delta_c}{\nu_\beta}} \end{vmatrix} = 0, \tag{A.89b}$$

where,

$$\Re_{\alpha 0} = \frac{\sigma_s}{2\sigma} \left[\mathrm{SA}_\alpha \left(\cos \frac{\Delta_c}{z_0} - 1 \right) + z_0 \mathrm{SB}_\alpha \sin \frac{\Delta_c}{z_0} \right], \tag{A.89c}$$

$$\Im_{\alpha 0} = \frac{\sigma_s}{2\sigma} \left[\mathrm{SA}_\alpha \sin \frac{\Delta_c}{z_0} + z_0 \mathrm{SB}_\alpha \left(\cos \frac{\Delta_c}{z_0} + 1 \right) \right], \tag{A.89d}$$

and,

$$\nu_0 = i z_0, \tag{A.89e}$$

$$\Delta_c = \sigma (x_c - 0), \tag{A.89f}$$

$$\mathrm{SA}_\alpha = \int_0^1 \mathrm{d}\eta \, \frac{\eta^2}{\eta^2 + z_0^2} \psi_\alpha(\eta), \tag{A.89g}$$

$$\mathrm{SB}_\alpha = \int_0^1 \mathrm{d}\eta \, \frac{\eta}{\eta^2 + z_0^2} \psi_\alpha(\eta). \tag{A.89h}$$

The determinant is found from the LU decomposition routine in Reference [24]. A bisection method is used to find Δ_c to satisfy the above relations.

A.8.2 Boundary and Interior Critical Flux Values

To determine the boundary flux, rewrite the matrix equation as

$$\sum_{\alpha=1}^{N} a_\alpha \left[B_\alpha(\nu_\beta) + A_\alpha(\nu_\beta)e^{-\Delta_c/\nu_\beta}\right] = -a_0 \left[B_0(\nu_\beta) + A_0(\nu_\beta)e^{-\Delta_c/\nu_\beta}\right], \quad \text{(A.90)}$$

where, a_0 is a normalization parameter. To calculate the additional a_α values, invert the matrix and use the normal post processor to find the fluxes.

To find the interior flux, the matrix equations for $\beta = 0, 1, \ldots, N-1$ are

$$\sum_{\alpha=0}^{N-1} [c_\alpha B_\alpha(\nu_\beta) - d_\alpha A_\alpha(\nu_\beta)] = -e^{-\sigma(x_c-x)/\nu_\beta} \sum_{\alpha=0}^{N-1} a_\alpha A_\alpha(\nu_\beta), \quad \text{(A.91a)}$$

$$\sum_{\alpha=0}^{N-1} [d_\alpha B_\alpha(\nu_\beta) - c_\alpha A_\alpha(\nu_\beta)] = -e^{-\sigma(x-0)/\nu_\beta} \sum_{\alpha=0}^{N-1} a_\alpha A_\alpha(\nu_\beta). \quad \text{(A.91b)}$$

However, for $\beta = 0$, the $A_\alpha(\nu_\beta)$'s and $B_\alpha(\nu_\beta)$'s are complex

$$A_\alpha(\nu_\beta) = \frac{\sigma_s}{2\sigma}\left[\mathrm{SA}_\alpha - iz_0\mathrm{SB}_\alpha\right], \quad \text{(A.92a)}$$

$$B_\alpha(\nu_\beta) = -\frac{\sigma_s}{2\sigma}\left[\mathrm{SA}_\alpha + iz_0\mathrm{SB}_\alpha\right]. \quad \text{(A.92b)}$$

The expansion coefficients are real, but the matrix terms and the matrix inversion routine need to be complex in order to calculate the expansion coefficients properly. Once the c_α and d_α values are found, the normal post processor can be used to determine the interior flux distribution.

A.8.3 F_N to ANISN/PC Normalization

To calculate the normalization factor between the F_N method and ANISN/PC, set the scalar flux found at $x = 0$ from both methods equal. The

scalar flux at the boundary for the F_N method is

$$\phi_{\text{fn}}(0) = \frac{\sigma_s}{2\sigma} a_0. \tag{A.93}$$

For a certain set of cross sections, $\nu\sigma_f + \sigma_s = c\sigma$, set the normalization factor used in the F_N algorithm as

$$\text{Scale} = \frac{2\phi_{\text{anisn}}(0)}{c}. \tag{A.94}$$

APPENDIX B

PROGRAM USER'S MANUAL

This chapter provides a user's manual for the operation of MGSLAB, MGSEMI, and FNCRIT. The input to and the output from the programs will be discussed. An example is included for clarity. The programs can be acquired through the University of Arizona's Nuclear Engineering Department.

Four versions of the program were created in the course of the research on the F_N method. The first version analyzed finite slab boundaries only, but included a degenerate eigenvalue algorithm. This version exists only to verify the algorithm and final program against existing scientific literature (References [11] and [12]). A second version of the program, referred to as MGSLAB, analyzes boundaries and interior slab positions without the degenerate eigenvalue algorithm which usually does not appear when normal material cross sections are used. This is the workhorse of the four programs. An algorithm that analyzes one group, homogeneous critical slabs is the third program created. It is referred to as FNCRIT. The last version is a homogeneous semi-infinite variant called MGSEMI. These programs use common subprograms shared in an object library.

B.1 Program Input

The input to each program is the same, whether or not the values are used by the particular program version being executed. The only exception is the scaling value used by FNCRIT. The pseudo-code below outlines the input flow. The programs read this file from FORTRAN unit 5. Under most operating systems, this unit can be defined as a file name outside the program.

Line 1:

Nslabs - Number of slabs [negative for diagnostic] (<MAXSLAB).

Ngroup - Number of energy groups (<MAXGROUP).

Inner - Number of boundary inner iterations for each slab at each FN iterate.

GLBoun - Inhomogeneous term integration quadrature (<MAXQUAD)

Line 2:

Nstart - Initial N for FN iteration:

- Negative value for collocation points of Chebyshev roots.
- Positive value for collocation points of Legendre roots.

Nend - Final N for FN iteration (<MAXN)

Nstep - Increment between approximations

Line 3:

EditMu - Number of positive direction edit points (<MAXEDIT)

EMType - Type of direction edit points to use:

1. Gauss-Legendre points of order EditMu
2. Evenly spaced points

3. User supplied point values

If EMType .eq. 1 then Line 4:

EMstrt - Starting edit direction value (0.0)

EMend - Final edit direction value (1.0)

If EMType .eq. 2 then Line 4:

EMstrt - Starting edit direction value (0.0)

EMend - Final edit direction value (1.0)

EMZero - The value to use for a Mu of zero (1.0d-10)

If EMType .eq. 3 then Line 4:

EMuser - User input positive edit directions (1..EditMu)

Line 5:

Tol - Flux convergence tolerance (1.0d-5)

Line 6:

Stype - The type of external source

0. No source
1. Beam source at left face of slab
2. Isotropic source at left face of slab

If Stype .eq. 1 then Line 7:

Mu0,S0 - Direction and Intensity of external source for each group (1..Ngroup)

If Stype .eq. 2 then Line 7:

S0 - Intensity of external source for each group (1..Ngroup)

Line 8:

Gsour - Number of energy groups that have distributed sources (if a -1, use the analytical GIT source)

If Gsour .lt. 0 then Line 9:

MuG - Direction of incoming GIT Beam

dens - Density of the target material

Line 10:

Width - Slab width in centimeter (ignored for the FNCRIT program).

EditX - Number of spatial edit points in this slab (<MAXEDIT)

EXType - Type of spatial edit points used

1. Evenly spaced points within slab (<MAXEDIT)
2. User supplied points within slab (<MAXEDIT)
3. Gauss-Legendre points of order EditX within slab (<MAXEDIT)

GLMatx - Gauss-Legendre integration order for evaluation of integrals in the matrix terms for this slab (<MAXQUAD)

BType - Type of basis functions to use in this slab

1. Shifted Legendre: $P_l(2x-1)$
2. Modified Shifted Legendre: $P_l(2(x^{\mathrm{md}}-1)$
3. Monomials: x^l
4. Modified Shifted Monomials: $(2x^{\mathrm{md}}-1)^l$

md - Parameter used for BType 2 and 4 (0.75)

Line 11:

Sg,Sgpg - Total and down scatter cross sections. Array dimensions for down scatter cross sections: (slab,from group,to group).

```
st(1) s1(1,1)    0        0     . . .
st(2) s2(1,2) s2(2,2)     0     . . .
st(3) s3(1,3) s3(2,3) s3(3,3)  . . .
  .       .       .        .     . . .
  .       .       .        .     . . .
  .       .       .        .     . . .
```

If EXType .eq. 2 then Line 12:

EXuser - User input spatial edit points (1..EditX)

Line 13 (used by FNCRIT only):

Scale - The flux scaling value

Last Line optional:

PNodes - Optional nodes to include in the boundary flux plot file (<100)

If the GIT source is used, two more file must be read. FORTRAN unit 40 contains the $\tilde{Y}^{J-l}_{i_1,r}$ values generated by the GIT program. These are in binary format. FORTRAN unit 41 contains the input deck used by the GIT program.

Line 1:

JJ - Maximum species (charge) number (<MAXJ)

LJJ - Charge number of last species

Line 2:

IRM -

-1. Use wilson stopping power

1. Use simplified stopping power

TOL - Relative error for romberg numerical integration

Line 3:

IDFL - 1 For flux profile for incident beam of species JJ (Only option used)

ISX -

-1. Use edit flux versus x

1. Use edit flux versus path length

Line 4:

IBIN -

-1. Read binary tape 40 for y coefficients

0. No action

1. Write binary tape 40 for y coefficients

IPR -

-1. All output on one file (unit 21)

1. Output on multiple files (units 21 through 39)

Line 5:

E0 - Input beam initial energy

LE - Number of energy edit points (<20)

LX - Number of spatial edit intervals (<100)

Line 6:

S0 - Model cross section normalization

FN - Fraction of neutrons produced in an interaction, f_n

E11 - First energy for simplified stopping power

E22 - Second energy for simplified stopping power

If ISX .lt. 0 then Line 7: Energy edit grid (EN(I),I=1,LE)

If ISX .gt. 0 then Line 7: Spatial grid (X(I),I=1,LX)

Section B.3 shows an example of an input deck.

B.2 Program Output

The output routines generate various types of output data. The list below shows FORTRAN unit number written and the type of data written to it. Under most operating systems, these units can be defined as file names outside the program.

- Unit 6: the Screen
- Unit 7: diagnostics file
- Unit 21: node and group angular fluxes in text format

- Unit 22: slab and group angular fluxes in text format
- Unit 23: group scalar fluxes in text format
- Unit 24: total scalar flux in text format
- Unit 25: total scalar flux in plot format
- Unit 26: screen echo to a file
- Unit 27: node and group angular fluxes in plot format
- Unit 28: slab and group angular fluxes in plot format
- Unit 29: group scalar flux in plot format
- Unit 30: the GIT ion flux in plot format
- Unit 31: the GIT neutron source in plot format
- Unit 49: energy group, slab position, and group scalar flux in three dimensional plot format
- Unit 50 to 69: energy group, direction, and group angular flux in three dimensional plot format

Section B.3 shows the text output from the example input deck.

B.3 Example

This section shows a typical example input deck and the associated output text files. The physical situation being modeled is a three energy group, three slab problem. A beam source of unit strength for group one only is incident on the left face of the media.

Input Deck:

```
3 3 3 35                    \ Nslabs Ngroup Inner GLBoun
11 49 2                     \ Nstart Nend Nstep
16 1                        \ EditMu EMType
0.0 1.0                     \ EMstart EMend
1.0d-04                     \ Tol
1                           \ Beam Source
1.0 1.0 1.0 0.0 1.0 0.0     \ Mu0 S0 for groups 1, 2, and 3
0                           \ No GIT Source
0.2d0 9 1 35 2 0.75d0       \ Width EditX EXType GLMatx BType md
2.0d0 1.0d0 0.0d0 0.0d0     \ Cross sections
5.0d0 1.0d0 3.0d0 0.0d0
3.0d0 0.1d0 0.2d0 1.5d0
0.4d0 19 1 35 2 0.75d0      \ Width EditX EXType GLMatx BType md
5.0d0 3.0d0 0.0d0 0.0d0     \ Cross sections
2.0d0 0.5d0 1.0d0 0.0d0
3.0d0 0.4d0 0.1d0 1.0d0
0.4d0 19 1 35 2 0.75d0      \ Width EditX EXType GLMatx BType md
3.0d0 2.8d0 0.0d0 0.0d0     \ Cross sections
2.0d0 0.1d0 0.9d0 0.0d0
5.0d0 0.9d0 0.9d0 1.0d0
5 20 40                     \ PNodes
```

Unit 26 - screen echo to a file:

```
3D Scalar Plot Data File Generated
Energy Group = 0001
  N  Conv ToCon Pos max err  Neg max err  Pos ave err  Neg ave err
0011 0000 0096  1.000000E+00 1.000000E+00 1.000000E+00 1.000000E+00
0011 0000 0096  1.000000E+00 1.000000E+00 1.000000E+00 1.000000E+00
0011 0000 0096  1.000000E+00 1.000000E+00 1.000000E+00 1.000000E+00
0013 0000 0096  3.553633E-03 5.712922E-03 1.167111E-03 1.301876E-03
0013 0000 0096  3.872581E-03 6.227630E-03 1.272876E-03 1.419210E-03
0013 0000 0096  3.901608E-03 6.274470E-03 1.282503E-03 1.429885E-03
0015 0093 0096  1.489162E-04 1.064508E-04 1.206050E-05 6.633653E-06
0015 0093 0096  1.488493E-04 1.064160E-04 1.209246E-05 6.696274E-06
0015 0093 0096  1.488428E-04 1.064128E-04 1.209542E-05 6.701626E-06
0017 0096 0096  3.640764E-05 2.877266E-05 4.588094E-06 2.083833E-06
Boundary Flux Converged
0017 0096 1600  1.000000E+00 1.000000E+00 9.400003E-01 9.400001E-01
0019 1584 1600  1.766174E-04 1.468803E-04 6.441155E-06 4.480234E-06
0021 1596 1600  1.158229E-04 1.116657E-04 1.090374E-06 9.166960E-07
0023 1600 1600  2.720663E-05 3.480179E-05 1.227406E-07 1.803098E-07
All Fluxes Converged
Including   0.100000000000000      in the boundary flux output
Including   0.400000000000000      in the boundary flux output
Including   0.800000000000000      in the boundary flux output
Energy Group = 0002
  N  Conv ToCon Pos max err  Neg max err  Pos ave err  Neg ave err
0011 0000 0096  1.000000E+00 1.000000E+00 1.000000E+00 1.000000E+00
0011 0000 0096  1.000000E+00 1.000000E+00 1.000000E+00 1.000000E+00
0011 0000 0096  1.000000E+00 1.000000E+00 1.000000E+00 1.000000E+00
0013 0000 0096  9.513772E-04 1.639784E-03 4.420175E-04 4.710332E-04
0013 0000 0096  1.016245E-03 1.755531E-03 4.723103E-04 5.034820E-04
0013 0000 0096  1.020552E-03 1.763143E-03 4.743243E-04 5.056349E-04
0015 0094 0096  1.350178E-04 2.991238E-05 1.619709E-05 3.357026E-06
0015 0094 0096  1.350328E-04 2.992016E-05 1.619631E-05 3.368438E-06
0015 0094 0096  1.350335E-04 2.992069E-05 1.619635E-05 3.369010E-06
0017 0096 0096  1.252745E-05 3.572194E-06 1.847479E-06 5.871654E-07
Boundary Flux Converged
0017 0096 1600  1.000000E+00 1.000000E+00 9.400001E-01 9.400000E-01
0019 1590 1600  1.325581E-04 1.302121E-04 5.260669E-06 4.477305E-06
0021 1600 1600  5.069402E-05 4.537826E-05 3.722857E-07 5.015554E-07
All Fluxes Converged
Including   0.100000000000000      in the boundary flux output
```

```
Including   0.400000000000000      in the boundary flux output
Including   0.800000000000000      in the boundary flux output
Energy Group = 0003
  N  Conv ToCon Pos max err  Neg max err  Pos ave err  Neg ave err
0011 0000 0096  1.000000E+00 1.000000E+00 1.000000E+00 1.000000E+00
0011 0000 0096  1.000000E+00 1.000000E+00 1.000000E+00 1.000000E+00
0011 0000 0096  1.000000E+00 1.000000E+00 1.000000E+00 1.000000E+00
0013 0063 0096  7.529517E-04 1.363943E-03 1.882021E-04 2.965920E-04
0013 0063 0096  7.670185E-04 1.400001E-03 1.922363E-04 3.036932E-04
0013 0063 0096  7.673035E-04 1.400694E-03 1.923174E-04 3.038329E-04
0015 0096 0096  1.967129E-05 2.913212E-05 2.491874E-06 1.872452E-06
Boundary Flux Converged
0015 0096 1600  1.000000E+00 1.000000E+00 9.400001E-01 9.400001E-01
0017 1590 1600  1.684172E-04 1.991901E-04 4.851583E-06 3.744157E-06
0019 1600 1600  5.225291E-05 6.332041E-05 6.616150E-07 5.106637E-07
All Fluxes Converged
Including   0.100000000000000      in the boundary flux output
Including   0.400000000000000      in the boundary flux output
Including   0.800000000000000      in the boundary flux output
```

Unit 21 - node and group angular fluxes in text format: (only including some of the spatial positions)

```
 Angular flux at the Direction Edit Points for group    1
      Spatial point    0.00000
              Mu              Mu  < 0          Mu  > 0
         5.29953E-03         3.219E-01         0.000E+00
         2.77125E-02         3.218E-01         0.000E+00
         6.71844E-02         3.188E-01         0.000E+00
         1.22298E-01         3.146E-01         0.000E+00
         1.91062E-01         3.103E-01         0.000E+00
         2.70992E-01         3.048E-01         0.000E+00
         3.59198E-01         2.977E-01         0.000E+00
         4.52494E-01         2.895E-01         0.000E+00
         5.47506E-01         2.808E-01         0.000E+00
         6.40802E-01         2.724E-01         0.000E+00
         7.29008E-01         2.647E-01         0.000E+00
         8.08938E-01         2.579E-01         0.000E+00
         8.77702E-01         2.522E-01         0.000E+00
         9.32816E-01         2.478E-01         0.000E+00
         9.72288E-01         2.447E-01         0.000E+00
         9.94700E-01         2.429E-01         0.000E+00
      Spatial point    0.02000
              Mu              Mu  < 0          Mu  > 0
         5.29953E-03         3.219E-01         3.222E-01
         2.77125E-02         3.201E-01         2.463E-01
         6.71844E-02         3.159E-01         1.447E-01
         1.22298E-01         3.115E-01         8.995E-02
         1.91062E-01         3.074E-01         6.091E-02
         2.70992E-01         3.020E-01         4.425E-02
         3.59198E-01         2.948E-01         3.398E-02
         4.52494E-01         2.864E-01         2.728E-02
         5.47506E-01         2.777E-01         2.272E-02
         6.40802E-01         2.692E-01         1.951E-02
         7.29008E-01         2.614E-01         1.721E-02
         8.08938E-01         2.546E-01         1.556E-02
         8.77702E-01         2.489E-01         1.436E-02
         9.32816E-01         2.445E-01         1.353E-02
         9.72288E-01         2.414E-01         1.300E-02
         9.94700E-01         2.397E-01         1.271E-02

(edited file here)
```

Spatial point 0.98000

Mu	Mu < 0	Mu > 0
5.29953E-03	6.656E-02	6.792E-02
2.77125E-02	5.714E-02	7.062E-02
6.71844E-02	3.763E-02	7.505E-02
1.22298E-01	2.460E-02	8.084E-02
1.91062E-01	1.706E-02	8.744E-02
2.70992E-01	1.256E-02	9.396E-02
3.59198E-01	9.723E-03	9.978E-02
4.52494E-01	7.846E-03	1.049E-01
5.47506E-01	6.556E-03	1.095E-01
6.40802E-01	5.644E-03	1.134E-01
7.29008E-01	4.989E-03	1.167E-01
8.08938E-01	4.513E-03	1.193E-01
8.77702E-01	4.171E-03	1.212E-01
9.32816E-01	3.933E-03	1.226E-01
9.72288E-01	3.778E-03	1.234E-01
9.94700E-01	3.695E-03	1.239E-01

Spatial point 1.00000

Mu	Mu < 0	Mu > 0
5.29953E-03	0.000E+00	5.925E-02
2.77125E-02	0.000E+00	6.262E-02
6.71844E-02	0.000E+00	6.760E-02
1.22298E-01	0.000E+00	7.381E-02
1.91062E-01	0.000E+00	8.081E-02
2.70992E-01	0.000E+00	8.779E-02
3.59198E-01	0.000E+00	9.412E-02
4.52494E-01	0.000E+00	9.970E-02
5.47506E-01	0.000E+00	1.046E-01
6.40802E-01	0.000E+00	1.089E-01
7.29008E-01	0.000E+00	1.125E-01
8.08938E-01	0.000E+00	1.153E-01
8.77702E-01	0.000E+00	1.174E-01
9.32816E-01	0.000E+00	1.189E-01
9.72288E-01	0.000E+00	1.198E-01
9.94700E-01	0.000E+00	1.203E-01

Angular flux at the Direction Edit Points for group 2

Spatial point 0.00000

Mu	Mu < 0	Mu > 0
5.29953E-03	1.886E-01	0.000E+00
2.77125E-02	1.932E-01	0.000E+00

6.71844E-02	1.985E-01	0.000E+00
1.22298E-01	2.032E-01	0.000E+00
1.91062E-01	2.067E-01	0.000E+00
2.70992E-01	2.081E-01	0.000E+00
3.59198E-01	2.070E-01	0.000E+00
4.52494E-01	2.035E-01	0.000E+00
5.47506E-01	1.983E-01	0.000E+00
6.40802E-01	1.924E-01	0.000E+00
7.29008E-01	1.864E-01	0.000E+00
8.08938E-01	1.808E-01	0.000E+00
8.77702E-01	1.760E-01	0.000E+00
9.32816E-01	1.722E-01	0.000E+00
9.72288E-01	1.696E-01	0.000E+00
9.94700E-01	1.681E-01	0.000E+00

Spatial point 0.02000

Mu	Mu < 0	Mu > 0
5.29953E-03	2.050E-01	2.000E-01
2.77125E-02	2.071E-01	1.969E-01
6.71844E-02	2.098E-01	1.541E-01
1.22298E-01	2.123E-01	1.108E-01
1.91062E-01	2.137E-01	8.066E-02
2.70992E-01	2.132E-01	6.102E-02
3.59198E-01	2.102E-01	4.802E-02
4.52494E-01	2.051E-01	3.917E-02
5.47506E-01	1.986E-01	3.297E-02
6.40802E-01	1.916E-01	2.853E-02
7.29008E-01	1.848E-01	2.531E-02
8.08938E-01	1.786E-01	2.296E-02
8.77702E-01	1.735E-01	2.126E-02
9.32816E-01	1.694E-01	2.007E-02
9.72288E-01	1.666E-01	1.929E-02
9.94700E-01	1.650E-01	1.888E-02

(edited file here)

Spatial point 0.98000

Mu	Mu < 0	Mu > 0
5.29953E-03	1.425E-02	1.458E-02
2.77125E-02	1.062E-02	1.526E-02
6.71844E-02	6.194E-03	1.644E-02
1.22298E-01	3.843E-03	1.822E-02
1.91062E-01	2.599E-03	2.141E-02

2.70992E-01	1.887E-03	2.700E-02
3.59198E-01	1.449E-03	3.481E-02
4.52494E-01	1.163E-03	4.358E-02
5.47506E-01	9.684E-04	5.194E-02
6.40802E-01	8.317E-04	5.905E-02
7.29008E-01	7.337E-04	6.463E-02
8.08938E-01	6.630E-04	6.876E-02
8.77702E-01	6.122E-04	7.166E-02
9.32816E-01	5.768E-04	7.360E-02
9.72288E-01	5.538E-04	7.479E-02
9.94700E-01	5.416E-04	7.540E-02

Spatial point 1.00000

Mu	Mu < 0	Mu > 0
5.29953E-03	0.000E+00	1.320E-02
2.77125E-02	0.000E+00	1.397E-02
6.71844E-02	0.000E+00	1.519E-02
1.22298E-01	0.000E+00	1.696E-02
1.91062E-01	0.000E+00	1.995E-02
2.70992E-01	0.000E+00	2.518E-02
3.59198E-01	0.000E+00	3.259E-02
4.52494E-01	0.000E+00	4.105E-02
5.47506E-01	0.000E+00	4.925E-02
6.40802E-01	0.000E+00	5.631E-02
7.29008E-01	0.000E+00	6.192E-02
8.08938E-01	0.000E+00	6.610E-02
8.77702E-01	0.000E+00	6.908E-02
9.32816E-01	0.000E+00	7.108E-02
9.72288E-01	0.000E+00	7.233E-02
9.94700E-01	0.000E+00	7.297E-02

Angular flux at the Direction Edit Points for group 3

Spatial point 0.00000

Mu	Mu < 0	Mu > 0
5.29953E-03	4.235E-02	0.000E+00
2.77125E-02	4.407E-02	0.000E+00
6.71844E-02	4.606E-02	0.000E+00
1.22298E-01	4.823E-02	0.000E+00
1.91062E-01	5.096E-02	0.000E+00
2.70992E-01	5.385E-02	0.000E+00
3.59198E-01	5.619E-02	0.000E+00
4.52494E-01	5.773E-02	0.000E+00
5.47506E-01	5.853E-02	0.000E+00
6.40802E-01	5.878E-02	0.000E+00

7.29008E-01	5.866E-02	0.000E+00
8.08938E-01	5.834E-02	0.000E+00
8.77702E-01	5.794E-02	0.000E+00
9.32816E-01	5.756E-02	0.000E+00
9.72288E-01	5.725E-02	0.000E+00
9.94700E-01	5.707E-02	0.000E+00

Spatial point 0.02000

Mu	Mu < 0	Mu > 0
5.29953E-03	4.661E-02	4.608E-02
2.77125E-02	4.761E-02	3.990E-02
6.71844E-02	4.898E-02	2.639E-02
1.22298E-01	5.078E-02	1.727E-02
1.91062E-01	5.343E-02	1.199E-02
2.70992E-01	5.622E-02	8.828E-03
3.59198E-01	5.835E-02	6.834E-03
4.52494E-01	5.963E-02	5.516E-03
5.47506E-01	6.017E-02	4.609E-03
6.40802E-01	6.020E-02	3.969E-03
7.29008E-01	5.989E-02	3.508E-03
8.08938E-01	5.942E-02	3.174E-03
8.77702E-01	5.891E-02	2.933E-03
9.32816E-01	5.844E-02	2.765E-03
9.72288E-01	5.808E-02	2.656E-03
9.94700E-01	5.786E-02	2.598E-03

(edited file here)

Spatial point 0.98000

Mu	Mu < 0	Mu > 0
5.29953E-03	2.054E-02	2.093E-02
2.77125E-02	1.966E-02	2.147E-02
6.71844E-02	1.535E-02	2.233E-02
1.22298E-01	1.099E-02	2.348E-02
1.91062E-01	7.993E-03	2.485E-02
2.70992E-01	6.042E-03	2.639E-02
3.59198E-01	4.753E-03	2.800E-02
4.52494E-01	3.875E-03	2.960E-02
5.47506E-01	3.261E-03	3.111E-02
6.40802E-01	2.822E-03	3.244E-02
7.29008E-01	2.503E-03	3.354E-02
8.08938E-01	2.270E-03	3.440E-02
8.77702E-01	2.102E-03	3.502E-02

9.32816E-01	1.984E-03	3.546E-02
9.72288E-01	1.908E-03	3.573E-02
9.94700E-01	1.867E-03	3.587E-02

Spatial point 1.00000

Mu	Mu < 0	Mu > 0
5.29953E-03	0.000E+00	1.815E-02
2.77125E-02	0.000E+00	1.885E-02
6.71844E-02	0.000E+00	1.987E-02
1.22298E-01	0.000E+00	2.115E-02
1.91062E-01	0.000E+00	2.262E-02
2.70992E-01	0.000E+00	2.423E-02
3.59198E-01	0.000E+00	2.592E-02
4.52494E-01	0.000E+00	2.759E-02
5.47506E-01	0.000E+00	2.916E-02
6.40802E-01	0.000E+00	3.057E-02
7.29008E-01	0.000E+00	3.174E-02
8.08938E-01	0.000E+00	3.266E-02
8.77702E-01	0.000E+00	3.335E-02
9.32816E-01	0.000E+00	3.383E-02
9.72288E-01	0.000E+00	3.414E-02
9.94700E-01	0.000E+00	3.430E-02

Unit 22 - slab and group angular fluxes in text format:

```
Angular flux at the Direction Edit Points for group     1
     Spatial point     0.00000
              Mu              Mu  < 0           Mu  > 0
         5.29953E-03         3.219E-01         0.000E+00
         2.77125E-02         3.218E-01         0.000E+00
         6.71844E-02         3.188E-01         0.000E+00
         1.22298E-01         3.146E-01         0.000E+00
         1.91062E-01         3.103E-01         0.000E+00
         2.70992E-01         3.048E-01         0.000E+00
         3.59198E-01         2.977E-01         0.000E+00
         4.52494E-01         2.895E-01         0.000E+00
         5.47506E-01         2.808E-01         0.000E+00
         6.40802E-01         2.724E-01         0.000E+00
         7.29008E-01         2.647E-01         0.000E+00
         8.08938E-01         2.579E-01         0.000E+00
         8.77702E-01         2.522E-01         0.000E+00
         9.32816E-01         2.478E-01         0.000E+00
         9.72288E-01         2.447E-01         0.000E+00
         9.94700E-01         2.429E-01         0.000E+00
     Spatial point     0.20000
              Mu              Mu  < 0           Mu  > 0
         5.29953E-03         3.331E-01         2.786E-01
         2.77125E-02         3.298E-01         2.813E-01
         6.71844E-02         3.233E-01         2.856E-01
         1.22298E-01         3.140E-01         2.806E-01
         1.91062E-01         3.025E-01         2.589E-01
         2.70992E-01         2.897E-01         2.296E-01
         3.59198E-01         2.768E-01         2.008E-01
         4.52494E-01         2.645E-01         1.760E-01
         5.47506E-01         2.532E-01         1.558E-01
         6.40802E-01         2.433E-01         1.397E-01
         7.29008E-01         2.346E-01         1.272E-01
         8.08938E-01         2.274E-01         1.176E-01
         8.77702E-01         2.215E-01         1.104E-01
         9.32816E-01         2.170E-01         1.052E-01
         9.72288E-01         2.139E-01         1.018E-01
         9.94700E-01         2.121E-01         9.995E-02
     Spatial point     0.60000
              Mu              Mu  < 0           Mu  > 0
         5.29953E-03         1.607E-01         1.030E-01
```

2.77125E-02	1.606E-01	1.031E-01
6.71844E-02	1.592E-01	1.041E-01
1.22298E-01	1.562E-01	1.065E-01
1.91062E-01	1.516E-01	1.103E-01
2.70992E-01	1.452E-01	1.160E-01
3.59198E-01	1.374E-01	1.229E-01
4.52494E-01	1.290E-01	1.301E-01
5.47506E-01	1.207E-01	1.364E-01
6.40802E-01	1.132E-01	1.412E-01
7.29008E-01	1.067E-01	1.445E-01
8.08938E-01	1.012E-01	1.465E-01
8.77702E-01	9.693E-02	1.476E-01
9.32816E-01	9.369E-02	1.481E-01
9.72288E-01	9.149E-02	1.482E-01
9.94700E-01	9.027E-02	1.482E-01

Spatial point 1.00000

Mu	Mu < 0	Mu > 0
5.29953E-03	0.000E+00	5.925E-02
2.77125E-02	0.000E+00	6.262E-02
6.71844E-02	0.000E+00	6.760E-02
1.22298E-01	0.000E+00	7.381E-02
1.91062E-01	0.000E+00	8.081E-02
2.70992E-01	0.000E+00	8.779E-02
3.59198E-01	0.000E+00	9.412E-02
4.52494E-01	0.000E+00	9.970E-02
5.47506E-01	0.000E+00	1.046E-01
6.40802E-01	0.000E+00	1.089E-01
7.29008E-01	0.000E+00	1.125E-01
8.08938E-01	0.000E+00	1.153E-01
8.77702E-01	0.000E+00	1.174E-01
9.32816E-01	0.000E+00	1.189E-01
9.72288E-01	0.000E+00	1.198E-01
9.94700E-01	0.000E+00	1.203E-01

Angular flux at the Direction Edit Points for group 2

Spatial point 0.00000

Mu	Mu < 0	Mu > 0
5.29953E-03	1.886E-01	0.000E+00
2.77125E-02	1.932E-01	0.000E+00
6.71844E-02	1.985E-01	0.000E+00
1.22298E-01	2.032E-01	0.000E+00
1.91062E-01	2.067E-01	0.000E+00
2.70992E-01	2.081E-01	0.000E+00

3.59198E-01	2.070E-01	0.000E+00
4.52494E-01	2.035E-01	0.000E+00
5.47506E-01	1.983E-01	0.000E+00
6.40802E-01	1.924E-01	0.000E+00
7.29008E-01	1.864E-01	0.000E+00
8.08938E-01	1.808E-01	0.000E+00
8.77702E-01	1.760E-01	0.000E+00
9.32816E-01	1.722E-01	0.000E+00
9.72288E-01	1.696E-01	0.000E+00
9.94700E-01	1.681E-01	0.000E+00

Spatial point 0.20000

Mu	Mu < 0	Mu > 0
5.29953E-03	2.187E-01	2.081E-01
2.77125E-02	2.142E-01	2.089E-01
6.71844E-02	2.056E-01	2.106E-01
1.22298E-01	1.937E-01	2.123E-01
1.91062E-01	1.799E-01	2.126E-01
2.70992E-01	1.652E-01	2.092E-01
3.59198E-01	1.508E-01	2.016E-01
4.52494E-01	1.377E-01	1.914E-01
5.47506E-01	1.262E-01	1.804E-01
6.40802E-01	1.165E-01	1.699E-01
7.29008E-01	1.085E-01	1.605E-01
8.08938E-01	1.021E-01	1.525E-01
8.77702E-01	9.712E-02	1.462E-01
9.32816E-01	9.348E-02	1.414E-01
9.72288E-01	9.102E-02	1.381E-01
9.94700E-01	8.968E-02	1.363E-01

Spatial point 0.60000

Mu	Mu < 0	Mu > 0
5.29953E-03	4.175E-02	8.061E-02
2.77125E-02	4.045E-02	8.263E-02
6.71844E-02	3.851E-02	8.696E-02
1.22298E-01	3.614E-02	9.424E-02
1.91062E-01	3.342E-02	1.043E-01
2.70992E-01	3.045E-02	1.155E-01
3.59198E-01	2.751E-02	1.255E-01
4.52494E-01	2.481E-02	1.326E-01
5.47506E-01	2.249E-02	1.368E-01
6.40802E-01	2.055E-02	1.385E-01
7.29008E-01	1.898E-02	1.385E-01
8.08938E-01	1.774E-02	1.376E-01

8.77702E-01	1.679E-02	1.362E-01
9.32816E-01	1.609E-02	1.349E-01
9.72288E-01	1.563E-02	1.339E-01
9.94700E-01	1.538E-02	1.332E-01

Spatial point 1.00000

Mu	Mu < 0	Mu > 0
5.29953E-03	0.000E+00	1.320E-02
2.77125E-02	0.000E+00	1.397E-02
6.71844E-02	0.000E+00	1.519E-02
1.22298E-01	0.000E+00	1.696E-02
1.91062E-01	0.000E+00	1.995E-02
2.70992E-01	0.000E+00	2.518E-02
3.59198E-01	0.000E+00	3.259E-02
4.52494E-01	0.000E+00	4.105E-02
5.47506E-01	0.000E+00	4.925E-02
6.40802E-01	0.000E+00	5.631E-02
7.29008E-01	0.000E+00	6.192E-02
8.08938E-01	0.000E+00	6.610E-02
8.77702E-01	0.000E+00	6.908E-02
9.32816E-01	0.000E+00	7.108E-02
9.72288E-01	0.000E+00	7.233E-02
9.94700E-01	0.000E+00	7.297E-02

Angular flux at the Direction Edit Points for group 3

Spatial point 0.00000

Mu	Mu < 0	Mu > 0
5.29953E-03	4.235E-02	0.000E+00
2.77125E-02	4.407E-02	0.000E+00
6.71844E-02	4.606E-02	0.000E+00
1.22298E-01	4.823E-02	0.000E+00
1.91062E-01	5.096E-02	0.000E+00
2.70992E-01	5.385E-02	0.000E+00
3.59198E-01	5.619E-02	0.000E+00
4.52494E-01	5.773E-02	0.000E+00
5.47506E-01	5.853E-02	0.000E+00
6.40802E-01	5.878E-02	0.000E+00
7.29008E-01	5.866E-02	0.000E+00
8.08938E-01	5.834E-02	0.000E+00
8.77702E-01	5.794E-02	0.000E+00
9.32816E-01	5.756E-02	0.000E+00
9.72288E-01	5.725E-02	0.000E+00
9.94700E-01	5.707E-02	0.000E+00

Spatial point 0.20000

Mu	Mu < 0	Mu > 0
5.29953E-03	9.879E-02	5.804E-02
2.77125E-02	9.788E-02	5.756E-02
6.71844E-02	9.570E-02	5.694E-02
1.22298E-01	9.233E-02	5.575E-02
1.91062E-01	8.817E-02	5.298E-02
2.70992E-01	8.379E-02	4.877E-02
3.59198E-01	7.965E-02	4.409E-02
4.52494E-01	7.596E-02	3.966E-02
5.47506E-01	7.274E-02	3.581E-02
6.40802E-01	6.994E-02	3.260E-02
7.29008E-01	6.755E-02	3.001E-02
8.08938E-01	6.554E-02	2.798E-02
8.77702E-01	6.391E-02	2.643E-02
9.32816E-01	6.266E-02	2.530E-02
9.72288E-01	6.179E-02	2.454E-02
9.94700E-01	6.131E-02	2.413E-02

Spatial point 0.60000

Mu	Mu < 0	Mu > 0
5.29953E-03	5.391E-02	4.129E-02
2.77125E-02	5.371E-02	4.145E-02
6.71844E-02	5.324E-02	4.217E-02
1.22298E-01	5.249E-02	4.367E-02
1.91062E-01	5.147E-02	4.601E-02
2.70992E-01	5.021E-02	4.875E-02
3.59198E-01	4.873E-02	5.107E-02
4.52494E-01	4.707E-02	5.247E-02
5.47506E-01	4.533E-02	5.294E-02
6.40802E-01	4.360E-02	5.271E-02
7.29008E-01	4.199E-02	5.204E-02
8.08938E-01	4.057E-02	5.120E-02
8.77702E-01	3.939E-02	5.035E-02
9.32816E-01	3.847E-02	4.962E-02
9.72288E-01	3.783E-02	4.907E-02
9.94700E-01	3.747E-02	4.875E-02

Spatial point 1.00000

Mu	Mu < 0	Mu > 0
5.29953E-03	0.000E+00	1.815E-02
2.77125E-02	0.000E+00	1.885E-02
6.71844E-02	0.000E+00	1.987E-02
1.22298E-01	0.000E+00	2.115E-02
1.91062E-01	0.000E+00	2.262E-02

2.70992E-01	0.000E+00	2.423E-02
3.59198E-01	0.000E+00	2.592E-02
4.52494E-01	0.000E+00	2.759E-02
5.47506E-01	0.000E+00	2.916E-02
6.40802E-01	0.000E+00	3.057E-02
7.29008E-01	0.000E+00	3.174E-02
8.08938E-01	0.000E+00	3.266E-02
8.77702E-01	0.000E+00	3.335E-02
9.32816E-01	0.000E+00	3.383E-02
9.72288E-01	0.000E+00	3.414E-02
9.94700E-01	0.000E+00	3.430E-02

Unit 23 - group scalar fluxes in text format:

```
Group Scalar Flux for group    1
      xb            Flux
  0.00000E+00   1.28432E+00
  2.00000E-02   1.28890E+00
  4.00000E-02   1.27715E+00
  6.00000E-02   1.26014E+00
  8.00000E-02   1.24036E+00
  1.00000E-01   1.21900E+00
  1.20000E-01   1.19682E+00
  1.40000E-01   1.17436E+00
  1.60000E-01   1.15213E+00
  1.80000E-01   1.13071E+00
  2.00000E-01   1.11225E+00
  2.20000E-01   1.06075E+00
  2.40000E-01   1.00266E+00
  2.60000E-01   9.43901E-01
  2.80000E-01   8.86170E-01
  3.00000E-01   8.30328E-01
  3.20000E-01   7.76878E-01
  3.40000E-01   7.26119E-01
  3.60000E-01   6.78219E-01
  3.80000E-01   6.33262E-01
  4.00000E-01   5.91277E-01
  4.20000E-01   5.52258E-01
  4.40000E-01   5.16184E-01
  4.60000E-01   4.83027E-01
  4.80000E-01   4.52768E-01
  5.00000E-01   4.25412E-01
  5.20000E-01   4.01012E-01
  5.40000E-01   3.79713E-01
  5.60000E-01   3.61861E-01
  5.80000E-01   3.48338E-01
  6.00000E-01   3.43891E-01
  6.20000E-01   3.43300E-01
  6.40000E-01   3.37939E-01
  6.60000E-01   3.30807E-01
  6.80000E-01   3.22562E-01
  7.00000E-01   3.13515E-01
  7.20000E-01   3.03852E-01
  7.40000E-01   2.93694E-01
```

7.60000E-01	2.83123E-01
7.80000E-01	2.72198E-01
8.00000E-01	2.60959E-01
8.20000E-01	2.49433E-01
8.40000E-01	2.37633E-01
8.60000E-01	2.25560E-01
8.80000E-01	2.13198E-01
9.00000E-01	2.00514E-01
9.20000E-01	1.87448E-01
9.40000E-01	1.73885E-01
9.60000E-01	1.59609E-01
9.80000E-01	1.44114E-01
1.00000E+00	1.24690E-01

Group Scalar Flux for group 2

xb	Flux
0.00000E+00	1.94270E-01
2.00000E-02	2.51740E-01
4.00000E-02	2.83754E-01
6.00000E-02	3.05655E-01
8.00000E-02	3.20727E-01
1.00000E-01	3.30516E-01
1.20000E-01	3.35915E-01
1.40000E-01	3.37475E-01
1.60000E-01	3.35525E-01
1.80000E-01	3.30200E-01
2.00000E-01	3.21957E-01
2.20000E-01	3.17179E-01
2.40000E-01	3.10880E-01
2.60000E-01	3.03654E-01
2.80000E-01	2.95773E-01
3.00000E-01	2.87427E-01
3.20000E-01	2.78751E-01
3.40000E-01	2.69845E-01
3.60000E-01	2.60789E-01
3.80000E-01	2.51648E-01
4.00000E-01	2.42470E-01
4.20000E-01	2.33295E-01
4.40000E-01	2.24150E-01
4.60000E-01	2.15053E-01
4.80000E-01	2.06008E-01
5.00000E-01	1.97009E-01
5.20000E-01	1.88030E-01

5.40000E-01	1.79015E-01
5.60000E-01	1.69851E-01
5.80000E-01	1.60282E-01
6.00000E-01	1.49053E-01
6.20000E-01	1.38195E-01
6.40000E-01	1.29726E-01
6.60000E-01	1.22260E-01
6.80000E-01	1.15486E-01
7.00000E-01	1.09246E-01
7.20000E-01	1.03439E-01
7.40000E-01	9.79969E-02
7.60000E-01	9.28664E-02
7.80000E-01	8.80063E-02
8.00000E-01	8.33824E-02
8.20000E-01	7.89658E-02
8.40000E-01	7.47310E-02
8.60000E-01	7.06547E-02
8.80000E-01	6.67145E-02
9.00000E-01	6.28879E-02
9.20000E-01	5.91494E-02
9.40000E-01	5.54677E-02
9.60000E-01	5.17967E-02
9.80000E-01	4.80459E-02
1.00000E+00	4.37958E-02

Group Scalar Flux for group 3

xb	Flux
0.00000E+00	5.52502E-02
2.00000E-02	6.58401E-02
4.00000E-02	7.31773E-02
6.00000E-02	7.93078E-02
8.00000E-02	8.46920E-02
1.00000E-01	8.95801E-02
1.20000E-01	9.41610E-02
1.40000E-01	9.86202E-02
1.60000E-01	1.03195E-01
1.80000E-01	1.08321E-01
2.00000E-01	1.16030E-01
2.20000E-01	1.22671E-01
2.40000E-01	1.25235E-01
2.60000E-01	1.26044E-01
2.80000E-01	1.25716E-01
3.00000E-01	1.24596E-01

3.20000E-01	1.22911E-01
3.40000E-01	1.20823E-01
3.60000E-01	1.18458E-01
3.80000E-01	1.15917E-01
4.00000E-01	1.13282E-01
4.20000E-01	1.10622E-01
4.40000E-01	1.07998E-01
4.60000E-01	1.05463E-01
4.80000E-01	1.03065E-01
5.00000E-01	1.00853E-01
5.20000E-01	9.88782E-02
5.40000E-01	9.71995E-02
5.60000E-01	9.58986E-02
5.80000E-01	9.51256E-02
6.00000E-01	9.55665E-02
6.20000E-01	9.58034E-02
6.40000E-01	9.44263E-02
6.60000E-01	9.24749E-02
6.80000E-01	9.01703E-02
7.00000E-01	8.76107E-02
7.20000E-01	8.48520E-02
7.40000E-01	8.19290E-02
7.60000E-01	7.88645E-02
7.80000E-01	7.56735E-02
8.00000E-01	7.23646E-02
8.20000E-01	6.89415E-02
8.40000E-01	6.54029E-02
8.60000E-01	6.17417E-02
8.80000E-01	5.79443E-02
9.00000E-01	5.39875E-02
9.20000E-01	4.98336E-02
9.40000E-01	4.54193E-02
9.60000E-01	4.06271E-02
9.80000E-01	3.51899E-02
1.00000E+00	2.77138E-02

Unit 24 - total scalar flux in text format:

```
Total Scalar Flux
      x            Flux
  0.00000E+00   1.53384E+00
  2.00000E-02   1.60648E+00
  4.00000E-02   1.63408E+00
  6.00000E-02   1.64511E+00
  8.00000E-02   1.64578E+00
  1.00000E-01   1.63910E+00
  1.20000E-01   1.62689E+00
  1.40000E-01   1.61046E+00
  1.60000E-01   1.59085E+00
  1.80000E-01   1.56923E+00
  2.00000E-01   1.55024E+00
  2.20000E-01   1.50061E+00
  2.40000E-01   1.43877E+00
  2.60000E-01   1.37360E+00
  2.80000E-01   1.30766E+00
  3.00000E-01   1.24235E+00
  3.20000E-01   1.17854E+00
  3.40000E-01   1.11679E+00
  3.60000E-01   1.05747E+00
  3.80000E-01   1.00083E+00
  4.00000E-01   9.47028E-01
  4.20000E-01   8.96176E-01
  4.40000E-01   8.48333E-01
  4.60000E-01   8.03543E-01
  4.80000E-01   7.61842E-01
  5.00000E-01   7.23275E-01
  5.20000E-01   6.87920E-01
  5.40000E-01   6.55928E-01
  5.60000E-01   6.27611E-01
  5.80000E-01   6.03746E-01
  6.00000E-01   5.88511E-01
  6.20000E-01   5.77298E-01
  6.40000E-01   5.62092E-01
  6.60000E-01   5.45542E-01
  6.80000E-01   5.28218E-01
  7.00000E-01   5.10371E-01
  7.20000E-01   4.92144E-01
  7.40000E-01   4.73620E-01
```

7.60000E-01	4.54854E-01
7.80000E-01	4.35878E-01
8.00000E-01	4.16706E-01
8.20000E-01	3.97341E-01
8.40000E-01	3.77767E-01
8.60000E-01	3.57956E-01
8.80000E-01	3.37857E-01
9.00000E-01	3.17390E-01
9.20000E-01	2.96431E-01
9.40000E-01	2.74772E-01
9.60000E-01	2.52033E-01
9.80000E-01	2.27350E-01
1.00000E+00	1.96200E-01

List of References

[1] Wilson, J. W., et. al.; *BRYNTRN: A Baryon Transport Model*, NASA Technical Paper, NASA TP-2887, March 1989.

[2] Filippone, W. L., *The theory and Application of SMART Electron Scattering Matrices*, Nuclear Science and Engineering, American Nuclear Society, Vol. 99, Pages 232-250, 1988.

[3] Filippone, W. L., Monahan, S. P., Woolf, S., Garth, J. C., *Three-Dimensional, Multi-region S_N Solutions of the Spencer-Lewis Electron Transport Equation*, Nuclear Science and Engineering, American Nuclear Society, Vol. 105, Pages 55-58, 1990.

[4] Irving, D. C., Alsmiller, R. G., Moran H. S.; *Tissue Current-to-Dose Conversion Factors for Neutrons With Energies From 0.5 to 60 Mev*, ORNL-4032, U.S. Atomic Energy Commision, Aug. 1967.

[5] Zerby, C. D., Kinney, W. E.; *Calculated Tissue Current-to-Dose Conversion Factors for Nucleaons Below 400 MeV*, ORNL-TM-1038, Oak Ridge National Laboratory, May 1965.

[6] Ganapol, B. D., et. al.; *Benchmark Solutions for the Galactic Heavy-Ion Transport Equations with Energy and Spatial Coupling*, NASA Technical Paper, NASA TP-3112, October 1991.

[7] Alsmiller Jr., R. G., Irving, D. C., Kinney, W. E., and Moran, H. S.; *The validity of the Straightahead Approximation in Space Vehicle Shielding Studies: Second Symposium on Protection Against Radiations in Space*, Arthur Reetz, Jr. ed., NASA SP-71, 1965, pp. 177-181.

[8] Wilson, J. W.; *Analysis of the Theory of High-Energy Ion Transport*, NASA Technical Note, NASA TN D-8381, March 1977.

[9] Wilson, J. W.; *Heavy Ion Transport in the Straight Ahead Approximation*, NASA Technical Paper, NASA TP-2178, June 1983.

[10] Pearson, C. E. (Editor), *Handbook of Applied Mathematics, Selected Results and Methods*, Second Edition, Van Nostrand Reinhold, Section 10.6.3, Page 564, 1990.

[11] Siewert, C. E., Benoist, P.; *Multigroup Transport Theory: I. Basic Analysis*, Nuclear Science and Engineering, American Nuclear Society, Vol 78, Pages 311-314, 1981.

[12] Garcia, R. D. M., Siewert, C. E.; *Multigroup Transport Theory: II. Numerical Results*, Nuclear Science and Engineering, American Nuclear Society, Vol 78, Pages 315-323, 1981.

[13] Siewert, C. E., Benoist, P.; *The F_N Method in Neutron-Transport Theory. Part I: Theory and Applications*, Nuclear Science and Engineering, American Nuclear Society, Vol 69, Pages 156-160, 1979.

[14] Grandjean, P., Siewert, C. E.; *The F_N Method in Neutron-Transport Theory. Part II: Applications and Numerical Results*, Nuclear Science and Engineering, American Nuclear Society, Vol 69, Pages 161-168, 1979.

[15] Bell, G. I., Glasstone, S.; *Nuclear Reactor Theory*, Robert E. Krieger Publishing Company, 1970.

[16] Duderstadt, J. J., Hamilton, L. J.; *Nuclear Reactor Analysis*, John Wiley & Sons, 1976.

[17] Cercignani, C.; *The Boltzmann Equation and Its Applications*, Applied Mathematical Sciences Series Volume 67, Springer-Verlag New York Inc., 1988.

[18] Case, K. M., Zweifel, P. F.; *Linear Transport Theory*, Addison-Wesley Publishing Company, 1967.

[19] Wilson, J. W., Townsend, L. W.; *A Benchmark for Galactic Cosmic-Ray Transport Codes*, Radiation Research, Society of Radiation Reasearch, Vol. 114, pages 201-206, May 1988.

[20] Ganapol, B. D., Townsend, L. W., Wilson, J. W.; *Benchmark Solutions for the Galactic Ion Transport Equations: Energy and Spatially Dependent Problems*, NASA Technical Paper, NASA TP-2878, March 1989.

[21] Mika, J. R.; *Neutron Transport with Anisotropic Scattering*, Nuclear Science & Engineering, American Nuclear Society, Vol. 11, pages 415-427, December 1961.

[22] Muskhelishvili, N. I. (translated from Russian by J. R. M. Radok); *Singular Integral Equations*, Second Edition, Dover Publications, Inc., 1992.

[23] *MathCAD 4.0*, MathSoft, Inc., March 1993.

[24] Vetterling, W. T., Press, W. H., Teukolsky, S. A., Flannery, B. P.; *Numerical Recipes, The Art of Scientific Computing, Second Edition*, Cambridge University Press, 1992.

[25] Parsons, K. D.; *ANISN/PC Manual*, EG&G Idaho, Inc., EGG-2500, December 1988.

[26] MacFarlane, R. E., Muir, D. W., Boicourt, R. M.; *The NJOY Nuclear Data Processing System*, Vols. I-IV, LA-9303-M, Los Alamos National Laboratory, May 1982.

[27] Wilson, J. W., Badavi, F. F., *Methods of Galactic Heavy Ion Transport*, Radiation Research, Society of Radiation Research, Vol. 108, Pages 231-237, 1986.